NUMERICAL INVESTIGATION ON THE RESPONSES OF EXISTING TUNNEL DUE TO ADJACENT LOADED PILE FOR DEVELOPMENT OF THE INFLUENCE ZONE AND CONSTRUCTION GUIDELINE

PRATEEP LUEPRASERT

A THESIS SUBMITTED IN PARTIAL FULFILLMENT
OF THE REQUIREMENT FOR THE DEGREE OF
DOCTORAL OF ENGINEERING IN CIVIL ENGINEERING
FACULTY OF ENGINEERING
KING MONGKUT'S INSTITUTE OF TECHNOLOGY LADKRABANG
2017

KMITL-2017-EN-D-098-209

หัวข้อวิทยานิพนธ์	การศึกษาการตอบสนองของอุโมงค์เดิมเนื่องจากผลกระทบของเสาเข็มรับแรงข้างเคียงเพื่อปรับปรุงเขตอิทธิพลและเป็นแนวทางการก่อสร้างเบื้องต้นโดยวิธีการวิเคราะห์เชิงตัวเลข
นักศึกษา	นาย ประทีป หลือประเสริฐ
รหัสประจำตัว	55610406
ปริญญา	วิศวกรรมศาสตรดุษฎีบัณฑิต
สาขาวิชา	วิศวกรรมโยธา
พ.ศ.	2560
อาจารย์ที่ปรึกษาวิทยานิพนธ์	ศาสตราจารย์ ดร. สุชัชวีร์ สุวรรณสวัสดิ์
อาจารย์ที่ปรึกษาวิทยานิพนธ์ร่วม	รองศาสตราจารย์ ดร. พรเกษม จงประดิษฐ์

บทคัดย่อ

ในปัจจุบันการพัฒนาโครงสร้างพื้นฐานมีจำนวนเพิ่มมากขึ้นอย่างรวดเร็วเพื่อตอบสนองการขยายตัวของเมืองสำคัญ เช่น กรุงเทพมหานคร แต่เนื่องจากพื้นที่สำหรับก่อสร้างที่มีอยู่อย่างจำกัดทำให้การก่อสร้างอาคารในอนาคตอยู่ใกล้เคียงกับอุโมงค์เดิมซึ่งเป็นโครงสร้างพื้นฐานสำหรับระบบคมนาคมและสาธารณูปโภคในปัจจุบันอย่างหลีกเลี่ยงไม่ได้ เขตคุ้มครอง (Protection Zone) ได้นำมาใช้เพื่อประเมินผลกระทบที่อาจเกิดขึ้นต่ออุโมงค์ อย่างไรก็ตามเขตคุ้มครองดังกล่าวได้พิจารณาจากทฤษฎีพื้นฐานการพังทลายของชั้นดินเท่านั้น และไม่คำนึงถึงการปฏิสัมพันธ์ระหว่างโครงสร้างและดิน โครงสร้างบนชั้นดินอ่อนใช้ระบบเสาเข็มเป็นหลัก ซึ่งเมื่อพิจารณาถึงการปฏิสัมพันธ์ของเสาเข็มรับน้ำหนักต่อดินรอบข้าง เขตคุ้มครองควรจะมีขนาดที่สัมพันธ์ต่ออิทธิพลของเสาเข็มฯ ดังนั้นการประเมินผลกระทบของเสาเข็มข้างเคียงรับน้ำหนักกระทำต่ออุโมงค์เดิมจึงเป็นสิ่งสำคัญเพื่อนำมาปรับปรุงเขตคุ้มครองให้มีความเหมาะสมกับผลกระทบที่เกิดจากเสาเข็มดังกล่าว โดยการศึกษานี้ใช้วิธีไฟไนต์เอลิเมนต์แบบ 3 มิติร่วมกับแบบจำลองที่สมเหตุสมผลกับพฤติกรรมของชั้นดินในการวิเคราะห์

ในการศึกษาเบื้องต้นในงานวิจัยนี้ซึ่งพิจารณาค่าการเปลี่ยนแปลงขนาดอุโมงค์ พิสูจน์ได้ว่าอิทธิพลของปลายเสาเข็มและลักษณะชั้นดินมีผลต่ออุโมงค์อย่างมีนัยยะและเขตอิทธิพลที่พิจารณาเฉพาะเสาเข็มสามารถมีขนาดเล็กลงและรูปร่างเปลี่ยนไปอย่างชัดเจน ชี้ให้เห็นถึงความจำเป็นที่จะต้องเข้าใจการปฏิสัมพันธ์ระหว่างโครงสร้างและดินและอิทธิพลของตัวแปรหลักอย่างถ่องแท้เพื่อประเมินผลกระทบทั้งการเสียรูปและเสถียรภาพอย่างสมเหตุสมผล นอกจากนี้พบว่าลักษณะการเสียรูปของอุโมงค์ไม่สมมาตร วิธีการวัดค่าการเปลี่ยนแปลงขนาดอุโมงค์ที่ใช้อยู่จึงไม่เหมาะสม งานวิจัยนี้จึงเสนอการพิจารณาวิธีจำลองการขุดเจาะอุโมงค์ด้วยหัวเจาะพร้อมกับการเทียบวัดกับผลการตรวจวัด

ให้ได้วิธีการจำลองที่เหมาะสมและได้ค่าแรงภายในผนังอุโมงค์ที่ถูกต้องก่อนการศึกษาการตอบสนองของอุโมงค์เดิมจากเสาเข็มรับแรงต่อไป

งานวิจัยนี้ยังได้เสนอวิธีการตรวจวัดค่าการเปลี่ยนแปลงขนาดอุโมงค์ที่สะท้อนถึงการเปลี่ยนแปลงสูงสุด และลักษณะการบิดเบี้ยว ผลการศึกษาเชิงตัวแปรเพื่อตรวจผลตอบสนองของอุโมงค์ทั้งในแง่การเสียรูปและการเปลี่ยนแปลงแรงภายในจากเสาเข็มรับแรงข้างเคียง ที่พิจารณาตำแหน่งปลายเข็มสัมพัทธ์กับอุโมงค์ ชั้นดิน ที่แตกต่างกัน ระบุว่ากลไกที่เกิดขึ้นคือเมื่อเสาเข็มรับแรงและส่งถ่ายให้กับดินรอบข้างและที่ปลายเสาเข็ม ทำให้ดินเกิดการเคลื่อนตัวและเหนี่ยวนำให้เกิดการเปลี่ยนแปลงของผนังอุโมงค์ ทำให้ตำแหน่งปลายเข็มสัมพัทธ์กับอุโมงค์และชั้นดินมีอิทธิพลอย่างยิ่ง รวมถึงได้ข้อแนะนำเบื้องต้นตำแหน่งปลายเข็มสัมพัทธ์กับอุโมงค์ที่มีผลกระทบรุนแรงต่ออุโมงค์เมื่ออุโมงค์อยู่ในชั้นดินแต่ละแบบ สำหรับในแง่ของเสถียรภาพพบว่าค่าการเปลี่ยนแปลงสูงสุดโมเมนต์ดัดมีอิทธิพลมากกว่าค่าการเปลี่ยนแปลงสูงสุดของแรงในแนวแกนอย่างชัดเจน

เมื่อพิจารณาค่าการเปลี่ยนแปลงสูงสุดของขนาดอุโมงค์และโมเมนต์ดัดซึ่งมีความสอดคล้องกัน สามารถนำมาเป็นแนวทางในการปรับปรุงพื้นที่อิทธิพลเนื่องจากผลกระทบของเสาเข็มรับน้ำหนักกระทำที่มีต่ออุโมงค์เดิมได้ ซึ่งเขตอิทธิพลใหม่ (new influence zone) สามารถระบุได้ดังนี้ ระยะห่างของขอบเสาเข็มถึงขอบผนังอุโมงค์ (clearance) ที่แนะนำ คือ 4.5 เมตร และ ระยะแนวดิ่งที่แนะนำ คือ 1.0 เท่าของขนาดเส้นผ่านศูนย์กลางอุโมงค์ (D_T) เหนือแกนอุโมงค์ (tunnel axis) และใต้แกนอุโมงค์ระยะแนวดิ่งมีความยาวเท่ากับความลึกของเสาเข็มที่ใช้ในการพิจารณา

คำสำคัญ: เขตคุ้มครอง, เสาเข็มรับแรง, ,อุโมงค์เดิม, การปฏิสัมพันธ์ของเสาเข็มรับแรง ดิน และอุโมงค์, แรงภายในผนังอุโมงค์

Thesis Title	Numerical Investigation on the Responses of Existing Tunnel due to Adjacent Loaded Pile for Development of the Influence Zone and Construction Guideline
Student	Mr. Prateep Lueprasert
Student ID.	55610406
Degree	Doctoral of Engineering
Program	Civil Engineering (Geotechnical Engineering)
Year	2017
Thesis Advisor	Professor Dr. Suchatvee Suwansawat
Thesis Co-advisor	Associate Professor Dr. Pornkasem Jongpradist

ABSTRACT

Nowadays, infrastructure developments have increased rapidly to contribute the urbanization of metropolis such as Bangkok. With limited space, the existing tunnels, which is generally used to facilitate transportation and service utilities, inevitably suffer impacts caused by those adjacent constructions. The protection zone is taken to evaluate possible impacts on the tunnel lining. However, this zone was conventionally assumed from the ideal shear plane of soil, rather than on the theoretical understanding of the pile-tunnel interaction. Under a soft ground condition, structures are principally supported by piles of various lengths. With considering pile-soil interaction, the protection zone should be in accordance to their interaction. The assessment of the impacts of adjacent pile under loading on the existing tunnel is thus essential to develop the proper protection zone. A 3D Finite Element Method (3D-FEM) with reasonable soil constitutive model are conducted to analyse the problem in this study.

The preliminary analysis in this study evaluating changes in tunnel diameter indicates that the pile tip position in relation to the tunnel axis and the soil type of which the existing tunnel is located, have significant effect on tunnel. Moreover, the obtained influence zone from the study is much smaller than the existing zone. These conclusions indicate that better understanding on pile-soil-tunnel interaction mechanism and key influence factors are necessary to reasonably assess the impact of loaded pile on the tunnel in terms of both tunnel deformation and tunnel stability. Besides, the unsymmetrical tunnel deformation has been observed, revealing that the current assessment method of the change in tunnel diameter is inappropriate. This dissertation thus developed tunnelling simulation method which is capable of reproducing both initial deformation and structural forces. The validation of the tunnelling simulation method is compared with the field measurement data. After that, the tunnel responses due to pile under loading is investigated.

This study also proposed the assessment method used to track changes in tunnel diameter regarding the maximum magnitude and distorted tunnel shapes. The results in terms of tunnel deformations and changes of lining forces due to adjacent pile under loading with various soil conditions and the positions of pile tip in relation to the tunnel axis are performed. The results indicate that the mechanisms behind the tunnel deformation are principally due to the movement behaviour (both magnitude

and direction) of soil surrounding the tunnel, which in turn is dependent on the load transfer behaviour from the pile. Thus, the relative position of the tunnel and pile tip together with soil profile is significantly affected. The relative positions of the tunnel and pile tip which contributes strong effect on existing tunnel in different soil conditions are also suggested. For considering the response in term of tunnel stability, it found that the maximum change in bending moment is more significant than the maximum change in axial force.

The relationship between the maximum change in tunnel diameter and the maximum change in bending moment and the relative position of the tunnel and pile tip can be used as a guideline to develop a new influence zone. The range of 1.0 D_T (D_T is tunnel diameter) above tunnel spring line and below tunnel spring line to the deepest level in engineering practice is recommended to be the zone in vertical direction. For the horizontal clearance, the value of 0.7 D_T or 4.5 m from tunnel surface seems to be sufficient.

Keyword: The protection zone, Pile under loading, Existing tunnel, Pile-soil-tunnel interaction, Lining forces

ACKNOWLEDGEMENT

When I have studied in a doctoral degree, there have been so many things I have learned and gotten to know from so many people. Firstly, it has been my true honor to work with Assoc.Prof. Pornkasem Jongpradist from King Mongkut's University of Technology Thonburi (KMUTT). He is very great both as a teacher and supervisor. He has always believed in my potential and suggested my initiative. Without his vision, effort and encouragement, this thesis could never have reached completion. Moreover, he has supported my research since the beginning and has always helped me to shape up my research. However, if I don't meet Prof. Suchatvee Suwansawat who has been the first advisor in graduated studies in Mongkut's Institute of Technology Ladkrabang (KMITL), the best opportunities for me is leave out. He provided me with some excellent engineering practices and helped all my problems. For the researching time in Austria, I am very thankful to Prof. Schweiger Helmut and Mr. Kamchai Choosrithong for supporting me and providing everything I need.

The authors wish to express their thankfulness to Thailand Research Fund (TRF), 1D2 Group Co. Ltd. for the financial support through Grant PHD56I0057 and King Mongkut's Institute of Technology Ladkrabang Grant KREF035001.

Sincere appreciation is also extended to the other members of the committees, Prof. Dr. Suched Likitlersuang, Asst. Prof. Dr. Thanadol Kongsomboon, Dr. Pastsakorn Kitiyodom and Dr. Salisa Chaiyaput, for their help, encouragement, suggestions and constructive comments.

I believe no research can be completed without having the support of friends and colleagues in a research group at the Ladkrabang Underground and Tunneling Innovation Center (LUTIC) in KMITL, Nattida Kwanlikit, Duangkamol Sirirak, Kodchamon Ruengwirojkul and Narunat Heama. They are my lovely juniors and made my office a great environment. Thanks for all the people who came to support me and helped make it a memorable and successful event.

Finally, I owe my deepest gratitude to my parents, Praphas and Thongyoo Lueprasert and my family; their love is the greatest power in the world and has driven me to succeed in every goal I have dreamed of.

Prateep Lueprasert
Ladkrabang underground and Tunneling Innovative Center (LUTIC)
October 2017

CONTENTS

LIST OF TABLES

LIST OF FIGURES

LIST OF SYMBOLS

c'	cohesion of soil
E_c	young modulus of concrete
E_{oed}^{ref}	reference tangent modulus for oedometer primary loading
E_{50}^{ref}	reference secant modulus from drained triaxial test
E_{ur}^{ref}	reference unloading/reloading modulus
G_0^{Ref}	Reference small strain shear modulus
$\gamma_{0.7}$	Shear strain amplitude at $0.722\,G_0$
R_f	Failure ratio
m	exponential power for modulus
p_{ref}	reference pressure
γ_c	unit weight of concrete
γ_{sat}	unit weight of saturated soil
υ_c	Poisson's ratio of concrete
υ_{ur}	unloading/reloading Poisson's ratio
ϕ'	internal friction angle
C_T	pile tip position beneath the tunnel spring line
D_T	tunnel diameter
L_p	pile tip position
L_T	depth of tunnel
ϕ_{H1}	tunnel diameter in horizontal direction before pile loading
ϕ_{H2}	tunnel diameter in horizontal direction after pile loading
$\phi_{T\text{-}C}$	tunnel diameter calculated from shortening behaviour before pile loading
$\phi_{T\text{-}E}$	tunnel diameter calculated from widening behaviour before pile loading
ϕ_{V1}	tunnel diameter in horizontal direction before pile loading
ϕ_{V2}	tunnel diameter in horizontal direction after pile loading
$\phi_{C\text{-}MAX}$	tunnel diameter calculated from shortening behaviour after pile loading
$\phi_{E\text{-}MAX}$	tunnel diameter calculated from widening behaviour after pile loading
$\Delta\phi_H$	change in tunnel diameter in horizontal direction
$\Delta\phi_V$	change in tunnel diameter in vertical direction
$M_{Max\_Initial}$	maximum value of bending moment after tunnel excavation complete
$N_{Max\_Initial}$	maximum value of axial force after tunnel excavation complete
ΔM_{Max}	maximum change in bending moment

ΔM_{Normal}	change in bending moment at generally observed positions of the tunnel lining
ΔN_{Max}	maximum change in axial force
ΔN_{Normal}	change in axial force at generally observed positions of the tunnel lining
$\Delta\phi_{C\text{-}MAX}$	the maximum contraction change in tunnel diameter
$\Delta\phi_{E\text{-}MAX}$	the maximum extension change in tunnel diameter
α	distortion degrees indicate the circumferential positions of the maximum extension change in tunnel diameter with respect to the tunnel horizontal axis
β	distortion degrees indicate the circumferential positions of the maximum contraction change in tunnel diameter with respect to the tunnel vertical axis
ω_D	position of maximum change in tunnel diameter defined the origin at tunnel crown
ω_M	position of maximum change in bending moment defined the origin at tunnel crown
ω_N	position of maximum change in axial force defined the origin at tunnel crown

Chapter 1

Introduction

1.1 Background

The amount of tunnel construction in many populous cities is increasing for many purposes, such as to effectively provide underground mass transit systems and a range of utilities. In most metropolises, tunnels are commonly routed underground along major streets to avoid being under buildings. Clearly, great care must be taken to maintain the safety and serviceability of these tunnels. For large and important public tunnels, the tunnel owners usually define the tunnel protection zone for any future construction activities in the adjacent area. Figure 1.1 illustrates tunnel influence zones for the new construction of the Land Transport Authority (LTA) [1] and the Mass Rapid Transit Authority (MRTA) [2]. Due to urbanization and traffic congestion, other new infrastructures, such as flyovers, elevated trains and tall buildings, are also being constructed. With limited space, the existing tunnels inevitably suffer impacts caused by these changes in their surrounding environment. Under a soft ground condition, structures are supported by piles of various lengths. Thus, the movement of the piles under loading would induce a certain degree of impact on the tunnels. An assessment of the impact of piles under loading on the stability and integrity of the tunnels is necessary. The assessment is typically carried out in two steps. The first step is to evaluate the potential impact of the pile foundation for a design modification of the pile position. At present, this is carried out by evaluating with the influence zone of the tunnel in combination with certain criteria. If the possible impact is serious, the second step of assessment is necessary, in which the design must be modified or a detailed assessment must be carried out.

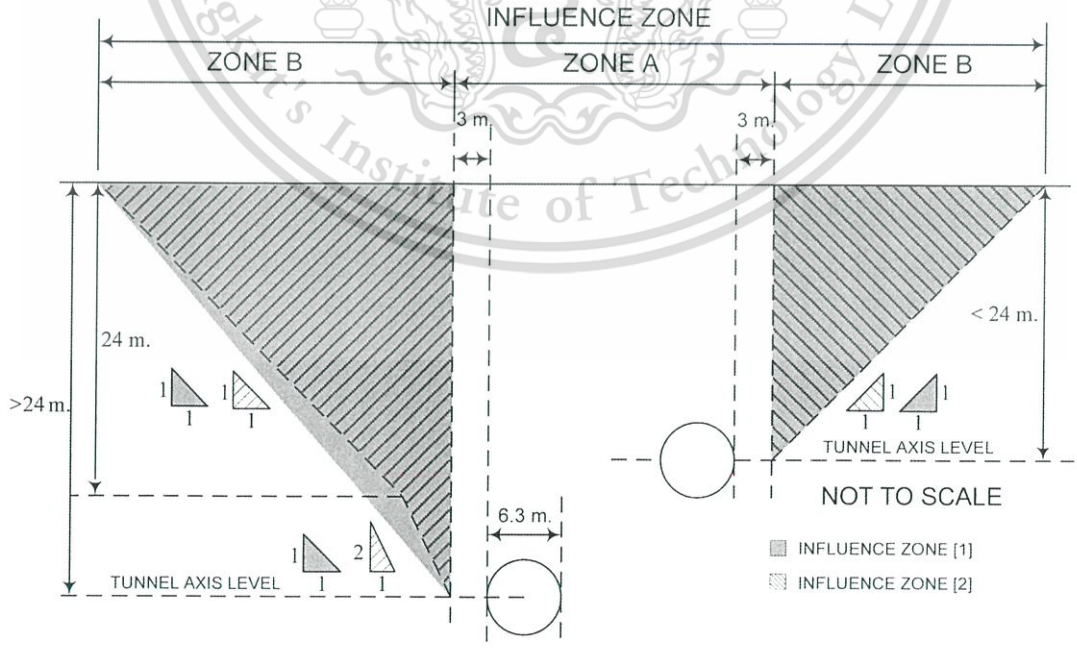

Figure 1.1 Tunnel influence zone utilised in current practice.

An influence zone was conventionally assumed from the ideal shear plane from the model test first proposed by Morton and King [3]. The influence zone is thus assumed from the shear plane of the ground due to tunnelling, rather than from the impact of a new construction on the existing tunnel. The zone is applied to all construction types but is proved to be inappropriate for piles. In addition, the restrictive guidelines were established based on experiences rather than on the theoretical understanding of the pile-tunnel interaction. According to the load transfer mechanism of pile, only the soil surrounding the pile perimeter and at the pile tip moves. Thus, the tunnel influence zone subject to pile under loading should be smaller than that assumed by the shear failure plane. A more reasonable and specific tunnel influence zone affected by nearby piles is therefore necessary for an efficient issuance of construction permits of pile-supported structures in an area near the existing tunnel. An understanding of pile-soil-tunnel interaction is essential for assessing the impact of loaded piles on the stability and integrity of tunnels, leading to establishment of appropriate influence zone.

However, studies on the effects of loaded piles on nearby existing tunnels are rather limited, Over the past 60 years, there have been only a small number of publications concerning the influence of bored piles on existing tunnels, mostly on those constructed in London, [4] – [8]. In 2006, the impacts of various bored pile types (single pile, pile row and pile group) on the existing tunnel in multi-layer soil focused on the Mass Rapid Transit (MRT) project were evaluated by Charoenpak (2006) [9]. The study revealed that the level of impact to tunnel depends on the pile tip position in relation to the tunnel position as well as the soil profile. However, since the existing tunnels considered in previous researches are primarily transportation tunnels, serviceability of existing metro tunnels is always under serious concern primarily. The tunnel response in terms of tunnel deformation is a common focus. To comprehensively investigate the impacts on the various type of existing tunnel, i.e., water supply tunnel, the tunnel stability also should be studied. In addition to studies concerning the influence of loaded piles on tunnels, there are studies concerning the impacts on tunnels due to adjacent constructions such as new subway tunnels [10] – [11] and deep excavation stages [12] – [14]. These studies continuously contribute to an understanding of tunnel response due to changes in surrounding conditions. Generally, soil excavation or tunnelling causes a release of in situ stress and thus soil displacement [15] – [17], which inevitably exerts an influence on existing tunnels. Construction at only one side of the tunnel imposes unsymmetrical stress relief and movement on the existing tunnel. Considering the tunnel deformation, it is revealed that the deformed tunnel is not an elliptical shape whose major axis aligns with the horizontal or vertical axis. The above literature reviews indicate that not only some key influencing factors (such as pile tip position and soil stratum) and impact (such as structural forces) have not yet sufficiently investigated, but also the appropriate evaluation method is required for better understanding of pile-soil-tunnel interaction. In this dissertation, all mentioned research gaps are aimed to be filled.

This study starts with preliminary evaluation on the new possible influence zone taking the pile tip position and soil stratum into consideration. This is to confirm that the zone with specific focus on pile would be much smaller than that available in present practice. This will be present in Chapter 3.

In engineering practice, the structural forces induced in tunnel lining are used for stability assessment. To properly evaluate the additional lining forces, the initial lining forces occurred from tunnel construction is essentially reproduced. The simulation techniques of tunnelling process with EPB shield are examined in Chapter

4. It is expected to obtain the suitable simulation method and accurate initial lining forces for further investigation.

Chapter 5 presents the proposed method that could appropriately trace the changes to the tunnel diameter and the global distortion of the tunnel lining. Moreover, in order to obtain a better understanding of the effects of the pile under loading on the existing tunnels, the pile-soil-tunnel interaction mechanism behind the tunnel deformation behaviour due to an adjacent loaded pile are revealed. The investigation of changes in lining forces are presented in Chapter 6. The relationship between the changes of lining forces and of tunnel diameters are exposed. Moreover, the influence zone for pile tip used restrictive guidelines for adjacent pile under loading to the existing tunnels are primarily introduced. For ease of understanding the analysis concept of this thesis, the schematic diagram of analysis process is illustrated in Figure 1.2

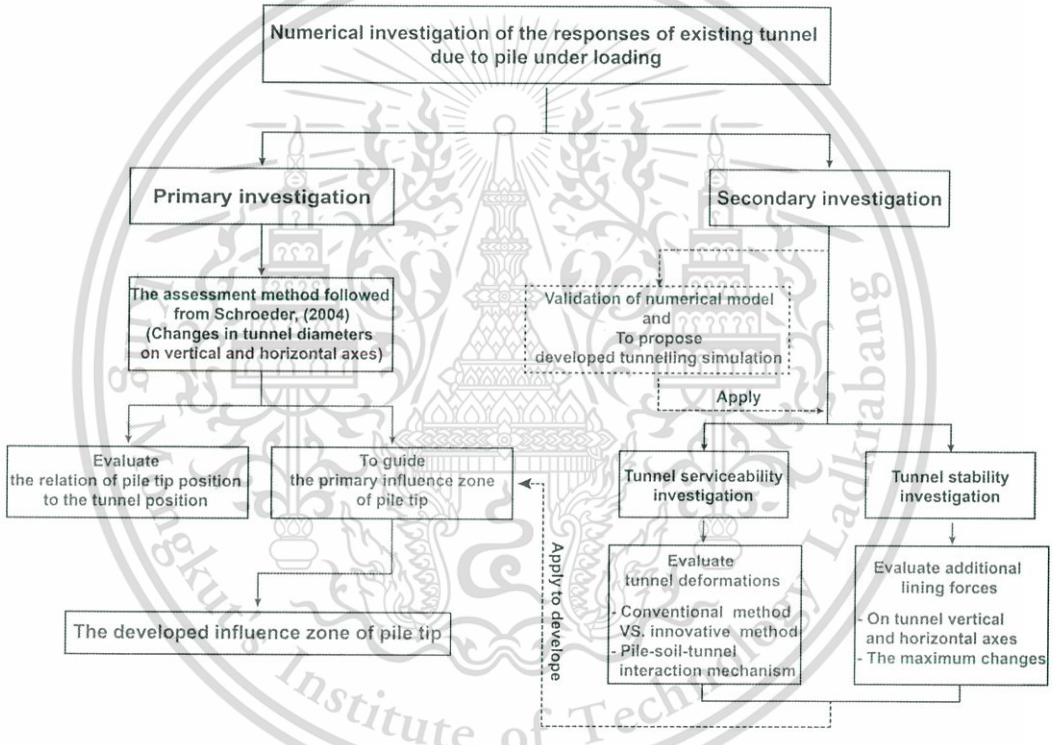

Figure 1.2 Flow chart of this study.

1.2 Purpose of study

The goals of this study are as follow:

1. To evaluate the effect of relative position of the pile tip with respect to the tunnel position as well as the soil type where the tunnel is located on tunnel responses.
2. To propose and validate the innovative technique of EPB tunnelling simulation in the numerical model.
3. To develop an innovative method for appropriately assessing the tunnel deformations due to pile under loading (pile located at only one side of the tunnel)
4. To investigate the changes of tunnel diameters and lining forces due to impacts of adjacent pile under loading.
5. To primarily suggest the tunnel influence zone for pile tip.

1.3 Scope of study

The case studies considered in this thesis are focused on the characteristics of the MRTA tunnel project in Bangkok subsoil. The existing tunnel with an outer diameter of 6.3 m, a lining thicknesses of 0.3 m and a depth of 20 m below the ground surface is fixed throughout for studying the impacts of pile under loading on the tunnel. The single bored pile of 1 m is on consider in this study.

For numerical analysis, the initial stress conditions, vertical effective stress and horizontal effective stress, were controlled by given soil unit weight and the coefficient of earth pressure at rest, K_0, for all strata and the piezometric drawdown of pore water pressure was also generated in the whole domain of investigation pile-tunnel interaction analyses. The undrained analysis was considered for all studies. Three-dimensional simulation using the finite element program ABAQUS [18] with simple constitutive soil model are conducted in the preliminary analysis (Chapter 3). Series of finite element analyses based on 3D PLAXIS [19] software with advanced soil models and reasonable assumptions are used to investigate the changes in tunnel diameters, the changes in lining forces and tunnel-pile-soil interaction mechanism, which carried out in Chapters 4-6.

1.4 Limitations

The limitations of this study are as follows.

1. Only single tunnel with only single diameter and thickness is considered
2. Adjacent bored piles are located on single side of a tunnel.
3. The effects due to the stage of bored pile construction are not considered.

1.5 References

[1] Land Transport Authority, "Code of Practice for Railway Protection", Development and Building Control Department, Singapore, 2004.

[2] Mass Rapid Transit Authority of Thailand, "Restrictive Guideline for Protection Zone in Blue Line Project", Engineering Specifications for MRT Tunnels, Bangkok, 2009 (in Thai).

[3] E.O. Measor, and D.H. New, "The design and construction of the Royal Festival Hall." *South Bank. J. Instn Civ. Engrs* 36, 241–318, 1951.

[4] L.J. Benton, and A. Phillips, "The behaviour of two tunnels beneath a building on piled foundation." *Deformation of Soils and Displacements of Structures; Proc. 10th Eur. Conf. Soil Mech. Fdn Engng*, Florence, 2, 665–668, 1991.

[5] K.G. Higgins, I. Chudleigh, H.D. St John, and D.M. Potts, "An example of pile tunnel interaction problems." *Proc. Int. Symp. Geotech. Aspects of Underground Construction in Soft Ground, IS-Tokyo '99* (eds O. Kusakabe, K. Fujita and Y. Miyazaki), 99–103. Rotterdam: Balkema, 1999.

[6] T. Chapman, D. Nicholson, and D. Luby, "Use of the observational method for the construction of piles next to tunnels," *Proc. Int. Conf. Response of Buildings to Excavation Induced Ground Movements*, (ed F. M. Jardine) London: CIRIA, 2001.

[7] F.C. Schroeder, "The Influence of Bored Piles on Existing Tunnels," A Thesis Submitted to the University of London for the Degree of Doctor of Philosophy and for the Diploma of the Imperial College of Science, Technology and Medicine, 2002.

[8] F. C. Schroeder, D. M. Potts, and T. I. Addenbrooke, "The influence of pile group loading on existing tunnels," *Géotechnique*, vol. 54, no. 6, pp. 351–362, 2004.

[9] K. Charoenpak, "Finite Element Analysis for Evaluating the Effects of Pile under Loading adjacent to Existing Tunnel," *Master Thesis, King Mongkut's University of Technology Thonburi, Thailand*, 2006.

[10] M. Abdel-Meguid, R. K. Rowe, and K. Y. Lo, "3D Effects of surface construction over existing subway tunnels," *Int. J. Geomech.*, vol. 2, no. 4, pp. 447–469, 2002.

[11] G. Zheng, T. Zhang, and Y. Diao, "Mechanism and countermeasures of preceding tunnel distortion induced by succeeding EPBS tunnelling in close proximity," *Comput. Geotech.*, vol. 66, pp. 53–65, 2015.

[12] M. Doležalová, "Tunnel complex unloaded by a deep excavation," *Comput. Geotech.*, vol. 28, no. 6–7, pp. 469–493, 2001.

[13] J. S. Sharma, A. M. Hefny, J. Zhao, and C. W. Chan, "Effect of large excavation on deformation of adjacent MRT tunnels," *Tunn. Undergr. Sp. Technol.*, vol. 16, no. 2, pp. 93–98, 2001.

[14] R. Chen, F. Meng, Z. Li, Y. Ye, and J. Ye, "Investigation of response of metro tunnels due to adjacent large excavation and protective measures in soft soils," *Tunn. Undergr. Sp. Technol.*, vol. 58, pp. 224–235, 2016.

[15] R. P. Chen, L. J. Tang, D. S. Ling, and Y. M. Chen, "Face stability analysis of shallow shield tunnels in dry sandy ground using the discrete element method," *Comput. Geotech.*, vol. 38, no. 2, pp. 187–195, 2011.G. W. Clough, B. P. Sweeney, and R. J. Finno, "Measured Soil Response to EPB Shield Tunneling," *J. Geotech. Eng.*, vol. 109, no. 2, pp. 131–149, 1983.

[16] R. P. Chen, J. Zhu, W. Liu, and X. W. Tang, "Ground movement induced by parallel EPB tunnels in silty soils," *Tunn. Undergr. Sp. Technol.*, vol. 26, no. 1, pp. 163–171, 2011.S. Bernat and B. Cambou, "Soil-structure interaction in shield tunnelling in soft soil," *Comput. Geotech.*, vol. 22, no. 3–4, pp. 221–242, 1998.

[17] R. P. Chen, J. Li, L. G. Kong, and L. jun Tang, "Experimental study on face instability of shield tunnel in sand," *Tunn. Undergr. Sp. Technol.*, vol. 33, pp.

[18] A. S. User, "Abaqus 6.3-1," *Dassault Systèmes Simulia Corp., Provid. RI, USA*, vol. Dassault S, 2008.

[19] R. Brinkgreve., E., Engin, W. Swolfs, "*PLAXIS 3D Version 2013 manual*," Chapman, 2013.

Chapter 2

Literature Reviews

2.1 Shield tunnelling method

As its name implies, a "shield of tunnelling" simply provides within a tunnel which is a working area protected against the collapse either of the walls or roof of the tunnel in construction sections, which has been recently excavated and tunnel lining or support of that excavation section has been erected yet. Obviously, the shield is necessary when the tunnel is being driven through stable ground. However, as its importance as a tunnelling tool extends beyond that of only supporting the ground, it is common for one to use a simple shield constructed tunnel in good ground. For instance, the shield provides shelter for segment erectors, muck disposal units, grouting equipment, etc. It also provides a bridge between the erected lining and the face so that work on extension of the lining and excavation of the face may be carried out simultaneously.

2.1.1 Types of shields

The general principle of a shield is based on a steel cylindrical assembly pushed forward in the axis of the tunnel while excavating the soil. The shield retrains the excavated void until the preliminary or final tunnel lining is installed. The shield has to resist the pressure of the surrounding soil and prevent the permeability of ground water while the void over the shield is held by the shield body itself. The additional measurement for retaining the tunnel face are required depending on the ground and water condition, five different measures for stabilizing the tunnel face are illustrated in Figure 2.1. These methods are a great advantage of the shield tunnelling method. Contrary to other tunnelling methods, the soil can be stabilized during the excavation.

Besides the specific mean of supporting the tunnel face, the specific method of soil excavation is also an important factor in shield machines. The classification of shield tunnelling machine, which means the method of support the tunnel face, is shown in Table 2.1. Equipment such as excavators and special cutter heads are used to excavate in Partial-face shield. They are guided and controlled either by the operating personnel or automatically. Full-face excavation depending on the geology encountered can be carried out by means of spoke wheels, rim wheels, or closed cutter heads as shown in Figure 2.2 through Figure 2.6.

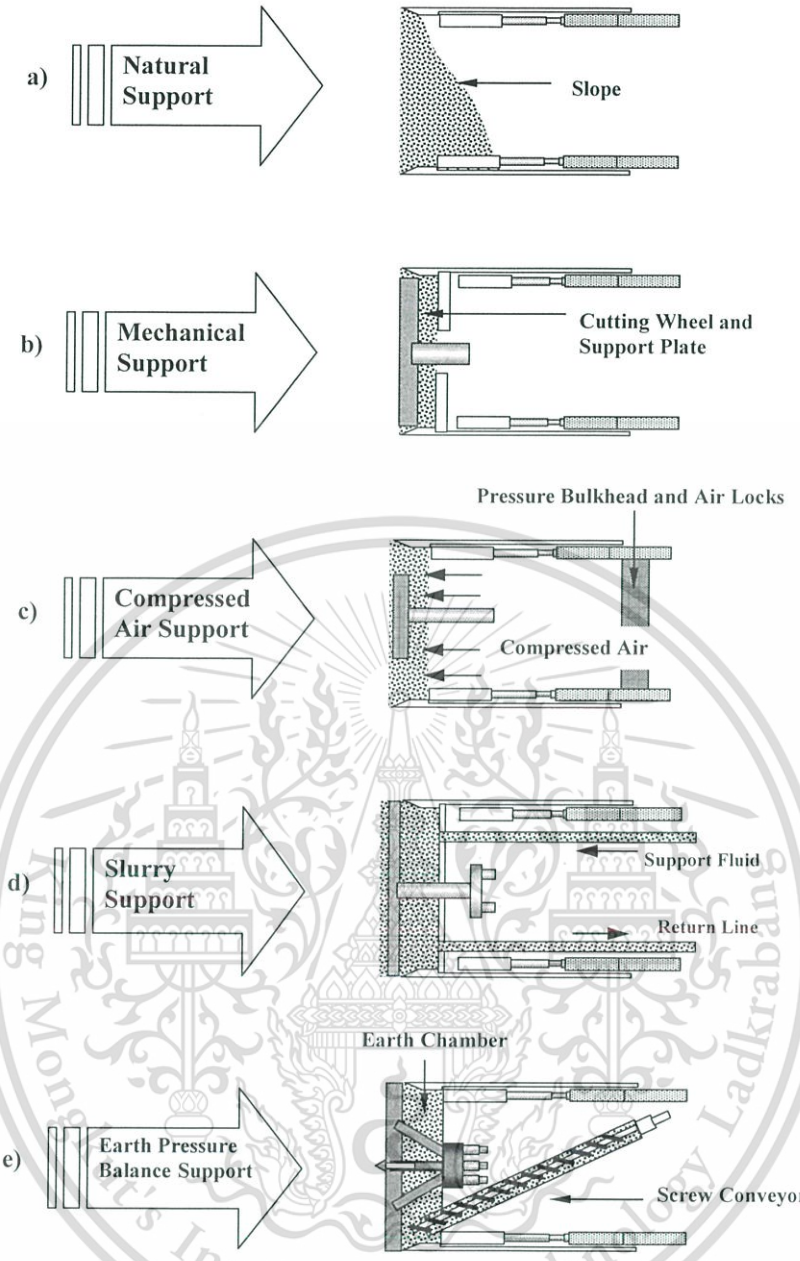

Figure 2.1 Different measures of face supporting (after [1]).

The principle of open-faced shields is of excavation soils without a system for pressure application at the tunnel face as shown in Figure 2.2. Generally, this shield can be used in ground conditions without ground water or where the ground water was lowered excavation level. If the shields are operated below the ground water level, the ingress of ground water is prevented, compressed air supporting excavation face can be applied. Compressed air shields (Figure 2.1c and Figure 2.3) can be hand shields as well as mechanical partial-face or full-face machines. A secure air supply is required as interruptions would lead to water entering the shield and the tunnel and the chambers under compressed air need to be airtight. For this purpose, a pressure bulkhead in the tunnel and an associated air lock separate the compressed air in the tunnel from the atmosphere.

Table 2.1 Classification of shield tunnelling machine [2].

	Face	Machine Type	Stabilization of Cutting Face	Excavating Method
Shield	Fully Open	Manual	Hood + Earth Retaining Jack	Hand
		Semi-Mechanical	Hood + Earth Retaining Jack	Back Hoe, etc.
		Mechanical	Cutter Disk or Spoke	Revolving Cutter
	Partially Open	Partial Face Extraction	Hood	Excavation shovel, bucket tooth
		Blind	Steel Bulkhead with slit	Extrusion
	Closed	Earth Pressure Balance (EPB)	Dug Soil + Cutter Disk or Spoke + (additive)	Revolving Cutter
		Slurry	Slurry + Cutter Disk or Spoke	Revolving Cutter
		Mixed	Slurry + EPB	Revolving Cutter

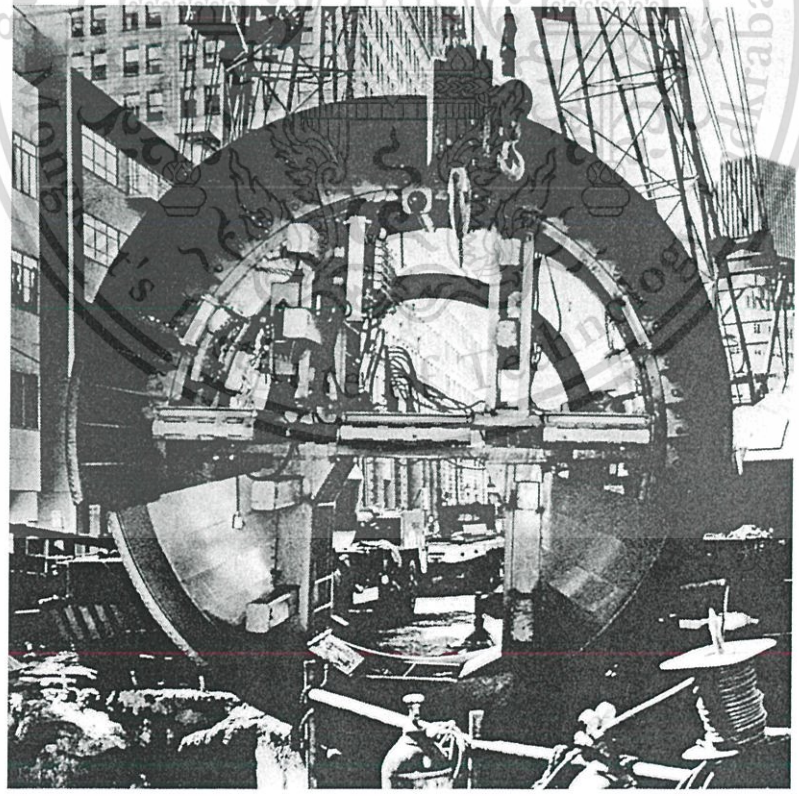

Figure 2.2 Open-faced shield used in Trans-Bay tube project (1969) [2].

Slurry shields, the tunnel face is supported by pressurized slurry as shown in Figure 2.1d and Figure 2.4. A frictionless fluid is used for intermediary supporting the face in slurry shields. It consists of water and an additive that can produce an impermeable layer at the fluid-soil interface. Bentonite is generally used as the slurry additive. In EPB shields as depicted in Figure 2.5, the soil material itself supports the face as shown in Figure 2.1e. The soil pressure acting on the shield face is maintained equal to the pressure inside the earth chamber.

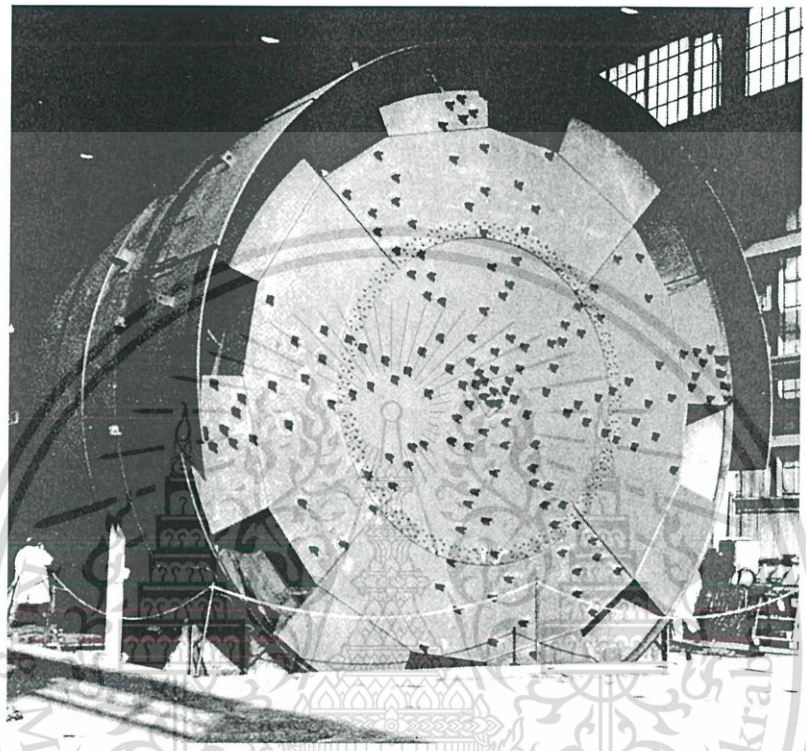

Figure 2.3 Compressed air shield used in the express subway tunnel in Paris (1964) [2].

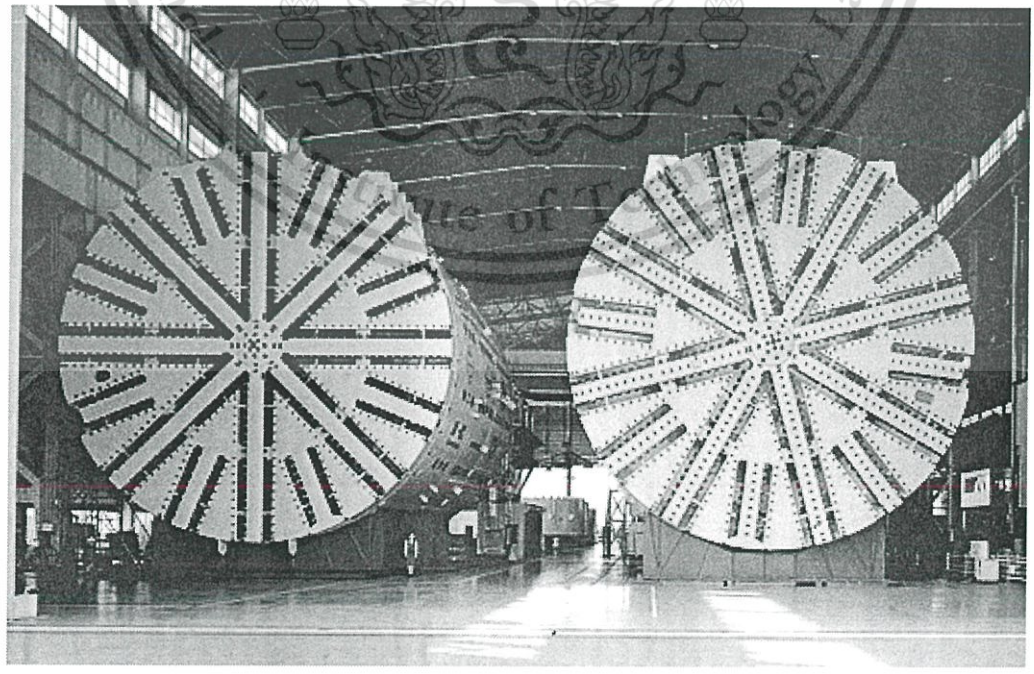

Figure 2.4 Slurry shield used for used for Tokyo Bay Aqua-Line Highway [3].

The construction sites where have special geological and hydro-geological conditions, it is sometimes not possible to excavate tunnel with a single shield type. For such reasons, the mix shield as shown in Figure 2.6 was developed which can deal with changing geological formations. The last type of shield, the blind or extrusion shield is normally used in cases where very homogeneous ground with a low shear strength and very plastic behaviour is encountered. The soil can be squeezed into the interior of the tunnel through several openings in the front of the shield.

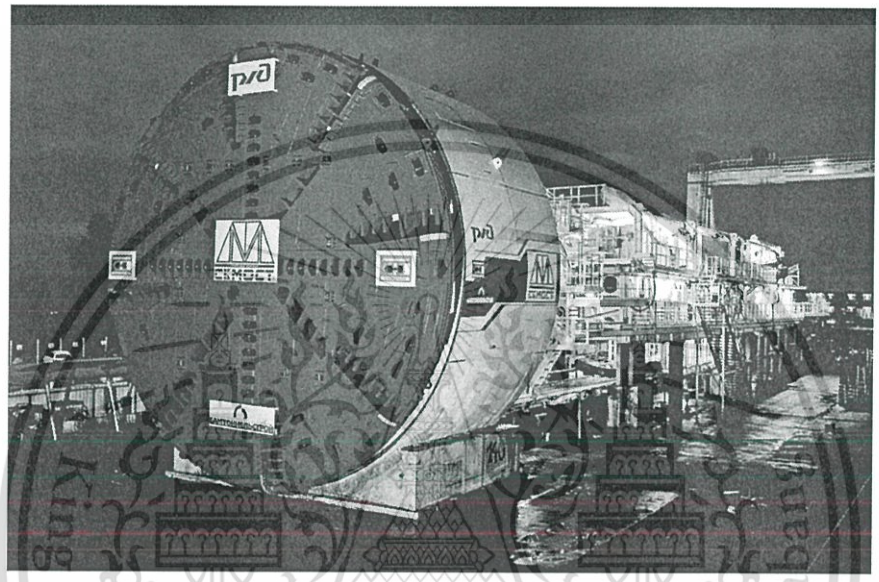

Figure 2.5 EPB shield used in the infrastructure planers in the Russian city Sochi on the Black Sea [4].

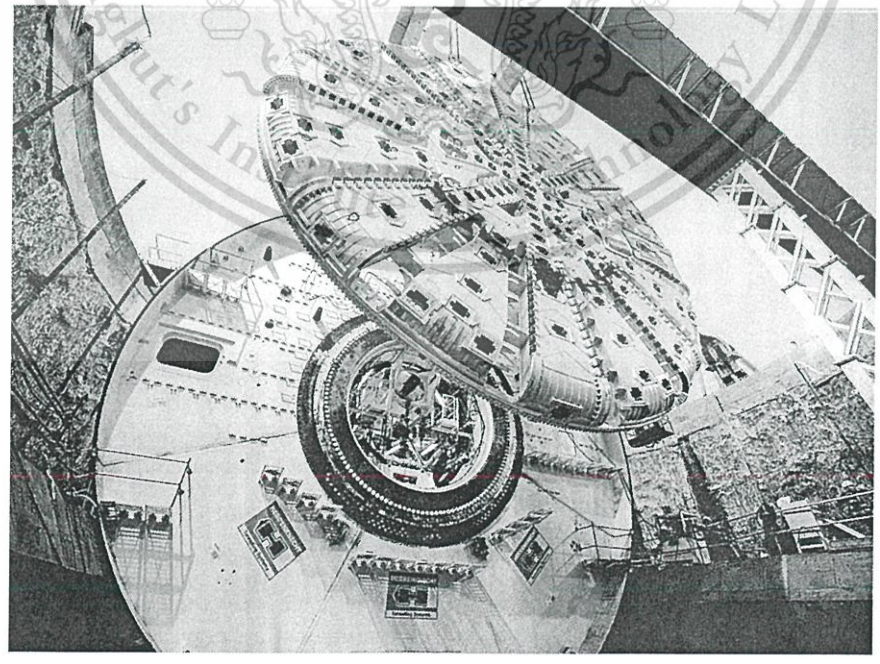

Figure 2.6 Mix shield used in Tuen Mun – Chek Lap Kok Link, Hong Kong [4].

In recent years, most tunnelling projects which are constructed in soft ground have adopted the Earth Pressure Balance (EPB) shield and slurry shield techniques. The EPB shield is commonly considered and particularly suitable for cohesive or silty ground that does not contain cobble or boulder obstructions and in which the water head at the face is not high. In other words, this technique is the more successful when tunnel is excavated in the more homogeneous and consistent the soil. Although the EPB shield is capable of working in sandy conditions, this might be problematic. The proper ground improvement methods are solution of that problems. On the other hand, the slurry shield method is rather suited for tunnelling in non-cohesive ground.

2.1.2 The Earth Pressure Balance (EPB) Shield

1) Introduction of EPB shield

The pioneer of the EPB shield is the Sato Kogyo Company Limited, a Japanese construction firm, who introduce the original concept of the shield due to tried to find a method of tunnelling through soft ground. Although, several tunnelling projects with compressed air and slurry shields had already been successful in Japan, there were disadvantages and limitations of these methods, which the Sato Kogyo Company desire to eliminate. At the time, slurry shields were widely applied in soft ground tunnelling, but this method has high capital and operating cost due to a slurry shield requiring a separation plant on the surface. Moreover, Sato Kogyo Company intended to find a machine, which would excavate efficiently and comply with the environmental regulations and laws of the many cities in Japan [5]. These included air and water pollution control laws, industrial water, waste disposal and public cleaning laws, and prevention of oxygen deficiency and prevention of compressed air hazard ordinances, etc. The earth pressure balance shield was thus begun to develop by the Sato Kogyo Company in 1963. The EPB shield was finally built by the Ishikawajima Harima Heavy Industries Company Ltd in 1966 after considerable research both in the laboratory and in the field., the first EPB shield with an outside diameter of 3.72 m was used for tunnelling of 1,900 m collector drive in Tokyo in 1974. The schematic diagram of the EPB shield first introduced by Sata Kogyo as illustrated in Figure 2.7.

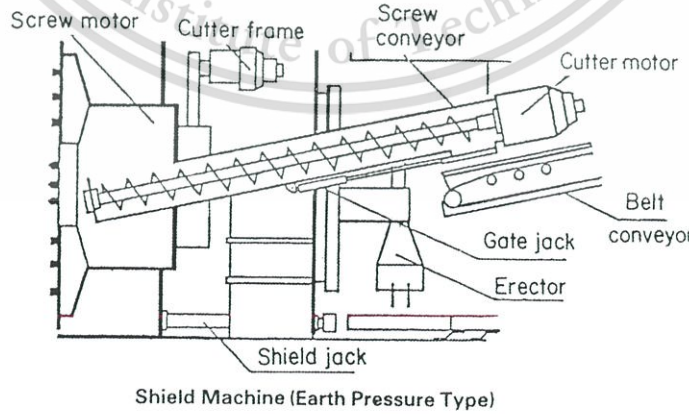

Figure 2.7 Earth Pressure Balance shield introduced by Sato Kogyo (1963) [2].

In the following years, earth pressure balance shields were produced an increasing number by various manufacturers under different names such as earth pressure balance shield, pressure holding shield, slime shield, soil pressure shield, confined soil shield, mud pressurized shield or muddy soil shield. All of these terms principally apply to the same method, known as the earth pressure balance system. The Earth Pressure Balance shield has advantages over other types of shields as shown in Table 2.2

Table 2.2 Typical advantages of the EPB shield over other shields [2].

Advantages over Slurry Shield	Advantages over Partial-face Shield	Advantages over Open-faced Shield
No separation plant, Economical application in ground with a high percentage of silt and clay	Can excavate a variety of soil conditions below the ground water	Can excavate a variety of soil conditions below the ground water
Can operate in both open mode and earth pressure balance mode	Full face cutter provides a better performance with lower ground loss	No compressed air-lock chamber needed

2) Excavation of EPB Shield

The EPB shield tunnelling technique, a tunnel can be excavated by a cutting wheel of shield that is disc cutters remove the soil from the tunnel face as shown in Figure 2.8, Tag 1. the tunnel face is then maintained in a compressed state within the excavation chamber as depicted Figure 2.8, Tag 2. Mixing arms at the cutting wheel and bulkhead transferred the thrust force to the soil paste mix the soil in the excavation chamber as shown in Figure 2.8, Tag 3 and Tag4., respectively. In general practice, to minimize ground movements, the earth pressure at the cutting face is carefully monitored and controlled as follows:

1. Target face pressure for each excavation cycle has to be determined prior to excavation depending on the design alignment and subsurface ground conditions. This target face pressure is used as a control parameter during excavation.
2. During excavation, the actual face pressure has to be recorded and controlled and maintained at the target pressure.
3. For each excavated ring or each excavation cycle, the target face pressure and the actual face pressure needs to be recorded in the excavation report which will be used as a reference.

The target pressure is used as a control parameter during excavation. The shield operator has to closely oversee the excavation in order to ensure that the shield is operated under the predetermined face pressure.

The excavated soil in the excavation chamber is removed through the screw conveyor (Figure 2.8, Tag 5.) and belt conveyor transported by means of pumping or muck skips pulled by locomotives. The pumping method is used for muck transport, there are some important concerns that need to be considered. In this method, the transport pipe is directly connected to the screw conveyor. The velocity in the transport pipe should be high enough to avoid blockage due to the soil settling in the pipe, but it should be also low enough to minimize pipe wear. Additionally, the EPB

tunnelling method, the controlled support pressure in front of the excavation chamber has to correspond to the rate of muck transport, the shield operator is required to balance the rate of muck pumping with the shield advance in order to control the face pressure. The EPB shield advance and control to sprightly excavate by hydraulic jack as shown in Figure 2.8, Tag 6. The hydraulic jacks behind the shield extend and push against tunnel lining to shove the shield ahead. For instance, the shield's jack force or applied thrust force is approximately between 600 and 1000 tons and the stroke of the jack is typically 1.60 m in the Bangkok Subway (Metropolitan Rapid Transit Authority, MRTA) project. The careful position control of target pitching, expected horizontal and vertical deviations, and current alignment are also required during shield advancing. Generally, all of these factors are also recorded in every excavation cycle. The shield tail consisted the shield skin, back filling and tunnel lining are shown in Figure 2.8, Tag 7-9., respectively. The working process of the assembled parts of shield tail will be described in next sections.

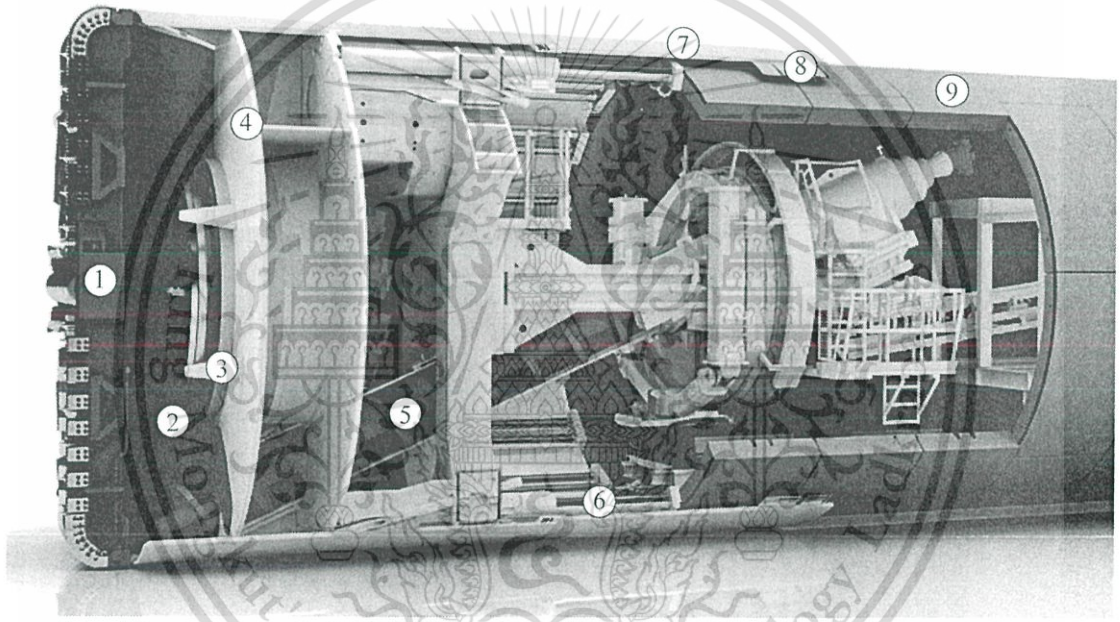

Figure 2.8 Earth Pressure Balance Shield [6].

3) Tunnel Lining

Segmental linings are usually associated with shield tunnelling. Figure 2.9 shows reinforced concrete segmental lining of The Bangkok MRTA (Blue Line Extension) Project. They are erected within the protection of a cylindrical tail shield. A one-pass system, providing both stabilization of the tunnel opening during construction and a permanent lining, is the installation system of the segmental lining in tail EPB shield. Segmental lining may also be constructed in two-pass systems. temporary segments provide only construction stabilization is a first-pass, and a second-pass cast in place concrete lining added for permanent service. Typically, segmental linings are smaller in diameter than the excavated size of tunnel, because they are erected inside a cylindrical shield that is part of the excavating equipment. The resulting annular void is usually filled with grout. In wet ground, segmental linings are usually bolted, to compress gaskets to seal against water leakage. In dry ground, unbolted segmental linings may be used. Additionally, in ground with

appreciable stand-up time, segmental linings may be expanded by jacking them after they have been cleared by the advancing shield.

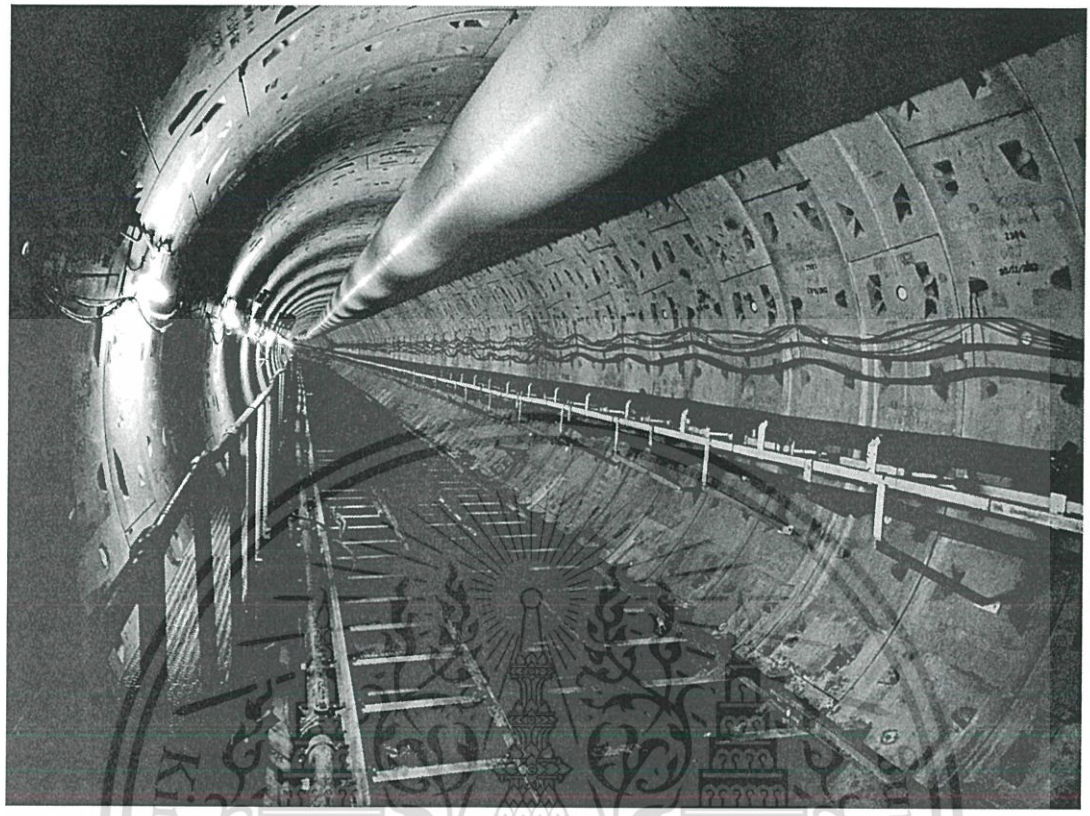

Figure 2.9 The Bangkok MRTA (Blue Line Extension) Project, reinforced concrete segmental lining.

4) Tail Void Grouting

In all shield tunnelling methods, the diameter of the shield is larger than that of the tunnel lining because the shield skin plate must overlap the lining to permit assembly of the lining and clearance must be provided between the outside of the lining and the inside of the tail plate to allow steering the shield around curves and to correct misalignment. These lead to an annulus or "tail void" around the outside of the lining. Therefore, tail void grouting must be used to minimize ground deformations outside the tunnel.

At the shield tail, there is a tailskin seal used to protect the rear end of the shield against ground water, the surrounding ground, and the support fluid or grout. The tailskin seal separates the shield from the ring annulus and is designed to reliably seal the joint between the tailskin and the segmental lining as shown in Figure 2.10. It can very high resist the earth pressure, the water pressure, and the grouting pressure. The wire brush seals, which was developed in Japan is firmly mounted on the tail skin as shown in Figure 2.10, were used to stuff the joint and prevent leakage of grout into the shield. For EPB shields of the Kawasaki and Herrenknecht used in the MRTA project, there are three rows of wire brush seals. Grease is injected into the chambers between the individual rows and kept at a high pressure to prevent water, ground or grout from infiltrating the sealing area.

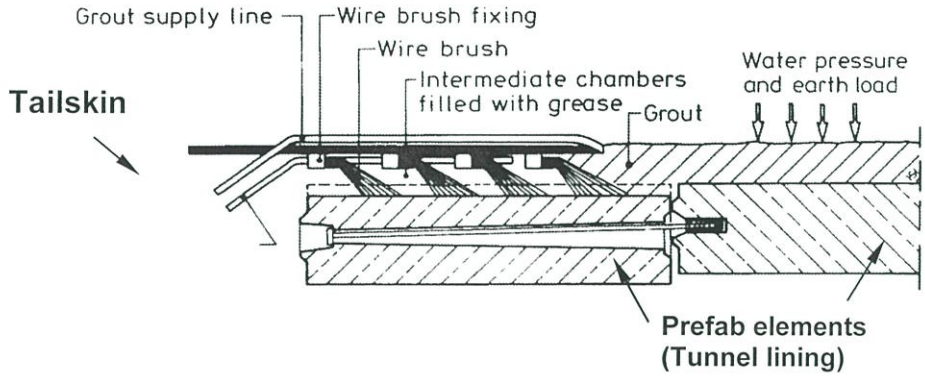

Figure 2.10 Tail skin seal (wire brush seal) [2].

The grout is injected through holes in the segments. The holes are fitted with screwed connection pieces and closed by plugs during the ring installation. In the MRTA project, plastic non-return valves were built into the segments. Grout is injected and flows down from the holes at the tunnel crown so that the grout is able to penetrate into the void by injected pressure and gravity. The injection is continuously performed under high pressure in the tail void developing behind the shield tail. Note that the back-fill grout injection is not only volume controlled (i.e. defined as percent grout filling) but also pressure-controlled, which is measured at the grout pipe or at the concrete segment. In the MRTA project, the pressure is automatically controlled to be as close as possible to 3 bars (300 kPa), which is the design condition of the segmental lining. With this high-pressure injection, the void can be filled in a short time and the grouting material can effectively prevent ground displacements towards the tunnel. Both volume and grouting pressure are monitored and recorded by the tunnel monitoring system at every excavation cycle.

2.2 Development of shield tunnelling simulation method

With the advancement of computer sciences and researches on tunnelling simulation in the past, the 3D finite element analysis of tunnel excavation by tunnel boring machines (TBMs) has been extensively used over the last decade. Due to that the complicated construction sequences and relevant loads can be taken into account, complex interaction problems can then be performed. Many simulation techniques have been proposed depending on the assumptions used in the modelling. For modelling the tunnel lining, solid elements are commonly used due to the ratio between the width and thickness of the lining is not large. In addition, most studies focused on the ground deformation, not the lining forces. However, in this study the lining forces are essentially observed as described in the Chapter 1. To reduce time consumption of the analysis, the structural elements which directly provide the values are preferred. Moreover, the induced structural forces in the lining are necessary during the design stage. Therefore, a part of this thesis will be described the simulation methods of EPBS with different techniques to validate before considering the impacts of adjacent pile under loading to tunnel lining.

Among various analysis methods, Finite Element Method (FEM) is one of the most widely used tool for tunnelling works. At the beginning, the simulations of tunnelling using TBMs were analysed in 2D finite element (FE) models [7] - [10]. In these models, the different stages of the TBMs advancement are considered by stress-relief method. The 3D FE models for TBMs tunnelling were first applied in the early

1990s. Various simulation methods considering different factors and simplifications have been developed [11]- [15]. Among different factors considered in the analysis by each researcher, the shield element and the tail void grout process have not been considered yet. These two parameters were measured and emphasized by Abu-Krisha [16] and Swoboda and Abu-Krisha [17]. The complicated simulations of 3D EPBS tunnelling models using several parameters e.g., face pressure, shield element or shield weight, tunnel lining element, tail void grout process, hydraulic jack, steering control, and backup trailer loads were gradually introduced [18] and [19]. The 3D FE models using face pressure, shield element, tunnel lining element, and grouting process as the parameters are used in studies [20] and [21]. As the studies mentioned above, only four main parameters (face pressure, shield element, grouting process and lining element) are generally used to model the 3D EPBS tunnelling. Thus, these parameters are also used to simulate the 3D EPBS tunnelling in the present work.

Various methods to model the grouting process have been proposed in the simulation of the excavation by EPBS in the past. For example, the method which uses a distributed pressure to represent the grouting process was introduced by Broere and Brinkgreve [22] and Plaxis [23]. In the grouting process in engineering practice, the grouting will change from the liquid state to solid. To realistically model this characteristic, solid elements having different stiffness are represented to simulate the grouting process [17], [20] and [24]. However, an actual behaviour of initial grout is in a fluid state with no stiffness. In practice, it is then difficult to specify the modulus of grouting during liquid state. The pressure boundary may thus be more appropriate than the solid elements.

In simulation of ground movement due to tunnelling, the solid elements or the brick elements are generally adopted to represent the tunnel lining [18], [19] and [22]. The lining which has a certain width and the actual excavated periphery of the soil can then properly be modelled. By using the solid elements, the structural forces (i.e., bending moment, normal force and shear force) cannot directly be obtained. In the circumstances that the structural forces are needed to be investigated, the modelling by the solid elements becomes inconvenient. In this situation, shell elements which offer the direct quantification of lining structural forces are preferable. The shell elements have been also used in the past researches, e.g., the influence of ground stratification on lining force and settlement due to tunnelling [24], the effects of tunnelling on adjacent building and existing tunnel respectively [20], [21] and [25]. However, using the shell elements to model the tunnel lining causes a problem due to that the shell elements have no thickness in the process of meshing. It is reasonable to model the shell element (as line on cross sectional plane) at the mid plane. Consequently, the treatment on the gap between the excavated soil periphery and mid plane during meshing is essential. To deal with the problems, the simulation method which introduce the grouting layer as solid element in the gap to represent the solid-state grouting while using pressure boundary to represent the liquid-state grouting will further described in Chapter 4.

2.3 Tunnel analysis

2.3.1 Background

There are often numerous tunnels for a modern urban environment. These tunnels have various purposes, i.e. road and rail tunnels that have large diameter or smaller diameter of tunnels that is constructed for telecommunications or service

tunnels. A satisfactory tunnel is introduced to follow requirements by Peck (1969b) [26] as below:

1. The tunnel is constructed that should be able to be guaranteed the stability of the tunnel at all times. In particular, this is relevant during the construction of the tunnel prior to the installation of the lining.

2. Excessive movements of the tunnel should not occur because these may lead to the damage of adjacent or overlying buildings or utilities. For tunnels constructed in modern urban environments this requirement is very imperative.

3. The tunnel should be able to withstand all the external influences that might be subjected to during its lifetime. The most noticeable one is the additional pressure of surrounding soil applied to the tunnel. The structural forces i.e., axial forces and moments in the tunnel lining, might however change due to external influences such as the construction of nearby tunnels or building.

Mair & Taylor (1997) [27] stated that the first requirements are particularly important in the urban environment. This is reflected by the fact that field measurements and numerical research have concentrated on ensuring the stability and the movements of the tunnel due to tunnelling. However, most measurements or assessment related to tunnelling activities are made of the short-term ground response in terms of surface and sometimes subsurface displacements. Long-term ground movements and responses of existing tunnel, such the forces or the deformation developing due to adjacent construction, have only a relatively small number of research or measurement. Thus, the responses of existing tunnel due to adjacent constructing structures should be considered interestingly.

Generally, tunnel behaviours relate to soil deformation or structural force in lining. The basic principle of that will be reviewed in next section. In addition, a Finite Element Method (FEM) widely used to analyse in tunnel problems will be also reviewed, the tunnel constructed in Bangkok subsoil particularly.

2.3.2 Ground and tunnel deformations due to closed shield tunnelling

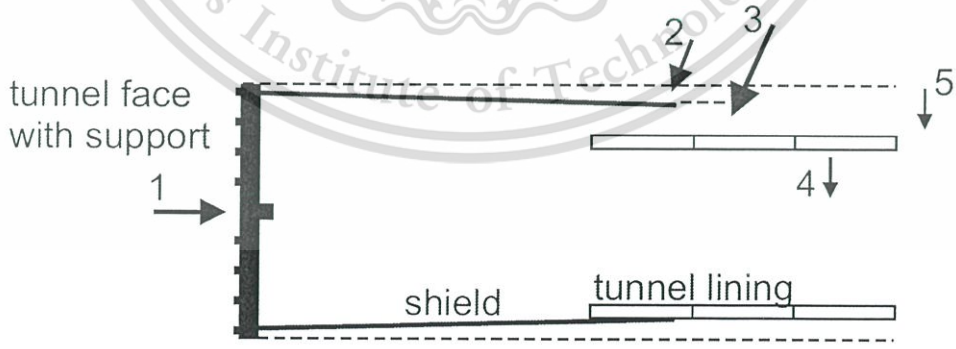

Figure 2.11 components of ground deformation due to closed shield tunnelling (after Mair & Taylor, 1997) [28].

The main components of ground deformation associated with closed-face systems such as tunnel boring machines with earth pressure or slurry shields was summarized by Mair & Taylor (1997) [2] as shown in Figure 2.11 and following;

1. Movement of the ground towards the face, due to stress relief.

2. Radial ground movement towards the shield, due to over-cutting and ploughing.

3. Radial ground movement into the tail void, due to a gap between shield and lining.

4. Radial ground movement towards the lining, due to deformation of the lining.

5. Radial ground movement towards the lining due to consolidation.

For shield tunnelling with adequate face support (Figure 2.11), the first component of ground deformation will be relatively small, but the second component may be appreciable. In particular, for a somewhat conical shield or in case of over-cutting, as well if there are steering problems in maintaining the alignment of the shield. The third component of ground deformation, which is usually the major cause of settlements, can be minimized by grouting, but this component is strongly influenced by the experience of the crew and the ground pressure control being implemented. Component four tends to be minor important regrading conventional tunnelling. Component five can be important for tunnelling in soft soils with low permeability. In case of insufficient face pressure, the pore water pressure dissipation/consolidation phenomenon may take place in front of the tunnel face.

Ground deformation due to ground loss manifests itself at the surface in a trough extending laterally and ahead of the advancing face. Figure 2.12 shows the typical three-dimensional shape of surface settlement trough caused by tunnelling in soft ground. However, in the case that less soil volume is excavated and removed than the volume of the shield advance (i.e., the shield is operated to have a positive volume balance), soil would heave (Figure 2.13). This case can be the result of applying too high a support pressure at the shield face.

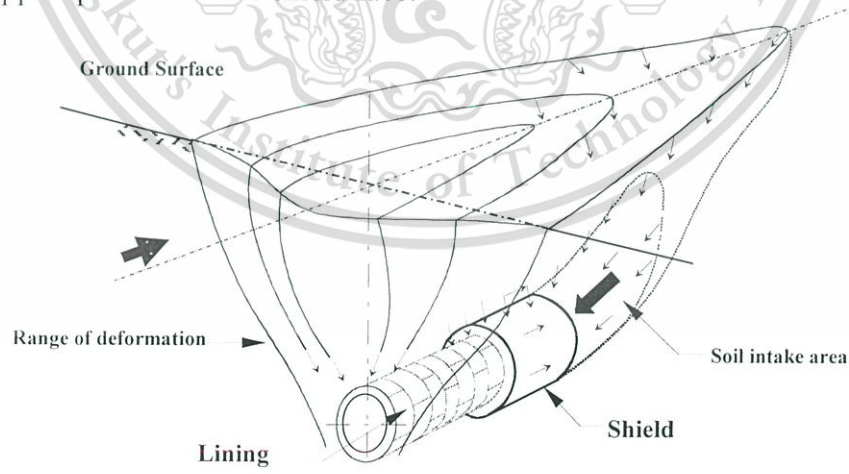

Figure 2.12 Typical ground deformation induced by shield tunnelling [2].

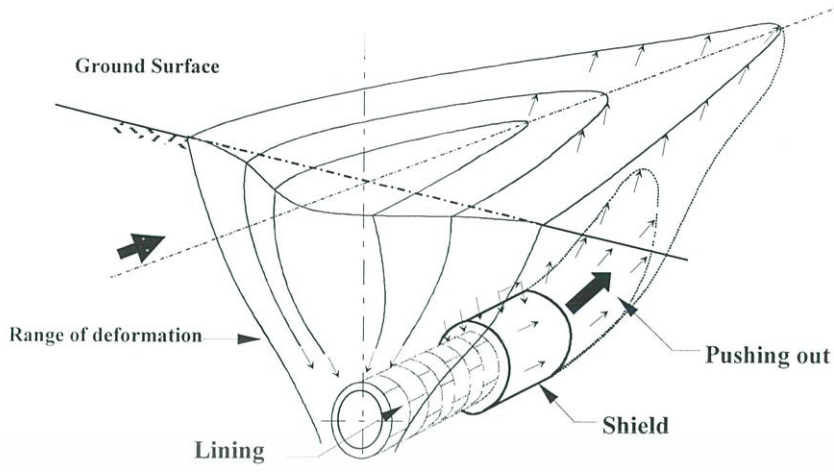

Figure 2.13 Surface heave ahead of the shield due to a positive volume balance [2].

The ground deformations as mentioned above (Section 2.3.2) are associated with the concept of "ground loss", usually expressed as the percentage of ground volume loss to the theoretical volume of the tunnel excavated per unit length. This parameter can be estimated from empirical observation or other methods considering aspects such as soil stability and tunnelling method [26] and [27]. Gonzalez and Sagaseta (2001) [28] proposed the deformation modes of tunnel constructed with circular shape in soft soil as shown in Figure 2.14. The first mode is a uniform radial contraction with ground loss, U_0. The second mode is an ovalization or distortion of the tunnel without the change of net volume, U_ϕ, in vertical direction and V_ϕ, in horizontal direction. The third mode is a vertical movement without distortion, U_y.

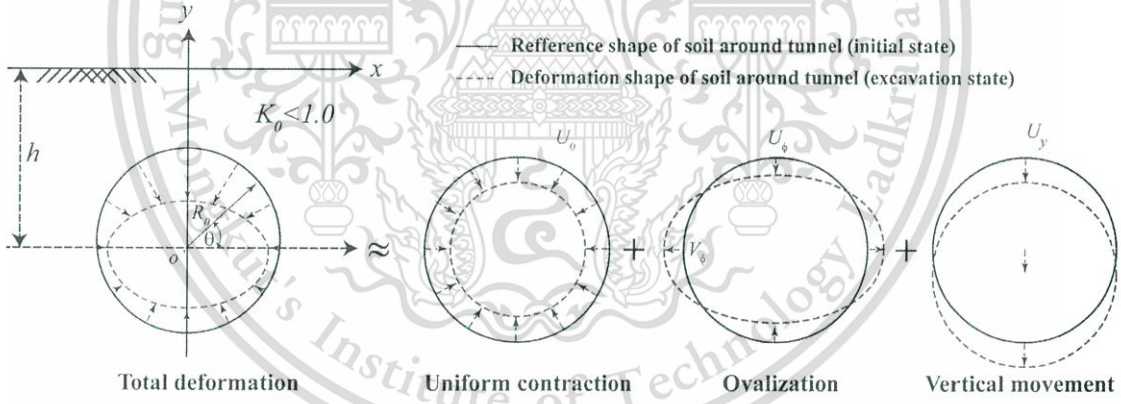

Figure 2.14 Deformation modes of tunnelling analysis.

2.3.3 Structural forces in tunnel lining

The lining, whether it be temporary or permanent, must withstand ground pressures with a sufficient margin of safety. The assessment of the water pressure is straight forward, but effective stresses on the lining depend again significantly on installation procedures. The effective stress may amount up to 50% of the overburden stress, the statement is revealed by Mair & Taylor (1997) [27]. In urban where tunnels are constructed by shield method, ground deformation is minimized by face support and grouting, but increase loads on linings so that effective stresses may get closer to the overburden stress. Craig and Muir wood (1978) [29] stated that monitoring of stresses in shield tunnel linings has shown that the average stresses generally increase during the first few months up to 50% - 70% of the equivalent overburden stress.

Higher stress concentrations have been recorded in the early measurements, but these may be partly associated with moment stress, as reported by Craig and Muir wood (1978) [29]. In the period of planning a tunnel structure, the engineers have to rely on a method of analysis, from which they may derive criteria whether the design is suitable, safe and economical. Relevant methods for the assessment of bending moments and normal forces are to be considered.

Structural design models of tunnel lining including analytical closed form solutions and bedded beam approaches have been widely used by the engineers for the analysis of both conventional and shield tunnelling. Installation procedures of these tunnelling methods (e.g. shield tunnelling, sequential excavation, etc.) significantly influence the magnitude and distribution of loads on tunnel lining Schmid (1926) [30] was probably the first to present an analytical solution for a continuum tunnel model. Later, analytical solutions for bending moments and normal forces were presented by various publications [31] – [40]. Some literatures mostly mentioned are extensively described follow.

Peck et al. (1972) [33] presented the definition of stiffness ratios, which are the flexibility ratio and the compressibility ratio, for tunnel linings. The flexibility ratio (F) is the flexural stiffness ratio between the ground and the liner and is defined as Eq 2.1.

$$F = \frac{E}{1+\nu} \Big/ \frac{6E_l I_l}{r^3(1+\nu_l^2)} \tag{2.1}$$

where E is the elastic modulus of the soil, E_l is the elastic modulus of the lining, I_l is the moment of inertia of the liner cross section per unit length along the tunnel axis, and E is the radius of the tunnel lining. The compressibility ratio (C) is obtained by dividing the extensional stiffness of ground by that of the tunnel lining and as formulated in Eq 2.2.

$$F = \frac{E}{(1+\nu)(1-2\nu)} \Big/ \frac{E_l t}{r(1-\nu_l^2)} \tag{2.2}$$

where t is the thickness of tunnel lining, ν is the Poisson's ratio of the soil, and ν_l^2 is the Poisson's ratio of the tunnel lining. The bending moment, M , and thrust force (normal force), T , in the tunnel lining can be theoretically obtained as Eq 2.3 and 2.4, respectively.

$$M = \frac{\mathrm{Pr}^2}{2}\left\{(1+K_0)\left[\frac{(1-2\nu)C}{6F}\right](1-L_n) + 0.5(1-K_0)(1+J_n-2N_n)\cos 2\theta\right\} \tag{2.3}$$

$$T = \frac{\mathrm{Pr}^2}{2}\left\{(1+K_0)(1-L_n) + (1-K_0)(1+J_n)\cos 2\theta\right\} \tag{2.4}$$

where K_0 is the earth pressure coefficient at rest, θ is the angle measured in counter-clockwise from horizontal plane, F is the flexibility ratio and C is the compressibility ratio. The parameters L_n , J_n , and N_n are defined in Eqs. 2.5 – 2.7.

$$L_n = \frac{(1-2\nu)(C-1)}{1+(1-2\nu)C} \tag{2.5}$$

$$J_n = \frac{\left[(1-2\nu)(1-C)\right]F - 0.5(1-2\nu)^2 C + 2}{\left[(3-2\nu)+(1-2\nu)C\right]F + 0.5(5-6\nu)(1-2\nu)C + (6-8\nu)} \tag{2.6}$$

$$N_n = \frac{\left[1+(1-2\nu)C\right]F - 0.5(1-2\nu)C - 2}{\left[(3-2\nu)+(1-2\nu)C\right]F + 0.5(5-6\nu)(1-2\nu)C + (6-8\nu)} \tag{2.7}$$

The analytical solutions are mostly based on simplifying assumptions regarding the soil and the lining. The circular tunnel is usually assumed to be so deep that the increase of stress due to gravity can be ignored. In 1975, Muir Wood [34] proposed the theory's which determines the tunnel in term of circular shape. The elastic analysis is used in this theory while shear force between tunnel lining and soil surrounding tunnel is not considered. The method developed form elastic theory was presented by Einstein (1979) [35]. The Einstein's theory considers that soil surrounding tunnel are homogeneous and isotropic. The tunnel lining is assumed thin-walled and flexibility. The pressure in vertical direction was considered at the centre of tunnel. The pressure in horizontal direction equals the pressure in vertical direction with coefficient of lateral earth pressure. The analytical solutions for a shallow tunnel in saturated ground considering two different drainage conditions (full drainage and no drainage at the ground-liner interface). The solutions covered different construction processes and soil conditions including (1) dry ground; (2) saturated ground with and without air pressure; (3) with and without a gap between the ground and the liner. It was also found that a smaller gap or a deeper tunnel produce larger stresses, while a stiffer ground or a smaller tunnel produce smaller stresses. However, the applicability of the analytical solutions as proposed by Bobet (2001) [39] is limited to tunnels in homogeneous, isotropic soils. As indicated above, ground pressure on linings depend seriously on the construction procedures (physical gap, lining installation method, workmanship, etc.). To incorporate the installation procedure, an analytical solution was developed to accounts for the installation method using a displacement approach [40].

For the design of the tunnel lining in the present day, the excavation and support sequence needs to be taken into consideration, in order to come to a reliable conclusion whether or not the design is adequate. With the rise of computer capacity, the use of appropriate 3D FE-simulation method with complex numerical model for closed face shield tunnels will be analysed to demonstrate their significant influence on the lining forces. For example, the comparison of the structural forces in tunnel lining analysed from different simulation methods and numerical models were introduced by Sven Moller (2006) [41]. This study indicated that the values and distributions of the lining forces are significantly different due to the using different simulation methods and numerical models. The selected simulation method with an appropriate numerical model for assessing the lining forces is essential.

Although the current design practice for tunnel lining considers all possible load scenarios during service of the tunnel, however, the future activities have not been included. It is then necessary to evaluate the possible effect of the adjacent pile under loading on tunnel lining in terms of changes in structural forces. There have only been a small number of researches concerning the response of existing tunnel in

term of changes in structural forces. For examples, the changes in the bending moment due to the influences of the overlying strata on the stresses developing in the tunnel lining was presented by experimental results [42]. The finite element method as a rapid and low-cost approach compared to filed measurement and centrifuge modelling test used to investigate the change of circumferential stresses in term of axial force and bending moment due to the impact of erosion voids established around existing tunnels [43]. This study revealed that the change in axial force is significant with comparing to the change in bending moment. The proper clear distances between new tunnel constructions and the existing tunnels in sand considered by lining forces were evaluated [44], it found that a slight difference in lining forces for the new tunnel construction occurred when distance between two tunnels is more than 2.20D (D is new tunnel diameter) for horizontal alignment, 1.80D for diagonal alignment and 1.25D for vertical alignment. The response of existing tunnel in term of change in lining forces observed at crown, invert and both spring lines due to adjacent pile under loading was investigated together with the changes in tunnel diameter in horizontal and vertical directions [45]. This study revealed that the change in lining forces are consistent with the change in tunnel diameter.

2.4 Pile Foundations

2.4.1 Introduction of piles

Piles are used when the bearing capacity of the foundation material when the ground surface is insufficient to carry loads determined by new buildings or reducing settlements. This section will only discuss points regarding bored cast in-situ piles which are formed by first boring a hole into the soil, and subsequently placing reinforcement and filling with concrete. Further, this section is only concerned with bored piles in soft clay and thus with so called friction piles. Friction piles obtain the greater part of their load carrying capacity by skin friction rather than by bearing on impenetrable or stronger strata at their tip.

2.4.2 A loading application on bored piles

In the assessment of the influence of piles on tunnels, it is important to know the magnitude of the loading that is commonly applied to bored piles in the field and the movements and stress changes in the ground caused by such loading. This section will thus describe design method that are currently used to determine the load capacity of bored piles in Bangkok subsoil. Moreover, some issues regarding good practice in the finite element modelling of vertically loaded piles will be reviewed.

1) Load transfer mechanism of bored pile

The ultimate load applied on the top of the pile is Q_u, a part of the load is transmitted to the soil along the length of the pile as called the ultimate friction load or skin load, Q_{uf}, and the balance is transmitted to the pile base as called the base or point load, Q_{ub}. The total ultimate load Q_u is expressed as Eq 2.8.

$$Q_u = Q_{ub} + Q_{uf} \tag{2.8}$$

where, Q_u = ultimate load applied on the top of the pile

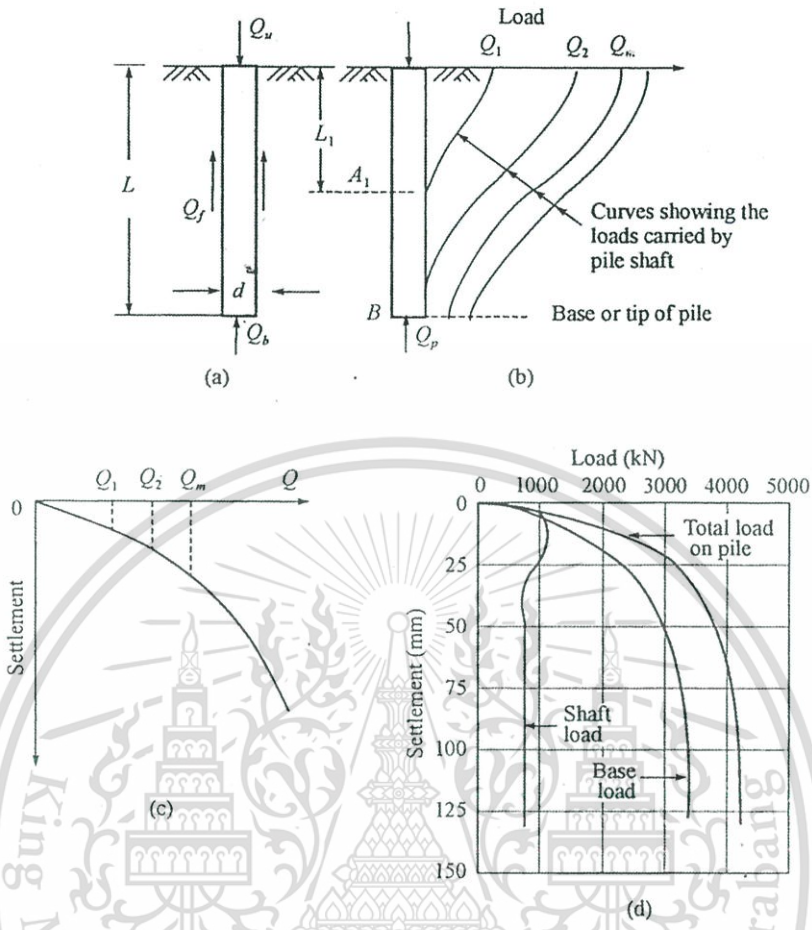

Figure 2.15 Load transfer mechanism: (a) Single pile, (b) load-transfer curves, (c) load-settlement curve, (d) load settlement relationships for large-diameter bored and cast-in-place piles (after [46]).

The mechanism of load transmitted to pile as shown in Figure 2.15. This figure(a) gives a single pile of uniform diameter, d (circular or any other shape), and length L driven into a homogeneous mass of soil of known physical properties. A static vertical load is applied on the top. It is required to determine the ultimate bearing capacity Q_u of the pile.

The consideration of the mechanism shown in Figure 2.15(b) if the pile is instrumented, the load distribution along the pile can be determined at different stages of loading and plotted. Figure 2.15(c) show that if settlement of the top of the pile is measured at every stage of loading after equilibrium condition is attained, a load settlement curve can be obtained like in its figure. A typical load-settlement relationship of friction load and base load is shown in Figure 2.15(d) for a large diameter bored and cast-in-situ pile in clay.

2) Ultimate load capacity

The ultimate load capacity of a single pile is given by the sum of the ultimate shaft and base capacities. Once the ultimate load capacity of a single pile has been determined the working load of the pile is assumed from the ultimate capacity by

applying a factor of safety. Building foundations will usually consist of pile groups, and therefore it might be necessary to apply a reduction factor to allow for the interaction of bored piles in a group. It is generally accepted that the ultimate base capacity, Q_{ub}, is given by the following Eq 2.9:

$$Q_{ub} + W = A_b(N_c c_{ub} + \gamma L_{pile}) \tag{2.9}$$

where W is the weight of the pile, A_b the area of the pile base, c_{ub} the undrained shear strength of the soil at the level of the base of the pile (more accurately the average shear strength within a depth below the base equal to about two thirds its diameter), N_c is a bearing capacity factor, the average density of the soil within the total length of the pile below ground level is L_{pile}. It can usually be assumed that the weight of the pile, W, is equal to $A_b L_{pile}$ and thus Eq. 2.10 reduces to:

$$Q_{ub} = A_b N_c c_{ub} \tag{2.10}$$

The calculation of the ultimate shaft capacity can be carried out using one of two methods; the α-method to calculate the undrained shaft capacity and the β-method to calculate the drained shaft capacity.

1) The α-method

The α-method for the calculation of the ultimate undrained shaft capacity was introduced by Skempton (1959) [47]. The method is based on the assumption that the loading behaviour of bored piles in clays with low permeability is undrained. The undrained shaft capacity, Q_{us}, is given by:

$$Q_{us} = A_s \overline{\tau_{sf}} \tag{2.11}$$

where A_s is the area of the shaft in interaction with the clay and $\overline{\tau_{sf}}$ is the average shaft friction over the length of the pile. Skempton (1959) [48] used the term average shaft adhesion, $\overline{c_a}$, instead of average shaft friction. The average shaft friction, $\overline{\tau_{sf}}$, is related to the average undrained shear strength, $\overline{c_u}$, through an empirical shaft adhesion factor, (α).

$$\overline{\tau_{sf}} = \alpha \overline{c_u} \tag{2.12}$$

Therefore, Eq. 2.13 can be written as:

$$Q_{us} = A_s \alpha \overline{c_u} \tag{2.13}$$

Generally, α is less than unity. The reduction of shaft adhesion in comparison to the undrained shear strength to softening of the clay adjacent to the shaft during the construction process is attributed by Skempton (1959) [47].

Results from twenty-five pile load tests are compiled by Skempton (1959) [47]. These results were interpreted in terms of the equivalent shaft adhesion factor,

α, that covers between 0.3 and 0.6 with an average of 0.45. The suggestion by Skempton (1959) [47] that in design the average shaft friction, $\overline{\tau_{sf}}$ should not be greater than 96 kN/m^2. As α is an empirical factor which is not only based on the pile test results but also the determining method of the average undrained shear strength, $\overline{c_u}$ of the soil over the depth of the piles. The design working load for a single pile suggested by Skempton (1959) [47], Q_w, should be use the following equation:

$$Q_w = \frac{\zeta(Q_{ub} + Q_{us})}{F} \tag{2.14}$$

where ζ is a group factor which is equal to 1.0 for an isolated pile and is less than 1.0 for piles in pile groups. F is a safety factor using a factor of safety of 2.5 for 'piles of the usual dimensions' and that for large diameter piles the factor of safety should be increased in order to restrict the settlements.

2) The β-method

Chandler (1966) [48] and Chandler (1968) [49] remarked that the shaft capacity of piles should be calculated in terms of effective stresses. The justification for this approach was that the probable mechanism of deformation on pile loading involves a narrow cylinder of clay immediately around the pile shaft subjected to simple shear. Providing the rate of loading is fairly slow (as in maintained load tests or in the case of pile loading due to the construction of a superstructure) drained conditions will exist in the clay along the pile shaft.

The assumption of fully drained conditions, Burland (1973) [50] and Burland & Twine (1988) [51] assumed the following;

1. Before loading the excess pore pressure set up during installation of the pile is completely dissipated.
2. As a result of remoulding of the clay during pile installation, the soil has no effective cohesion. Hence the shaft friction at failure, τ_{sf} at any point is given by

$$\tau_{sf} = \sigma'_h \tan\delta' \tag{2.15}$$

where σ'_h is the effective horizontal stress acting on the pile and δ' is the effective angle of friction between the clay and the pile shaft. The initial horizontal effective stress, σ'_{h0} in the soil is related to the initial vertical effective stress, σ'_{v0} through the earth pressure coefficient at rest, K_0 ($K_0 = \sigma'_{h0}/\sigma'_{v0}$). Additional assumed that the horizontal effective stress acting on the pile can also be related to the initial vertical effective stress through a factor (K) [38].

$$\sigma'_h = K\sigma'_{v0} \tag{2.16}$$

Eq. 2.15, therefore can be written as:

$$\tau_{sf} = K\sigma'_{v0} \tan\delta' \tag{2.17}$$

Burland (1973) [50] proposed the empirical parameter, β as Eq. 2.18

$$\beta = \frac{\tau_{sf}}{\sigma'_{v0}} = K \tan \delta' \tag{2.18}$$

The ultimate shaft capacity is then given by:

$$Q_{us} = 2\pi \frac{D_{pile}}{2} \int (K\sigma'_{v0} \tan \delta')dl = 2\pi \frac{D_{pile}}{2} \int (\beta\sigma'_{v0})dl \tag{2.19}$$

where D_{pile} is the diameter of the pile.

2.4.3 Bored pile constructions in the Bangkok sub soil

1) Overview of applications

Table 2.3 The structures constructed by Wet-Processed Bored Piles in Bangkok (modified after [52]).

Project Name	Year of Construction	Construction Method	Diameter (m)	Depth (m)
Pinkloa Bridge	1971	Reverse circulation	1.5	45
Sathorn Bridge	1979		1.5	46
New Memorial Bridge	1982		1.5	49
Royal Orchid Hotel	1979	Rotary-drilling with auger and bucket	0.8-1.0	33
Taiping Tower	1980		0.8-1.5	32
River city Hotel	1982		0.8-1.0	27.5
Asoke Tower	1983		0.8-1.5	50
Time Square Building	1983		0.8-1.5	50

Using tripod rigs, small diameter dry-processed bored pile construction was started in early 1970. The first wet-process large diameter bored pile, which use reverse circulation method, a 1.50m diameter bored pile was installed up to 45m in the second sand layer, was constructed for Pinklao Bridge in Bangkok 36 years ago. The bored pile using the reverse circulation method was used to construct three major bridges in Bangkok from early 1970 to 1980. The rotary-drilling method utilized in

wet-process of bored pile was constructed in Bangkok in the late 1970s for high-rise building project, the Royal Orchid Hotel located at the bank of Chao Phraya River. After that, this method has been extensively used for foundation of various large-scale structures such as high-rise buildings, elevated expressways, overpass-bridges, underground car park buildings, waste-water treatment plants and most recently underground train stations of Bangkok's first subway project (MRTA project). In 1980s, bored piles became the choice of foundation for large-scale structures, particularly in the urban area of Bangkok. The versatility of the construction method and the high-load capacity because of that offered the constructability and cost-saving, are the main factors contributing to the incremental construction of deep-seated large diameter bored piles. Most of the early wet-process bored piles (1980s) in Bangkok were constructed up to 50 m depth. Sizes of bored piles constructed in early days are 0.6 to 1.5 m in diameter. Summarized information of bored piles constructed in Bangkok is listed in Table 2.3

2) Design concept and parameters selection

In the initial stage of introducing bored piles in Thailand, the design concepts and parameters were mainly based on the available literature from research carried out in other parts of the world such as Tomlinson (1957) [46], Skempton (1959) [47], Broms (1966) [53], Bowles (1968) [54], Meyerhof (1976) [55] etc. The work of Chiruppapa (1968) [56] was believed to be the first research data available for design parameters of bored piles in Bangkok soft clay. Design methods and selection of parameters for local subsoil (i.e., adhesion factor (α), shaft friction factor (β) and bearing capacity factor (N)) were improved as a result of research works carried out in 1980s [46]- [51]. However, the design parameters obtained from these research works were mainly based on shaft friction loads from plain static pile load test results estimated from numbers of assumptions because the results of instrumented pile load test were limited. With Thailand constructing boom, in particularly in Bangkok, large numbers of instrument with full-scale static load tests on bored piles were proceeded throughout 1990's which provided better understanding on behaviour of these deep-seated foundations. The design parameters and methods based on these test data were thus proposed by Thasnanipan et al. (2007) [52]. With improved design methods, the wet-process cast-in-place foundations came to be regarded as reliable foundations in the construction industry of Thailand.

From published research of Thasnanipan et al. (2007) [52], the bored piles embedded in the multi layered soils of Bangkok, estimation of ultimate shaft friction capacity needs to consider the brittle type of failure mechanism of stiff to hard clay layers and the α values selected need to be adjusted accordingly. Peak and residual of α values mobilized in the stiff clay layers were plotted as shown in Figure 2.16 along with the suggested curves by different researchers. It can be seen from the figure that the residual α value of 2nd stiff clay layer (undrained shear strength values of 25 ton/m^2), at the maximum test load, drops below the curve suggested by Pimpasugdi (1989) [57]. So, the α values proposed by the author in Figure 2.16 for the stiff to hard clay layers overestimate the ultimate shaft friction under these conditions.

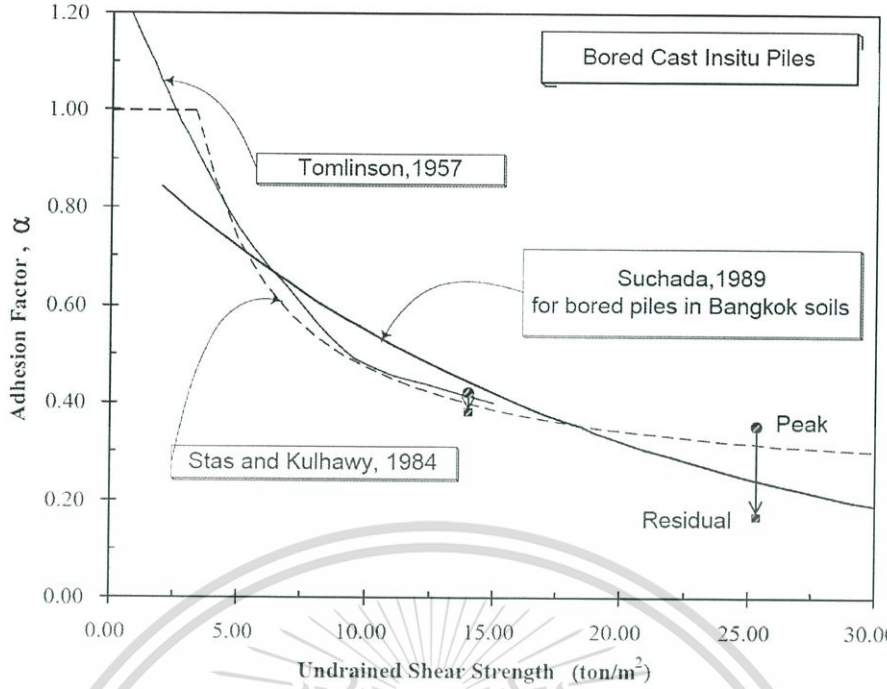

Figure 2.16 Comparison of adhesion factor, α, suggested by different researchers with the actual mobilized in the stiff clay layers (after Thansnanipan et. al 1999 [58]).

A primary breakthrough for both construction and design engineers with the polymer-based slurry for wet-process bored piles was reviewed by Thasnanipan et al. (2007) [52]. From this research, bored piles constructed with polymer-based slurry have higher capacity than those constructed with bentonite slurry. Figure 2.17 depicts the shaft friction factors β of sand layers for polymer-based bored piles in comparison with the design line of bentonite bored piles. The higher load capacity of bored piles constructed with polymer-based slurry allows the use of a single, large diameter deep-seated bored pile in place of a group of smaller size shallow-seated bored piles or driven piles. Moreover, this research performed the static pile load test result of 1.80m diameter bored pile of 60 m depth constructed with polymer-based slurry in urban area of Bangkok as shown in Figure 2.18. The maximum applied load 48,000 kN in this test is believed to be the highest static pile load test performed on a single bored pile in Thailand. Apparently, from the test result, the pile (diameter 1.80m x 60m deep) could carry a significantly higher load than the original pre-defined safe design load of 16,000 kN.

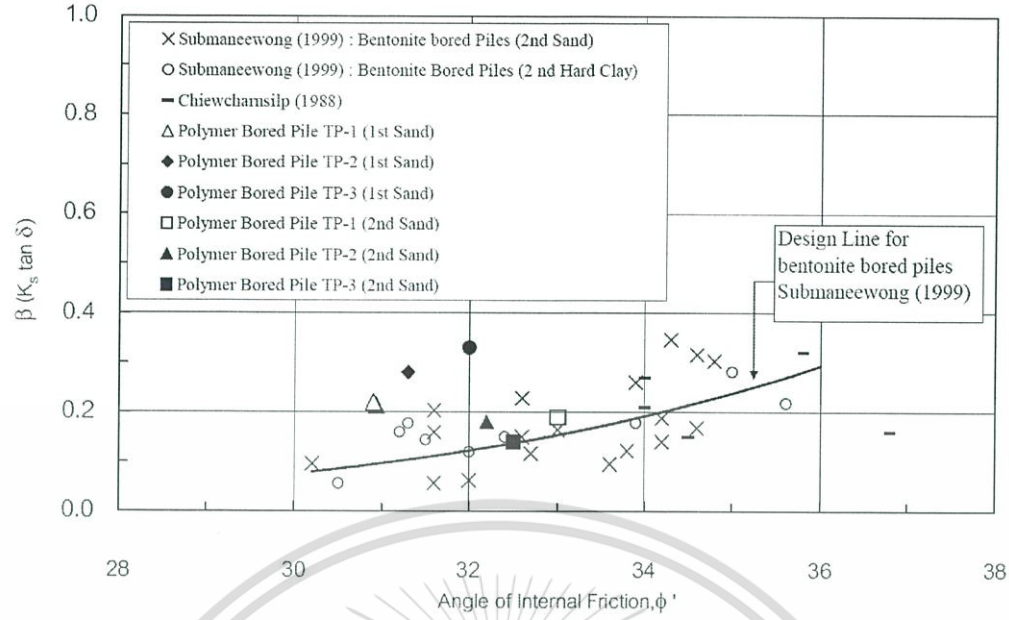

Figure 2.17 Back-calculated β values of polymer bored piles at maximum test load plotted on design line of bentonite bored piles constructed in Bangkok subsoil (after Thansnanipan et. al 2002b [59]).

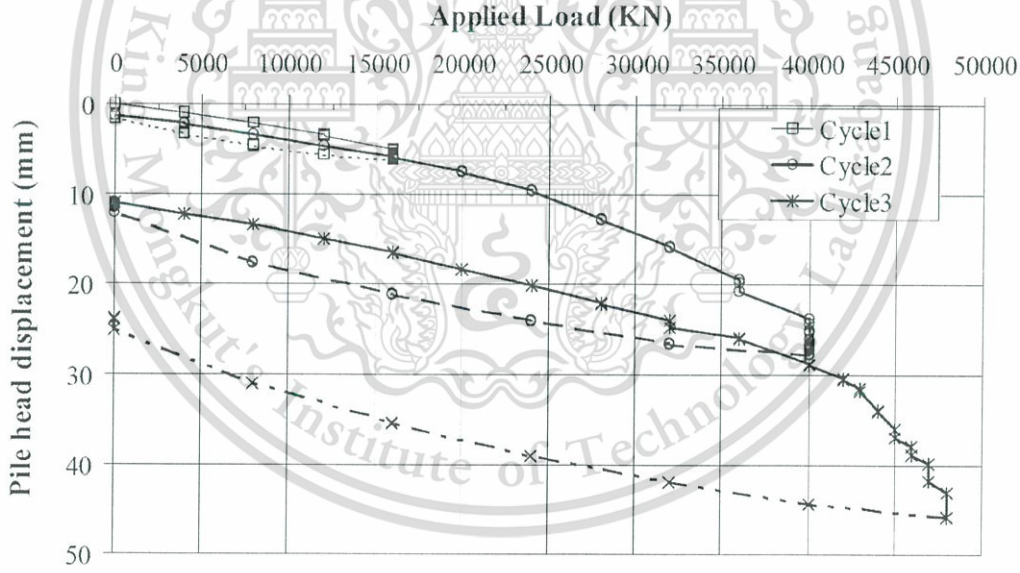

Figure 2.18 Static pile load test result of 1.80m diameter bored pile of depth 60m in Bangkok.

2.5 Tunnel influence zone and pile-soil-tunnel interaction

2.5.1 The influence zone concept

An assessment of the impact of adjacent structure on the stability and integrity of the existing tunnels or the tunnel construction on existing structure is necessary. The assessment is typically carried out in two steps. The first step is to evaluate the potential impact of new structures on protecting structures for a design modification.

At present, this is carried out by defining the influence zone of the tunnel in combination with certain criteria. An influence zone refers to an area of land where future developments or construction activities to be undertaken could result in the imposition of additional load on the tunnel structure or affect an operational system [60]. If the possible impact is serious, the second step of assessment is necessary, in which the design must be modified or a detailed assessment must be carried out. Tunnel owners have used restrictive guidelines for new constructions adjacent to the tunnels. The guidelines could include one or more influence zones or a minimum clearance between structures, maximum allowable tunnel deformation, and stress changes in tunnel lining. Figure 2.19 illustrates tunnel influence zones for the new construction of the Land Transport Authority (LTA) [60] and the Mass Rapid Transit Authority (MRTA) [61]. An influence zone was conventionally assumed from the ideal shear plane from the model test which be further described in the next section. The zone is applied to all construction types but is proved to be inappropriate for piles. In addition, the restrictive guidelines were established based on experiences rather than on the theoretical understanding of the pile-tunnel interaction.

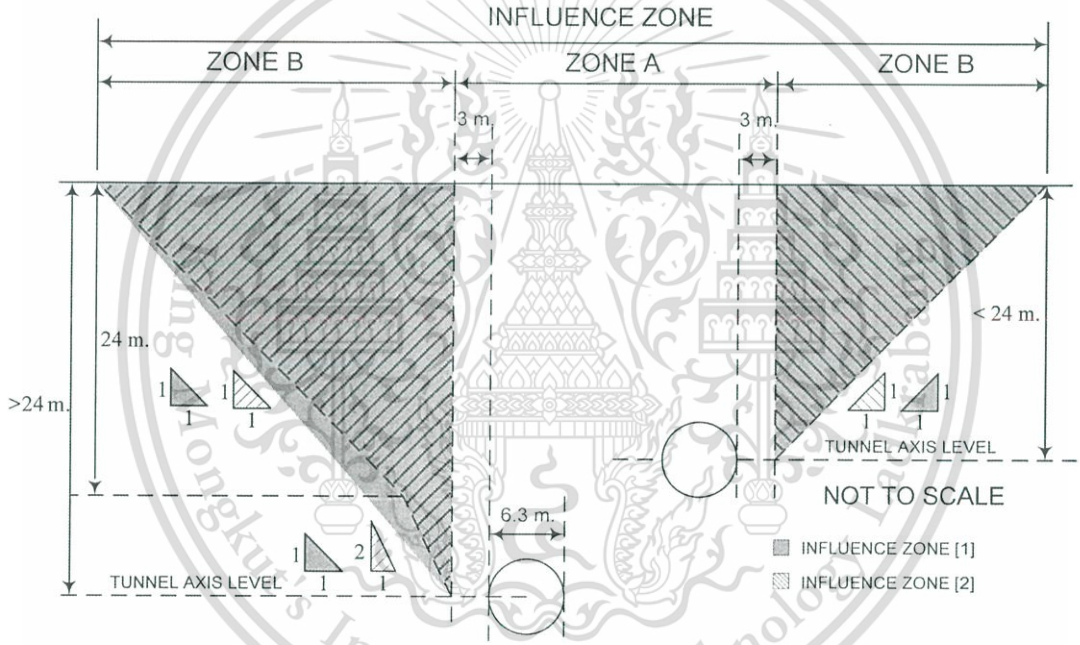

Figure 2.19 Tunnel influence zone utilised in current practice.

Numerous researchers have attempted to investigate the mechanism of pile-soil-tunnel interaction that can divide into two main groups as the influence of tunnel construction on existing piles and the influence of pile construction and loading on existing tunnels. However, most of the researches and the publications focus on the influence of tunnelling on adjacent piled foundations of existing buildings. The study of the effect of pile under loading on existing tunnels are even more limited. To obtain better understanding of the mechanism of pile-soil-tunnel interaction, this thesis will extensively review on the influences of pile under loading and adjacent constructions on existing tunnels, however, the influence of tunnel construction on existing piles will be also summarised.

2.5.2 The influence of tunnel construction on adjacent existing piles

There have been a number of studies addressing the mechanisms of soil-tunnel-pile interactions. However, the majority of the attention has focused on the influence of tunnelling on nearby piled foundations, for instance, field observation [62], full-scale tests [63], physical model tests [64] - [66] and analyses by the analytical method [67] and the numerical method [65], [68] – [71]. Among these, due to time and budget constraints in the field, full-scale and physical model tests, analytical and numerical analyses have become the primary methods used. Based on these studies, a knowledge base of soil-tunnel-pile interaction mechanisms has been developed and continually updated.

Besides, most studies interested to focus on the concept of an influence zone, which is commonly used in engineering practice as a guideline to control tunnel position adjacent to pile foundations [65] and [72] - [74] as depicted in Figure 2.20. This figure shows that the influence zone is conventionally assumed to rise at an angle of b =45 ± (ϕ/2) to the vertical from the tunnel axis to the ground surface where ϕ is the friction angle. The b lines are based on the typical shear surfaces first proposed from model test results by Morton and King [74] which principally assumed to define the influence zone as mention in Section 2.5.1. These surfaces can also be defined by a wedge of width ±2.5i at the ground surface with its source at the tunnel lining, where i is the distance from the tunnel centre line to the inflection point [72] - [73], [75].

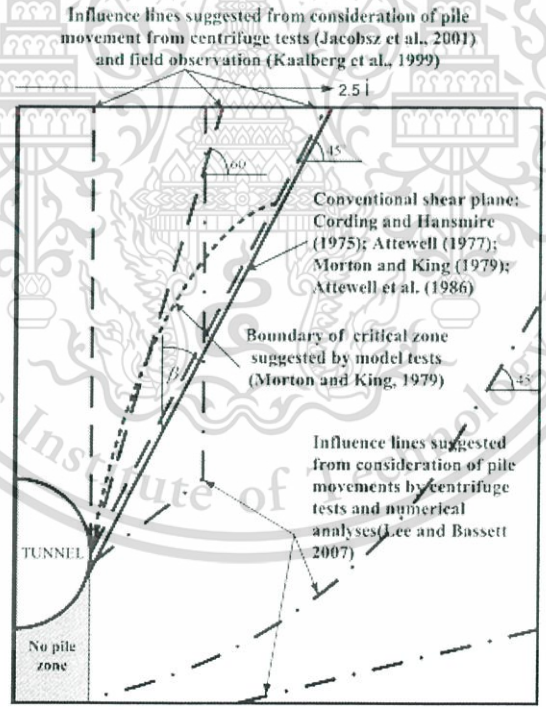

Figure 2.20 Influence line proposed in previous studies [76].

In addition to the concept of a typical shear surface, influence lines have also been proposed based on consideration of pile settlements in recent studies. Kaalberg et al. (1999) [77] and Jacobsz et al. (2001) [78] proposed a critical influence line (60° to the tunnel axis) and a normal influence line (45° to the tunnel axis) from full-scale and centrifuge model tests, respectively. Lee and Bassett (2007) [65] presented influence zones based on the normalized pile tip settlement from both model tests and

numerical analysis and Selemetas et al. (2005) [63] suggested influence zones from field observation. These suggested zones are different from those based on the shear plane concept. with limited data from results of a specific test condition for a series of model tests or field observation cases, each proposed zone in previous studies was roughly suggested based on limited information where only a few significant influencing factors are considered. Interactions depend on many factors including the tunnel and pile dimensions, volume loss, the position of the pile tip with respect to the tunnel horizontal axis and clearance. More data reflecting the influence of those factors are required to reliably suggest influence zones

In 2013, Jongpradist et al., [76] developed tunnelling influence zones with suitable criteria being considered for adjacent pile foundations by using artificial data of pile responses generated from a series of finite element analyses (FEA) as shown in Figure 2.21. This zone was adopted from two primary behaviour types that can be defined, depending on the relative pile length compared to the tunnel depth: short pile (deep tunnelling) and long pile (shallow tunnelling). For the long pile condition, the width of the influence zone is *1D* from the nearest pile, *D* is tunnel diameter. The vertical distance for transition of the zone from the tunnelling (above pile tip) to the deep one refers to 0.75*D* from the pile tip regardless of the length of the pile. The inclination of the zone for deep tunnelling is *H*:*V* = 2:3.5. The transition from inclined to vertical lines as the boundary for deep tunnelling zone (short pile condition) is 2*D* wide from pile and 2.5*D* deep from pile tip. If a tunnel is to be constructed within these zones, detailed assessment and volume loss control with a comprehensive instrumentation program are necessary during the design and construction stages, respectively.

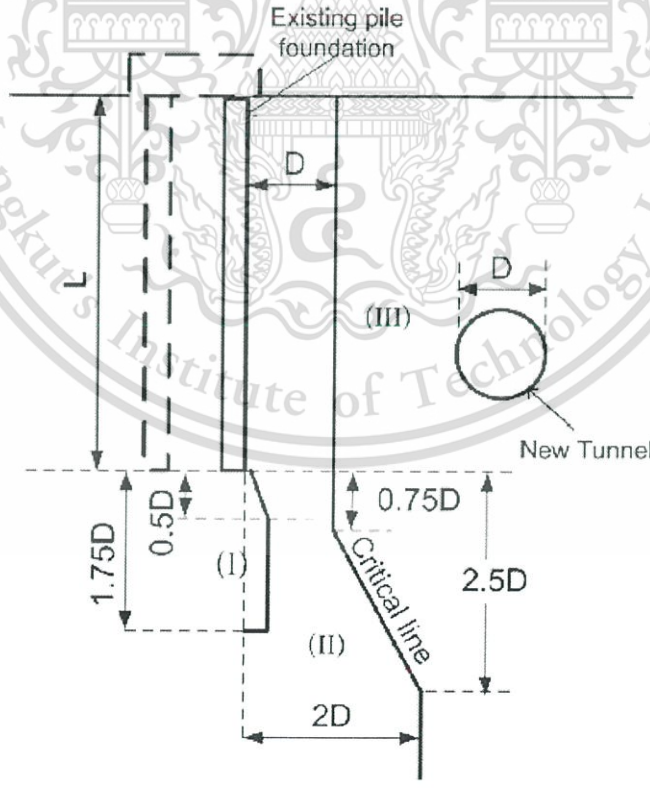

Figure 2.21 Proposed influence zones of pile (combination of maximum pile head settlement and maximum pile bending moment consideration) [76].

2.5.3 The influence of pile loading and adjacent constructions on existing tunnels

Despite several attempts focused on the influence of tunnelling on adjacent pile foundations, studies on the effects of loaded piles on nearby existing tunnels are rather limited, although the issue has been recognized since the 1950s in London [79]. Over the past 30 years, the studies concerning the influence of bored piles on existing tunnels have only small published, mostly on those constructed in London [80]- [83]. Due to the tunnels considered in previous studies are primarily subway tunnels, train operational safety is of major concern. In order to protect their tunnel infrastructure, tunnel owners often impose limitations on the construction and loading of adjacent piles to their tunnels. The limitations generally imposed by tunnel owners were summarized by Chudleigh et al. (1999) [82] as example following;

1) Tunnel deformation

Chudleigh et al. (1999) [82] imposed limitations on tunnel deformations as a very reasonable method of tunnel owners as the limits on deformations are often an easily determined quantity. Deformations on rail tunnels are limited by the clearance between the dynamic envelope surrounding a moving train and the tunnel lining. In the case of pedestrian travellators and escalators, limits on movements will be prescribed by the manufacturer of the machinery, and are frequently in the order of millimetres. However, it is often uncertain whether the restrictions on tunnel deformations relate to the absolute movements of a tunnel (movements in space) or distortions of the tunnel (relative movements). Another factor often ignored in the restrictions is the direction of the movements. Deformations in a certain direction might even be beneficial if they correct previous distortions of the tunnel lining.

2) Pile offset

The distance between piles and an existing tunnel at which piles may be installed are also defined. It is supposed to allow for inaccuracies in setting out and verticality of the pile. A pile located at the specified distance is presumed not to cause excessive deformation of or stress changes in the tunnel lining. LUL commonly impose an exclusion zone to the side of their tunnels of 3 m for the construction of bored piles and 15 m for the construction of driven piles. In additionally, the investigated reports of Parker (2000) [84] for the construction of piles for the Millennium Dome the Highways Agency initially set a 10-m exclusion zone around the Blackwall Tunnel. However, the piling contractor agreed to use continuous flight auger piling in the vicinity of the tunnel such that the 750 mm diameter piles could be located at a distance of 3 m from the tunnel.

However, the limitations as above mentions were established based on experiences rather than on the theoretical understanding of the pile-tunnel interaction. In order to extend the better understanding of the limitations, a finite element method was used to analyse the impacts of pile under loading on an existing tunnel. The effects of piles on existing tunnel by 3-D finite element analysis were studied that emphasis is placed on the function of debonding /sleeving, which is usually taken as a measure to mitigate the effects of pile foundations on the tunnel [85]. The results of this study indicated that the interaction behaviour is strongly affected by tunnel depth to pile length ratio and soil properties where the pile tips was located. Moreover, the tunnel deformations in circumferential direction due to those effects are primary revealed. The effects in terms of tunnel distortions and global movements in relation to the loading of pile rows supporting a 15-storey building was examined by

Schroeder (2002, 2004) [86] and [87]. The changes in tunnel diameter in vertical and horizontal directions was considered to observe the tunnel deformation. The changes in tunnel diameter can use to define a specific clearance (pile offset of the limitations) between the pile rows and the tunnel. Moreover, the distortion shapes of the tunnel induced from adjacent pile under loading located on both and single sides of the tunnel were performed obviously, the unsymmetrical tunnel shape can be observed for the case of pile located at the single side of the tunnel. However, the soil was homogeneous, the pile length was identical, and the pile tip position was much lower than that of the tunnel, are restrictions of the study. In 2006, Charoenpak [88] investigated the effects of the pile tip position with various types (single pile, pile row and pile group) on the existing tunnel in multi-layer soil focused on the MRTA tunnel and on Bangkok subsoil. The results of the study were performed in terms of tunnel deformations based on the study of Schroeder (2004) [87], i.e. changes of tunnel diameter in both vertical and horizontal directions.

In addition, the series of centrifuge tests carried out to investigate the effects of loading of bored piles on existing tunnels were presented by and Zou et al. (2002) [85] and Yao et al. (2008) [89].

With the small publications of the effects of adjacent loaded pile on existing tunnel as reviewed above, the responses of an existing tunnel to adjacent constructions are reviewed together. There were studies concerning the impacts on tunnels due to adjacent constructions such as new subway tunnels [90] and [91], and deep excavation stages [92] – [94]. These studies continuously contribute to an understanding of tunnel response due to changes in surrounding conditions inducing a release of in situ stress and thus soil displacement, which inevitably exerts an influence on existing tunnels. Besides, the tunnel deformations investigated by those researches, there were few researches interesting in other behaviours of existing tunnel, stress, strain and structural forces, affected from adjacent constructions. The stress-strain changes in tunnel lining due to tunnel excavation crossing underneath existing tunnel were considered to identify the influence zone of new tunnel excavation [95]. The change in tunnel diameter, the bending stress-strain, the structural forces of tunnel lining in the transverse direction due to basement excavation were investigated by Ng et al (2015) [96].

2.6 References

[1] B. Maidl, M. Herrenknecht, and L. Anheuser, L, "*Mechanised Shield Tunneling*," 1996.

[2] S. Suwansawat, "Earth Pressure Balance (EPB) Shield Tunneling in Bangkok: Ground Response and Prediction of Surface Settlements Using Artificial Neural Networks", Ph.D. Thesis, Massachusetts Institute of Technology, USA, 2002

[3] Kawasaki Heavy Industries, Ltd., "Kawasaki Heavy Industries" [Online], Japan, Available: https://global.kawasaki.com/en/industrial_ equipment/ construction/civil/hydraulic [19 August 2016].

[4] Herrenknecht AG, "Herrenknecht" [Online], Germany, Available: https://www.herrenknecht.com/en/references/references-tunnelling.html [19 August 2016].

[5] B. Stack, "Handbook of Mining and Tunneling Machinery," *John Wiley & Sons*, New York, 1982.

[6] Herrenknecht AG, "Herrenknecht" [Online], Germany, Available: https://www.herrenknech t.com/en/products/core-products/tunnelling/epb-shield.html [5 April 2016].

[7] G. W. Clough, B. P. Sweeney, and R. J. Finno, "Measured Soil Response to EPB Shield Tunneling," *J. Geotech. Eng.*, vol. 109, no. 2, pp. 131–149, 1983.

[8] R.J. Finno, G.W. Clough, "Evaluation of soil response to EPB shield tunnelling," *J. of Geotechnical Engineering-ASCE*, 111(2), pp. 155-173, 1985.

[9] S. Bernat and B. Cambou, "Soil-structure interaction in shield tunnelling in soft soil," *Comput. Geotech.*, vol. 22, no. 3–4, pp. 221–242, 1998.

[10] S. Bernat, B. Cambou, and P. Dubois, "Assessing a soft soil tunnelling numerical model using field data," *Geotechnique*, vol. 49, no. 4, pp. 427–452, 1999.

[11] K. M. Lee and R. K. Rowe, "Finite element modelling of the three-dimensional ground deformations due to tunnelling in soft cohesive soils: Part I - Method of analysis," *Comput. Geotech.*, vol. 10, no. 2, pp. 87–109, 1990.

[12] K. M. Lee and R. K. Rowe, "Finite element modelling of the three-dimensional ground deformations due to tunnelling in soft cohesive soils: Part II - Results," *Comput. Geotech.*, vol. 10, no. 2, pp. 87–109, 1990.

[13] K. M. Lee and R. K. Rowe, "An analysis of three-dimensional ground movements: The Thunder Bay tunnel," *Can. Geotech. J.*, vol. 28, no. 1, pp. 25–41, 1991.

[14] K. M. Lee, R. K. Rowe, and K. Y. Lo, "Subsidence owing to tunnelling. I. Estimating the gap parameter," *Can. Geotech. J.*, vol. 29, no. 6, pp. 929–940, 1992.

[15] R. K. Rowe and K. M. Lee, "Subsidence owing to tunnelling. II. Evaluation of a prediction technique: Reply," *Can. Geotech. J.*, vol. 31, no. 3, pp. 467–469, 1994.

[16] Abu-Krisha "A. Numerical modelling of TBM tunnelling in consolidated clay," Ph.D. Thesis, University of Innsbruck, 1998.

[17] G. Swoboda, "Three-Dimensional Numerical Modelling for TBM Tunnelling in Consolidated Clay," *Tunn. Undergr. Sp. Technol.*, vol. 14, no. 3, pp. 327–333, 1999.

[18] T. Kasper and G. Meschke, "A 3D finite element simulation model for TBM tunnelling in soft ground," *Int. J. Numer. Anal. Methods Geomech.*, vol. 28, no. 14, pp. 1441–1460, 2004.

[19] T. Kasper and G. Meschke, "A numerical study of the effect of soil and grout material properties and cover depth in shield tunnelling," *Comput. Geotech.*, vol. 33, no. 4–5, pp. 234–247, 2006.

[20] H. Chakeri, Y. Ozcelik, and B. Unver, "Effects of important factors on surface settlement prediction for metro tunnel excavated by EPB," *Tunn. Undergr. Sp. Technol.*, vol. 36, pp. 14–23, 2013.

[21] G. Zheng, T. Zhang, and Y. Diao, "Mechanism and countermeasures of preceding tunnel distortion induced by succeeding EPBS tunnelling in close proximity," *Comput. Geotech.*, vol. 66, pp. 53–65, 2015.

[22] W. Broere, R. Brinkgreve, ''Phased simulation of a tunnel boring process in soft soil,'' *in Proc. Conf. on Numerical Methods in Geotechnical*

Engineering, in Mestat (Ed.), Presses de 1'ENPC/ LCPC, Paris, pp.529-536, 2002.

[23] Brinkgreve, R., Engin, E., Swolfs, W., "*PLAXIS 3D Version 2013 manual*," Chapman, 2013.

[24] H. Katebi, A. H. Rezaei, M. Hajialilue-Bonab, and A. Tarifard, "Assessment the influence of ground stratification, tunnel and surface buildings specifications on shield tunnel lining loads (by FEM)," *Tunn. Undergr. Sp. Technol.*, vol. 49, pp. 67–78, 2015.

[25] E. M. Comodromos, M. C. Papadopoulou, and G. K. Konstantinidis, "Numerical Assessment of Subsidence and Adjacent Building Movements Induced by TBM-EPB Tunneling," *J. Geotech. Geoenvironmental Eng.*, vol. 140, no. 11, p. 4014061, 2014.

[26] R. Peck, "Deep excavations and tunnelling in soft ground," *Proc. 7th Int. Conf. SMFE*, pp. 226–290, 1969.

[27] R. J. Mair and R. N. Taylor, "Bored tunnelling in the urban environment," *14Th International Conference on Soil Mechanics and Foundation Engineering*, vol. 4. pp. 2353–2385, 1997.

[28] C. González and C. Sagaseta, "Patterns of soil deformations around tunnels. Application to the extension of Madrid Metro," *Comput. Geotech.*, vol. 28, no. 6–7, pp. 445–468, 2001.

[29] R.N. Craig, and A.M.M Wood, "A review of tunnel lining practice in the United Kingdom," *Transport and Road Research Laborat*ory, TRRL Supplementary Report 335, 1978.

[30] H. Schmid, "Statische Probleme des Tunnel-und Druckstollenbaues," Berlin, 1926.

[31] H. Schulze, and H. Duddeck, "Stresses in shield driven tunnels," Beton and Stahlbetonbau 8, 169–175, 1964.

[32] D.H. Morgan, "A contribution to the analysis of stress in a circular tunnel," *Geotechnique*, 11 (3), 37–46, 1971.

[33] R.B. Peck, A.J. Hendron, and B. Mohraz, "State of the art of soft-ground tunneling," *In: Proceedings of the North American Rapid Excavation and Tunneling Conference*, Chicago, IL, pp. 259–286, 1972.

[34] A. M. M. Wood, "The circular tunnel in elastic ground," *Géotechnique*, vol. 25, no. 1, pp. 115–127, 1975.

[35] H.H. Einstein, and C.W. Schwartz, "Simplified analysis for tunnel supports," *Journal of the Geotechnical Engineering Division, American Society of Civil Engineers*, 105, 499–518, 1979.

[36] C. Sagaseta, "Analysis of undrained soil deformation due to ground loss," *Géotechnique*, 37 (3), 301–320, 1987.

[37] A. Verruijt and J. R. Booker, "Surface settlements due to deformation of a tunnel in an elastic half plane," *Géotechnique*, vol. 46, no. 4, pp. 753–756, 1996.

[38] N. Loganathan and H. G. Poulos, "Analytical Prediction for Tunneling-Induced Ground Movements in Clays," *J. Geotech. Geoenvironmental Eng.*, vol. 124, no. 9, pp. 846–856, 1998.

[39] A. Bobet, "Analytical Solutions for Shallow Tunnels in Saturated Ground," *Journal of Engineering Mechanics*, vol. 127, no. 12. pp. 1258–1266, 2001.

[40] W. I. Chou and A. Bobet, "Predictions of ground deformations in shallow tunnels in clay," *Tunn. Undergr. Sp. Technol.*, vol. 17, no. 1, pp. 3–19, 2002.

[41] S. Moller, "Tunnel Induced Settlements and Structural Forces in Linings," 2006.

[42] M. A. Nunes and M. A. Meguid, "A study on the effects of overlying soil strata on the stresses developing in a tunnel lining," *Tunn. Undergr. Sp. Technol.*, vol. 24, no. 6, pp. 716–722, 2009.

[43] M. A. Meguid and H. K. Dang, "The effect of erosion voids on existing tunnel linings," *Tunn. Undergr. Sp. Technol.*, vol. 24, no. 3, pp. 278–286, 2009.

[44] H. H. A. Hamdy, M. Enieb, A. Abdelmoamen Khalil, and A. S. H. Ahmed, "Twin tunnel configuration for Greater Cairo metro line No. 4," *Comput. Geotech.*, vol. 68, pp. 66–77, 2015.

[45] N. Heama, P. Jongpradist, P. Lueprasert, and S. Suwansawat, "Investigation on tunnel response due to adjacent loaded pile by 3D finite element analysis," *Int. J. GEOMATE*, vol. 12, no. 31, pp. 63–70, 2017.

[46] M.J. Tomlinson, "The adhesion of piles driven in clay soils". *Proc. 4th ICSMFE*, England , pp. 66-71, 1957.

[47] A.W. Skempton,1959. "Cast In-Situ Bored Piles in London Clay," *Géotechnique* 9(4): 153–73, 1959.

[48] R.J. Chandler, "Discussion on Whitaker and Cooke," *Proc. Symp. Large Bored Piles*. p. 95-97, 1966.

[49] R.J. Chandler, "The shaft friction of piles in cohesive soils in terms of effective stress" *Civ. Eng. and Pub. Works Rev.* Jan 1968. p. 48-51, 1968.

[50] J.B. Burland, "Shaft friction of piles in clay - a simple fundamental approach." Ground Engineering. 6, No. 3, p. 30-42, 1973.

[51] J.B. Burland and D. Twine, "The shaft friction of bored piles in terms of effective strength." *Proc. 1 st Int. Conf. Deep Foundations on Bored and Augered Piles*. p. 411-420, 1988.

[52] N. Thasnanipan, A. W. Maung, T. Navaneethan and Z. Z. Aye, "Development and Achievements of Deep-seated Bored Piles and Barrettes Construction in Thailand for the Past Forty Years, A Country Report", *Proc. of the 16th Southeast Asian Geotechnical Conference 8-11 May 2007*, Kuala Lumpur, Malaysia, 2007.

[53] B.B. Broms, "Methods of calculating the ultimate bearing capacity of piles – a summary," *Soils-Soils, No. 18- 19:* 21-32, 1966.

[54] J.E. Bowles, "*Foundation analysis and design*," *McGRaw-Hill,* New York, 1968.

[55] G. G. Meyerhof, "Bearing Capacity and Settlement of Pile Foundations," *J. Geotech. Eng. Div.*, vol. 102, no. 3, pp. 195–228, 1976.

[56] P. Chiruppapa, *"Cast in-situ bored piles in Bangkok Clay*," M. Eng. Thesis No. 213, Asian Institute of Technology, Bangkok, Thailand, 1968.

[57] P. Suchada, *"Performance of Bored, Driven and Auger Press Piles in Bangkok Subsoils,"* M. Eng. Thesis No. GT 88-12, Asian Institute of Technology, Bangkok, Thailand, 1989 (in Thai).

[58] N. Thasananipan, and M. A. Maung, "Failure Mechanism of Long Bored Piles in Layered Soils of Bangkok," *Civil and Environmental Engineering Conference*, Bangkok, Thailand: V-69 to V-73, 1999.

[59] N. Thasnanipan, Zaw Zaw Aye, C. Submaneewong and W Teparaksa, "Performance of Wet- Process Bored Piles Constructed with Polymer-Based Slurry in Bangkok Subsoi," *Proceedings of the International Deep Foundations Congress 2002, Geotechnical Special Publication No. 116,*

Volume One, ASCE, February 14-16 2002, Orlando, Florida, USA :143- 157, 2002b.

[60] Land Transport Authority, "Code of Practice for Railway Protection", Development and Building Control Department, Singapore, 2004.

[61] Mass Rapid Transit Authority of Thailand, "Restrictive Guideline for Protection Zone in Blue Line Project", Engineering Specifications for MRT Tunnels, Bangkok, 2009 (in Thai).

[62] R. J. Mair, R. N. Taylor, and a. Bracegirdle, "Subsurface settlement profiles above tunnels in clays," *Géotechnique*, vol. 45, no. 2, pp. 361–362, 1995.

[63] D. Selemetas, J. R. Standing, and R. J. Mair, "The response of full-scale piles to tunnelling," *Geotech. Asp. Undergr. Constr. Soft Gr. - Proc. 5th Int. Conf. TC28 ISSMGE*, pp. 763–769, 2006.

[64] Y. J. Lee and R. H. Bassett, "A model test and numerical investigation on the shear deformation patterns of deep wall–soil–tunnel interaction," *Can. Geotech. J.*, vol. 43, no. 12, pp. 1306–1323, 2006.

[65] Y. J. Lee and R. H. Bassett, "Influence zones for 2D pile-soil-tunnelling interaction based on model test and numerical analysis," *Tunn. Undergr. Sp. Technol.*, vol. 22, no. 3, pp. 325–342, 2007.

[66] C. W. W. Ng, H. Lu, and S. Y. Peng, "Three-dimensional centrifuge modelling of the effects of twin tunnelling on an existing pile," *Tunn. Undergr. Sp. Technol.*, vol. 35, pp. 189–199, 2013.

[67] Y. Xiang and S. Feng, "Theoretical prediction of the potential plastic zone of shallow tunneling in vicinity of pile foundation in soils," *Tunn. Undergr. Sp. Technol.*, vol. 38, pp. 115–121, 2013.

[68] H. Mroueh and I. Shahrour, "Three-dimensional finite element analysis of the interaction between tunneling and pile foundations," *Int. J. Numer. Anal. Methods Geomech.*, vol. 26, no. 3, pp. 217–230, 2002.

[69] P. Kitiyodom, T. Matsumoto, and K. Kawaguchi, "A simplified analysis method for piled raft foundations subjected to ground movements induced by tunnelling," *Int. J. Numer. Anal. Methods Geomech.*, vol. 29, no. 15, pp. 1485–1507, 2005.

[70] H. Y. Liu, J. C. Small, J. P. Carter, and D. J. Williams, "Effects of tunnelling on existing support systems of perpendicularly crossing tunnels," *Comput. Geotech.*, vol. 36, no. 5, pp. 880–894, 2009.

[71] C. J. Lee, "Three-dimensional numerical analyses of the response of a single pile and pile groups to tunnelling in weak weathered rock," *Tunn. Undergr. Sp. Technol.*, vol. 32, pp. 132–142, 2012.

[72] E.J. Cording, and W.H. Hansmire, "Displacements around soft ground tunnels," *In: 5th Pan American Congress on Soil Mechanics and Foundation Engineering, General Report-Session IV*, Buenos Aires, pp. 571–632, 1975.

[73] P.B. Attewell, "Ground movements caused by tunneling in soil," *In: Proceedings International Conference on Large Movements and Structures*, London, pp. 812–948, 1977.

[74] J.D. Morton, and K.H. King, "Effects of tunneling on the bearing capacity and settlement of piled foundations," *In: Tunneling '79. IMM*, London, pp. 57–68, 1979.

[75] P.B. Attewell, J. Yeates, and A.R. Selby, "Soil Movements Induced by Tunneling and their Effects on Pipelines and Structures." Blackie, Glasgow, pp. 256, 1986.

[76] P. Jongpradist, T. Kaewsri, A. Sawatparnich, S. Suwansawat, S. Youwai, W. Kongkitkul, and J. Sunitsakul, "Development of tunneling influence zones for adjacent pile foundations by numerical analyses," *Tunn. Undergr. Sp. Technol.*, vol. 34, pp. 96–109, 2013.

[77] F.J. Kaalberg, H.J. Lengkeek, E.A.H. Teunissen, "*Evaluatie van de meetresulaten van het proefpalenprojek ter plaatse van de tweede Heinenoordtunnel.*" Adviedbureau Noord/Zuidlijn Report No. R981382, Amsterdam. (in Dutch), 1999.

[78] S.W. Jacobsz, J.R. Standing, R.J. Mair, K. Soga, T. Hagiwara, T. Sugiyama, "Tunneling effect on driven piles," *In: Proceedings of the International Conference on Response of buildings to excavation-induced ground movements*. Imperial College, CIRIA, London, pp. 1–15, 2001.

[79] E.O. Measor, and D.H. New, "The design and construction of the Royal Festival Hall." *South Bank. J. Instn Civ. Engrs* 36, 241–318, 1951.

[80] L.J. Benton, and A. Phillips, "The behaviour of two tunnels beneath a building on piled foundation." *Deformation of Soils and Displacements of Structures; Proc. 10th Eur. Conf. Soil Mech. Fdn Engng*, Florence, 2, 665–668, 1991.

[81] K.G. Higgins, I. Chudleigh, H.D. St John, and D.M. Potts, "An example of pile tunnel interaction problems." *Proc. Int. Symp. Geotech. Aspects of Underground Construction in Soft Ground, IS-Tokyo '99* (eds O. Kusakabe, K. Fujita and Y. Miyazaki), 99–103. Rotterdam: Balkema, 1999.

[82] I. Chudleigh, K.G. Higgins, H.D. St John, D.M. Pott, and F.C. Schroeder, "Pile-tunnel interaction problems," *Proc. of Tunnel Construction and Piling, London*, Great Britain, 172-185, 1999.

[83] T. Chapman, D. Nicholson, and D. Luby, "Use of the observational method for the construction of piles next to tunnels," *Proc. Int. Conf. Response of Buildings to Excavation Induced Ground Movements*, (ed F. M. Jardine) London: CIRIA, 2001.

[84] D. Parker, "Pinning hopes," *New Civil Engineer Supplement: Engineering the Millennium Dome*, 24 February, xiv–xv, 2000.

[85] J. Zou, Y. K. Chow, G. R. Dasari, C. F. Leung, and C. S. Ng, "Pile-soil-tunnel interaction in some layered soil profiles," pp. 1–4, 2002.

[86] F.C. Schroeder, *"The Influence of Bored Piles on Existing Tunnels*," A Thesis Submitted to the University of London for the Degree of Doctor of Philosophy and for the Diploma of the Imperial College of Science, Technology and Medicine, 2002.

[87] F. C. Schroeder, D. M. Potts, and T. I. Addenbrooke, "The influence of pile group loading on existing tunnels," *Géotechnique*, vol. 54, no. 6, pp. 351–362, 2004.

[88] K. Charoenpak, "Finite Element Analysis for Evaluating the Effects of Pile under Loading adjacent to Existing Tunnel," *Master Thesis, King Mongkut's University of Technology Thonburi, Thailand*, 2006.

[89] J. Yao, R. N. Taylor, and a M. Mcnamara, "The effects of loaded bored piles on existing tunnels," *Geotech. Asp. Undergr. Constr. Soft Gr. - 6th Int. Symp.*, no. 1988, pp. 735–741, 2008.

[90] M. Abdel-Meguid, R. K. Rowe, and K. Y. Lo, "3D Effects of surface construction over existing subway tunnels," *Int. J. Geomech.*, vol. 2, no. 4, pp. 447–469, 2002

[91] Zheng, T. Zhang, and Y. Diao, "Mechanism and countermeasures of preceding tunnel distortion induced by succeeding EPBS tunnelling in close proximity," *Comput. Geotech.*, vol. 66, pp. 53–65, 2015.

[92] M. Doležalová, "Tunnel complex unloaded by a deep excavation," *Comput. Geotech.*, vol. 28, no. 6–7, pp. 469–493, 2001.

[93] J. S. Sharma, A. M. Hefny, J. Zhao, and C. W. Chan, "Effect of large excavation on deformation of adjacent MRT tunnels," *Tunn. Undergr. Sp. Technol.*, vol. 16, no. 2, pp. 93–98, 2001.

[94] R. Chen, F. Meng, Z. Li, Y. Ye, and J. Ye, "Investigation of response of metro tunnels due to adjacent large excavation and protective measures in soft soils," *Tunn. Undergr. Sp. Technol.*, vol. 58, pp. 224–235, 2016.

[95] C. W. W. Ng, T. Boonyarak, and D. Masin, "Three-dimensional centrifuge and numerical modeling of the interaction between perpendicularly crossing tunnels," *Can. Geotech. J.*, vol. 50, no. 9, pp. 935–946, 2013.

[96] C. W. W. Ng, H. S. Sun, G. H. Lei, J. W. Shi, and D. Mašín, "Ability of three different soil constitutive models to predict a tunnel's response to basement excavation," *Can. Geotech. J.*, vol. 52, no. 11, pp. 1685–1698, 2015.

Chapter 3

Preliminary Analysis

3.1 Concepts and background

With the limitations of the study by Schoroeder et al. [1] as described in Section 2.5.3 of Chapter 2, many actual conditions cannot be reflected. In previous study, the soil condition was homogeneous and the pile tip position was much lower than that of the tunnel. However, in some situations where the foundations of a bridge approach or small buildings having varied lengths are constructed adjacent to the tunnel, e.g. as shown in Figure 3.1, the position of pile tips is close to that of the tunnel. To comprehensively investigate the conditions mentioned above, this chapter presents the preliminary analysis of the impacts of piles under loading on the subway tunnel of the Mass Rapid Transit Authority of Thailand in Bangkok using the 3D finite element method. The preliminary analysis focuses on the evaluation of the effect of relative position between the pile tip and tunnel on tunnel deformation. Moreover, the possible tunnel influence zone regarding to the adjacent pile is also preliminarily observed. The simple constitutive models and simulation techniques are adopted to investigate the responses of existing tunnel. The results show that the significant factors are the relative position of the pile tip with respect to the tunnel position as well as the soil type where the tunnel is located. In addition, a new influence zone for pile construction adjacent to the existing tunnel is tentatively proposed.

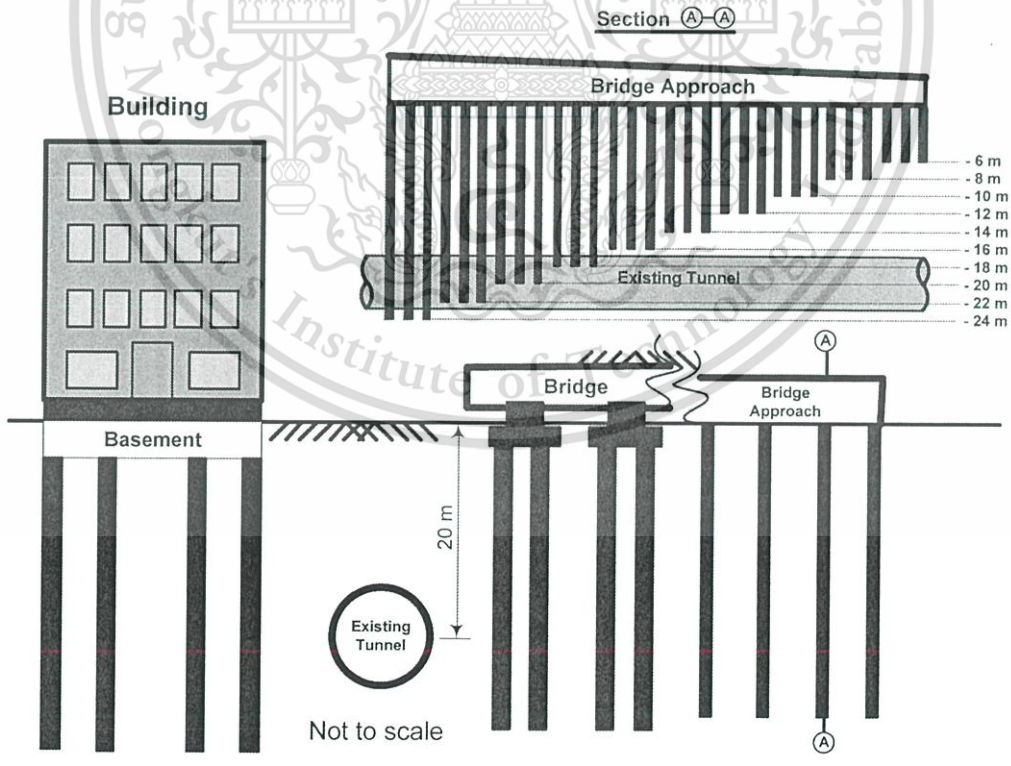

Figure 3.1 Pile foundations adjacent to existing tunnel.

3.2 Problem consideration

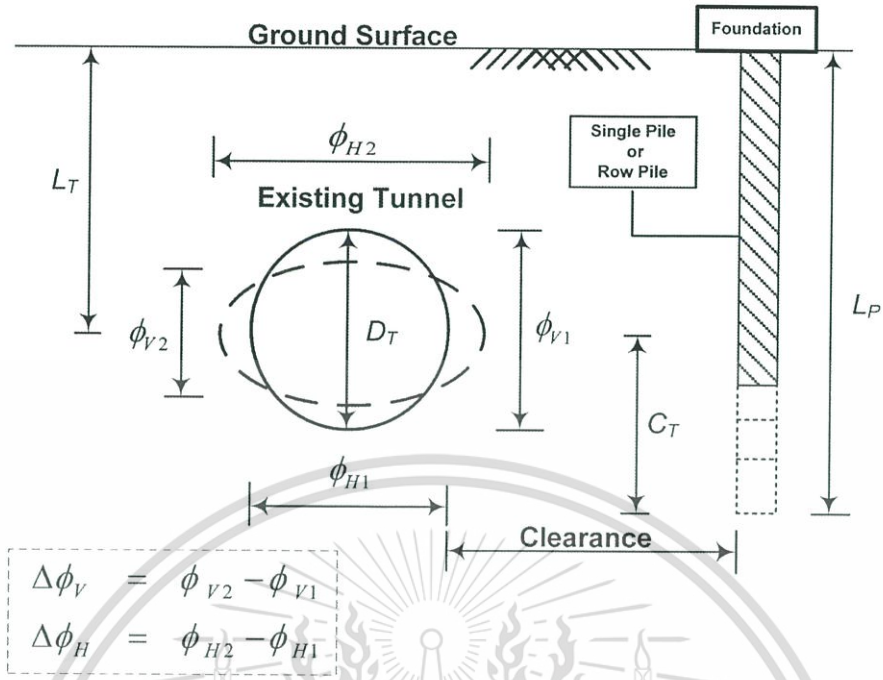

Figure 3.2 Illustration of piles under loading adjacent to an existing tunnel (D_T = tunnel diameter; L_T = tunnel depth; L_P = pile tip; C_T = vertical distance from centre of tunnel to pile tip; ϕ_H and ϕ_V = tunnel deformations).

The response of tunnel lining when subjected to pile loading, particularly in a single pile case, is principally a three-dimensional problem. The simulation of the effects of adjacent piles under loading on the tunnel was performed by means of a three-dimensional simulation using the finite element program ABAQUS [2]. The analysis consists of two parts: single pile and pile row under loading. The first part, single pile analysis, is to investigate the significance of pile tip position relative to the tunnel and of soil stratum in which the tunnel is located. The geometric parameters in the analysis are depicted in Figure 3.2. The thickness of the lining is 0.30 m. The outer tunnel diameter, D_T, of 6.3 m and the depth, L_T, of 20 m below the ground surface are fixed throughout the study. The position of the tip of the bored piles with the diameter of 1 m is varied over a range of 0.20-1.80 L_T to investigate its impact.

As shown in Figure 3.3, four cases of ground conditions in relation to the tunnel position are considered. Based on the soil profiles along the tunnel alignment and from the tunnel transition part to the ground level maintenance centre, the subsoil condition was varied to account for soft clay and stiff clay as shown in Figure 3.3. The piles were wished-in-place at the beginning of analysis. In the analysis, the piles were loaded to their working load, which depends on the pile length and soil condition, using a safety factor of 2.5 of their ultimate capacity, which was calculated based on the alpha method as mentioned in Section 2.4.2 of Chapter 2. From past experiences of a construction project in the UK, where the bored pile was successfully located at a distance of 3 m from the tunnel [3], a maximum clearance of 3.5 m (approximately 0.6 D_T) is adopted in this study.

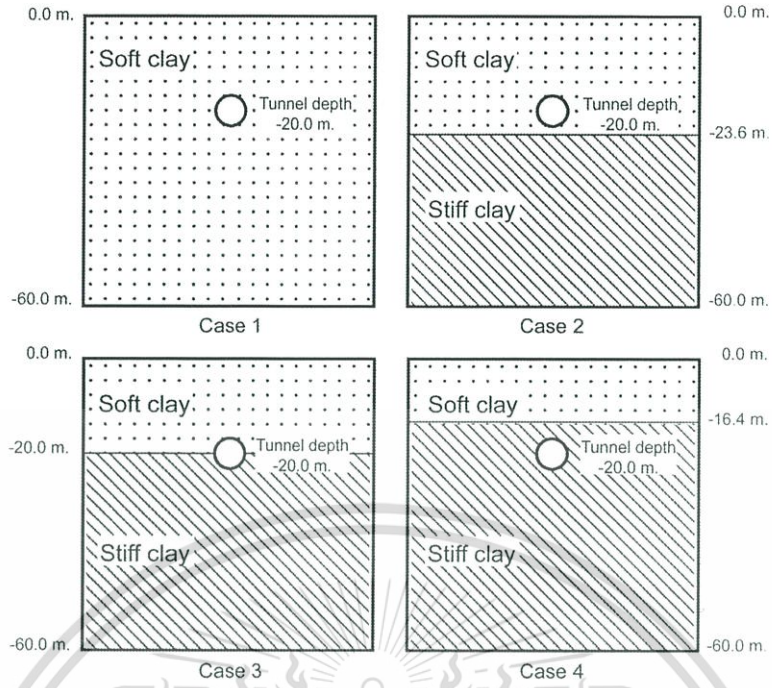

Figure 3.3 Soil profiles in this study.

3.3 Finite element analysis

3.3.1 Numerical model

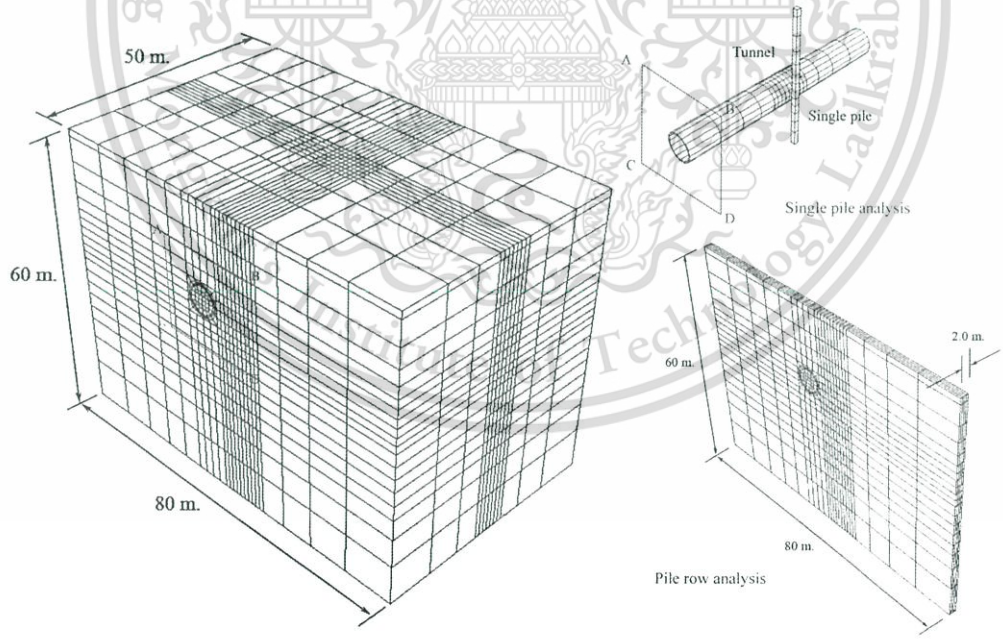

Figure 3.4 Finite element meshes for single-pile and pile-row cases.

The soil and piles were discretised into hexahedral (or brick) elements with a suitable aspect ratio. The shell elements were used to represent the tunnel lining. For the region of greater interest, finer discretisation mesh is used to obtain accurate solutions, especially in the tunnel lining and the zone between pile and tunnel. A tied interaction was assigned to the soil-pile and soil-lining interfaces to prevent the

relative displacement of adjacent nodes on the interfaces. Figure 3.4 shows examples of the analytical meshes for single-pile and pile-row problems. For the single-pile case, the dimension of the mesh is 50 m in the longitudinal direction, 60 m in the vertical direction and 80 m in the transverse direction. The mesh dimension of the pile row is similar to that of the single pile but with a thickness (in longitudinal direction) of 2.0 m. The pile is located on one side of the tunnel.

3.3.2 Material properties

Table 3.1 Material properties of tunnel lining and bored pile [5].

Young modulus of Concrete, E_c (kN/m^2)	Poisson's Ratio of concrete, ν_c	Unit weight of concrete, γ_c (kN/m^3)
3.1 x 10^7	0.20	24

Table 3.2 Geotechnical design parameters in MRT Project [5] and [6].

Soil layer	Weathered crust	Soft clay	1st Stiff clay	1st Dense sand	2nd Stiff clay	2nd Dense sand
Material model	Elastic	MC	MC	MC	MC	MC
k_0 (-)	0.60	0.75	0.85	0.80	0.80	0.80
E_u (kPa)	13500	6250	66000	-	82500	-
E' (kPa)	10800	5000	52800	110000	66000	150000
υ (-)	0.33	0.33	0.33	0.25	0.30	0.25
C_u (kPa)	-	20	120	-	120	-
C' (kPa)	5	5	5	0	5	0
ϕ (°)	25	20	26	36	26	36
γ (kN/m^3)	18	16.5	20.5	20	20	20
k (m/day)	0.08	0.0004	0.0009	0.08	0.0002	0.08
GS	2.70	2.75	2.75	2.65	2.65	2.70

The concrete bored pile and lining were assumed to be linearly elastic. For the soil, several recently developed advanced models such as the hardening soil [4] can reproduce the behaviour of soil under loading with a higher degree of satisfaction.

However, the Mohr-Coulomb model [2] is commonly used in current engineering practice due to its simplicity, with only five parameters being required. In this study, the observed values for the determination of influence zone are the changes in tunnel diameter. Therefore, the Mohr-Coulomb (MC) model is considered appropriate. The model parameters can be readily obtained from the literature [5, 6]. The parameters used in the analysis, including lateral earth pressure (k_0), undrained and drained Young's modulus (E_u , E'), undrained and drained shear strengths (C_u, C'), angle of friction (ϕ), unit weight of soil (γ), permeability (k) and specific gravity (GS), are garnered and listed in Tables 1 and 2. Note that the parameters for the hardening soil model for Bangkok subsoil can also be found in prior researches [e.g. 7, 8].

3.3.3 Analysis conditions

In the initial condition, the initial distributions of vertical effective stress and horizontal effective stress were controlled by the given soil unit weights and the coefficient of earth pressure at rest, k_0, for all strata. The bulk unit weight and k_0 of each soil layer were adopted from the MRT tunnel project [9]. The hydrostatic pore water pressure condition was considered to analyse in this study.

The displacement boundary condition was for performing the simulation in this study. The side and bottom boundaries were sufficiently extended from the area of greatest change in the model to avoid the boundary effect and minimise significant impacts on the analysis results. In the finite element model, the front and rear sides of the mesh were restrained against lateral movements but allowed for free vertical movement. Thus, no movement perpendicular to these sides was expected. Since the bottom of the mesh was fixed, there were no vertical and horizontal movements. These conditions were applied to all finite element meshes throughout the study.

Each analysis part was performed in 2 stages. The first involved the construction of the tunnel, which was simply modelled by consecutively removing the soil elements situated in the excavation zone and activating the tunnel lining with simultaneous application of pressure on the tunnel face to stabilise the excavation face. The excavation processes with Earth Pressure Balance (EPB) shield, i.e. shield elements, grouting pressure, and the hardening of grouting, are not simulated. Thus, the initial stresses in tunnel lining induced from the excavation processes are not considered. The second stage was the application of the pile axial loading, which was the design working load to a wished-in-place concrete pile. The undrained analysis was considered.

3.4 Analysis results

3.4.1 Single pile

Figure 3.5 illustrates the changes in tunnel diameters in vertical and horizontal directions for the single-pile case with a clearance of 0.5 m. The changes in tunnel diameter are normalised by the tunnel diameter (D_T) and plotted against the normalised depth of pile tip, L_P/L_T, for different cases (i.e. soil types). The normalised depth of tunnel position to tunnel diameter, C_T/D_T, is also provided in the y-axis on the right side. The negative and positive signs of magnitude in the x-axis denote a shortening and widening of the tunnel diameter respectively. It is clear from the Figure that, with identical clearance, the depth of the pile tip position relative to the tunnel has a strong influence on the tunnel deformations. The distribution patterns of

changes in tunnel diameter in both vertical ($\Delta\phi_V$) and horizontal ($\Delta\phi_H$) directions are very similar for all analysis cases. The tunnel deformations become large when the pile tip is situated in the range of *2 DT* above and *2 DT* underneath the tunnel axis. Note that the pile in each case (with different length and soil profile) is loaded with different working load. However, the magnitude of tunnel deformation is extremely large for the tunnel in soft clay despite the smallest working load (for the same pile length), whereas it becomes small for the tunnel in stiff clay. The pile tip position that induces the maximum change in tunnel diameter is the point above the tunnel crown by 0.5 *DT* to 1 *DT*. With regard to the pile tip position which induces the maximum tunnel deformation, it is found that this position is higher in stiffer soil than in softer soil. The maximum deformation occurs when the pile tip is embedded in the soft clay layer. The deformation rapidly decreases when the pile tip reaches the stiff clay layer underneath.

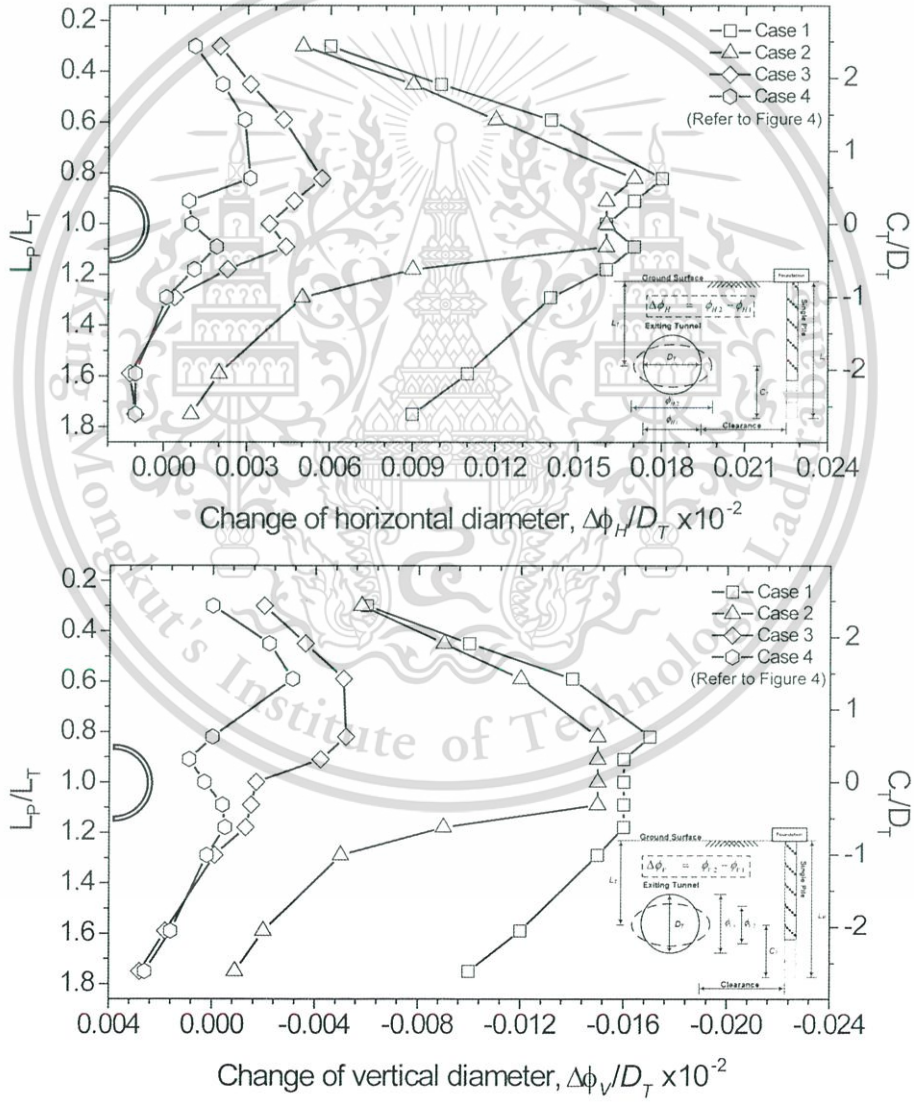

Figure 3.5 Impact of pile tip position relative to the tunnel and in relation to soil profile on the change in tunnel diameter for single pile (clearance 0.5 m).

The tunnel-pile interaction behaviour can be determined by interpreting the numerical results. When a pile is loaded, the force is transmitted to the soil along the

shaft and around the pile tip. This leads to an increase in stresses in soil. Simultaneously, the pile moves downward and causes the soil surrounding the pile to move. The soil movement interacts with the nearby existing tunnel and induces additional forces, stresses and displacements or distortion of the tunnel. The tunnel deformations by the pile tip located in soft clay are thus large due to large movements of the soil, as illustrated in Figure 3.6, which shows the distortion shapes by the same magnitude factor in the four cases of soil profile. The non-symmetric nature of the tunnel deformation can be observed. The tunnel diameter is reduced in the vertical direction and increased in the horizontal direction in all cases. The preliminary results of this part confirm that the position of the pile tip relative to the tunnel and the soil type in which the tunnel is located have a significant impact on the tunnel deformation. In engineering practice, the tunnel deformation induced by a pile row or pile group is regularly encountered and is more severe due to more load concentrations. Thus, further investigation is carried out in the next section.

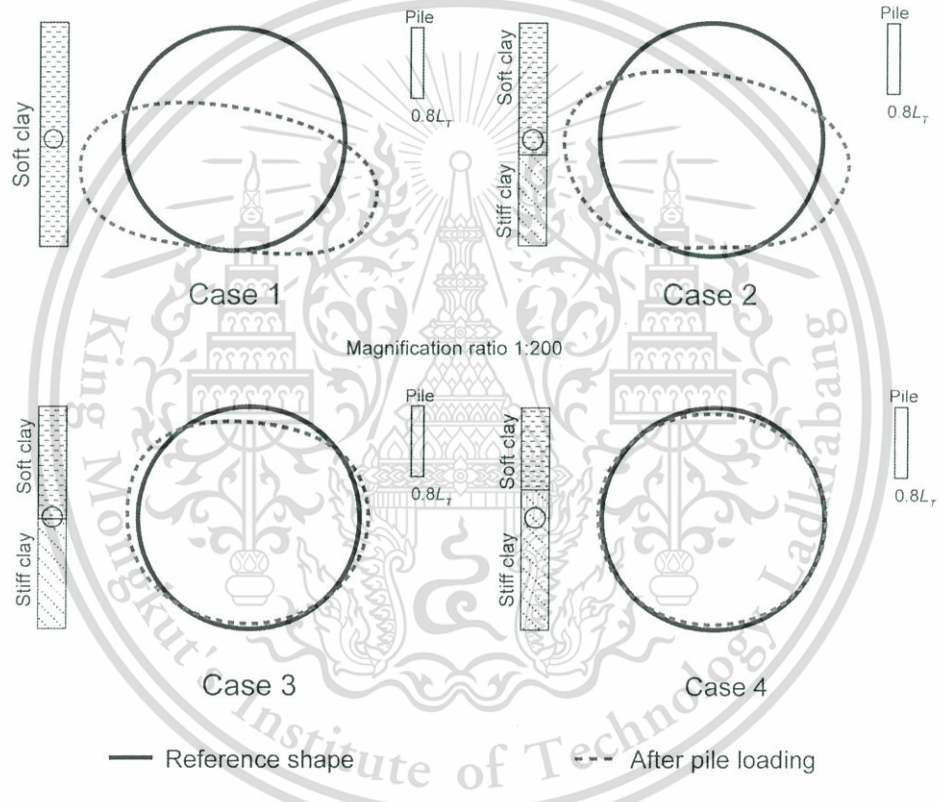

Figure 3.6 Tunnel distortions caused by pile under loading with the same pile tip position and clearance for four different cases of soil profile.

3.4.2 Row pile

Figure 3.7 illustrates the changes in tunnel diameter in the vertical ($\Delta\phi_V$) and horizontal ($\Delta\phi_H$) directions for the first case of soil profile (i.e. tunnel in soft clay) at various values of pile tip position and clearance. As seen in the Figure, the magnitude of $\Delta\phi_V$ and $\Delta\phi_H$ decreases when the clearance increases. The negative values indicate the shortening of tunnel diameter. For ease of understanding, absolute values are considered, so an 'increase' means that the absolute value becomes larger regardless of the sign. For the zone above the tunnel axis, $\Delta\phi_V$ increases with lower pile tip position. The increase rate of $\Delta\phi_V$ drastically changes when the pile tip position

reaches approximately 2.0 D_T (positive: above tunnel axis) and the maximum value occurs at a depth of about 0.80 L_T (for the clearance of 0.50 m and 1.50 m) before slightly decreasing with increasing pile length. When the pile tip is extended below the tunnel axis, $\Delta\phi_V$ gradually increases again. At the clearance of 3.50 m, $\Delta\phi_V$ continues increasing with deeper pile tip position. The maximum $\Delta\phi_V$ occurs when the pile tip (for all three cases of clearance) is at about 1.1 L_T. As the pile length increases, thereby extending its tip below 1.1 L_T, $\Delta\phi_V$ decreases significantly. The decrease rate of $\Delta\phi_V$ approaches zero when the pile tip reaches about -2.0 D_T (negative: beneath tunnel axis). To recap, $\Delta\phi_V$ becomes large when the pile tip is situated in the range of 2.0 D_T above and 2.0 D_T underneath the tunnel axis. For $\Delta\phi_H$, a similar tendency to that of $\Delta\phi_H$ can be observed and the magnitude is also similar. The area with large $\Delta\phi_H$, therefore, covers the range of 2.0 D_T above and 2.0 D_T underneath the tunnel axis as well.

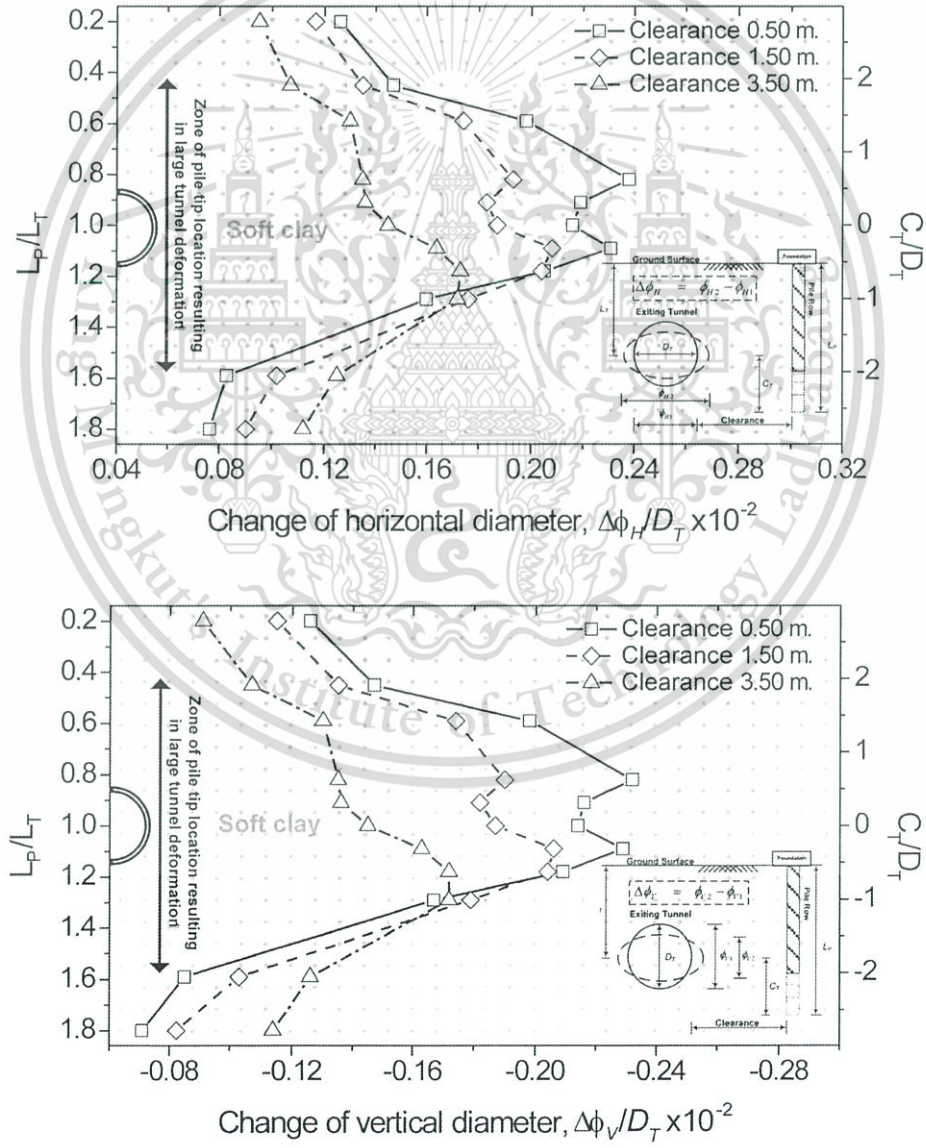

Figure 3.7 Impact of pile tip position relative to tunnel axis on the changes in tunnel diameter for tunnel in soft clay layer (case 1, Figure 3.3).

Investigating the three other cases of soil profile reveals that both the trend and magnitude of $\Delta\phi_V$ and $\Delta\phi_H$ are almost identical to one another, so only $\Delta\phi_V$ is shown for the three other cases. Figure 3.8 shows $\Delta\phi_V$ as a function of pile tip position for the tunnel in case 2 (Figure 3.3). Generally, the results are similar to case 1, where the tunnel is in soft clay, although the maximum values are lower. Besides, the level of pile tip at which $\Delta\phi_V$ rapidly decreases with increasing pile length is at the border between soft and stiff clays. Beneath this level, the rate of decrease for $\Delta\phi_V$ becomes noticeable. This implies that the existence of stiff layer underneath the tunnel could account for smaller tunnel deformations and a narrower influence zone. The zone with large tunnel deformations appears to cover a range from 2.0 D_T above the tunnel axis to the border between soft and stiff clays, which is 0.5 D_T.

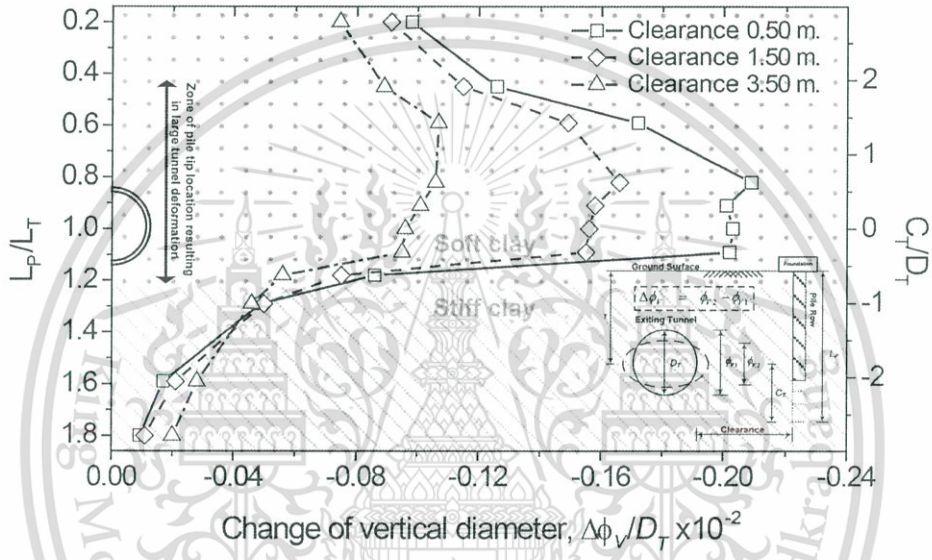

Figure 3.8 Changes in tunnel diameter in vertical direction subject to pile row loading with various pile tip positions for tunnel in case 2 (Figure 3.3).

The results for tunnel located between soft clay and stiff clay layers (case 3, Figure 4) are presented in Figure 3.9. The border between soft and stiff clays is set at the tunnel axis. For all three values of clearance, the values of $\Delta\phi_V$ are smaller than those from the two previous cases. In comparison to the previous cases, the maximum values are significantly smaller and occur when the pile tip is in soft clay at a higher level. Similar to case 2, the level of pile tip at which $\Delta\phi_V$ suddenly decreases with increasing pile length is at the border between soft and stiff clays. However, when the pile tip is extended below this level, which is stiff clay, $\Delta\phi_V$ slightly increases again for a certain depth before it gradually decreases with increasing pile length. This is probably because at that depth the piles have a larger working load (due to end bearing capacity) and their tips are at the same level as the tunnel axis.

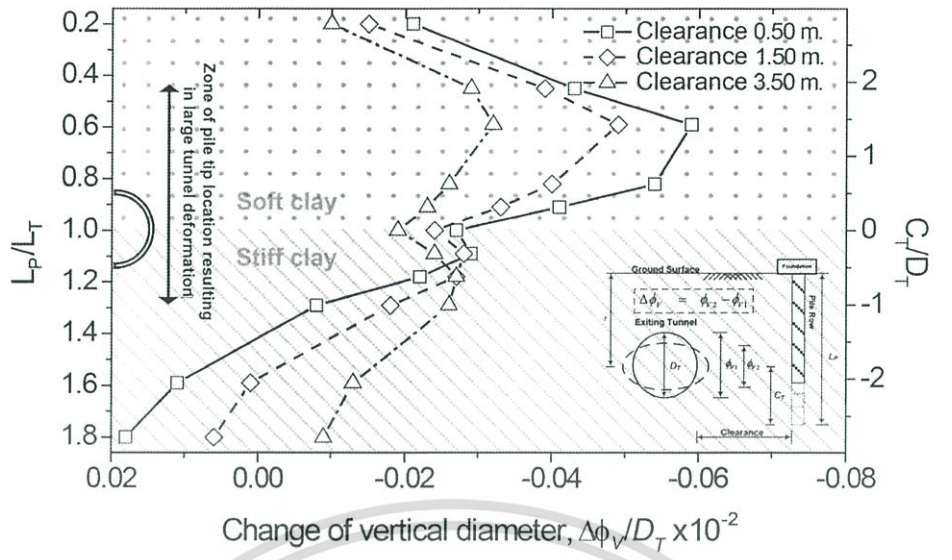

Figure 3.9 Changes in tunnel diameter in vertical direction subject to pile row loading with various pile tip positions for tunnel located between soft and stiff clays (case 3, Figure 3.3).

Figure 3.10 depicts the results for the case of the tunnel constructed in stiff clay (case 4, Figure 3.3). The tunnel deformations as well as their maximum values are smallest among the four cases in this study. The tunnel in stiff soil is thus safer than that in soft soil due to smaller soil movements in the tunnel vicinity. The maximum values still occur when the pile tip is in soft clay even with a small working load. Therefore, caution should be exercised in the construction of the bearing unit pile adjacent to the tunnel. When the pile tip is near the tunnel in stiff clay, $\Delta\phi_V$ increases again with a relatively higher value and longer range (compared to the previous case) after a large decrease at the clay border.

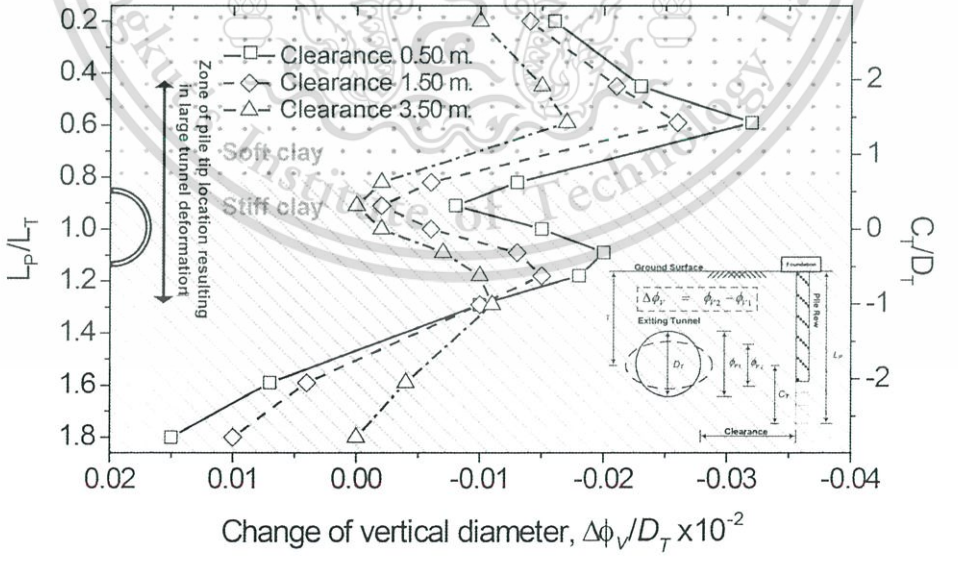

Figure 3.10 Changes in tunnel diameter in vertical direction subject to pile row loading with various pile tip positions for tunnel in stiff clay layer (case 4, Figure 3.3)

The numerical results have confirmed that the deformations of an existing tunnel caused by a pile-row loading are similar to those caused by a single-pile

loading, although the magnitude of the deformations in the former case is larger than in the latter. The deformations of the tunnel constructed in soft clay are much larger than in stiff clay and a large tunnel deformation occurs when the pile tip is close to the tunnel. The tunnel influence zone subject to nearby bored pile loading should therefore be determined by taking into account the relative position between the pile tip and the tunnel. The drastic changes of tunnel deformation are noticeable between about 2.0 D_T above and 2.0 D_T below the tunnel axis or down to the stiff layer, depending on the ground conditions, as listed in Table 3. For the horizontal clearance, a value of 0.6 D_T (approximately 3.5 m) from the tunnel surface seems to be sufficient.

Table 3.3 Significant influence zone from pile-row analyses.

Soil stratum	Significant influence zone	
	Change of vertical diameter	Change of horizontal diameter
Case 1	$2D_T$ - ($-2D_T$)	$2D_T$ - ($-2D_T$)
Case 2	$2D_T$ - ($-0.5D_T$)	$2D_T$ - ($-0.5D_T$)
Case 3	$2D_T$ - ($-1D_T$)	$2D_T$ - ($-1D_T$)
Case 4	$2D_T$ - ($-1D_T$)	$2D_T$ - ($-1D_T$)

A new influence zone for the existing tunnel subject to nearby piles can then be proposed as shown in Figure 3.11. By comparison with the previously used influence zones, the developed zone obtained in this study (shaded rectangular area in Figure 12) is much smaller. This increases the likelihood of new construction projects in the area near the tunnel alignment. However, the proposed influence zone is specified based on one specific tunnel (i.e. that of the MRTA) and one pile size (1 m). A broader set of data is required to enhance its reliability.

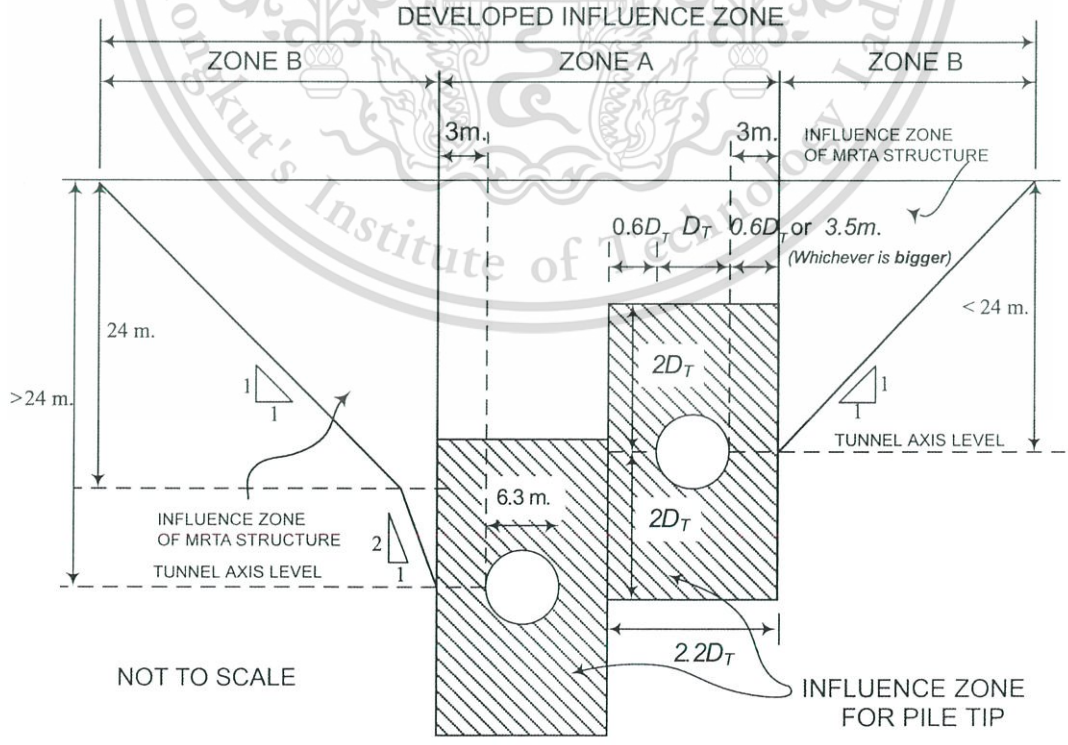

Figure 3.11 Developed tunnel influence zone from nearby pile tip position.

3.5 Summary

The position of pile tip in relation to the tunnel axis and the soil type in which the tunnel is situated have a significant impact on deformations of the existing tunnel. The numerically generated data and the consideration of the relative position of the pile tip can suggest a new influence zone. The following observations have been made from the study:

1. The tunnel deformations become drastically large when the pile tip is situated in a specific range, depending on the soil type in which the tunnel is situated. However, the ranges for the four different soil types hardly alter.

2. It is reasonable to recommend the range of 2.0 D_T above and 2.0 D_T underneath the tunnel centre as the influence zone.

3. For the horizontal clearance, the value of 0.6 D_T from tunnel surface seems to be sufficient.

4. By considering the lining deformation induced by the movement of soil surrounding the pile, the proposed influence zone is much smaller than the existing zone in which all construction activities are taken into consideration. The smaller zone increases the possibility of new construction projects in the area near the tunnel alignment.

However, as more complex behaviours in engineering practice, i.e. the excavation process of EPB shield, are excluded from this study. This exclusion is considered to validate the numerical model in future study, the descriptions will be presented in the next chapter. Moreover, further study on the correlation between pile settlement, pile force distribution and soil stress distribution around pile with lining deformation should enhance the understanding of this soil-structure interaction problem.

3.6 References

[1] F. C. Schroeder, D. M. Potts, and T. I. Addenbrooke, "The influence of pile group loading on existing tunnels," *Géotechnique*, vol. 54, no. 6, pp. 351–362, 2004.

[2] A. S. User, "Abaqus 6.3-1," *Dassault Systèmes Simulia Corp., Provid. RI, USA*, vol. Dassault S, 2008.

[3] I. Chudleigh, K.G. Higgins, H.D. St John, D.M. Pott, and F.C. Schroeder, "Pile-tunnel interaction problems," *Proc. of Tunnel Construction and Piling, London*, Great Britain, 172-185, 1999.

[4] T. Schanz, a Vermeer, and P. Bonnier, "The hardening soil model: formulation and verification," *Beyond 2000 Comput. Geotech. 10 years PLAXIS Int. Proc. Int. Symp. beyond 2000 Comput. Geotech. Amsterdam Netherlands 1820 March 1999*, p. 281, 1999.

[5] S. Timpong, "Analysis of ground movements in Bangkok MRT Blue Line project", *Master Thesis, Asian Institute of Technology*, Thailand, 2002.

[6] C. T. Tseng, "Three dimension simulation of EPB shield tunneling in Bangkok soft ground", *Master Thesis, Asian Institute of Technology, Thailand*, 2000.

[7] C. Surarak, S. Likitlersuang, D. Wanatowski, A. Balasubramaniam, E. Oh, and H. Guan, "Stiffness and strength parameters for hardening soil model of soft and stiff Bangkok clays," *Soils Found.*, vol. 52, no. 4, pp. 682–697, 2012.

[8] P. Jongpradist, T. Kaewsri, A. Sawatparnich, S. Suwansawat, S. Youwai, W. Kongkitkul, and J. Sunitsakul, "Development of tunneling influence zones for adjacent pile foundations by numerical analyses," *Tunn. Undergr. Sp. Technol.*, vol. 34, pp. 96–109, 2013.

[9] R. Prust, J. Davies, and S. Hu, "Part 6: Tunnels and Underground Structures: Pressuremeter Investigation for Mass Rapid Transit in Bangkok, Thailand," *Transp. Res. Rec. J. Transp. Res. Board*, vol. 1928, no. 1, pp. 205–217, 2005.

CHAPTER 4

Validation of Tunnelling Simulation Method

4.1 Background

Many simulation techniques of Tunnel Boring Machines (TBMs), which were described in Section 2.2 of Chapter 2, have been proposed depending on the assumptions used in the modelling. Therefore, the selection of tunnelling simulation method is essential to investigate the responses of the tunnel lining, especially the structural forces of tunnel lining. To reduce time consumption of the analysis, the structural elements which directly provide the lining forces are preferred. Thus, this chapter attempts to propose the innovative technique of EPB tunnelling simulation by using the shell elements as tunnel lining together with the grouting layer. In order to validate the proposed numerical model, the analysis results from the proposed method and the conventional one are compared and discussed in terms of ground deformation and lining forces together with the field measurement data. The results reveal that the simulation by the proposed method is sufficient and can reasonably reproduce the soil and lining responses.

4.2 Site description of tunnelling simulation

The geotechnical conditions of the Mass Rapid Transit Authority (MRTA) Blue Line Project is used for modelling in this study. The geotechnical conditions along the MRTA project can be separated into the North Tunnel section and the South Tunnel section. The soil profile is very uniform with soft clay underlain by stiff clay along the tunnel alignment in the North section. In this section, tunnelling with horizontal-twin tunnel is conducted mostly within the stiff clay layer. For the South section, most of the tunnel alignment is also located within a stiff clay layer [1]. The section CS-8B of the South section is chosen to simulate in this study as shown in Figure 4.1.

Geological conditions can be described as follows. The uppermost first layer consists of weathered crust or fill material. The second layer is the very soft clay layer overlaying on the first stiff clay. A thin seam of clayey sand is found below the first stiff clay as the fourth layer. The second stiff clay is found below the upper sand. Tunnel with inner and outer diameter of 5.7 m and 6.3 m, respectively, is located into the stiff clay layers at the depth of about 19 m from ground surface. A typical pore water pressure profile in Bangkok is a piezometric drawdown as shown in Figure 4.1. The pore water at the depth of about 20 m is almost zero and restored condition to hydrostatic pressure at the depth about lower than 20 m.

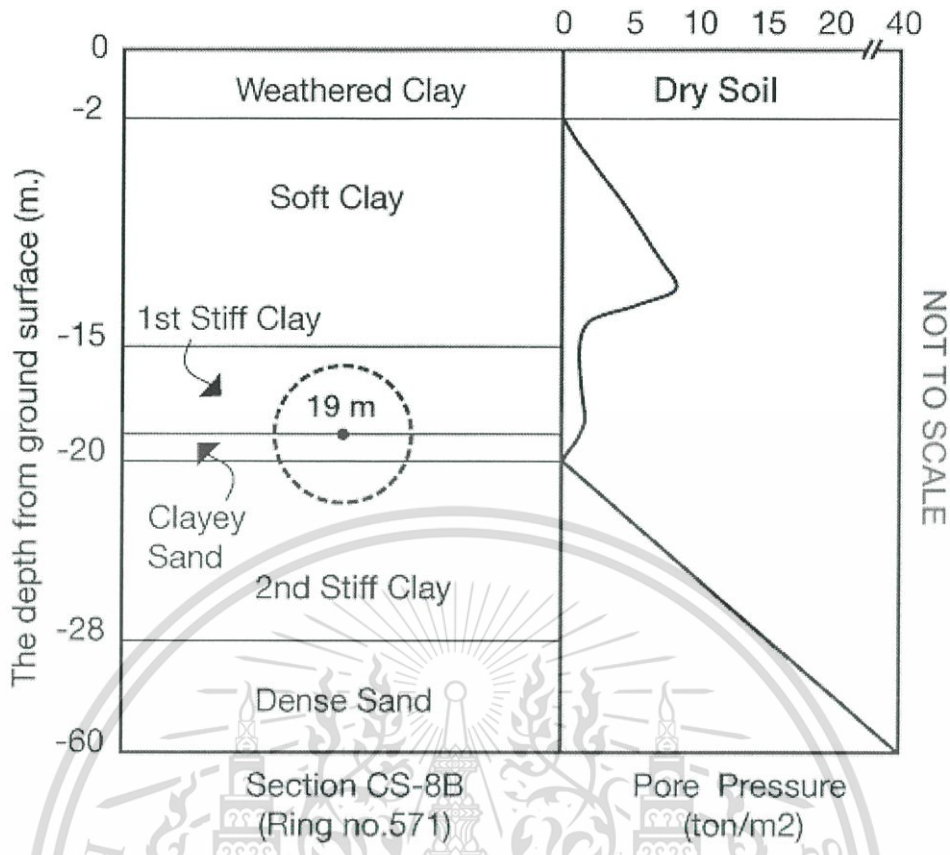

Figure 4.1 Soil profile and pore pressure of case study in MRTA Blue Line Project.

4.3 Finite element analysis

4.3.1 Numerical model

The 3D FE mesh presenting the sample case of the proposed method (the final method) is depicted in Figure 4.2. The soil layers were discretized into the six-node bricks or the solid elements with a suitable aspect ratio. The simulation of tunnel components consisted of three layers, EPB shield layer, grouting layer and tunnel lining layer. The four-node shell elements were used to model the tunnel lining and EPB shield. The hardened grouting layer was simulated by the solid elements. Their information will be detailed in next section.

Previous study on three-dimensional analysis of TBM tunnelling [2] indicated that a lateral distance of $4D_T$ from the tunnel axis and the advancement of $4DT$ ahead and behind the tunnel excavation face are sufficient for 3D-FE mesh of tunnelling problem. Thus, the distance of $5D_T$ ahead and behind the monitoring section, and of $6D_T$ in lateral direction from the tunnel axis, are enough to fully simulate the tunnelling problem in this study. The dimension of model is 80 m ($\approx 12.5D_T$) in the transverse direction, 60 m ($\approx 9.5DT$) in the longitudinal and vertical directions. D_T is the outer diameter of a tunnel lining. At centre of longitudinal direction is the monitoring section. The PLAXIS 3D 2013.1 software [3] was implemented for mesh generation and analysis.

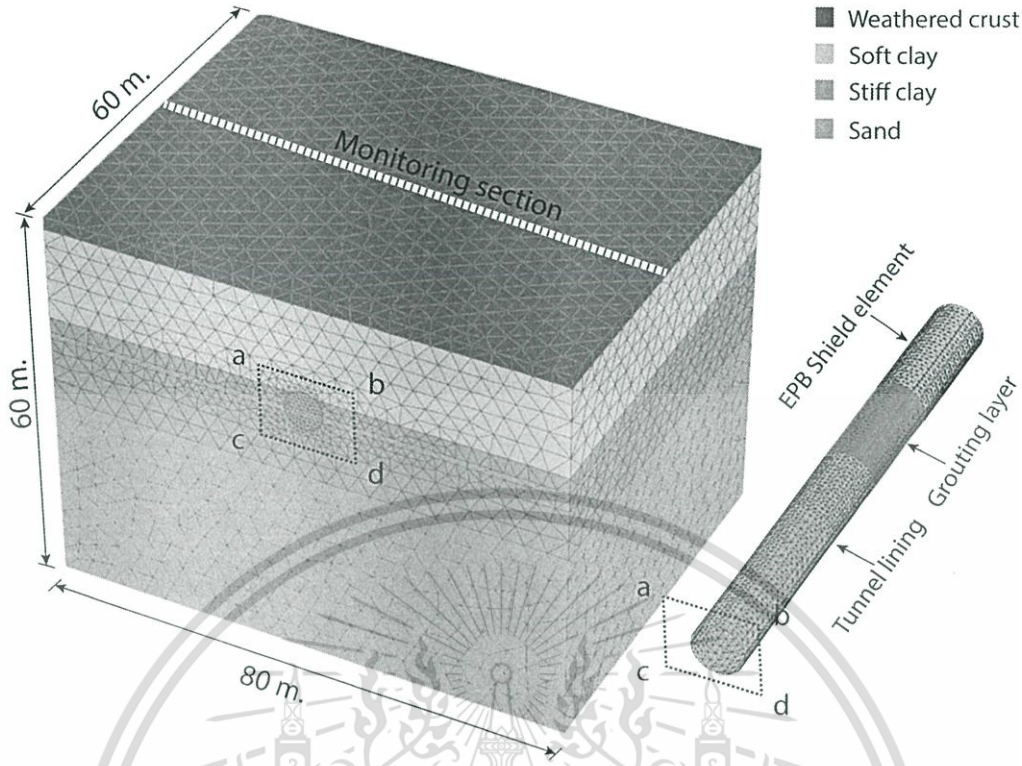

Figure 4.2 The mesh in FE model (the proposed method).

4.3.2 Analysis conditions

The initial distribution of vertical effective stress and horizontal effective stress are controlled by the given soil unit weight, the coefficient of earth pressure at rest, K_0, for all strata. The pore water pressure was generated in the whole geometry domain as piezometric drawdown. The undrained analysis was considered.

The displacement boundary was adopted in this study. The sides of the mesh including the front side and rear side are restrained against lateral movements but free to move vertically. Therefore, no movement perpendicular to their side of meshes is allowed. The bottom of the mesh is fixed (no vertical and horizontal movements). These conditions were used for all finite element meshes throughout this study.

4.3.3 Material properties

The properties of soils are determined from the MRTA projects [4]. The soil layers, stiff and soft clays, were assumed by hardening soil model (HS) [5]. The Mohr-Coulomb model (MC) was assumed to represent the weathered clay and sand layer. The soil properties in this study are calibrated from field testing data [6] and testing data of previous studies as shown in Table 4.1. *1 **Poisson's ratio for Mohr Coulomb model**

*2 Poisson's ratio for Hardening Soils model

Table 4.2 shows the properties of the components of EPBS tunneling simulation. The EPB shield, tunnel lining and grouting layer were assumed to be linear elastic. The properties of grouting layer at 28 days of curing are obtained from Kasper and Meschke [7] and Kasper and Meschke [8] while those of EPBS are acquired from Katebi et al. [9].

Table 4.1 Soil parameters for modelling [6].

Soil layer	Weathered crust	Soft clay	Stiff clay	Sand
Material model	Mohr Coulomb	Hardening Soils (HS) model		Mohr Coulomb
E' (kPa)	6,000	-	-	80,000
E_{oed}^{ref} (kPa)	-	5,000	63,158	-
E_{50}^{ref} (kPa)	-	5,000	63,158	-
E_{ur}^{ref} (kPa)	-	15,000	189,474	-
γ_{sat} (kN/m^3)	17	16	18	20
υ^{*1}, υ_{ur}^{*2} (-)	0.32	0.20	0.20	0.30
ϕ' (°)	22	22	22	36
c' (kPa)	8	5	18	0
m (-)	-	1	1	-
p_{ref} (kPa)	-	100	100	-

*1 Poisson's ratio for Mohr Coulomb model
*2 Poisson's ratio for Hardening Soils model

Table 4.2 Material properties of EPB shield, tunnel lining and grouting layer.

EPB Elements	Young modulus [E] (kN/m^2)	Poisson's ratio [υ] (-)	Unit weight [γ] (kN/m^3)
Tunnel lining	31 x 10^6	0.20	24
EPB shield	21 x 10^7	0.28	78
Grouting layer	1 x 10^6	0.30	21

4.3.4 Earth Pressure Balance Shield (EPBS) advancement and simulation procedures

The tunnelling process of EPBS was simulated using a step-by-step approach. Each excavation step corresponded to an advancement of the tunnel face of 1.2 m which is equal to the width of the tunnel lining. A simplified geometry of EPBS as cylindrical shape is assumed in steading of modelling the original cone shape. The schematic of simulated process with EPBS was shown in Figure 4.3. The simulation process can be described as follows.

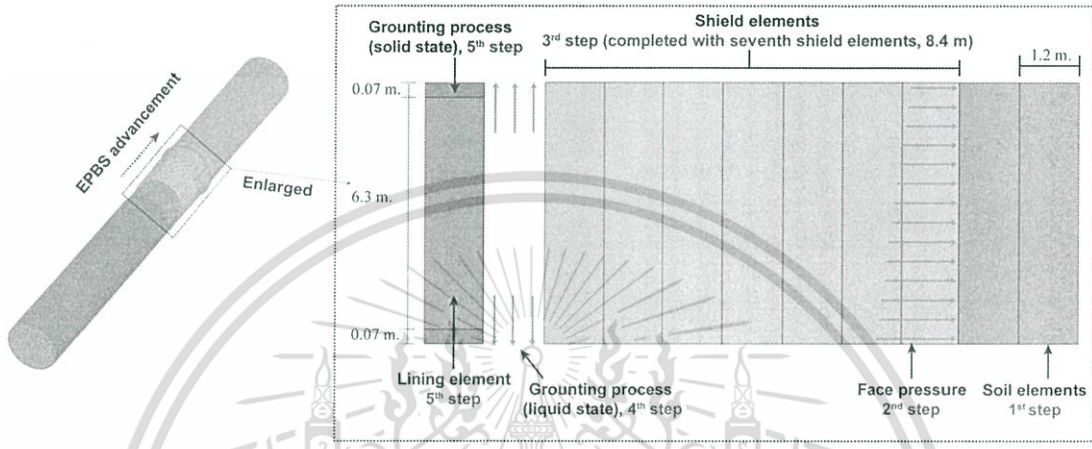

Figure 4.3 Schematic illustration of the process of tunnelling simulation in 3D-FE.

Step 1, the soil elements in the targeted excavation zone were deactivated. When over cutting is not considered, the dimension in radial direction equals to the outer radius of lining (6.30/2 m in this study) for case of using solid elements and shell elements with grouting layer. This can be larger when the shield driving quality (over cutting and pitching-yawing) is taken into consideration. The support of excavation face was modelled by applying a pressure distribution with linear increase of pressure with depth in step 2. The face pressure in this study is about 150 to 200 kPa at crown and invert of tunnel, respectively [1]. The shell elements were activated to represent the EPB shield with contraction ratio of 0.4% in step 3, which was calibrated from the previous FE analysis of tunnelling projects in Bangkok subsoil. These procedures were repeated until the advancement of shield was completed with seventh rings for the length of about 8.4 m in longitudinal direction. Step 4, the simulation of tail void grouting in a first phase, the grout has not yet fully hardened, the liquid state of grouting was simulated by applying a radial pressure with 200 kPa [1] acting on soil around tunnel. The simulation of tunnelling process in steps 1 and 2 follows ones recommended by manual of PLAXIS 2013.1 [3]. Step 3, the tail void grouting in a second phase is considered to be hardened, the grouting layer was simulated by the solid elements. Step 4, the shell or solid elements representing the tunnel lining were activated in the same grouting layer section. These steps, 4 and 5, are differed for the simulation by each method in this study. The details are described in next section.

4.3.5 Patterns of Simulation Method

Three simulation methods of EPBS tunnelling with different modelling techniques are carried out in this study. The main differences are the techniques to

simulate the tunnel lining and grouting layer section as schematically shown in Figure 4.4.

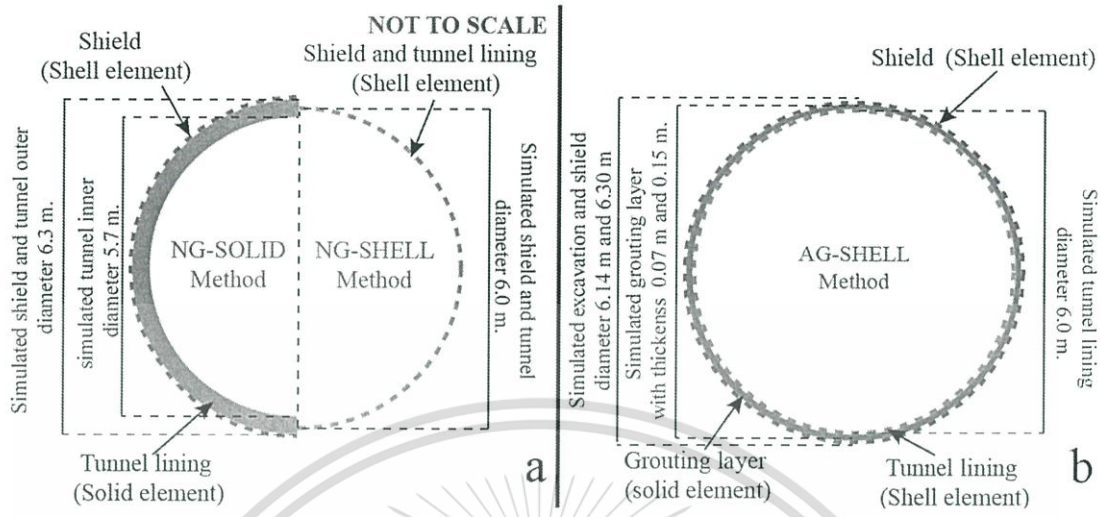

Figure 4.4 The cross sections of simulation patterns.

In the first method that is called "NG-SOLID method", the tunnel linings are modelled by the solid elements with thickness of 0.30 m. The step 3 of simulation procedures is not considered in this method. The second method, that is called "NG-SHELL method", is similar to the first method. The shell elements are represented to simulate the tunnel lining and the geometry of simulation is thus different. The difference between using the solid or shell elements is that the geometry of thin shell element is modelled as zero-thick line at mid plane. Thus, the diameter of excavated soil periphery in this modelling is 6.0 m which is the same as shield diameter. The details of two simulation methods are depicted in Figure 4.4a.

For the method proposed in this study, the shell elements were used to represent the tunnel lining together with introduction of the grouting layer, that is called "AG-SHELL method". The thicknesses of grouting layer considered in this study are 0.07 m and 0.15 m to represent ideal TBM driving and effect from over cutting together with pitching-and-yawing, respectively. The diameter of excavated soil periphery in each model is thus as 6.14 m and 6.30 m respectively. The grouting layer of 0.07 m which is equal to the thickness of EPBS in the case that the pitching angle of excavation process and over cutting of EPBS are not considered. In other words, the thickness of grouting layer is a theoretical tail-void gap. To take the effect of over cutting and pitching angle into consideration, grouting layer of 0.15 m, which is average value of tail void gap during shield excavation as reported by Babendererde [10], is chosen. The schematic cross section of AG-SHELL method is depicted in Figure 4.4b.

4.4 Analysis results

The results in terms of surface settlement and lining forces from the three simulation methods are compared and discussed together with the measurement data if available. The observations of FE analysis results are carried out after the process of tunnelling simulation is completed.

4.4.1 Surface settlement

Figure 4.5 shows the surface settlement profiles compared between FE analyses and MRTA monitoring data in section CS-8B [1]. The surface settlement profiles analysed by FEM are similar in shape but quantitatively different. The surface settlement profile of the NG-SOLID method is noticeably deeper than that obtained from the NG-SHELL method. It is clear that the selection of simulation method significantly affects the nature of the computed surface settlements. The difference of the surface settlement profiles may be presumed to be associated with properties of the elements or the excavated cavity of tunnelling. Although the excavated cavity of NG-SOLID is larger than that of the AG-SHELL method with grouting thickness of 0.07 m (the $AG_{0.07}$-SHELL method), the surface settlement profile of the $AG_{0.07}$-SHELL method is close to that of the NG-SOLID and the MRTA monitoring data. Moreover, when increasing the grouting thickness to 0.15 m (the $AG_{0.15}$-SHELL method), the surface settlement becomes larger than that of the NG-SOLID. This implies that the quality of TBM shield control during excavation (due to over cutting and pitching-and-yawing of TBM) can be reflected by varying the thickness of the grouting layer.

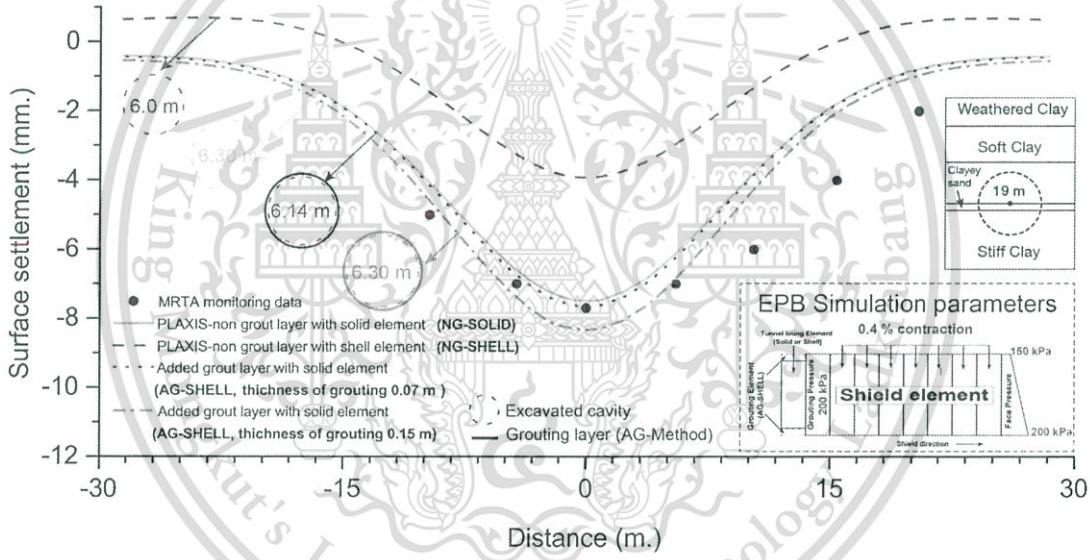

Figure 4.5 Comparing transverse settlement profile from MTRA section CS-8B with FEM analyses.

4.4.2 Induced structural forces in the circumferential direction due to tunnelling

The comparison of the computed structural forces in the tunnel lining for three simulation methods is presented hereafter. The structural forces of the tunnel lining in circumferential direction are plotted from the reference lining ring located at the mid-section of the model.

1) The bending moment

Figure 4.6 shows the computed bending moments resulted by the three simulation methods. From this figure, the significant differences of the computed bending moments are revealed. Especially, the distribution of the computed bending moments by the NG-SHELL method is drastically different with those by the others.

The computed bending moment of tunnelling simulation located in soft clay (K_0 < 1.0) is positive values at the spring line and negative values at crown and invert.

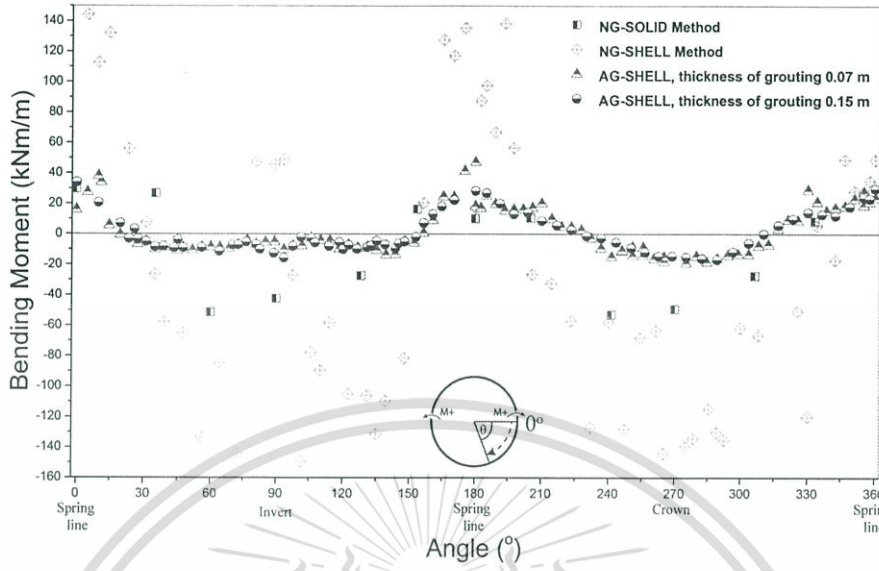

Figure 4.6 The computed bending moment in linings for three different methods.

This behaviour is obtained by NG-SOLID and AG-SHELL methods. Although the trends of the computed bending moments for NG-SOLID and AG-SHELL methods are similar, the magnitudes are different. However, the ranges of magnitude of computed bending moment obtained from the NG-SOLID and AG-SHELL methods are close to those reported in the previous studies [11], [12]. For the AG-SHELL method, although the excavated cavity of the $AG_{0.15}$-SHELL method is larger than the $AG_{0.07}$-SHELL method, their computed bending moments are close.

2) The axial force

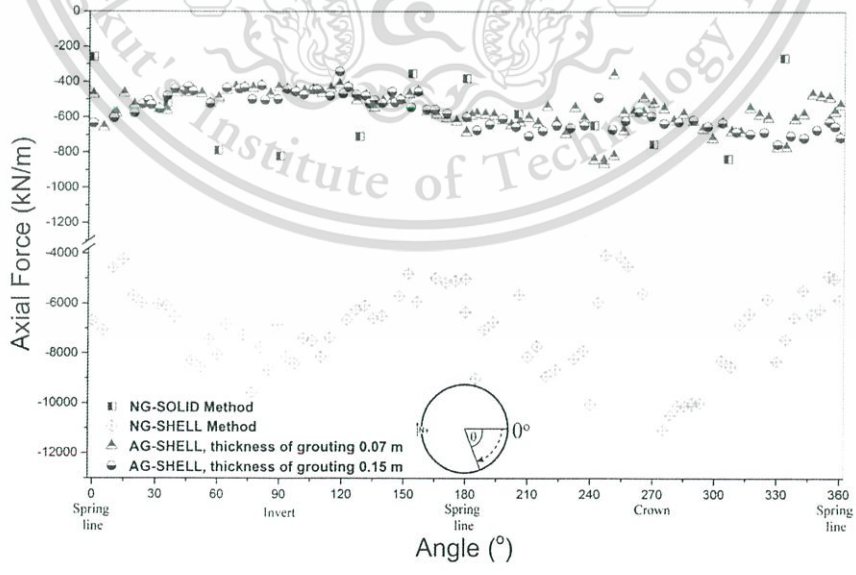

Figure 4.7 The computed axial force in linings for three different methods.

Figure 4.7 depicts the computed axial forces resulted by three simulation methods. The tendency of the computed axial forces is similar to the computed

bending moments. The computed axial forces of the NG-SOLID method and both of AG-SHELL methods are in the same range. This range agrees well with the previous researches [11], [12], which should be in the range of 0 to 1000 kN/m. In contrast, the distribution of the computed axial forces by the NG-SHELL method becomes differed and the magnitudes are much higher.

For the AG-SHELL methods, although the excavated cavity of $AG_{0.15}$-SHELL method is larger than $AG_{0.07}$-SHELL method, their computed bending moments and axial forces are close. This indicates that the grouting layer with greater thickness can absorb more stress transmitted from the soil. Consequently, the induced structural forces become smaller.

Recapitulating, the above described results of using the shell elements alone to model the tunnel lining in tunnelling simulation cannot provide satisfaction in terms of both the surface settlement and the structural forces. This drawback can be solved by introduction of grouting layer proposed in this study. Although the simulated thickness of grouting layer obtained from real construction may provide more accurate results, the ideal thickness of grouting layer which is equal to the thickness of TBM can be satisfactorily used in the simulation.

4.5 Summary

In this study, the modelling of tunnel lining with the shell elements together with the grouting layer in tunnelling analysis by TBM in soft ground was proposed. The grouting is modelled as pressure boundary and solid elements in liquid and solid states, respectively. By the proposed method, grouting process and actual excavated boundary of the soil can then be realistically modelled. Analysis of tunnel excavation using the proposed method in conjunction to 4 main factors (face pressure, shield element, grouting process and lining element), provides good agreement with results from the conventional method and field measurement data. Besides, the structural forces obtained from the current method are in ranges of history records.

4.6 References

[1] S. Suwansawat, "Earth Pressure Balance (EPB) Shield Tunneling in Bangkok: Ground Response and Prediction of Surface Settlements Using Artificial Neural Networks", Ph.D. Thesis, Massachusetts Institute of Technology, USA, 2002.

[2] H. Mroueh and I. Shahrour, "A simplified 3D model for tunnel construction using tunnel boring machines," *Tunn. Undergr. Sp. Technol.*, vol. 23, no. 1, pp. 38–45, 2008.

[3] R. Brinkgreve., E., Engin, W. Swolfs, "*PLAXIS 3D Version 2013 manual*," Chapman, 2013.

[4] P. Jongpradist, T. Kaewsri, A. Sawatparnich, S. Suwansawat, S. Youwai, W. Kongkitkul, and J. Sunitsakul, "Development of tunneling influence zones for adjacent pile foundations by numerical analyses," *Tunn. Undergr. Sp. Technol.*, vol. 34, pp. 96–109, 2013.

[5] T. Schanz, a Vermeer, and P. Bonnier, "The hardening soil model: formulation and verification," *Beyond 2000 Comput. Geotech. 10 years PLAXIS Int. Proc. Int. Symp. beyond 2000 Comput. Geotech. Amsterdam Netherlands 1820 March 1999*, p. 281, 1999.

[6] R. Prust, J. Davies, and S. Hu, "Part 6: Tunnels and Underground Structures: Pressuremeter Investigation for Mass Rapid Transit in Bangkok, Thailand," *Transp. Res. Rec. J. Transp. Res. Board*, vol. 1928, no. 1, pp. 205–217, 2005.

[7] T. Kasper and G. Meschke, "A 3D finite element simulation model for TBM tunnelling in soft ground," *Int. J. Numer. Anal. Methods Geomech.*, vol. 28, no. 14, pp. 1441–1460, 2004.

[8] T. Kasper and G. Meschke, "A numerical study of the effect of soil and grout material properties and cover depth in shield tunnelling," *Comput. Geotech.*, vol. 33, no. 4–5, pp. 234–247, 2006.

[9] H. Katebi, A. H. Rezaei, M. Hajialilue-Bonab, and A. Tarifard, "Assessment the influence of ground stratification, tunnel and surface buildings specifications on shield tunnel lining loads (by FEM)," *Tunn. Undergr. Sp. Technol.*, vol. 49, pp. 67–78, 2015.

[10] S. Babendererde, "Underground Construction in Germany 2000", chapter Verpressen der Schildschwanzfuge hinter einer Tunnelvortriebsmaschine mit T¨ ubbingausbau, STUVA, DAUB, pp. 113–116, 2000.

[11] Working Group No. 2, ITA, "Guidelines for the Design of Shield Tunnel Lining," Elsevier Science Ltd: Published, 2000.

[12] S. Moller, "Tunnel Induced Settlements and Structural Forces in Linings," 2006.

Chapter 5
Tunnel Deformations due to Adjacent Loaded Pile and Their Mechanisms

5.1 Background

To establish a preventive measure in the design stage, a proper assessment method for the impacts of an adjacent pile under loading on a tunnel and an understanding of pile-soil-tunnel interaction are essential. In Chapter 3, by observing the dependence of the changes of the tunnel diameter in the horizontal and vertical directions on the relative position of the pile tip with respect to the tunnel position (Figure 3.3), a new influence zone for pile construction adjacent to an existing tunnel can be tentatively suggested as illustrated in Figure 3.12. However, there are studies concerning the impacts on tunnels due to adjacent constructions such as new subway tunnels and deep excavation stages as described in Chapter 2 with references no. 89-93. Generally, soil excavation or tunnelling causes a release of in situ stress and thus soil displacement [1] - [3], which inevitably exerts an influence on existing tunnels. Construction at only one side of the tunnel imposes unsymmetrical stress relief and movement on the existing tunnel. Considering the tunnel deformation, it is revealed that the deformed tunnel is not an elliptical shape whose major axis aligns with the horizontal or vertical axis. This indicated that for the problem of loaded piles on a single side of an existing tunnel (which is a common situation), the changes in the tunnel diameter in the horizontal and vertical directions as used in Chapter 3 seems to be unsuitable to represent the tunnel deformation. The assessment of tunnel deformation based on changes of the tunnel diameter in the horizontal and vertical directions is thus inappropriate in this situation. This chapter has a goal of understanding the pile-soil-tunnel interaction mechanism for the tunnel response due to an adjacent pile under loading based on analysed data with consideration of various influence factors. The data are obtained from a large number of tunnel responses generated from the Finite Element Analysis (FEA) of selected cases with advanced constitutive soil model. The analysis results begin with exploring the assessment of tunnel deformation following the method used in Chapter 3 and the shape of deformed tunnels before emphasizing the necessity of a more suitable assessment method. A new assessment method is proposed based on the concept of out-of-roundness. A reassessment of tunnel deformation is performed using the proposed method to highlight its efficiency. Furthermore, supplemental analyses of pile loading simulations are performed to provide an explanation of the mechanism behind the pile-soil-tunnel interaction.

5.2 Characteristics of the case studies

The characteristics of the Mass Rapid Transit Authority (MRTA) tunnel project in Bangkok subsoil as described in the chapter 3 are considered in this study. The existing tunnel with an outer diameter, D_T, of 6.3 m, a lining thicknesses of 0.3 m and a depth, L_T, of 20 m below the ground surface is fixed throughout this study. The more considering of the case studies in this chapter are the lengths and clearances of 1 m diameter bored pile. The pile tips are varied over a range of 3.0 D_T above to 4.0 D_T below the tunnel spring line to investigate their impact and the clearances of 0.5, 1.5,

3.5 and 4.5m are considered. The clearance is herein defined as the distance between the edge of the tunnel lining and the closer edge of the bored pile. A schematic diagram of the different pile tip positions (indicating the different pile lengths and their clearances) considered in this study compared to the outer tunnel diameter (D_T) is illustrated in Figure 5.1.

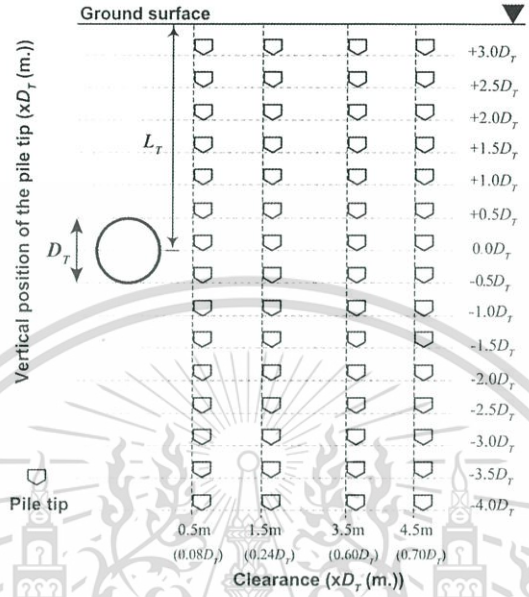

Figure 5.1 Illustration of pile tip positions and geometrical parameters.

In engineering practice, the tunnel alignment is preferably located in a stiff clay layer. A previous study [4] also indicated that a tunnel situated in the soft clay layer, referred to as the tunnel transition section, exhibits the largest deformation due to an adjacent pile under loading. Figure 5.2 shows two ground conditions with regard to the tunnel position, considered as the case studies. The tunnel depth is fixed at 20 m for comparison. A typical pore water pressure profile in Bangkok is a piezometric drawdown, as depicted in the figure.

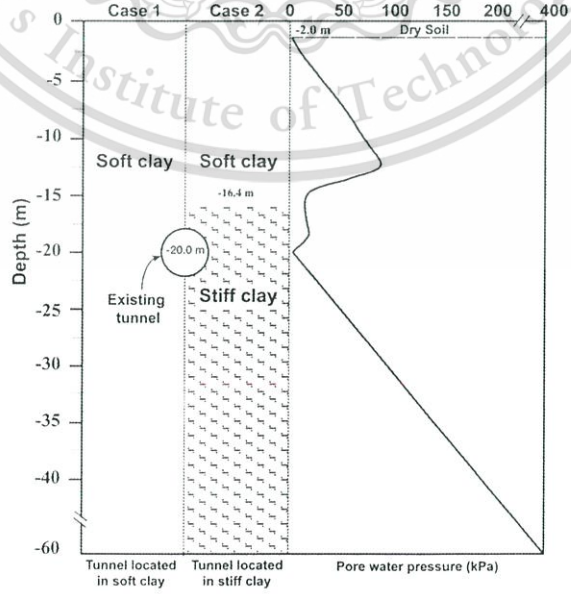

Figure 5.2 Soil profiles and ground water conditions considered in this study.

5.3 Finite element analysis

The FE analyses include two parts. The first part is the investigation of the effects of loaded pile on the tunnel deformation whose results are presented in the next Section 5.4.1-5.4.4. The latter part is the pile loading simulation to observe the pile-soil interaction mechanism as described in Section 5.4.5. The details of simulation method, meshing, analysis conditions, material properties and simulation process are described below.

5.3.1 Finite element mesh

Series of finite element analyses were carried out using the 3D FE method with reasonable soil models and assumptions. An example of 3D FE mesh (for the tunnel constructed in stiff clay) indicating the relevant geometry, soil profile and element discretization is illustrated in Figure 5.3. The boundary size of FE model for tunnelling simulation is sufficiently extended from the area of the extreme change in the model to avoid the boundary effect and minimize significant effects on the analysis results. Previous study on three dimensional analyses of TBM tunnelling [5] indicated that a lateral distance of 4.0 D_T from the tunnel axis and the advancement of 4.0 D_T ahead and behind the tunnel excavation face are sufficient for 3D FE mesh of tunnelling problem. Thus, the advancements of about 5.0 D_T ahead and behind the monitoring section, and of 6.0 D_T in lateral direction from the tunnel axis, are enough to fully model the tunnelling problem for this study. The dimension of FE mesh is 60 m (≈9.5 D_T) in the vertical and longitudinal directions and 80m (≈12.5 D_T) in the transverse direction. The monitoring section is at the centre of longitudinal direction. The soil stratum and bored pile were discretized into the 10-node tetrahedral elements or the volume elements. The six-node triangular plate elements were used to simulate the tunnel lining.

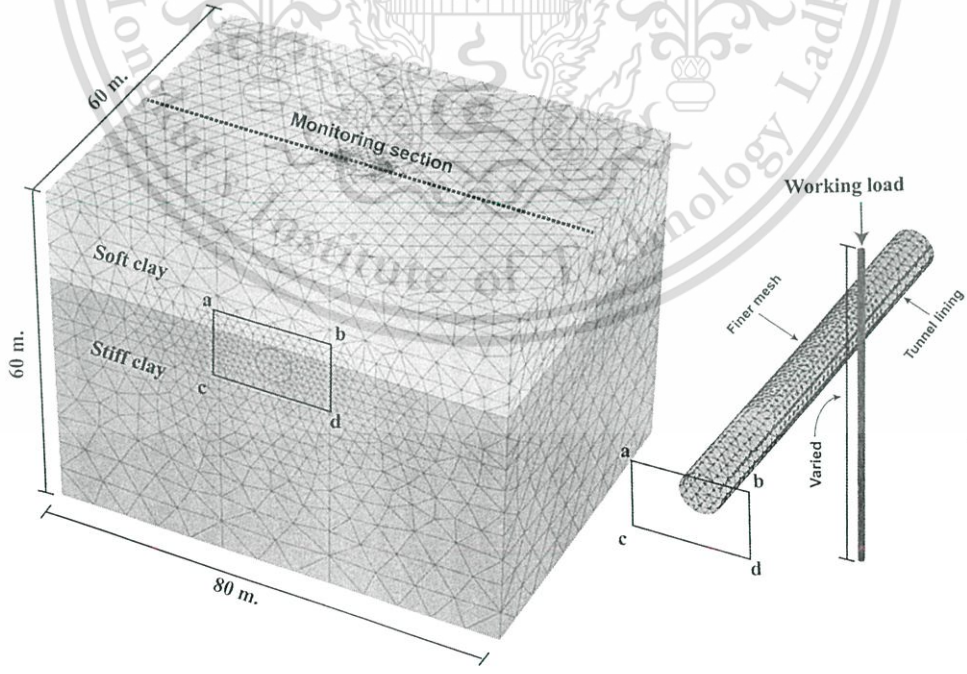

Figure 5.3 Finite element mesh for the tunnel constructed in stiff clay.

For the region of greater interest where severe plastic strains are expected to develop, especially in the zone between pile and tunnel, finer discretization mesh with

suitable aspect ratio is used to accommodate the accuracy of the solutions. The PLAXIS 3D (version 2013) software was implemented for mesh generation and analysis [6]. For modelling the tunnel lining, some recent researches (e.g., Ye et al., 2014 [7]; Kavvadas et al., 2017 [8]) revealed that considering as segmental concrete pieces bolted together provides more realistic tunnel deformation shape, particularly, the local deformation at the joints. However, the global tunnel deformation shape is not much affected. In this study, the observed values are the changes in tunnel diameter and tunnel global distortion, modelling as continuous lining commonly used in current engineering practice is considered appropriate.

5.3.2 Constitutive model and material properties

Advanced soil constitutive models were used to simulate in this study. The Hardening Soil (HS) model assumed to be elasto-plastic with stress dependent stiffness and shear dilatancy properties [9] was employed to simulate the soil element as soft and stiff clay layers. The material parameters for Bangkok subsoil were determined from correlating local investigated data with in situ tests of MRTA projects [10] and previous laboratory testing data. Before implementing in previous work [11] – [13], the validations have been performed with measured data of tunnel excavations, deep excavations and pile load tests [14].

Table 5.1 Soil model parameters [14].

Soil layer	Soft clay	Stiff clay
Material model	Hardening Soils (HS) model	
E_{oed}^{ref} (kPa)	5,000	63,158
E_{50}^{ref} (kPa)	5,000	63,158
E_{ur}^{ref} (-)	15,000	189,474
γ_{sat} (kN/m^3)	16	18
υ' (kPa)	0.2	0.2
ϕ' (°)	22	22
c (kN/m^3)	5	18
m (m/day)	1	1
p_{ref}	100	100

Table 5.2 Material properties of the bore pile and tunnel lining [11].

Structural elements	Young modulus $[E]$ (kN/m^2)	Poisson's ratio $[\upsilon_C]$ (-)	Unit weight $[\gamma_C]$ (kN/m^3)
Tunnel lining	31 x 10^6	0.20	24
Bored pile	31 x 10^6	0.20	24

The concrete lining and bored pile were assumed to be a linear elastic material model. The material parameters used in the numerical analyses are summarized in Table 5.1 and Table 5.2. The value of interface friction (R_{inter}) between the surrounding soil and structural elements (EPB, tunnel lining or bored piles) was chosen to be 0.9 in this study [6].

5.3.3 Analysis conditions

The initial stress conditions, vertical effective stress and horizontal effective stress, were controlled by given soil unit weight and the coefficient of earth pressure at rest, K_0, for all strata and the piezometric drawdown of pore water pressure was also generated in the whole domain. With regard to the hydraulic boundary conditions, a no-flow condition was assigned and the undrained analysis was considered. The pore water pressures on all sides of boundaries are assumed to be constant throughout the analysis at the original groundwater (the piezometric drawdown). The displacement boundary condition was adopted in this study. The lateral boundaries of the mesh were restrained against lateral movements but allowed for vertical movements. Thus, no movement perpendicular to their sides is allowed. The bottom boundary is fixed (no vertical and horizontal movements). These conditions were applied to all finite element models throughout the study.

5.3.4 Numerical procedure

The simulation process for the investigation of the responses of the tunnel lining due to a loaded pile was divided into two stages. The first stage is the simulation of the tunnelling process with the Earth Pressure Balance (EPB) shield method proposed in Chapter 4. The second stage concerns the application of the pile axial loading, which is the predetermined working load. The wished-in-place pile is modelled in the analysis.

5.4 The assessment of tunnel lining deformation due to an adjacent loaded pile

5.4.1 The changes in tunnel diameter in the vertical and horizontal directions

The changes in the tunnel diameter in the vertical ($\Delta\phi_V$) and horizontal ($\Delta\phi_H$) directions (as suggested by Schroeder et al. (2004) [15] and followed by Lueprasert et al. (2015) [4]; the assessment method was schematically shown in Figure 3.3, in the

Chapter 3) are investigated in this section. Normalized $\Delta\phi_V$ and $\Delta\phi_H$ (with D_T) for the tunnel located in soft clay (Figure 5.2, case 1) against various normalized depths of the pile tip (L_P/L_T) and clearance are illustrated in Figure 5.4. The normalized positions of the pile tip beneath the tunnel spring line to the tunnel diameter, C_T/D_T, are also provided on the right side of the y-axis. The positive and negative signs denote the positions of the pile tip located above or below the tunnel spring line, respectively. In addition, the deformed shapes (for the case with a clearance of 0.5 m) with a magnification ratio of 1:3000 and the parameters to assess the change of tunnel diameter are illustrated in the figure. The negative and positive signs of magnitude in the x-axis denote a shortening and a widening of the tunnel diameter, respectively. It is seen in the figure that, in most situations considered in this study, the tunnel diameter shortens in the vertical direction and widens in the horizontal direction. The exception is when the pile tip is located between the tunnel crown and the invert at the farthest clearances (3.5 and 4.5 m in this study).

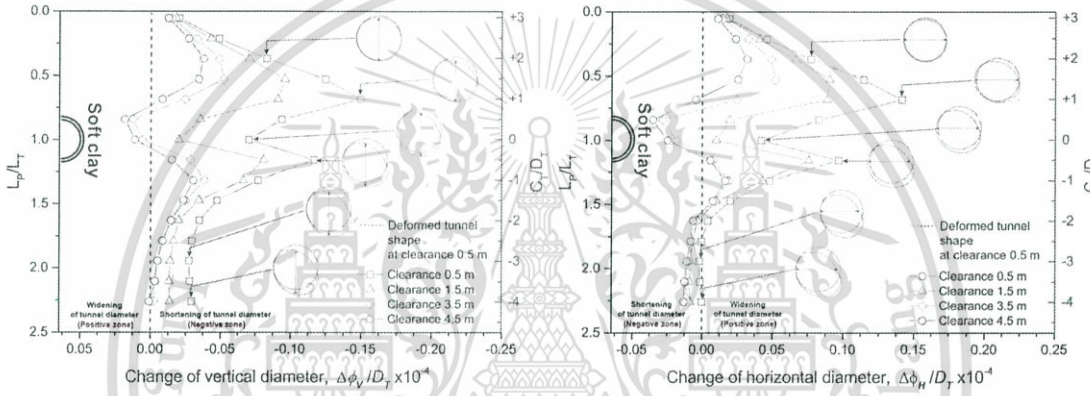

Figure 5.4 Impact of the pile tip position relative to the tunnel axis on the changes in tunnel diameter for a tunnel in a soft clay layer; (a) $\Delta\phi_V$ and (b) $\Delta\phi_H$.

As seen in Figure 5.4, the distribution patterns along the soil depth of changes in the tunnel diameter in both the vertical ($\Delta\phi_V$) and horizontal ($\Delta\phi_H$) directions are very similar for all clearances. Nevertheless, the absolute values of $\Delta\phi_V$ and $\Delta\phi_H$ decrease with increasing clearance. The values of the cases with clearances of 3.5 m and 4.5 m are very close. Therefore, the $\Delta\phi_V$ and $\Delta\phi_H$ for the clearances of 0.5 m and 1.5 m are described in detail. For ease of understanding, the absolute values (not considering − (shortening) or + (widening)) are considered, so an 'increase' means the absolute value is becoming larger, regardless of the sign. The $\Delta\phi_V$ and $\Delta\phi_H$ gradually increase with a lower pile tip position, and the maximum value occurs when the pile tip is at a depth of +1.0 D_T (positive: above the tunnel spring line). Then, the $\Delta\phi_V$ and $\Delta\phi_H$ gradually decrease with increasing pile length before increasing again when the pile tip is located at the tunnel spring line (0.0 D_T). When the pile tip is extended below −0.5 D_T (negative: beneath the tunnel spring line), the $\Delta\phi_V$ and $\Delta\phi_H$ decrease significantly before approaching certain values with extending pile tip from −2.0 D_T to −4.0 D_T. The $\Delta\phi_H$ for all clearances becomes a negative value (shortening).

The investigation of another case of the soil profile reveals that both the trend and magnitude of $\Delta\phi_V$ and $\Delta\phi_H$ are almost identical to each other, so only the results for $\Delta\phi_H$ are shown. The normalized $\Delta\phi_H$ values for the case of the tunnel located in

stiff clay (Figure 5.2, case 2) against various normalized depths of the pile tip and clearance are illustrated in Figure 5.5. The changes in tunnel diameter are smaller than those of the case of the tunnel located in soft clay. The distribution patterns of $\Delta\phi_H$ for cases with various clearances are similar. For the pile tip position in soft clay (+3.0 D_T to +1.0 D_T), the $\Delta\phi_H$ gradually increases as the lining widens (positive value) with increasing pile length. With continually increasing pile length, the $\Delta\phi_H$ abruptly decreases. The values become negative (shortening), and the maximum negative value is exhibited when the pile tip is located at a depth in the range between the tunnel crown and the spring line level, depending on the clearance. The $\Delta\phi_H$ then temporarily returns to an additional widening behaviour (the total behaviour still remains as shortening except for the case with a clearance of 0.5 m) when the pile tip extends to the invert level. Beneath this level, the $\Delta\phi_H$ returns to an additional shortening behaviour before approaching an approximately certain value with increasing pile length.

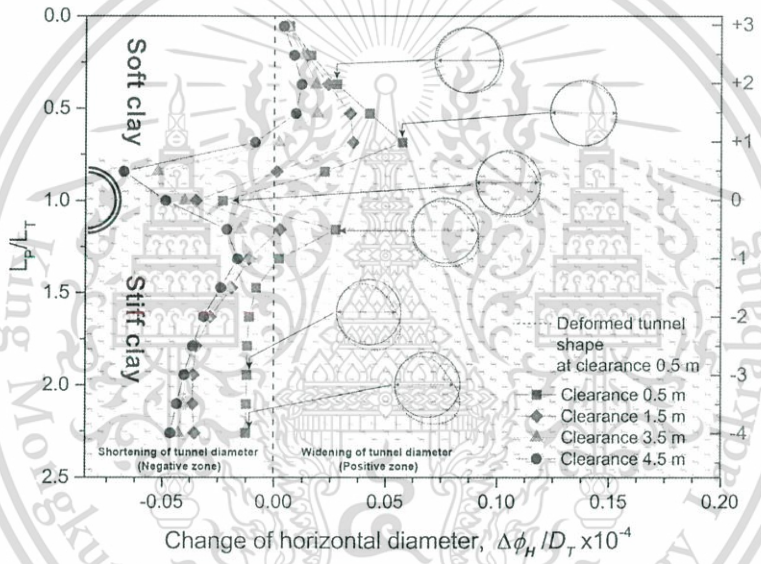

Figure 5.5 Impact of the pile tip position relative to the tunnel axis on the changes in tunnel diameter (horizontal direction, $\Delta\phi_H$) for a tunnel in a soft clay layer.

The results in terms of changes in tunnel diameter in both the vertical ($\Delta\phi_V$) and horizontal ($\Delta\phi_H$) directions investigated in this study are consistent with the findings in preliminary analysis (the chapter 3) based on the same case. The pile tip position with respect to the tunnel has a strong influence on the tunnel deformations. The maximum deformation occurs when the pile tip is close to the crown of the tunnel (+1.0 D_T). The change rate of tunnel deformation gradually decreases when the pile tip is located below the invert of the tunnel to the deepest level considered in the study (−4.0 D_T). The results of the study imply that caution should be exercised in the construction of a pile whose pile tip is located 2 D_T above and 2 D_T beneath the spring line, as indicated in the proposed influence zone as mentioned in the chapter 3. However, this conclusion seems to be inconsistent with the distorted shapes of the tunnel lining shown in Figure 5.4 and Figure 5.5.

To provide a suitable assessment of the changes in the tunnel diameter, the clearly illustrated shapes of tunnel deformations due to adjacent pile loading with various pile lengths are further observed. It is also suggested from the obtained results that the changes in tunnel diameter from the influence of the pile tip for a tunnel constructed in soft clay are much larger than those in stiff clay. This indicates that the tunnel in stiff soil should thus be safer than that in soft soil because of smaller tunnel deformations.

5.4.2 The shapes of the tunnel lining affected by various pile tip positions of the loaded pile

The deformation evolutions of the circular shaped lining due to adjacent pile loading for both cases with a clearance of 0.5 m are illustrated in Figure 5.6 and Figure 5.7. Note that deformation due to the construction process is not considered. The unsymmetrical nature of the global movement and a distortion to the pile can be observed clearly in both cases. In the previous study of Schroeder et al., (2004) [15], the global movement of the tunnel in terms of only crown settlement was investigated. In this study, the observation points for the global movement are specified as the reference nodes at the crown, both sides of the spring line and the invert of the tunnel lining to provide a better understanding. The deformed shapes of the tunnel lining based on various tip positions of the adjacent loaded pile are illustrated in Figure 5.6 and Figure 5.7 for cases of tunnels located in soft clay and stiff clay, respectively.

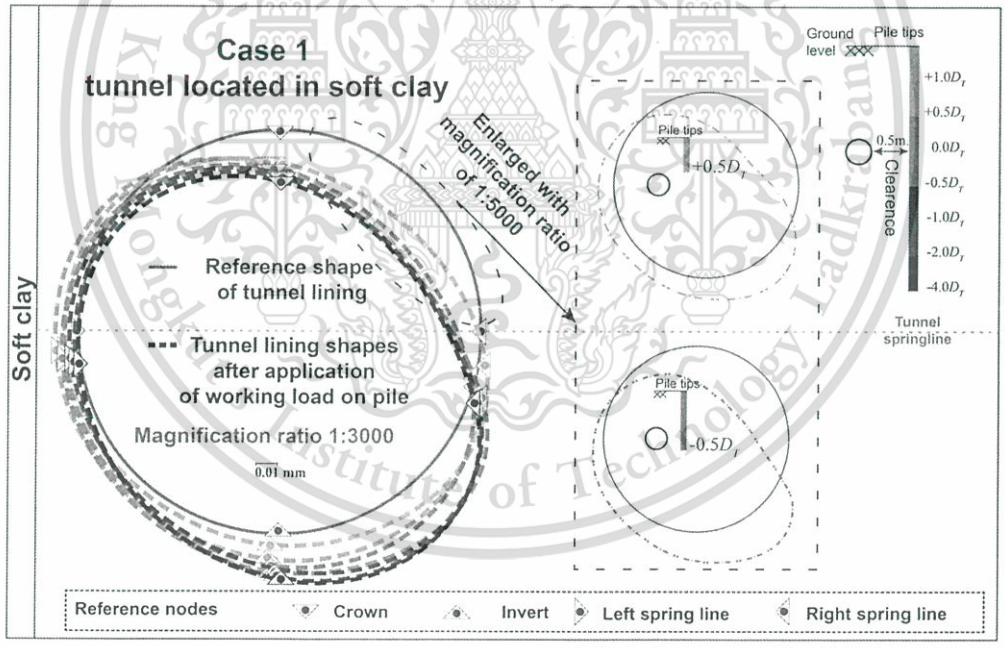

Figure 5.6 The deformed shapes of the tunnel lining due to a pile under loading with various tips for the tunnel located in soft clay.

As seen in Figure 5.6, the crown of the tunnel noticeably moves downward and outward from the pile when the pile tip is located above the tunnel spring line (the blue and green circles). When the pile tip extends below the tunnel spring line, only a small increment of downward movement of the crown is observed. The movement towards the pile is also noted with increasing pile length. Similarly, the downward movement of the tunnel invert can be observed, but with a smaller magnitude when the pile tip is located above the tunnel spring line. However, with increasing pile length at which the tip is below the tunnel spring line, the invert moves downward and

towards the pile with a large movement increment. When the pile tip is at −4.0 D_T, the magnitude of the invert movement becomes approximately the same as that of the crown.

By contrast, the tunnel spring line on the side closer to the pile moves downward and towards the pile when the pile tip is located above the tunnel spring line (the blue and green circles). When the pile tip is below the spring line level, it moves downward and outward towards the pile, but with a smaller movement increment. The movement of the tunnel spring line at the side far of the pile is comparatively smaller. This results in the tunnel lining becoming distorted into a shape such as a kidney or ellipse shape with the major axis inclined with respect to the horizontal axis, indicating that the maximum tunnel lining deformation is along neither the horizontal nor vertical axis. Moreover, it can be seen that the length of the major axis becomes longer with increasing pile length in the range of the study. To clearly observe the shape of the deformed tunnel lining, the enlarged shapes with a magnification ratio of 1:5000 for cases where the pile tips are located above (+0.5 D_T) and below (−0.5 D_T) the spring line are depicted in the figure. It can be seen that the distorted shapes of the tunnel lining are kidney and ellipse shapes when the pile tips are located above and below the spring line, respectively.

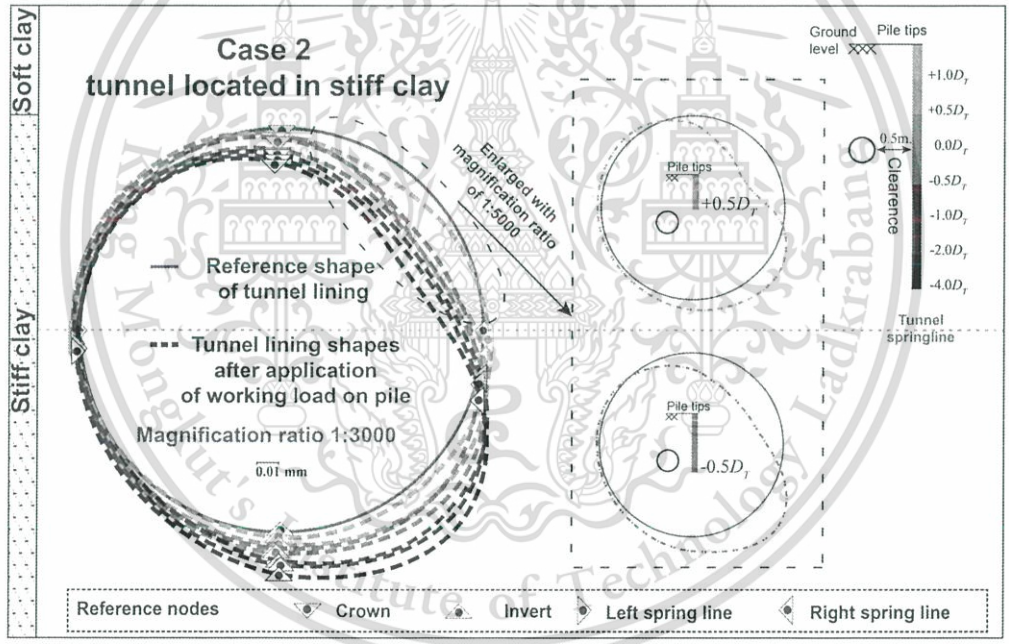

Figure 5.7 The deformed shapes of the tunnel lining due to a pile under loading with various tips for the tunnel located in stiff clay.

For the case of a tunnel in stiff clay (Figure 5.7), global movement behaviour similar to that in the case of the tunnel in soft clay can be observed. Two main differences are observed. First, a smaller movement increment occurs when the pile tip is located above the tunnel spring line; however, a larger movement increment is noted with increasing pile length (the pile tip under the spring line). When the pile tip extends to −4.0 D_T, the deformation of the tunnel in stiff clay becomes equal to or larger than that of the tunnel in soft clay. Note that the magnitude of the pile load in the case of a tunnel in stiff clay is larger than that of the tunnel in soft clay for the same pile tip. This indicates that a tunnel in stiff clay can suffer impacts from the adjacent loaded pile to the same degree or larger compared to the tunnel in soft clay. The degree of impact depends not only on the soil condition where the tunnel is

situated but also on the magnitude of the load applied to the pile. The second difference is that the movements of the crown, invert and spring line on the side closer to the pile are downward and always outward from the pile. A much smaller movement is seen for the spring line on the side farther from the pile.

As described above, the major axis of the deformed lining does not align in the horizontal and vertical directions. Therefore, the use of parameters $\Delta\phi_V$ and $\Delta\phi_H$ is no longer suitable for assessing the tunnel deformation in this situation.

5.4.3 Proposal of an assessment method for tracing the behaviour of a deformed tunnel

A suitable assessment method for tracing the maximum deformation of a tunnel lining in terms of the changes in tunnel diameter (in the case of an adjacent bored pile located on one side of the existing tunnel) is proposed. In the case of a circular section of shell structures (e.g., pipelines, tanks, and steel lining), the unsymmetrical distortion of structure shapes is generally assessed by the out-of-roundness in various design codes, e.g., the Eurocode 3 [16]. The out-of-roundness is defined in terms of parameters including the maximum, minimum, and nominal diameters of a deformed structure. Therefore, the assessment method in terms of the maximum extension change ($\Delta\phi_{E-MAX}$) and the maximum contraction change ($\Delta\phi_{C-MAX}$) in tunnel diameter inferred from the out-of-roundness are proposed together with a distortion degree. The distortion degree indicates the position in the circumferential direction at which the maximum tunnel deformation occurs with respect to the horizontal or vertical axis. In engineering practice, one needs to trace the maximum deformation and its position to be aware of possible damage.

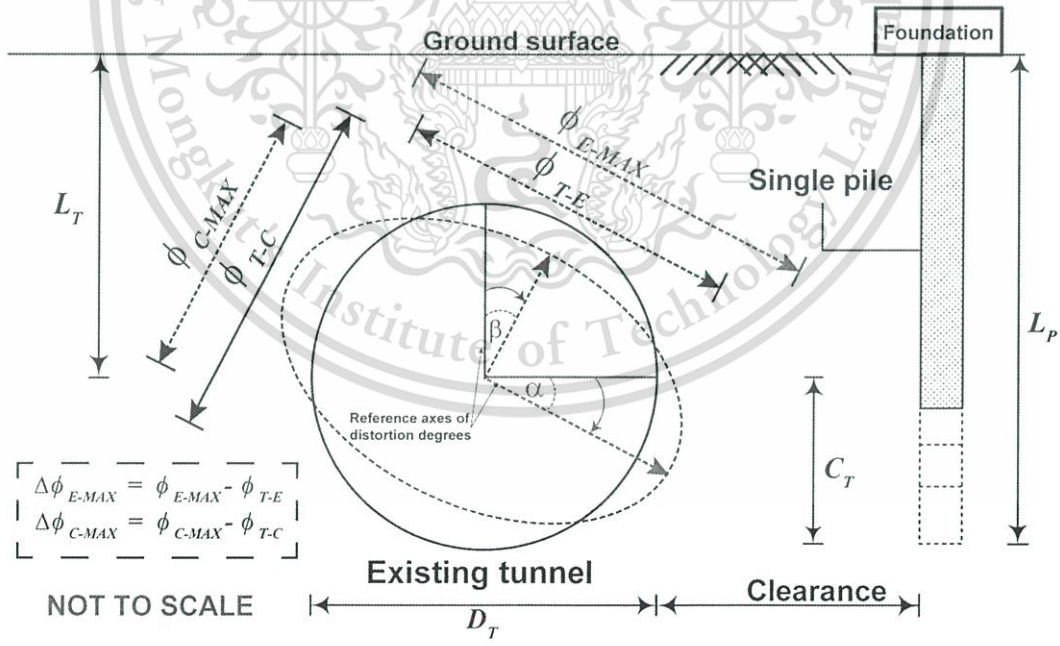

Figure 5.8 The schematic of the assessment method for changes in tunnel diameter proposed in this study.

The proposed assessment is schematically illustrated in Figure 5.8. The $\Delta\phi_{E-MAX}$ and $\Delta\phi_{C-MAX}$ represent the largest widening and shortening of the tunnel diameter, respectively. Note that only the deformation due to an adjacent pile under

loading is considered; those due to the excavation process are not included. The distortion degrees α and β indicate the circumferential positions of $\Delta\phi_{E-MAX}$ and $\Delta\phi_{C-MAX}$ with respect to the horizontal and vertical axes, respectively.

5.4.4 Tunnel deformation assessment by the proposed method

The maximum extension change ($\Delta\phi_{E-MAX}$) and maximum contraction change ($\Delta\phi_{C-MAX}$) in tunnel diameter with distortion degrees (α and β) due to pile loading are presented and discussed in this section. The presentation is similar to that of the $\Delta\phi_V$ and $\Delta\phi_H$ in Section 5.4.1. For the case of a tunnel in soft clay, the $\Delta\phi_{E-MAX}$ and α against the pile tip position for various clearances are illustrated in Figure 5.9a and b, respectively.

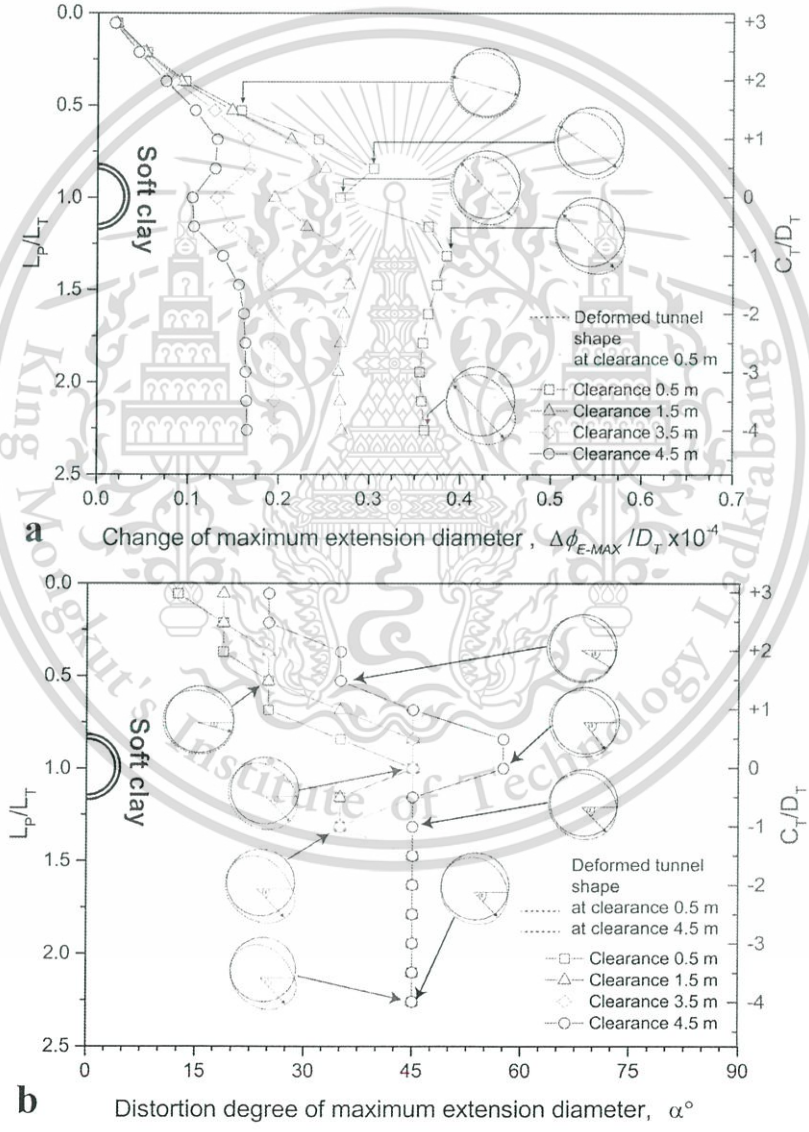

Figure 5.9 Tunnel deformation due to a pile under loading with various tips for a tunnel located in soft clay. (a) Maximum extension changes in tunnel diameter. (b) Distortional degree, α .

It is clearly seen that the distribution patterns of $\Delta\phi_{E-MAX}$ against L_P/L_T (or C_T/D_T) are significantly different from those of $\Delta\phi_V$ and $\Delta\phi_H$. The $\Delta\phi_{E-MAX}$ increases with increasing L_P when the pile tip is located above the tunnel crown ($C_T/D_T \geq 0.5$) and becomes decreasing in the range of $0.5 \geq C_T/D_T \geq 0.0$ before increasing again in a manner similar to the $\Delta\phi_V$ and $\Delta\phi_H$. However, unlike the $\Delta\phi_V$ and $\Delta\phi_H$ that rapidly decrease when the pile tip is located under the tunnel invert and approach a certain value with a longer pile length, the $\Delta\phi_{E-MAX}$ continues increasing with a decreasing rate or remains almost constant with extending pile tip location beneath the tunnel invert. Moreover, the magnitude (absolute value) of $\Delta\phi_{E-MAX}$ is much larger than that of the $\Delta\phi_V$ and $\Delta\phi_H$ for the same pile length and clearance, for example, 3.5 times greater at the clearance of 0.5m and $C_T/D_T = -1$. This reveals that using the $\Delta\phi_V$ and $\Delta\phi_H$ for assessment of tunnel lining deformation results in underestimation. Additionally, it leads to misunderstanding of the assessment when the pile tip is below the tunnel invert level.

Together with the distortional degree (α) in Fig. 13b, a better understanding of tunnel lining deformation behaviour can be achieved. Surprisingly, the larger α belongs to the larger clearance case (for the same pile tip level). With a longer pile, until the pile tip is at the level of the spring line, α continues to increase (at the same pile tip, α at a clearance of 4.5m remains the largest). With increasing pile length, the α decreases when the pile tip is located in the range of 0.0 D_T to −1.0 D_T. Below this level, the α begins approaching and becomes 45° regardless of the clearance. This implies that in this case (a tunnel in soft clay and a clearance in the range of 0.5 – 4.5 m), the tunnel deformation reaches its maximum and remains constant after the pile tip extends below −2.0 D_T. This finding is very interesting and worth further investigation, which is performed in the next section. Note that the discretization of the tunnel lining might affect the accuracy of the provided results. However, with the elaborate mesh used in this study (approximately every 5° in the circumferential direction for the tunnel lining), this small discrepancy has no influence on the conclusion drawn from this study.

The maximum contraction changes of the tunnel diameter ($\Delta\phi_{C-MAX}$) and the associated direction of the minor axis with respect to the vertical tunnel axis (β) for all clearances in the case of the tunnel located in soft clay are shown in Figure 5.10a and b, respectively. Although the $\Delta\phi_{C-MAX}$ represents the tunnel deformation in a contraction mode, the distribution patterns of $\Delta\phi_{C-MAX}$ are similar to those of $\Delta\phi_{E-MAX}$ for the same case, and their absolute values are very close for all clearances and all pile tips. This is also true for β. The distribution patterns of β are similar to those of α for the same case. However, a small discrepancy can be seen, for example, in the case of a clearance of 3.5 m. This is attributed to the finite element discretization of the analysis model.

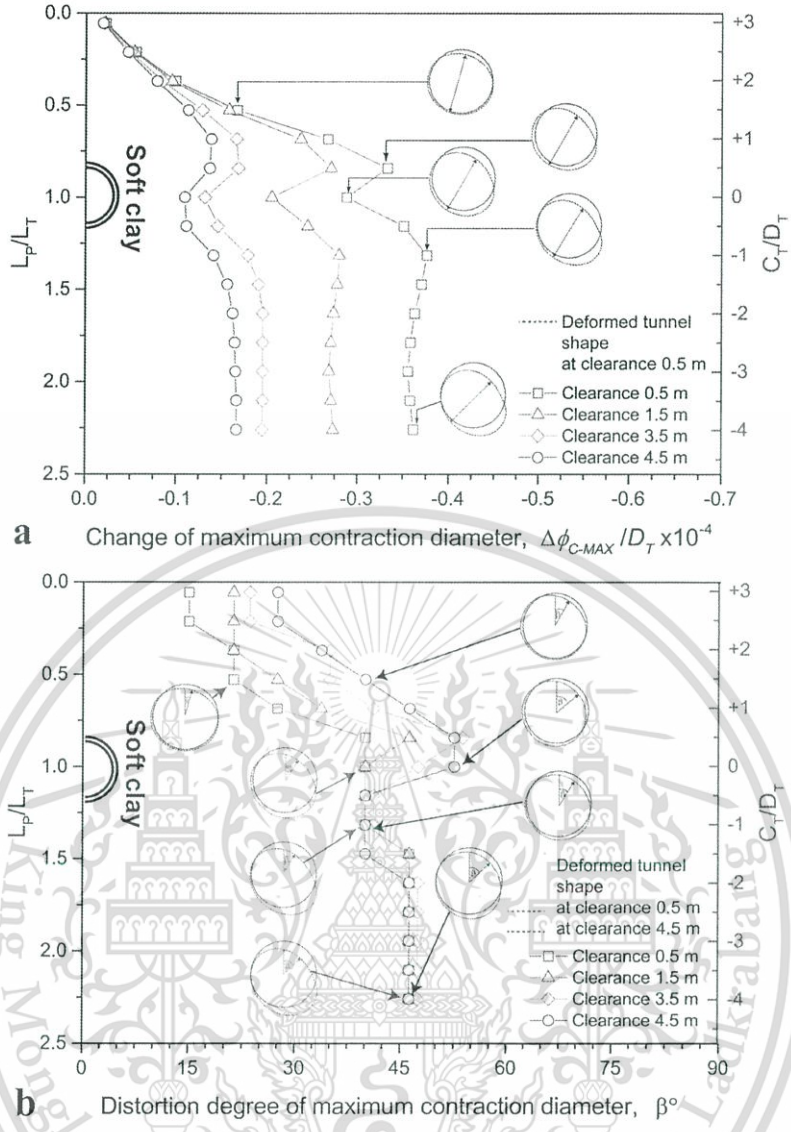

Figure 5.10 Tunnel deformation due to a pile under loading with various tips for a tunnel located in soft clay. (a) Maximum contraction changes in tunnel diameter. (b) Distortional degree, β.

For the case of the tunnel located in stiff clay, the distributions and magnitudes of $\Delta\phi_{C-MAX}$ and $\Delta\phi_{E-MAX}$ are almost identical, so only the results for $\Delta\phi_{E-MAX}$ and α are shown. Figure 5.11a show the relationships between $\Delta\phi_{E-MAX}$ and L_P/L_T (or C_T/D_T) for all clearances. When the pile tip is still located in soft clay (+3.0 D_T to +1.0 D_T), the $\Delta\phi_{E-MAX}$ increases with increasing pile length. At the same pile length and clearance, the $\Delta\phi_{E-MAX}$ in this case is much smaller than in the previous condition (a tunnel in soft clay). This indicates that, when subjected to the same working load, the deformation of the tunnel in stiff clay is smaller. When the pile tip is extended into stiff clay (+0.5 D_T), the $\Delta\phi_{E-MAX}$ drastically increases before slightly decreasing when the pile tip is at the tunnel spring line. This is probably because the piles have a larger working load when extending the pile tip into the stiffer layer. However, more clarification is needed to explain why the $\Delta\phi_{E-MAX}$ decreases when the pile tip is extended to the spring line. The $\Delta\phi_{E-MAX}$ continually increases again with extending

pile tip, and the maximum value of $\Delta\phi_{E-MAX}$ occurs at the deepest level considered in this study (−4.0 D_T). This tendency is completely different from that of the case of the tunnel in soft clay, in which the $\Delta\phi_{E-MAX}$ is nearly constant after the pile tip extends to −2.0 D_T. Moreover, for the case of the pile tip at −4.0 D_T, the $\Delta\phi_{E-MAX}$ in the case of the tunnel in stiff clay becomes larger than that of the tunnel in soft clay. This reveals that it is not true that the tunnel in stiff clay is safer. The magnitude of the load applied to the pile also has a strong influence on the tunnel deformation.

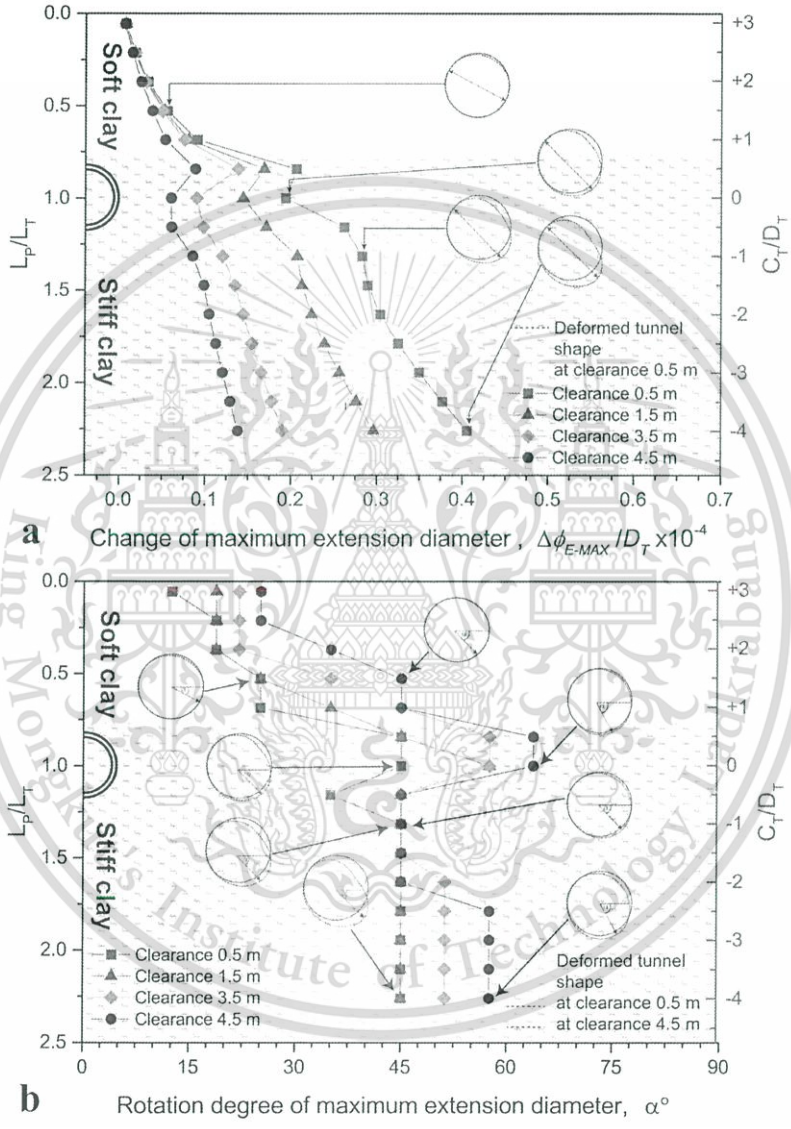

Figure 5.11 Tunnel deformation due to a pile under loading with various tips for a tunnel located in stiff clay. (a) Maximum extension changes in tunnel diameter. (b) Distortional degree, α .

The variation of α against L_P/L_T (or C_T/D_T) for the case of the tunnel located in stiff clay is depicted in Figure 5.11b. The variation of α in this case is similar to that of the previous case when the pile tip is located in the range of +3.0 D_T to−2.0 D_T. When the pile tip is extended below−2.0 D_T, the α for the clearances of 3.5 m and 4.5 m can be observed to be approximately 52° and 60°, respectively; the α for the clearances of 0.5 m and 1.5 m still remain at 45°. Note that the α values for the

clearances of 3.5 m and 4.5 m are larger than those for the clearances of 0.5 m and 1.5 m; however, the $\Delta\phi_{E-MAX}$ is much smaller.

5.4.5 The mechanism of soil-pile interaction

1) The soil movement behaviour due to application of working load on the bored piles.

Generally, a pile under loading causes the in-situ stress to change and thus soil displacement, which inevitably exerts influence on nearby existing structures. With the expected applied working load (Q_a) of 40% of the ultimate pile capacity (Q_u) calculated based on the alpha method [17], the load applied to the pile is commonly largest at the pile head and decreases with depth by transferring to the surrounding ground along the pile length. The degree of soil disturbance, change of stress and soil displacement at each depth are therefore dependent on the load transfer mechanism. With increasing pile length (as well as Q_a), the zone of the soil disturbance extends to a greater depth. Considering when the tunnel is located adjacent to the loaded pile at different depths, different degrees of impact on the tunnel may be expected. This logically depends on the degree of impact to the soil, which in turn depends on the relative position between the tunnel and the pile tip. In the same manner, for a tunnel at a certain depth, the degree of impact on the tunnel can be varied depending on the pile length and the associated degree of soil disturbance at that depth.

To comprehensively understand the mechanism behind the impact on the existing tunnel due to the adjacent loaded pile presented in the previous section, it is worth obtaining insight into the impact of the pile under loading on the surrounding soil at a certain depth. It is believed that the mechanism behind the tunnel deformation due to an adjacent loaded pile is principally the displacement of soil surrounding the tunnel. Additionally, the effect of the relative position between the considered location and the pile tip (both depth and clearance) and that of the ground condition are investigated. The analysis method described in Section 5.3 was also used to investigate the impact of a pile under loading on the soil in the vicinity of the tunnel lining. However, no tunnel exists in the analysis, and consequently, the steps for tunnel excavation are disregarded.

The results of pile-soil interaction are presented in terms of the total displacement vectors and shear strain distribution in the soil, as illustrated in Figures 5.12 and 5.13 for the cases of a single homogeneous soft clay layer and a multiple clay layer, respectively. The soil stratum considered and their mechanical properties are the same as those in the previous section. The investigation reveals that with the application of 40% Q_u, no plastic strain is generated in the soil, along the shaft or at the pile tip. The HS model, which does not consider strain softening, assumed for stiff clay in this study is sufficient. The vectors in the figures depict the relative magnitudes of soil total movement and their directions with a magnification ratio of 1:1500. The dotted circles in the figures represent the positions of the adjacent tunnel if its existence is considered in Section 5.4. The circles have clearances of 0.5m and 4.5m from the pile to represent the cases in Section 5.4 with clearances of 0.5m and 4.5 m, respectively. The positions of the pile tip located above or below the centre of the dotted circle are denoted by positive and negative signs, respectively. The movement vectors of the soil around and in the dotted circle are observed.

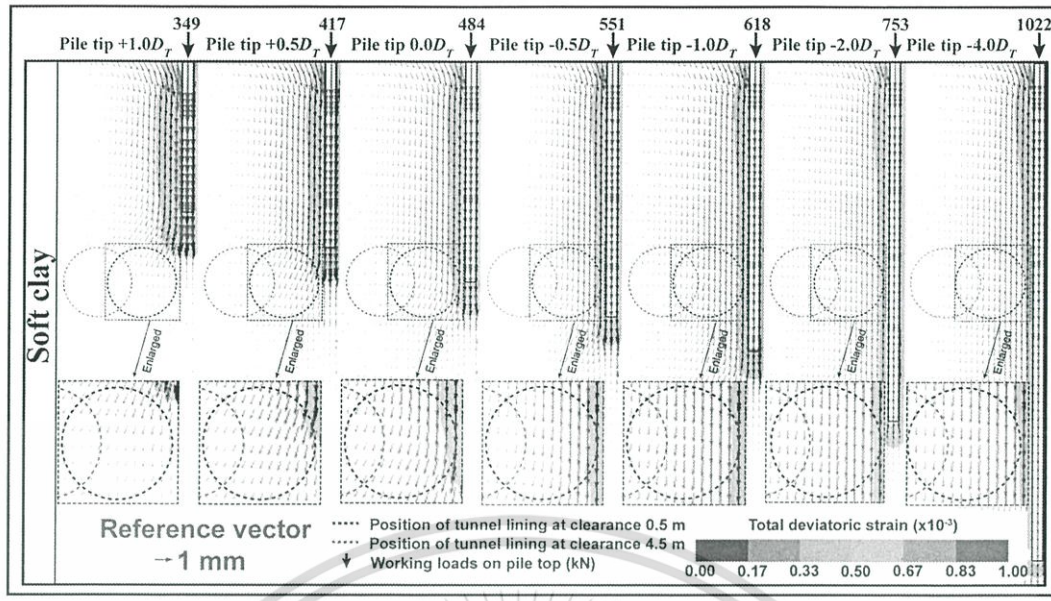

Figure 5.12 Vectors of total soil movement and contour of the shear strain in soil surrounding the loaded pile with various pile lengths in soft clay.

The development of soil movement vectors and shear strain distribution based on increasing pile length (and pile load) in soft clay are illustrated in Figure 5.12. The applied load at the pile head and position of the pile tip with regard to that of the dotted circle of each case are also indicated in the figure. In this situation, D_T represents the diameter of the dotted circles, which is equal to 6.3 m. It is seen that the movement vectors of soil along the pile surface and at the end are larger than those farther away from the pile. Except around the pile top and tip, the vectors of soil movement direct downward, and their magnitudes decrease with depth. At the soil surface and shallow depth near the pile top, the vectors are larger and directed towards the pile. Larger soil movement vectors are also observed under the pile tip, but they direct outward from the pile. With increasing pile length and associated applied working load, the zone of large downward vectors extends to greater depth, but their magnitudes decrease compared to those in the case of the shorter pile. Moreover, the magnitude of soil movement vectors around the pile top and under the tip are also smaller with increasing pile length, particularly under the pile tip. This indicates that these piles (having the pile tip under the centre line level of the circle) behave as a friction pile.

Considering the soil movement at certain locations (the same as those of the tunnel considered in the previous section), special attention is paid to the vectors in the vicinity of the dotted circles. In all cases with various pile tip positions, it is clearly seen that the soil movement vectors in the vicinity of the closer dotted circle (0.5 m clearance) is larger than those in the vicinity of the farther dotted circle (4.5 m clearance). This tendency is in agreement with the results in the previous section that the induced tunnel deformation in the case with a larger clearance decreases for the same considered pile tip position. This also implies that the tunnel deformation is induced by the soil movements surrounding the tunnel, which are a result of the pile being subjected to the load. The following consideration is thus focused on the soil vectors in the vicinity of the dotted circle that has a clearance of 0.5 m from the pile. For the case of the pile tip level of +1.0 D_T, in which the tip is located above the right side of the circle, the dotted circles cover the area of soil below the left side of the pile tip. The vectors in the area of the dotted circle are larger in the upper right section and

their directions are towards the centre of the circle. Focusing on the periphery of the upper right section of the dotted circle, the soil movement vectors are perpendicular to the periphery. With the existence of the tunnel lining in the previous case, these soil movement vectors would induce a compression force in the radial direction of the upper right section of the tunnel lining, and the largest deformation of the tunnel lining would occur in this section, as shown in Figure 5.6.

The soil movement vectors in the other zones become gradually smaller with distance from the pile tip and gradually change direction downward, particularly at the spring line and in the lower right section. This provides the explanation for a tunnel deforming into a kidney shape, as described in the previous section and as shown in Figure 5.6. With a deeper pile tip position at a level of +0.5 D_T, the soil movement vectors in the area of the dotted circle become larger than those in the case of the pile tip level of +1.0 D_T, explaining why the tunnel deformation in the case of the pile tip level of +0.5 D_T is larger than that in the case of the pile tip level of +1.0 D_T. For the case of the pile tip level of +0.0 D_T, or at the spring line level, the soil movement vectors in most sections of the dotted circle direct downward, particularly in the upper right section, where the vectors are the largest. Inclined vectors are only noted in the lower right section. Although the soil movement vectors in this case are overall larger than those in the case of the pile tip level of +0.5 D_T, the tunnel deformation (in Section 5.4.4) decreases, particularly in the upper right section. This indicates that not only the magnitude but also the direction of the soil movement in the vicinity of the tunnel has an influence on the tunnel deformation. These downward soil movements would pull the tunnel lining (in the previous section) down, and the larger movements in the right section cause the deformed shape to be a rotated ellipse. With deeper pile tip positions from −0.5 D_T to −4.0 D_T (and a larger pile load), only downward soil movement vectors can be observed in the focused area. The magnitude of soil movement seems to insignificantly change for the cases with pile tip positions at and lower than −1.0 D_T, particularly for the cases in which the pile tip positions are lower than −2.0 D_T. This is in agreement with the findings in the previous section that the tunnel deformation does not significantly change and almost remains constant for the cases of pile tip positions lower than −1.0 D_T and −2.0 D_T, respectively.

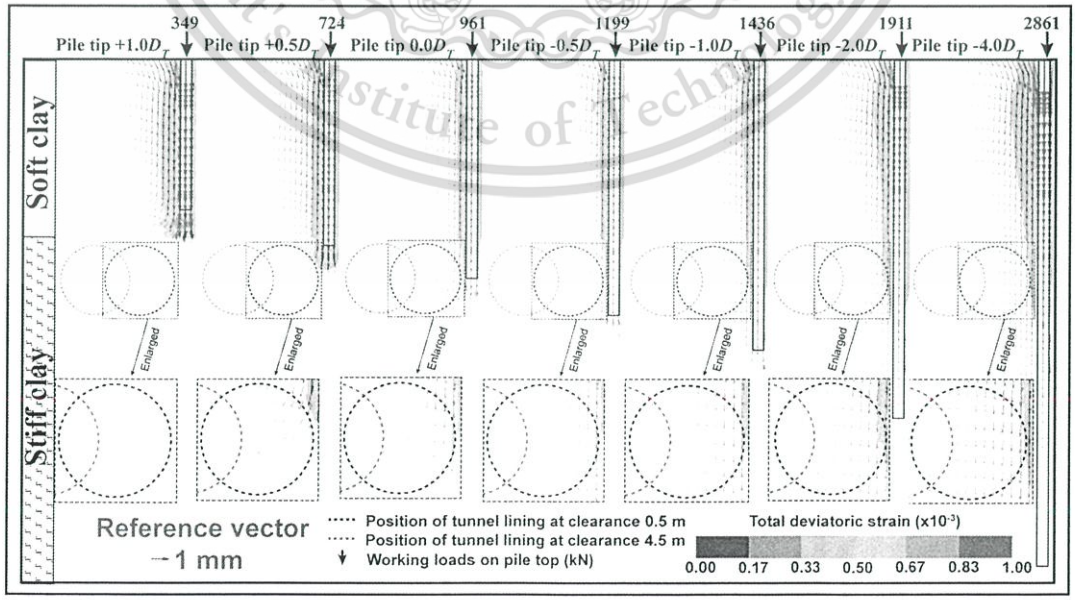

Figure 5.13 Vectors of total soil movement and contour of the shear strain in soil surrounding the loaded pile with various pile lengths in stiff clay.

In the cases when the dotted circles are located in stiff clay (Figure 5.13), similar tendencies in the results can be observed. Two main differences are noted. First, in the dotted circles, the soil movement vectors are shorter, except for the case of the pile tip at −4.0 D_T. This is in accordance with the tunnel deformation tendency in the previous section that a smaller tunnel lining deformation can be captured for a tunnel in stiff clay, except for the case of a pile tip at−4.0 D_T. The observation of shear strain distribution reveals that the degree of shear strain development along the pile shaft is smaller than that for the pile in a soft clay condition with the same pile tip. However, for the case of the pile tip at −4.0 D_T, the degree of shear strain development in the focused zone becomes equivalent. This confirms that the mechanisms behind the tunnel deformation due to an adjacent pile under loading are principally due to the movement behaviour of soil surrounding the tunnel, particularly in the zone between the pile and the tunnel, which is dependent on the load transfer behaviour from the pile. Thus, the relative position of the tunnel and pile tip and the soil layer in which the tunnel is located play an important role in tunnel deformation behaviour.

2) The load transfer behaviour of the bored piles

The load transfer behaviour from the pile to the soil is further investigated, focusing on the soil at the depth at which the tunnel is located in the previous section. Generally, after application of a load at the pile top, the pile moves downward. This movement will be resisted by the side frictions mobilized along the shaft of the pile (unit skin friction) and the soil below the tip of the pile (end bearing). Figure 5.14 illustrates the mobilized unit skin friction or the incremental vertical stress (every 2 m) that transfers to the soil at each depth from a pile subjected to its working load for a) a single homogeneous soft clay layer and b) a multiple soil layer. The mobilized unit skin friction is calculated as the difference between the loads that transferred to the pile depth every 2 m divided by the perimeter surface area of a 2 metre interval. It is seen that the incremental force transferred to soil increases with greater depth due to higher soil stiffness. Attention is paid to the depth in the range of 16.5–23 m, where the tunnel is located if it exists. In Figure 5.14a, when the pile tip is above the considered depth of +1.0 D_T and +0.5 D_T, the soil in the vicinity of the considered depth is affected by only the load transfer from the pile tip as it is pushing in a downward manner. For cases 0.0 D_T and−0.5 D_T, both the skin friction (pulling down) and the load transfer from the pile tip (pushing sideways) have an influence on the soil in the considered zone. With the deeper pile tip position, the contribution from skin friction becomes larger and that from the pile tip decreases. This is why the tunnel deformation decreases (compared to case +0.5 D_T) for case 0.0 D_T and increases again for case −0.5 D_T. With increasing depth of the pile tip below this level, most influence on the soil in the considered zone comes from skin friction, which slightly decreases with a longer pile and approaches a certain value. This provides an explanation as to why the tunnel deformation slightly decreases and almost remains constant.

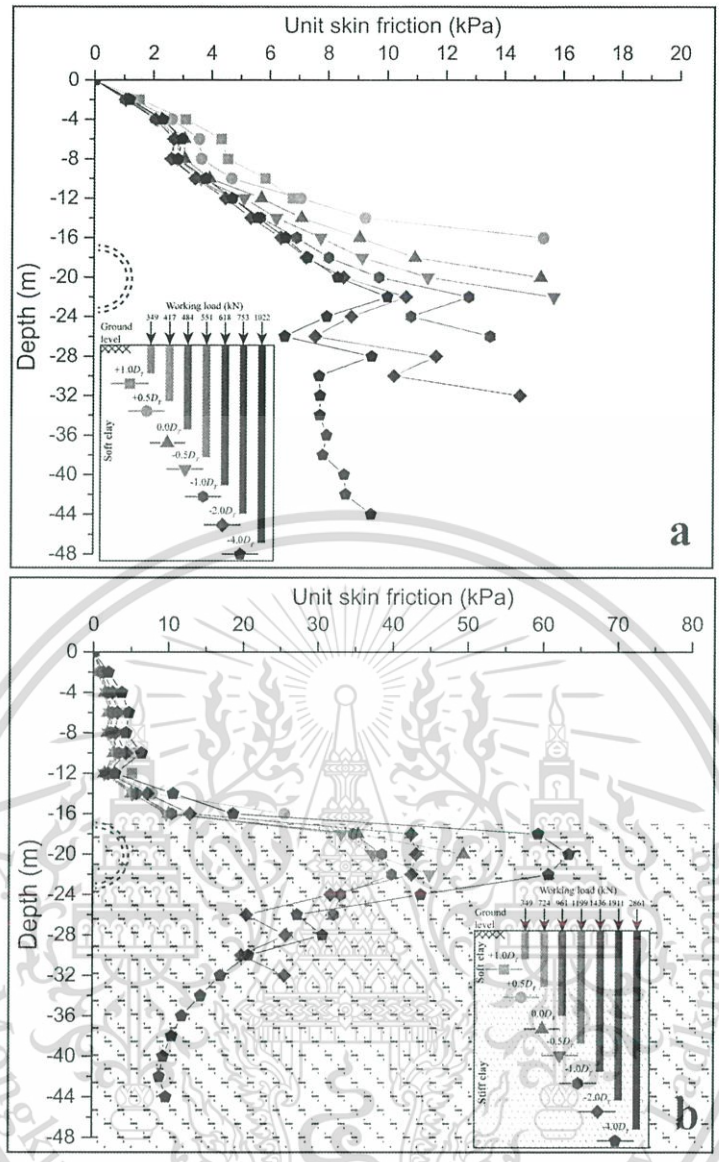

Figure 5.14 The mobilized skin friction along the pile with different soil types. (a) Tunnel located in soft clay. (b) Tunnel located in stiff clay.

In Figure 5.14b, in which the considered depth is in the stiff clay, the abrupt increase of load transfer in stiff clay can be seen. The distinct difference from the case of a single homogeneous clay layer is that the skin friction transferred to the considered depth (16.5–23 m) increases with a longer pile. This is in accordance with the increasing tunnel deformation against a longer pile in the previous section. Thus, it can be concluded that the tunnel deformation behaviour due to an adjacent loaded pile depends on the movement behaviour of the soil surrounding the tunnel, which in turn is affected by the load transfer behaviour of the soil in the vicinity of the tunnel. This load transfer includes both the skin friction and end bearing.

Figure 5.15 depicts the comparisons of the deformed tunnel shape in Section 5.4.2 and the deformed shape of the soil along the same perimeter (the dotted circle in this section) at the same magnification ratio (1:3000). Only some cases of pile tip positions are chosen for illustration. It is clearly seen that the deformed shapes of both are principally similar and that the magnitude of the tunnel deformation is smaller. This reconfirms that the tunnel deformation depends on the movement behaviour of the surrounding soil. When the tunnel lining is stiffer than the soil, the magnitude of

the tunnel deformation is smaller. It is interesting to note that for the case of +1.0 D_T, the tunnel lining deformation in the upper right section is much smaller than that of the soil due to the greater stiffness of the tunnel lining. However, the tunnel lining deformation in the lower right section becomes slightly larger.

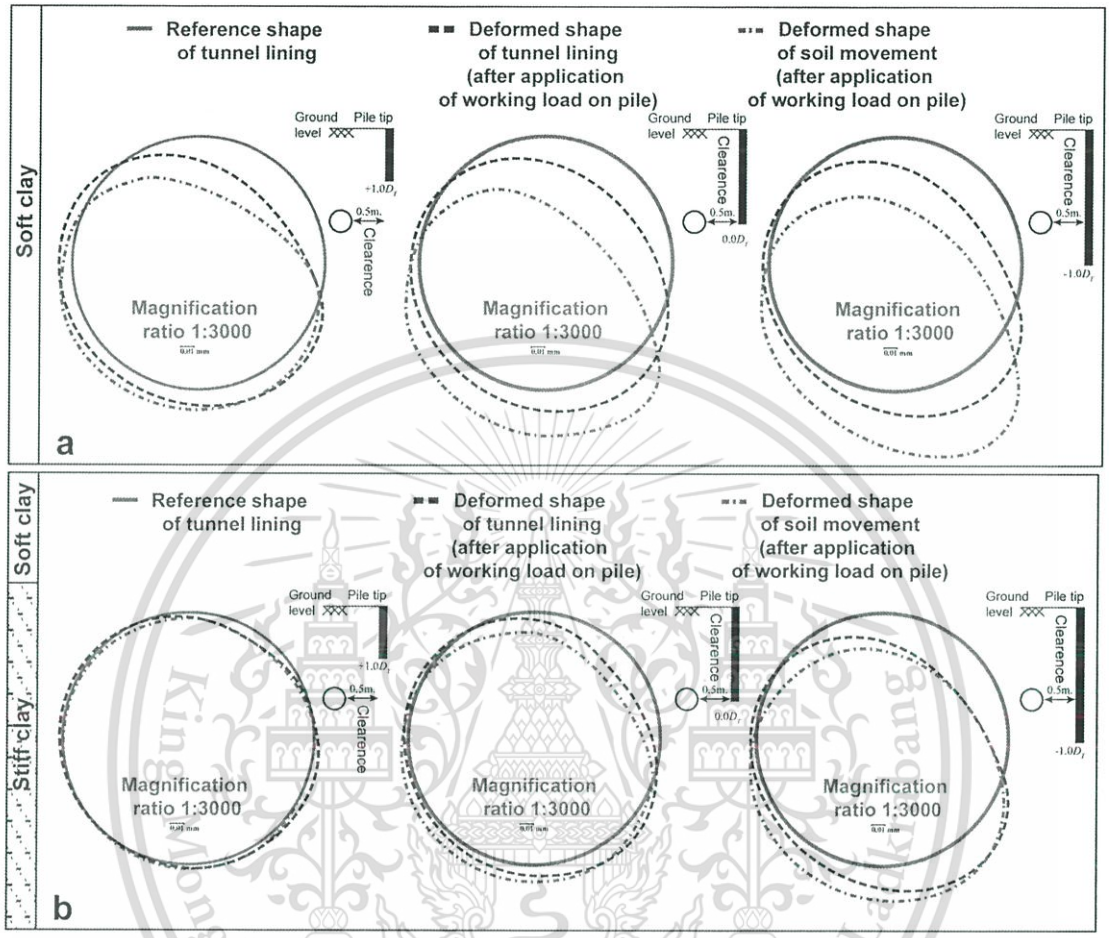

Figure 5.15 Comparisons of deformation shapes of tunnel lining and soil (along the periphery of the tunnel lining if no lining exists), with various loaded pile tips. (a) Tunnel located in soft clay. (b) Tunnel located in stiff clay.

This implies that the induced force in the lining structure from the soil movement around the upper right section is sufficiently large to expand the lining in the lower right section. Further investigation of induced force in lining structure can enhance the understanding of this soil-tunnel-pile interaction. Moreover, the relevant parameters excluded in this study, e.g., the tunnel diameter and thickness of the tunnel lining, are necessary to investigate the impacts of adjacent pile loading on an existing tunnel.

5.5 Summary

A series of 3D-FEA were conducted to investigate the tunnel response due to an adjacent pile under loading, in the case of a single pile located on a single side of the tunnel. Additional analyses of pile loading simulation were also performed to assist in explaining the pile-soil-tunnel interaction mechanism behind the tunnel response due to an adjacent pile under loading. The results are as follows:

1. The tunnel deforms as a kidney or rotated ellipse shape when the pile tip is above or below the tunnel spring line, respectively.

2. The assessment by $\Delta\phi_V$ and $\Delta\phi_H$ employed in previous works is not suitable for tracing the tunnel deformation due to an adjacent single pile under loading on one side. The impact in terms of changes in the diameter should be assessed by the method presented in this study. The proposed maximum contraction change ($\Delta\phi_{C-MAX}$) and maximum extension change ($\Delta\phi_{E-MAX}$) in a tunnel diameter with distortion degrees (α and β) effectively provide reasonable deformation evaluation of the existing tunnel in this situation.

3. The mechanisms behind the tunnel deformation due to an adjacent pile under loading are principally due to the movement behaviour (both magnitude and direction) of soil surrounding the tunnel, which in turn is dependent on the load transfer behaviour from the pile. Thus, the relative position of the tunnel and pile tip, magnitude of the applied load and stiffness of the soil layer in which the tunnel is located play a key role in this complex behaviour.

4. By tracing the tunnel deformation with $\Delta\phi_{E-MAX}$ or $\Delta\phi_{C-MAX}$ and α or β, respectively, the deformation of a tunnel in soft clay increases with pile length (and applied working load) up to the level of a pile tip at–2.0 D_T. The deformation of a tunnel in stiff clay continues to increase with pile length (and applied working load) up to the deepest level of pile tip in this study, −4.0 D_T. The α or β values principally increase with the pile length. The maximum α or β value appears when the pile tip is located either +0.5 D_T above or at the spring line before converging to a certain value with a greater pile tip depth. The value is 45° for a tunnel in soft clay regardless of the clearance between the pile and tunnel, while the value in stiff clay is in the range of 45–60°, depending on the clearance. The larger value (60°) is observed for larger clearance; however, note that the deformation is smaller.

5. It is postulated that the pile tip at +0.5 D_T above and −2.0 D_T below the spring line should be considered for existing tunnel assessment regarding an adjacent pile under loading for a short pile and long pile condition, respectively, in soft clay. For stiffer soil, greater depth below −4.0 D_T to the deepest level in engineering practice should be taken into consideration.

However, the evaluation of tunnel structural safety is not discussed in this chapter. To gain a better understanding of existing tunnel response due to applications of load on bored pile, the stress changes of the tunnel lining in term of axial force and bending moment will be presented in the next chapter.

5.6 References

[1] R. P. Chen, L. J. Tang, D. S. Ling, and Y. M. Chen, "Face stability analysis of shallow shield tunnels in dry sandy ground using the discrete element method," *Comput. Geotech.*, vol. 38, no. 2, pp. 187–195, 2011.

[2] R. P. Chen, J. Zhu, W. Liu, and X. W. Tang, "Ground movement induced by parallel EPB tunnels in silty soils," *Tunn. Undergr. Sp. Technol.*, vol. 26, no. 1, pp. 163–171, 2011.

[3] R. P. Chen, J. Li, L. G. Kong, and L. jun Tang, "Experimental study on face instability of shield tunnel in sand," *Tunn. Undergr. Sp. Technol.*, vol. 33, pp. 12–21, 2013.

[4] P. Lueprasert, P. Jongpradist, K. Charoenpak, P. Chaipanna, and S. Suwansawat, "Three dimensional finite element analysis for preliminary establishment of tunnel influence zone subject to pile loading," *Maejo Int. J. Sci. Technol.*, vol. 9, no. 2, pp. 209–223, 2015.

[5] H. Mroueh and I. Shahrour, "A simplified 3D model for tunnel construction using tunnel boring machines," *Tunn. Undergr. Sp. Technol.*, vol. 23, no. 1, pp. 38–45, 2008.

[6] Brinkgreve, R., Engin, E., Swolfs, W., 2013. PLAXIS 3D Version 2013 manual.

[7] F. Ye, C. fei Gou, H. dong Sun, Y. peng Liu, Y. xu Xia, and Z. Zhou, "Model test study on effective ratio of segment transverse bending rigidity of shield tunnel," *Tunn. Undergr. Sp. Technol.*, vol. 41, no. 1, pp. 193–205, 2014.

[8] M. Kavvadas, D. Litsas, I. Vazaios, and P. Fortsakis, "Development of a 3D finite element model for shield EPB tunnelling," *Tunn. Undergr. Sp. Technol.*, vol. 65, pp. 22–34, 2017.

[9] T. Schanz, a Vermeer, and P. Bonnier, "The hardening soil model: formulation and verification," *Beyond 2000 Comput. Geotech. 10 years PLAXIS Int. Proc. Int. Symp. beyond 2000 Comput. Geotech. Amsterdam Netherlands 1820 March 1999*, p. 281, 1999.

[10] R. Prust, J. Davies, and S. Hu, "Part 6: Tunnels and Underground Structures: Pressuremeter Investigation for Mass Rapid Transit in Bangkok, Thailand," *Transp. Res. Rec. J. Transp. Res. Board*, vol. 1928, no. 1, pp. 205–217, 2005.

[11] P. Jongpradist, T. Kaewsri, A. Sawatparnich, S. Suwansawat, S. Youwai, W. Kongkitkul, and J. Sunitsakul, "Development of tunneling influence zones for adjacent pile foundations by numerical analyses," *Tunn. Undergr. Sp. Technol.*, vol. 34, pp. 96–109, 2013.

[12] A. Wonglert and P. Jongpradist, "Impact of reinforced core on performance and failure behavior of stiffened deep cement mixing piles," *Comput. Geotech.*, vol. 69, pp. 93–104, 2015.

[13] P. Jamsawang, N. Yoobanpot, N. Thanasisathit, P. Voottipruex, and P. Jongpradist, "Three-dimensional numerical analysis of a DCM column-supported highway embankment," *Comput. Geotech.*, vol. 72, pp. 42–56, 2016.

[14] T. Rukdeechuai, P. Jongpradist, A. Wonglert, and T. Kaewsri, "Influence of soil models on numerical simulation of geotechnical works in Bangkok subsoil," *EIT Res. Dev. J.* vol. 20 (3), pp. 17–28, 2009

[15] F. C. Schroeder, D. M. Potts, and T. I. Addenbrooke, "The influence of pile group loading on existing tunnels," *Géotechnique*, vol. 54, no. 6, pp. 351–362, 2004.

[16] European Committee for Standardization (CEN), Design of steel structures, Part 1–6 general rules: Supplementary rules for shell structures. Eurocode 3. Brussels, Belgium, 1999.

[17] A. W. Skempton, "Cast In-Situ Bored Piles in London Clay," *Géotechnique*, vol. 9, no. 4, pp. 153–173, 1959.

CHAPTER 6

Changes of Structural Forces in Tunnel Lining due to Adjacent Loaded Pile

6.1 Background

Since considered existing tunnels due to the impacts of adjacent loaded pile in previous researches are transportation tunnels, serviceability is always under serious concern primarily. The tunnel response in terms of tunnel deformation is a common focus. To comprehensively investigate the impacts on the various type of existing tunnel, i.e., water supply tunnel, the tunnel stability also should be studied. There has only been a small number of researches concerning the response of existing tunnel in terms of changes in lining forces as mentioned in Section 2.3.3 of Chapter 2. Generally, the traditional reinforced concrete lining is designed based on short column method which subject to combined normal force and bending moment [1] and [2]. The maximum values of axial force or bending moment considered to design the steel reinforcement are often located at the crown, invert, or both of spring line. The number and type of rebar used to reinforce the concrete lining are then governed by lining forces at those positions. Although the current design practice for tunnel lining considers all possible load scenarios during service of the tunnel, however, the future activities have not been included. Moreover, the design of any tunnel structure has to fulfil important requirements concerning structure stability and serviceability. To achieve these requirements, it is necessary to predict unwanted effects. It is then necessary to evaluate the possible effect of the adjacent pile under loading on tunnel lining in terms of changes in lining forces including tunnel deformation.

In this chapter, the investigation of changes in lining forces is divided into two parts. First part, to evaluate the changing stability of tunnel lining governed by the maximum design values of lining forces, which is generally located at tunnel crown, invert or spring lines, the changes in lining forces at their positions are observed. Second part, with the revelation of the previous study as mentioned in Chapter 5, the maximum tunnel deformation impacted by adjacent loaded piles on a single side of an existing tunnel (which is a common situation) is along neither the tunnel horizontal nor tunnel vertical axis. Thus, the maximum change in lining forces are also should be investigated. The FEM code, PLAXIS, is selected as the numerical tool for analysis in this study. With the investigations as mentioned above, it probably can be used to guide designing, planning and constructing for new adjacent structures constructed close to the existing tunnel. Moreover, the tunnel owner can use the investigated assessment to appropriately prepare or manage those impacts. It also can reduce the instrument costs if the observing positions are appropriately chosen.

6.2 Characteristics of the case studies

The characteristics of Mass Rapid Transit Authority of Thailand (MRTA) tunnel project in Bangkok subsoil were used to represent for investigating the response of existing tunnel due to adjacent bored pile in this study. The similar characteristics of case studies as previous study described in Chapter 5 are used to be

investigated again in this chapter. To obtain the reliable results, however, the more positions of pile tips compared to the outer tunnel diameter (D_T) are considered. The pile tips are varied over a range of 3.0 D_T above to 6.0 D_T below the tunnel spring line. The distance between the edge of the tunnel lining and the closer edge of the bored pile are the clearances that are defined as 0.5 m to 4.5 m in this study. Two ground conditions with regard to the tunnel position are considered as the case studies following the previous chapter (Chapter 5). The tunnel depth is fixed at 20 m for comparison. A typical pore water pressure profile in Bangkok is a piezometric drawdown. A schematic diagram of the soil profiles and the pile tip positions (indicating the different pile lengths and their clearances) is illustrated in Figure 6.1.

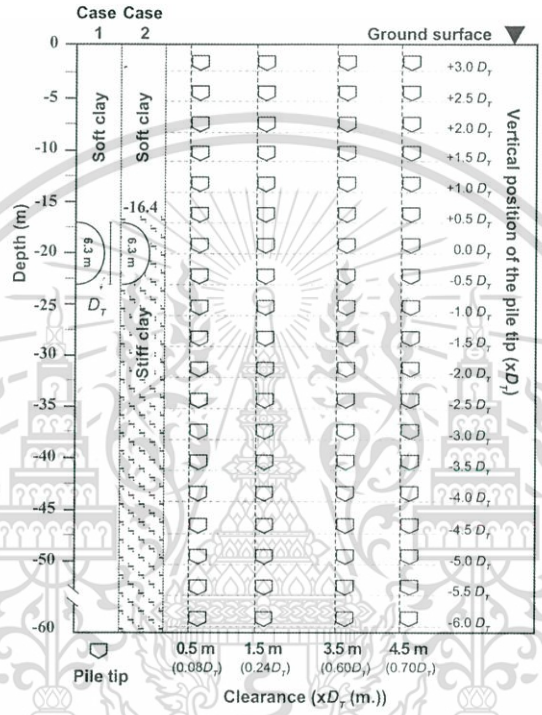

Figure 6.1 Soil profiles and illustration of pile tip positions considered in this study.

6.3 Finite element analysis

In this analysis, the PLAXIS 3D (version 2016) software was utilized to generate the mesh and to analysis (Brinkgreve et.al, 2016) [3]. The details of simulation method, meshing, analysis conditions, material properties and simulation process are described below.

6.3.1 Finite element mesh and analysis conditions

A series of finite element analyses were carried out using the three-dimensional (3D) FE method with advanced elasto-plastic soil models and reasonable assumptions. An example of 3D FE mesh (for the tunnel constructed in stiff clay, Case 2) indicating the relevant geometry, soil profile, element discretization and displacement boundaries is illustrated in Figure 6.2.

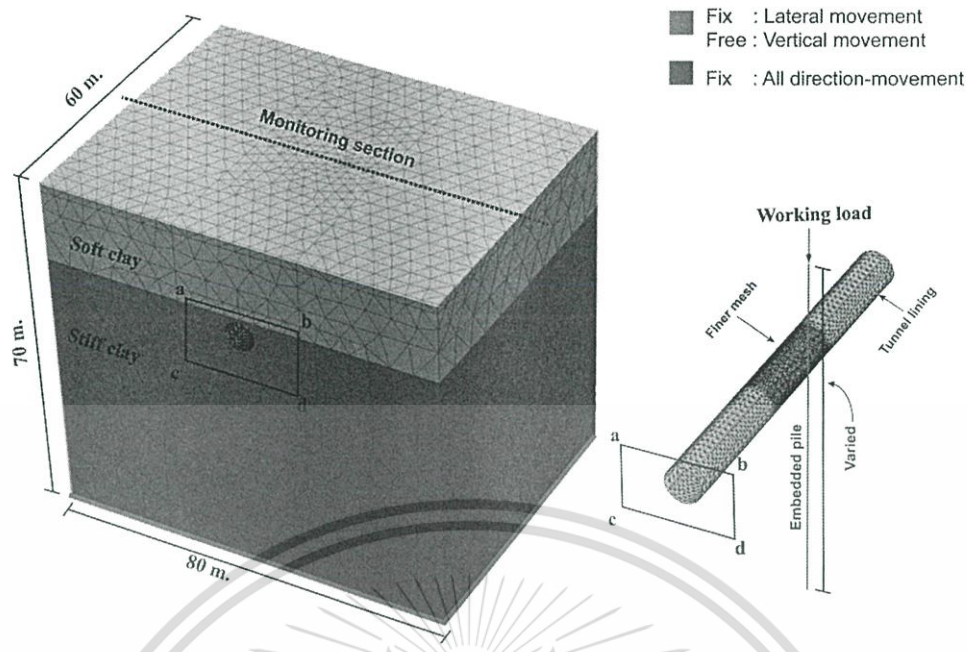

Figure 6.2 Finite element mesh for the tunnel constructed in stiff clay.

Before analysing the responses of the existing tunnel due to the impacts of loaded piles, the tunnel excavation, which is further detailed in Section 3.3, is simulated to validate the stress developed in tunnel lining. The sufficient boundary of FE model for tunnel excavation simulation is proposed by Mroueh and Shahrour (2008) [4]. To cover the boundary size of the previous study [4], the dimension of the FE mesh is 60 m (≈9.5 D_T) in longitudinal direction, 70 m (≈11.0 D_T) in the vertical direction and 80 m (≈ 12.5 D_T) in the transverse direction. The monitoring section is at the centre of the longitudinal direction. The soil stratum was discretized into 10-node tetrahedral elements. The 6-node shell elements were used to model the tunnel lining simplified by continuous ring model. An attractive method reducing the complication of such models is the modelling of the bored pile by embedded pile elements, where piles are not explicitly modelled with continuum finite elements but replaced by a special formulation with beam elements [5].

Noted that, mesh in this study is generated automatically by PLAXIS software used to analysis in this study. Controlling of generated mesh are difficult to examine mesh sensitivity However, for the region of greater interest where severe plastic strains are expected to develop, especially in the zone between pile and tunnel, finer discretization mesh with the suitable aspect ratio is refined to offer the accuracy of the solutions (approximately every 3° of the tunnel lining element in the circumferential direction). With the refined mesh used in this study, this minor discrepancy has no influence on the conclusion drawn from this study.

The analysis conditions used in this study are similar to those of Chapter 5, then it is not to mention in this chapter.

6.3.2 Constitutive model and material properties

To comprehensively investigate the responses of the existing tunnel located in the subsoils of the MRTA project, another soil constitutive model with the Hardening Soil Model with Small Strain Stiffness (HSsmall), which was studied for investigating geotechnical problems in the project [6] and [7], are employed to simulate the soil element as soft and stiff clay layers. The HSsmall is a modification of the Hardening

Soil Model (HS) [7], incorporating the small strain stiffness of soils [8]. Two additional parameters are needed to describe the stiffness behaviour at small strains. These are the initial or very small-strain shear modulus (G_0^{Ref}) and the shear strain level $\gamma_{0.7}$ at which the secant shear modulus is reduced to 70 % of G_0^{Ref}. A comprehensive set of experimental data on Bangkok subsoils from oedometer and triaxial tests were conducted to determine the stiffness and strength parameters of the HS for soft and stiff Bangkok clays [9]. In addition, the detail of small strain parameters, G_0^{Ref} and $\gamma_{0.7}$, of the Bangkok clays were studied by Likitlersuang et al., (2013) [6]. The HSsmall parameters for Bangkok clay were validated by numerical analysis with calibrating measured data of deep excavations in MRT project [7]. The concrete lining and bored pile were assumed to be a linear elastic. The material parameters used in the numerical analyses are summarized in Table 6.1 and Table 6.2.

Table 6.1 Soil model parameters [10].

Soil layer	Soft clay	Stiff clay
Material model	The Hardening Soil Model with Small Strain Stiffness (HSS)	
E_{oed}^{ref} (kPa)	800	8,500
E_{50}^{ref} (kPa)	850	9,000
E_{ur}^{ref} (kPa)	8,000	30,000
γ_{sat} (kN/m^3)	16.5	19.5
ϕ' (°)	23	25
c (kPa)	1	10
υ_{ur} (-)	0.2	0.2
m (-)	1	1
K_0^{nc} (-)	0.7	0.5
R_f (-)	0.9	0.9
G_0^{Ref} (kPa)	10,000	30,000
$\gamma_{0.7}$ (%)	0.08	0.002

Table 6.2 Material properties of the bored pile and tunnel lining [11].

Structural elements	Young modulus $[E]$ (kN/m^2)	Poisson's ratio $[\upsilon_C]$ (-)	Unit weight $[\gamma_C]$ (kN/m^3)
Tunnel lining	31 x 10^6	0.20	24
Bored pile	31 x 10^6	0.20	24

6.3.3 Numerical procedure of the finite element analysis

Similarly, the numerical procedure was conducted to investigate tunnel deformations due to loaded pile as described in Chapter 5. The simulation process was divided into two stages. On the first stage, the initial responses of the tunnel lining are examined by the tunnelling simulation with the Earth Pressure Balance (EPB) shield method as described in Chapter 4. The second stage concerns the application of the single pile axial loading modelled wished-in-place, which is the predetermined working load.

6.4 The responses of the tunnel lining

6.4.1 The considering the induced lining forces due to pile under loading

Figure 6.3 shows a tunnel lining element considered the induced lining forces for the 3D and 2D analysis.

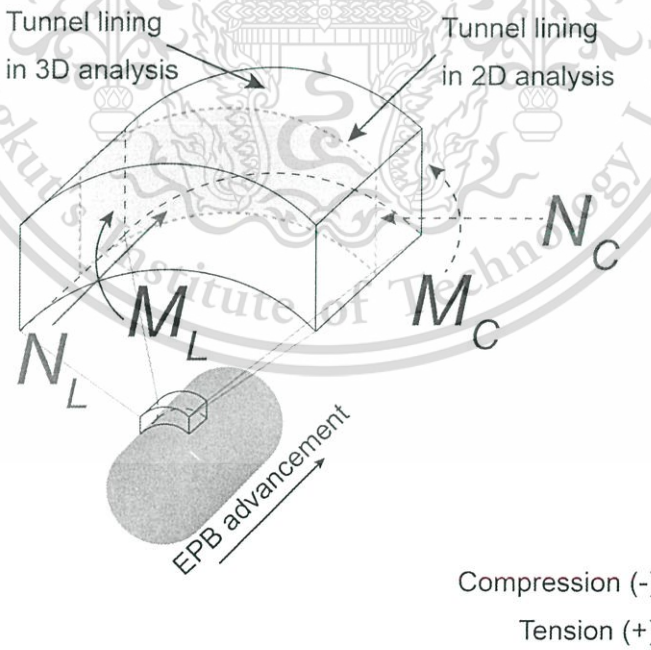

Figure 6.3 Considering the structural forces in tunnel lining due to single loaded pile.

Generally, the induced lining forces in the tunnel lining due to the various adjacent constructions or the load scenarios for tunnel design are evaluated based on 2D plane strain assumption. Then, the induced lining forces in circumferential direction, axial force (N_C) and bending moment (M_C) are only considered. However,

considering the response of the tunnel lining due to pile under loading, particularly in a single pile case, is principally a three-dimensional problem. With the 3D simulation analysis, the influence of single pile on the tunnel lining in longitudinal directions probably occurs.

To clear this suspicion, the changes of lining forces in longitudinal direction, axial force (N_L) and bending moment (M_L) are also considered firstly. For induced normal force (N_L) after complete tunnel excavation, the maximum values are about 582.36 and 451.20 kNm for tunnel excavated in soft and stiff clay respectively. When the pile tip is located at the deepest level considered in this study (-6.0 D_T), the reducing of induced axial forces occurs with the maximum values of 537.82 and 407.91 kNm for tunnel located in soft and stiff clay respectively. When considering the induced bending moment after complete tunnel excavation, the maximum values are about 4.54 and 6.41 kNm/m. The maximum values of induced bending moment due to pile under loading are about 7.31 and 8.52 kNm/m for tunnel located in soft and stiff clay respectively, and they occur when the pile tip is located at -6.0 D_T. For considering the changes of lining forces in circumferential direction, the maximum values of induced axial force (N_C) and bending moment (M_C) after complete tunnel excavation are about -781.38 kNm and 15.33 kNm/m for tunnel located in soft clay, and -626.85 kNm and -22.95 kNm/m for tunnel located in stiff clay. When tunnel lining is impacted by pile under loading, the induced lining forces still increase in certain pile tip levels, especially the change in bending moment. The changes in lining force in circumferential direction reach the maximum value of about 125%, this are further described in next section.

As mentioned above, the changes of lining forces in longitudinal directions, N_L and M_L, due to the tunnelling and impact of loaded pile are insignificant by comparing with the changes of lining forces in circumferential direction. Thus, the lining forces in circumferential directions, N_C and M_C, are only considered to investigate the impacts of pile under loading on the tunnel lining in this study.

6.4.2 The responses of tunnel lining after completed excavation

The responses of the tunnel lining after complete tunnel excavation are depicted in Figure 6.4. A polar coordinate system defined an origin radian (θ) at the tunnel crown is performed to describe the tunnel deformation, the bending moment and axial force along the tunnel circumferential direction. They are extracted when EPB shield advances for 30 m (5 D_T), the tunnelling process is completely simulated, to ensure that present excavation process has no influence on the lining forces and deformations at the monitoring section. For tunnel constructed in soft clay (Case 1, Figure 6.1), Figure 6.4a shows the tunnel displacement (I) with a magnification ratio of 1:30. The tunnel deformed shape, which is oval with its major axis aligns with the horizontal axis, can be clearly observed. The magnitudes at tunnel crown and invert are larger than the magnitudes at both of tunnel spring lines, the largest magnitude can be observed at the tunnel crown. This behaviour occurs due to the tunnel constructed in soft soil where the lateral earth pressure coefficient, K_0, is less than 1.0.

Note that the inward displacements around the tunnel lining can be observed due to the simulation technique from PLAXIS code. The displacement of the tunnel lining is simulated by volume loss assumption becoming the contraction ratio in PLAXIS code. The tunnel lining is then controlled by prespecified displacement values.

For the lining forces illustrated in subfigures (II, III), the bending moment and axial force were not symmetrical distributions. This may be attributed to the 3D

simulation of tunnel construction process; in fact, the symmetrical distribution of lining forces is hardly occurred in practical engineering. In subfigure (II), the distribution of bending moment within the areas from 328° to 45° and from 135° to 225° was the negative sign, which means that these areas are subjected to compressive bending stress. The maximum magnitude of negative bending moment about 10.42 kNm/m occurred at crown tunnel. Meanwhile, the positive bending moment occurred at the areas from 45° to 135° and from 225° to 315°, the maximum magnitude of the tunnel lining belonging to the positive bending moment about 15.33 kNm/m occurred at the right spring line.

According to subfigure (III), the uneven distribution of axial force can be seen. The axial force was negative in the entire section, which means that the tunnel lining was compressed entirely. The magnitudes at the tunnel crown and the invert are the smaller than that at tunnel spring lines, the magnitudes of about 600 kNm occur at the tunnel crown and about 700 kNm occur at tunnel spring lines. The maximum value for tunnel constructed in soft clay is 781.38 kN/m, but not located at tunnel crown, invert or both of spring lines.

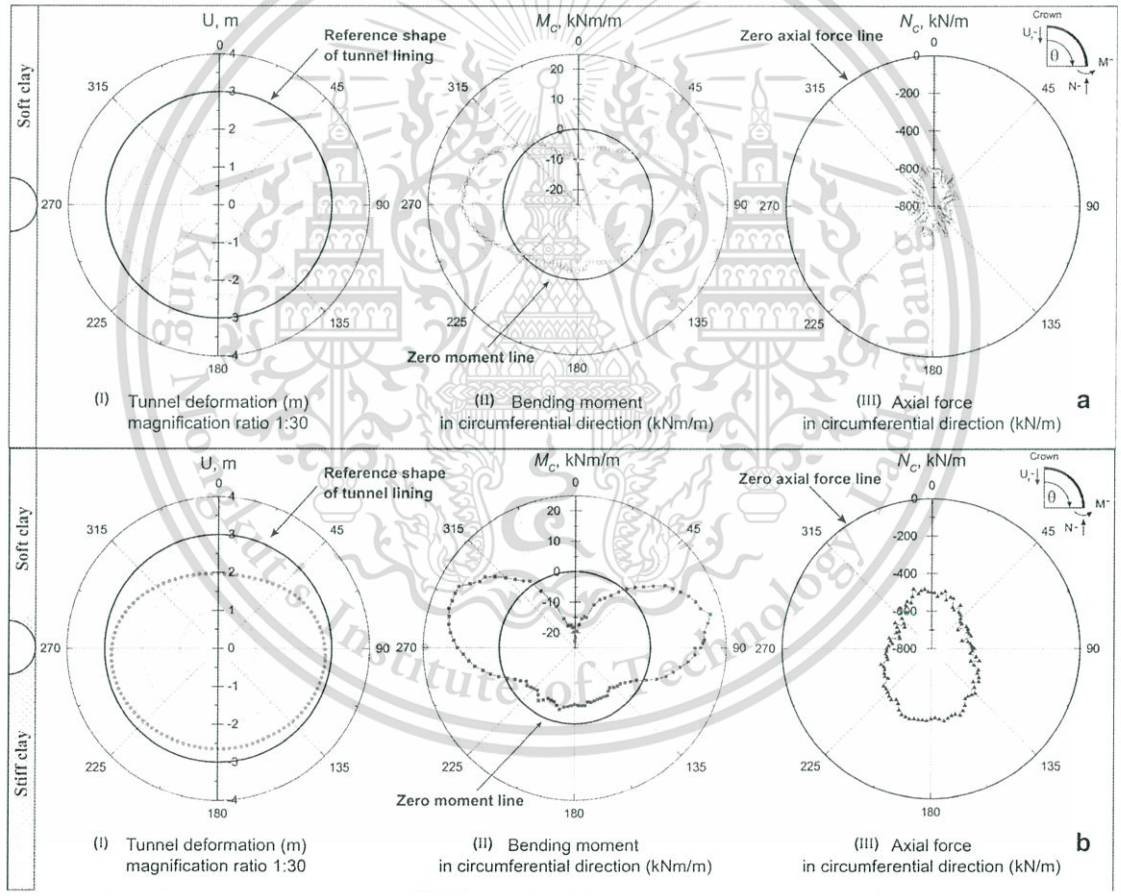

Figure 6.4 The tunnel responses after tunnel excavation in circumferential direction, (I) tunnel displacement, (II) bending moment and (III) axial force. (a) for tunnel constructed in soft clay. (b) for tunnel constructed in stiff clay.

The responses of tunnel lining for tunnel constructed in stiff clay (Case 2, Figure 6.1) are depicted in Figure 6.4b. The deformation of tunnel located in stiff clay is similar to that of tunnel constructed in soft clay, but the displacement value is little smaller. The moment distribution is also similar to that of tunnel constructed in soft clay. The negative bending moments occur at 328° to 38° and 117° to 245°, the

maximum negative moment of about 22.95 kNm/m occurs at tunnel crown (0°). The positive moments occur at the areas from 41° to 114° and 249° to 325°, the positive maximum moment of about 21.00 kNm/m occurred at about of 76° (above the tunnel right spring lines). The maximum value of the bending moment is much larger than that of the tunnel constructed in soft clay. The distribution of the axial force can be clearly seen. The magnitudes of the axial force are smaller than those of the tunnel constructed in soft clay. However, the smaller magnitudes about 500 kN/m still occur at the crown and invert of the tunnel while the magnitudes of about 550 kN/m occur at the spring lines, similarly to the tunnel constructed in soft clay. The maximum value for tunnel constructed in stiff clay is 626.85 kN/m which is smaller than that of tunnel constructed in soft clay.

With the design criteria of tunnel lining, the stability of the tunnel lining is subjected to a concrete capacity and reinforcement. The tunnel stability is considered form combined lining forces, the axial forces and the bending moment, in critical section of the construction projects. Generally, all possible load scenarios during service and construction of the tunnel are only considered to provide the tunnel stability. However, the future activities have not been included. To achieve these requirements, the changes in axial force and bending moment of tunnel lining are further investigated.

6.4.3 The distributions of the structural forces in tunnel lining due to the application of working load on pile

To initially obtain a clear view of changes in lining forces, the distributions of the lining forces in the circumferential direction of the tunnel lining due to pile under loading with various tips are firstly presented as shown in Figure 6.5 and Figure 6.6 for observing the distributions of axial forces and bending moments induced by application of working on pile with various tip positions.

1) The distributions of the axial forces induced by loaded pile

Figure 6.5a show the distributions of axial forces along with circumferential tunnel lining defined the origin (0°) at tunnel crown. The distributions of axial forces induced by the impact of loaded pile with various tips and complete tunnel excavation are represented by symbols and bold line respectively. The similar distributions of both axial forces with close values can be observed. The axial force distributions due to pile under loading by comparing with the axial force after complete tunnel excavation (bold line) can visibly observe at 0° to 210°, whereas the difference of these axial forces at higher degrees of 210° are insignificant. The maximum change of the axial forces can be seen at 30° to 150° (dot line area), this is further observed. When considering the impacts of loaded pile, the axial force distributions due to pile under loading increase with extending pile tip. Especially when the pile tip is located at tunnel invert (-0.5 D_T), the maximum change of axial force due to pile under loading can be seen. The increasing of axial force due to loaded pile at certain degrees exceeds the maximum axial force induced by excavated tunnel, especially at degree occurring the maximum axial force due to complete tunnel excavation.

For tunnel located in stiff clay as shown in Figure 6.5b, the distribution patterns of the axial forces due to excavated tunnel and pile under loading are similar. By the comparing the axial forces after excavated tunnel and pile under loading, the different values are larger than the previous case (tunnel located in soft clay). However, the differences of those axial forces are similar to those of tunnel located in soft clay, significant difference occur at 0° to 210° and insignificant difference occur

at higher degrees of 210°. The exceeded axial force due to impacts of loaded pile can be seen. Especially, when the pile tip is located at tunnel invert (-0.5 D_T), the maximum value of axial force induced by loaded pile with exceeding the initial axial forces can be observed. It is similar to the case of tunnel located in soft clay.

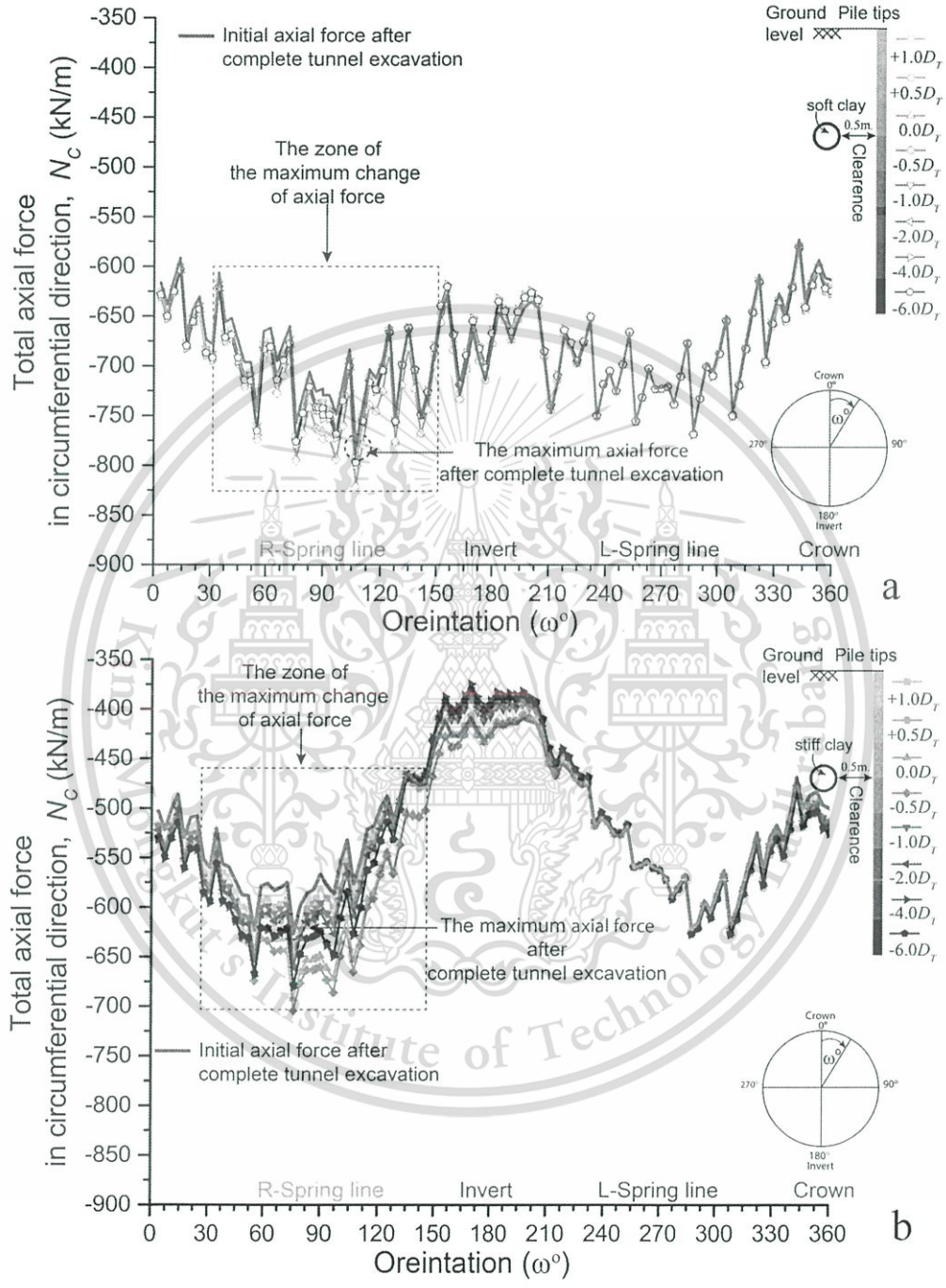

Figure 6.5 The distributions of the axial force in tunnel circumferential direction induced by pile under loading with various pile tips for tunnel located in. (a) soft clay. (b) stiff clay.

2) The distributions of the bending moments induced by loaded pile

Figure 6.6a and b illustrate the distributions of bending moment in the circumferential direction of the tunnel lining due to pile under loading with various pile tips for tunnel located in soft clay and stiff clay respectively.

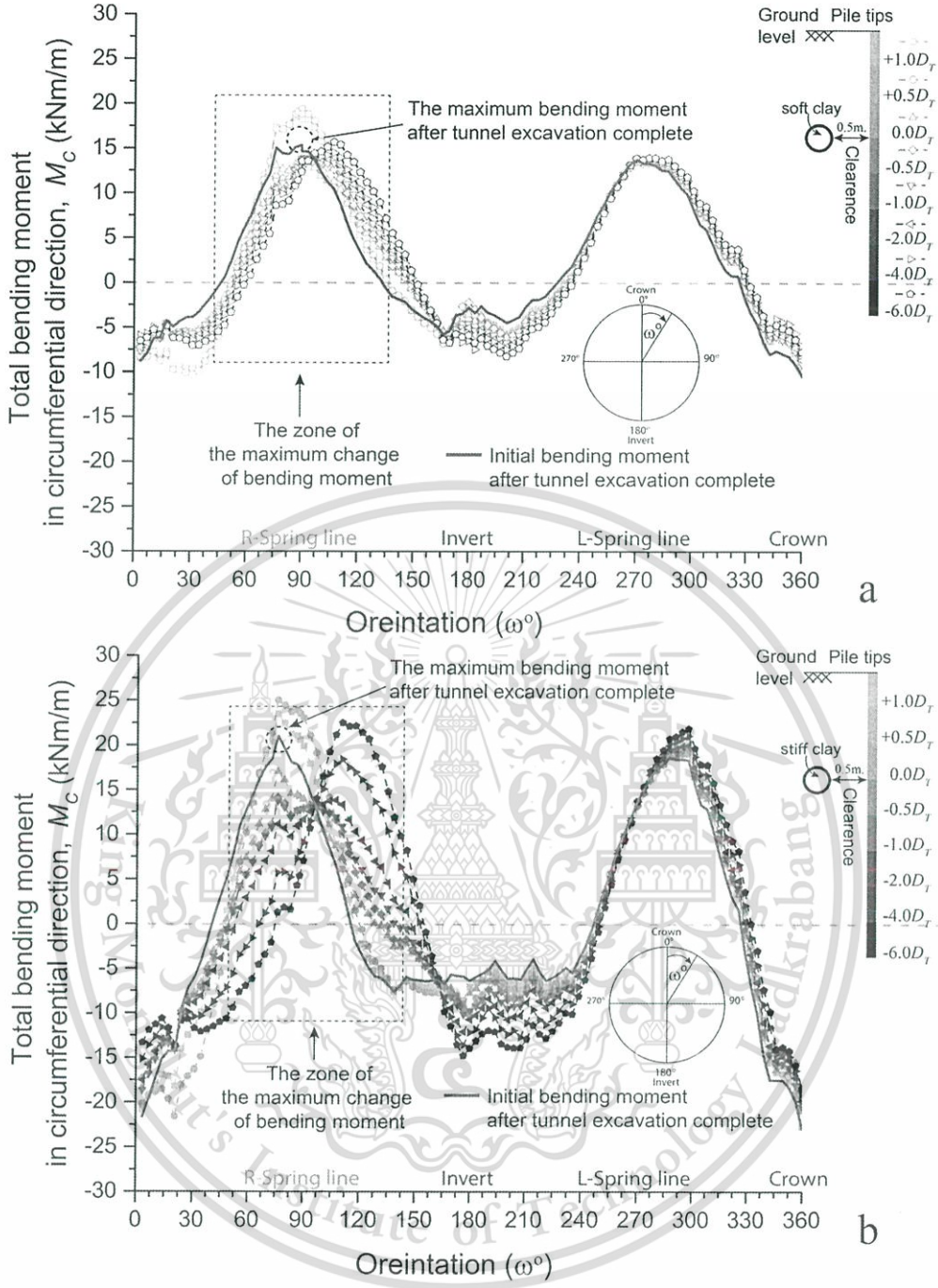

Figure 6.6 The distributions of the bending moment in tunnel circumferential direction induced by pile under loading with various pile tips for tunnel located in. (a) soft clay. (b) stiff clay.

It can be clearly seen that the different values of the bending moments induced from complete tunnel excavation and pile under loading are more than that of the axial force. The bending moment induced excavated tunnel represented by bold line are regularly distributed (positive values at the spring line and negative values at crown and invert) in both cases. For tunnel located in soft clay as shown in Figure 6.6a, the distribution patterns of the bending moment induced by pile under loading with various tips are similar to that of the induced bending moment after complete tunnel excavation. Whereas, the distributions of induced bending moment due to loaded pile seem to be rotated that the positions of the bending moment distributions

are changed with increasing orientation degree. The difference of bending moments between impacts of excavated tunnel and loaded pile with considering at same positions then occurs. The significant difference of the bending moments can be seen clearly at 0° to 240°, especially on the side closer to the pile (0° to 180°). At higher degrees of 240°, the smaller difference of the bending moments can be observed. Moreover, the maximum value of changes in bending moment approximately can be seen at 0° to 30°. For investigating the impacts of pile under loading on induced bending moment in tunnel lining, at the upper part of the tunnel lining on side closer pile (30° to 90°), the induced bending moment due to the pile tip located above the tunnel in the range from +1.0 D_T to +0.5 D_T increase to exceed the maximum bending moment induced by excavated tunnel. This indicates that the induced bending moment in the lining is affected by the load transfer from the pile tip as it is pushing manner. When the pile tip is extended to the deepest position considered in this study (-6.0 D_T), the bending moment induced by the pile under loading gradually decrease because the pushing manner of transferred load gradually become the pulling manner. In the other hand, the bending moment induced by pile under loading gradually increase with increasing pile length when the observation is considered at lower part of the tunnel lining on side closer pile (90° to 150°). This is caused by increasing of the load transfer from the pile tip as it is pulling manner. With the pile tip located at -6.0 D_T, the induced bending moment exceeds the maximum bending moment induced by excavated tunnel.

For tunnel located in stiff clay as shown in Figure 6.6b, the distributions of induced bending moment in tunnel lining due to complete tunnel excavation and pile under loading are similar. The changes of bending moments due to impacts of loaded pile are similar to those of case located in soft clay, but the larger quantity can be observed. The induced bending moments due to pile tips located at above tunnel (+1.0 D_T and +0.5 D_T) and below tunnel (-6.0 D_T) exceed the induced bending moment after complete tunnel excavation at upper and lower parts on side closer pile respectively, similarly the previous case.

For providing passengers with safe and comfortable transportation operations, the tunnels are generally constructed at the shallow depth. With considering the design of the tunnel lining located at shallow depth as this study, the steel reinforcement with using traditional rebar is subject primarily to the bending moment over the axial force. Then, the tunnel stability combining from concrete capacity and steel reinforcement is also governed by the bending moment due to complete tunnel excavation. As results described in Section 6.4.2, for tunnel located in soft clay, the maximum bending moments after complete tunnel excavation occur at the crown and right spring lines for negative and positive bending moment, respectively. For tunnel located in stiff clay, the maximum negative and positive bending moments occur at crown and above right tunnel spring line respectively. Thus, the tunnel stability in this situation are governed by either the bending moment at crown or that at right tunnel spring line. For this reason, the positions along the horizontal and vertical axes of tunnel lining, which can be provided the induced maximum bending moment due to tunnelling, are primarily investigated the change in bending moment due to loaded piles. To better understand the tunnel response in terms of change in lining forces, however, the change in axial force due to loaded piles should be investigated together. Additionally, the lining forces due to pile under loading at certain pile tips exceed those of complete tunnel excavation provided for the tunnel lining capacity. Thus, the special attention should be paid to protect or be aware the damage to the existing tunnel lining due to adjacent loaded pile.

6.4.4 The changes in lining forces observed at tunnel horizontal and vertical axes due to the application of working load on pile

1) The changes in axial force of the tunnel lining

The changes in axial force observed at tunnel crown, invert, and both spring lines at clearance 0.5 m are represented by ΔN_{Normal} for the tunnel in soft and stiff clay as illustrated in Figure 6.7a and b respectively. The percentage of ΔN_{Normal} are normalized with the maximum axial force due to constructed tunnel ($N_{Max\_Initial}$) against various normalized depths of the pile tip (L_P/L_T). The normalized positions of the pile tip beneath the tunnel spring line to the tunnel diameter, C_T/D_T, are also provided on the right side of the y-axis. The positions of the pile tip located above and below the tunnel spring line represented by the positive and negative signs, respectively.

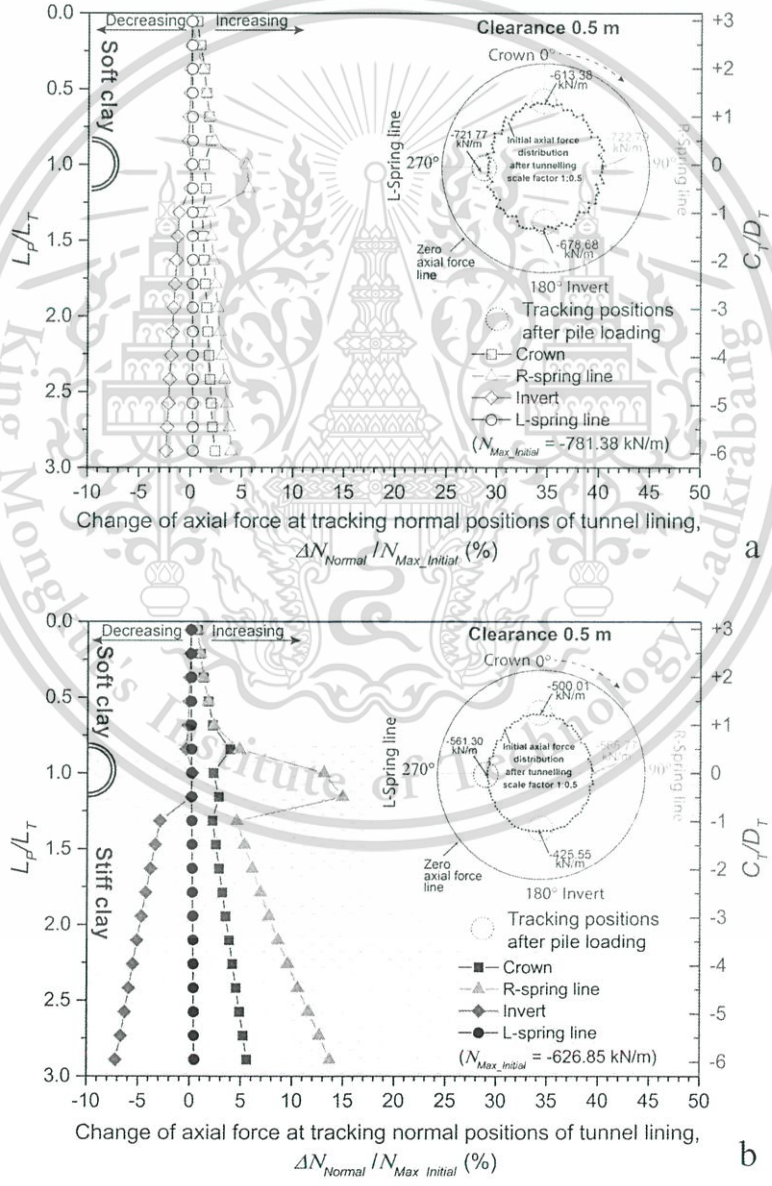

Figure 6.7 Changes of axial force at generally observed positions due to a pile under loading at clearance of 0.5 m with various tips for. (a(tunnel located in soft clay. (b(tunnel located in stiff clay.

ΔN_{Normal} at tunnel crown and right spring line represented by square and triangle symbols slightly increase and their magnitudes are close when the pile tip is located at above tunnel (+3.0 D_T to + 0.5 D_T). When the pile tip is located at tunnel axis (0.0 D_T), only ΔN_{Normal} at right spring line significantly increase with reaching the maximum value of 5% (by comparing with $N_{Max\_Initial}$ of -781.38 kN/m). For ease of understanding, the "increase or decrease" means the change values is becoming larger or smaller, with regarding of the sign performing the compressive or tensile behaviour of the tunnel lining. For investigating the change in axial forces which only behave the compressive behaviour, the increasing of change in axial forces means the larger changes of compressive axial forces. ΔN_{Normal} at crown and right spring line gradually increase with extending pile tip from -1.0 D_T to -6.0 D_T. ΔN_{Normal} at left spring line and invert of the tunnel represented by circle and diamond symbols respectively are close when the pile tip is located in the range of +3.0 D_T to -1.0 D_T. With extending the pile tips to the deepest level considered in this study (-6.0 D_T), ΔN_{Normal} at left spring line are still unchanged, but ΔN_{Normal} at tunnel invert gradually decrease.

For tunnel located in stiff clay as depicted in Figure 6.7b, the distribution patterns of ΔN_{Normal} are similar to those of the case of the tunnel located in soft clay, especially ΔN_{Normal} observed at tunnel crown and left spring line. However, the more increments of ΔN_{Normal} can be seen. Particularly ΔN_{Normal} is observed at right spring line, the maximum magnitude reached about 15% by comparing with smaller maximum of initial axial force (-626.85 kN/m), when the pile tip is located at the pile tip of -0.5 D_T. ΔN_{Normal} observed at tunnel invert are significantly decreased when the pile tip is extended in the range from -1.0 D_T to -6.0 D_T.

The results mentioned above can confirm again that the existing tunnel located in stiff clay is not safer than the existing tunnel located in soft clay when it is affected by adjacent pile under loading. Not only the tunnel deformation as mentioned in Chapter 5, the magnitude of the load applied to the pile subjected to soil stiffness has a strong influence, but also the induced axial forces in tunnel lining. The maximum value of ΔN_{Normal} at right spring line for both cases are probably insignificant by comparing the $N_{Max\_Initial}$ of each case study. However, as seen in Figure 6.5a and b, the axial forces induced by pile under loading exceeds the maximum value of the initial axial force. More attention should be thus paid on this situation.

2) The changes in bending moment of the tunnel lining

The changes in bending moment observed at tunnel crown, invert, and both spring lines at clearance 0.5 m are represented by ΔM_{Normal} for the tunnel located in soft and stiff clay as depicted in Figure 6.8a and b respectively. The same pattern of the considered changes in axial forces as the previous section is also performed for the changes in bending moment. The percentages of ΔM_{Normal} are normalized with the maximum bending moment due to constructed tunnel ($N_{Max\_Initial}$). For ease of the description, ΔM_{Normal} , are presented by regarding sign of bending moment which means that the increasing or decreasing of ΔM_{Normal} is larger or smaller changes in bending moment with the same sign of initial bending moment (the bending moment after complete tunnel construction).

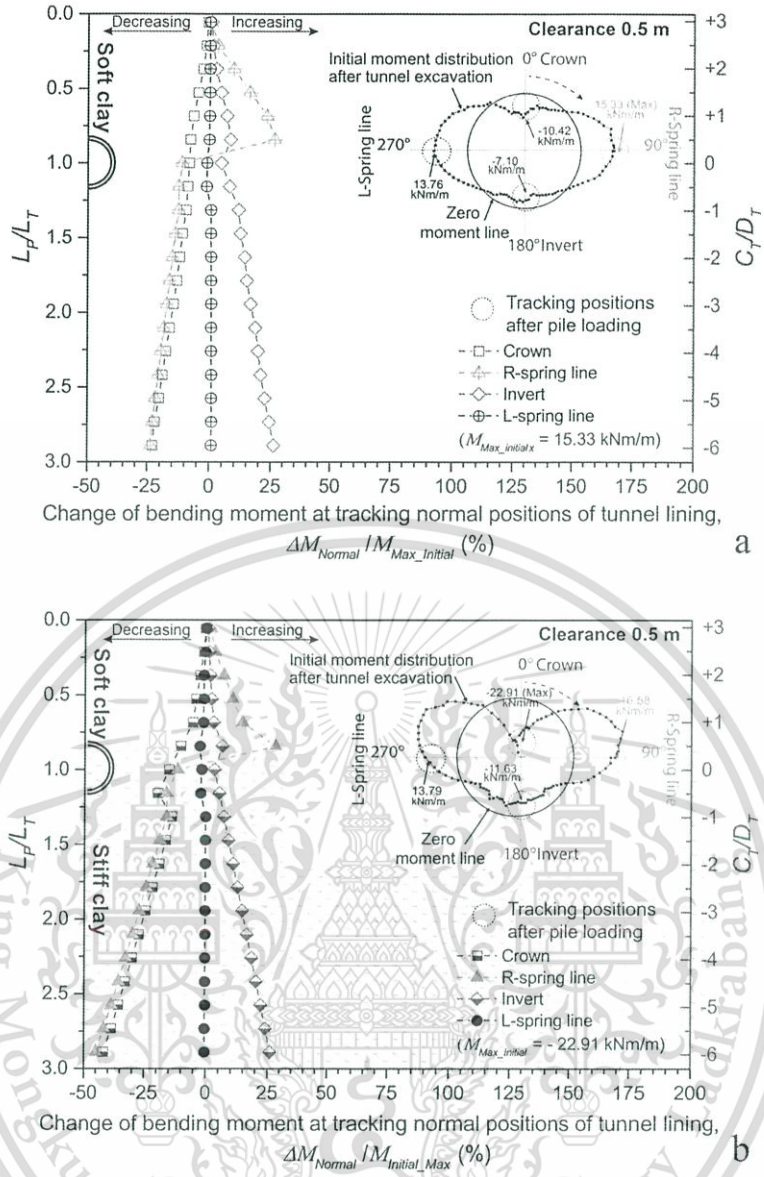

Figure 6.8 Changes of bending moment at generally observed positions due to a pile under loading at clearance of 0.5 m with various tips for. (a(tunnel located in soft clay. (b(tunnel located in stiff clay.

In Figure 6.8a for tunnel located in soft clay, it can be seen that ΔM_{Normal} at tunnel crown represented by clear square symbol (initial bending moment is negative bending moment) gradually decreases before slightly increases at which the pile tip is located at -1.0 D_T. When the pile tips are extended from -1.0 D_T to -6.0 D_T, ΔM_{Normal} at crown decreases again. ΔM_{Normal} at right spring line represented by triangle symbol with positive sign (initial bending moment is positive bending moment) significantly increases when the pile tip is located in the range from +3.0 D_T to +0.5 D_T (above the tunnel). At this level of the pile tip (+0.5 D_T), the maximum value of 27% by comparing with $M_{Max\_Initial}$ of 15.33 kNm/m occurs. When the pile tip is located at tunnel axis (0.0 D_T), ΔM_{Normal} at right spring suddenly decreases before it gradually decreases as well as ΔM_{Normal} at tunnel crown when the pile tip is

located below the tunnel axis (0.0 D_T to -6.0 D_T). ΔM_{Normal} observed at left spring line (circle symbol with positive sign) is remains constant with all positions of pile tips. When ΔM_{Normal} are observed at tunnel invert (clear diamond symbol), the small increasing occurs to reach the maximum value of about 27% at the pile tip of -6.0 D_T. Except when the pile tip is located at the tunnel spring line (0.0 D_T), small decreasing of ΔM_{Normal} occurs. Although the maximum values of increasing changes in bending moment at right tunnel spring line and invert are close, the critical position of tunnel lining, where the induced bending moment exceeds the initial value as shown in Figure 6.6a and should be specially traced, is the right tunnel spring line. In addition, the maximum value of 27% observed at tunnel invert does not exceed the maximum value of initial bending moment.

For the tunnel located in stiff clay as shown in Figure 6.8b, the positions of observing ΔM_{Normal} having the initial bending moment with positive and negative sign are represented by solid and half solid respectively. The distribution patterns of ΔM_{Normal} are similar to those of tunnel located in soft clay, but the larger decreasing of ΔM_{Normal} at tunnel crown (square symbol) and right spring line (triangle symbol) can be seen. Their maximum decreasing values reaching about 50% by comparing with larger $M_{Max\_Initial}$ of -22.99 kNm/m, when the pile tip is located below the tunnel (-0.5 D_T to -6.0 D_T). The changes in bending moment with decreasing values can imply that the deformation behaviour of tunnel lining has changed, e.g. compressive behaviour of the tunnel lining represented by negative bending moment in initial stage (after tunnel excavation) has been changed to become positive bending moments (after the tunnel affected from loaded pile) resulting in increased tensile behaviour of the tunnel lining. However, the reversed signs of considering ΔM_{Normal} do not occur in this section. The maximum increasing of 27% belongs to ΔM_{Normal} observed at right spring line when the pile tip is located at +0.5 D_T and ΔM_{Normal} observed tunnel invert when the pile tip is located at -6.0 D_T. Although, the induced bending moment due to pile under loading for tunnel located in stiff clay are larger than those of tunnel located in soft clay, the maximum increasing values of ΔM_{Normal} at tunnel invert and right spring line still close to those of the previous case (tunnel located in soft clay) because the initial bending moment used to normalize is larger. These results in this section can indicate that the impact of pile under loading on the induced bending moment are more influence than that of the induce axial force. However, when considering the distributions of lining force as depicted in Section 6.4.3 that shows the area where the maximum changes in lining force should be located, not located at tunnel horizontal or vertical axes. The position of maximum changes in lining forces should be consistent with that of the maximum changes in tunnel diameter investigated in Chapter 5. To preliminary offer a suitable observation of the changes in the lining forces, the tunnel shapes due to adjacent loaded pile with various depths are investigated in the next section.

6.5 The tunnel deformation shapes due to the application of working load on pile

The tunnel shape evolutions due to adjacent pile under loading with a clearance of 0.5m for cases of tunnels located in soft and stiff clay are illustrated in

Figure 6.9 and Figure 6.10 respectively. Note that the tunnel deformation due to the construction process is not considered. In this study, the observation positions of the contraction or extension changes in tunnel diameter, the assessment methods of the maximum changes in tunnel diameter are depicted in the figures, are specified as the reference nodes with inward or outward directions respectively.

As seen in Figure 6.9, the unsymmetrical shape of the global movement with extending length of its major axis (inclined with respect to the tunnel axis) and a distortion to the pile can be seen clearly as mentioned in the previous chapter (Section 5.4.2) The contraction and extension distortions of deformed tunnel shapes due to increasing the pile length can be clearly observed on the closer pile side, the contraction and extension distortions appear at the upper part and lower part of the tunnel lining respectively. When the pile tip is located at +1.0 D_T (the blue circle), the maximum tunnel deformations with contraction and extension behaviours occurred at about 27° and 115°, the larger magnitude of the tunnel deformation belongs to the contraction behaviours. When the pile tip is located at the spring line (0.0 D_T), the maximum tunnel deformations with contraction and extension behaviours are located at about 45° and 140°, their magnitudes are close to that of the pile tip located at +1.0 D_T. With extending pile tip below the tunnel to the deepest level considered in study (-1.0 to -6.0 D_T), the maximum tunnel deformations of both the contraction and extension behaviours are closely located at 45° and 135° whereas that the increment of the maximum extension deformation is more than the maximum contraction deformation.

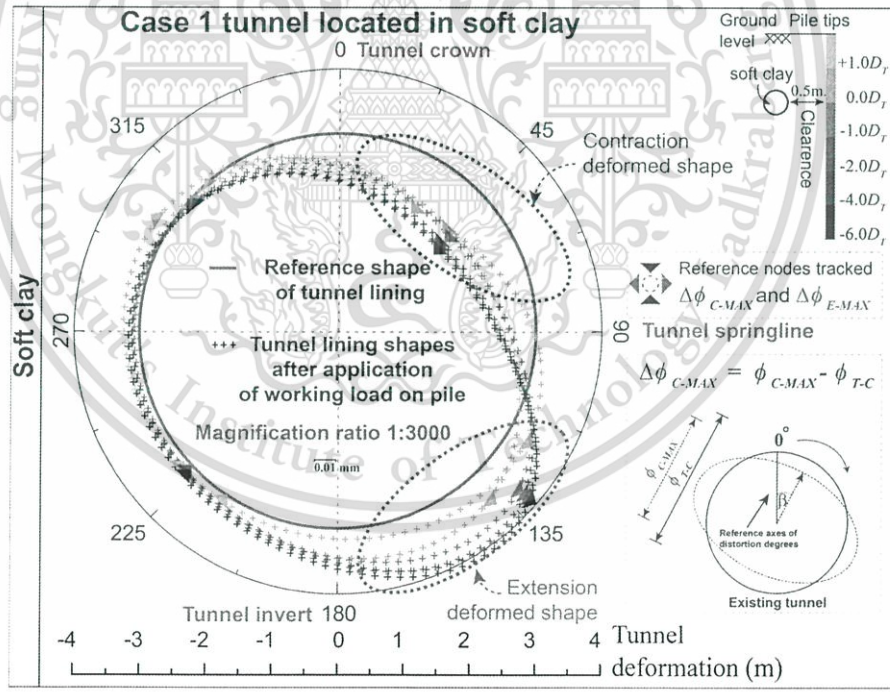

Figure 6.9 Deformed tunnel shapes after application of working load on pile for tunnel located in soft clay.

For the case of a tunnel in stiff clay as depict in Figure 6.10, global movement behaviour of the tunnel lining with the positions of the maximum deformations is similar to that in the case of the tunnel located in soft clay. The main differences are observed. First, a smaller movement increment of the maximum contraction behaviour occurs when the pile tip is located above the tunnel spring line (+1.0 D_T); however, a larger movement increment belonging to the maximum extension

behaviour is noted with increasing pile length (the pile tip under the spring line, -1.0 D_T to -6.0 D_T). Note that the application of working load on the pile in the case of a tunnel located in stiff clay is larger than that of the tunnel located in soft clay for the same pile tip.

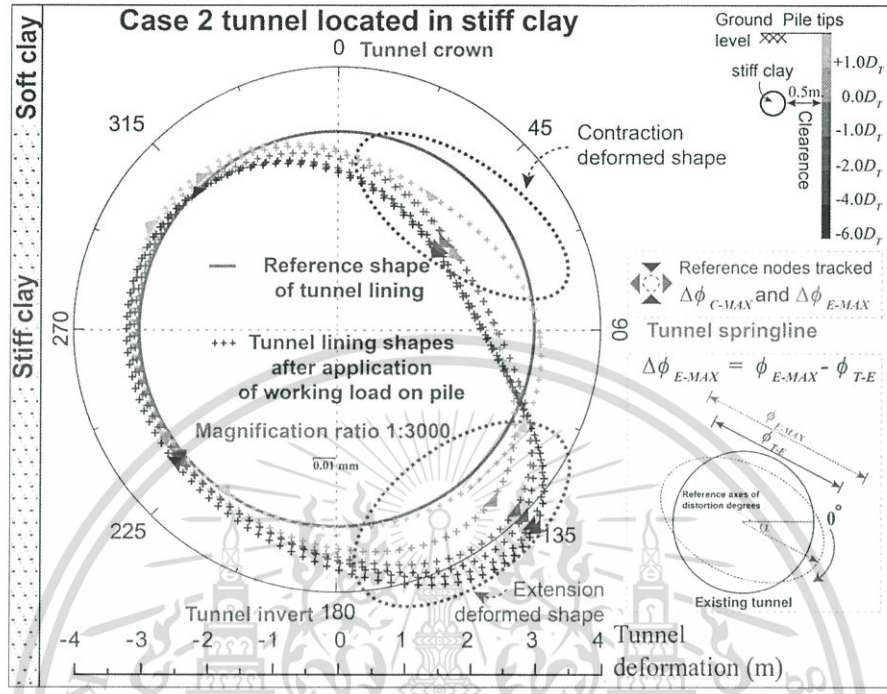

Figure 6.10 Deformed tunnel shapes after application of working load on pile for tunnel located in stiff clay.

As described above, the maximum deformations are located at about 27° to 45° on the tunnel upper part as contraction deformation and at about 115° to 135° on the tunnel lower part as extension deformation. Interestingly, according to the ITA guidelines for the design of tunnels [1] and the study of Abdel-Motaal et al., (2014) [12], the distributions of the lining forces in tunnel lining are associated with the tunnel deformation. Then, the changes in lining forces due to a loaded pile at which the maximum contraction or extension deformation occurs should be more significant than the changes in lining forces observed at tunnel horizontal and vertical axes. The observation of the maximum changes in axial force and bending moment due to application of load on the pile with various tips are thus explored in the next section.

6.6 The maximum changes in structural forces of the tunnel lining due to application of working load on pile

1) The maximum changes in axial force of the tunnel lining

The maximum changes in axial force ($\Delta N_{\max}$) with observed degrees (ω_N) due to pile under loading are presented and discussed in this section. The presentation of $\Delta N_{\max}$ is similar to those of the ΔN_{Normal} in Section 6.4.4. For the case of a tunnel in soft clay, the ΔN_{Max} and ω_N against the position of pile tip for various clearances are depicted in Figure 6.11a and b, respectively. It is seen that the distribution patterns of $\Delta N_{\max}$ against Lp/L_T (or C_T/D_T) are similar to those of ΔN_{Normal} observed at right spring line as shown in Figure 6.7a. $\Delta N_{\max}$ for clearances of 3.5 and 4.5 with all

depths of pile tips are insignificant and very close. ΔN_{max} significantly increase to reach the maximum value of about 5% when the pile tip is located at lower part of the tunnel ($0.0 \geq C_T/D_T \geq -0.5$) before decreasing at the pile tip of -1.0 D_T.

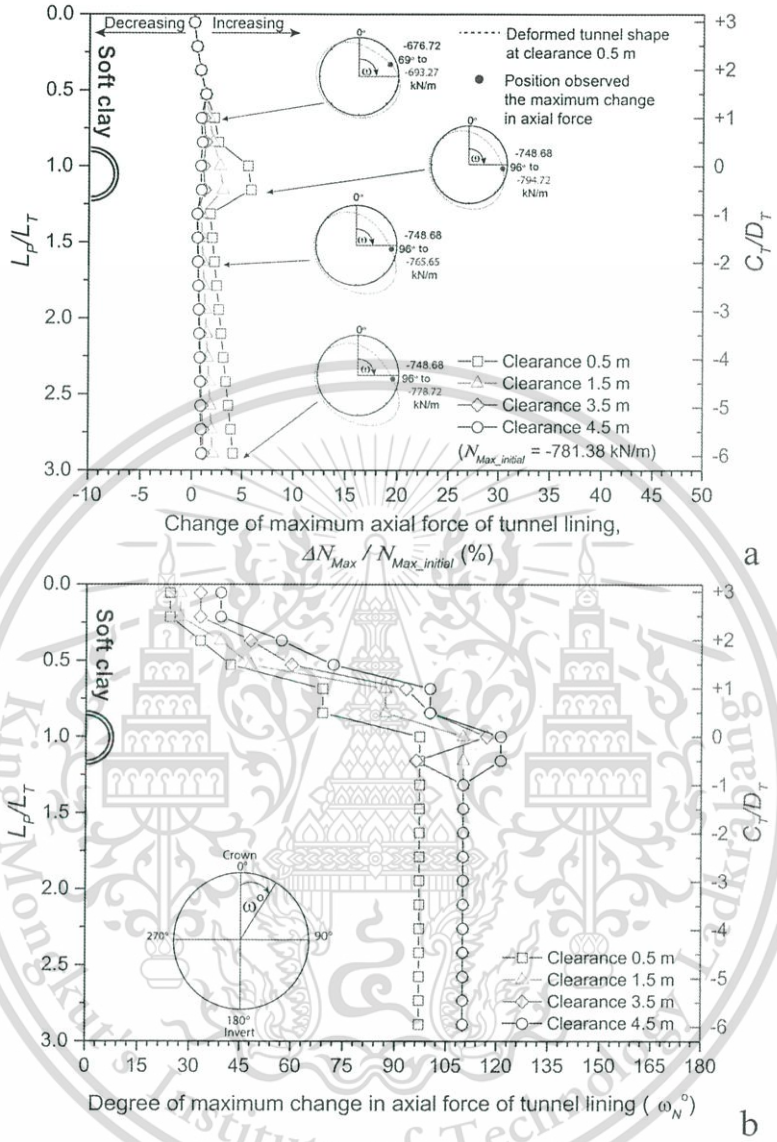

Figure 6.11 Changes of axial forces for tunnel located in soft clay (a) the maximum change in axial force (b) degrees of the maximum change in axial force, ω_N.

Surprisingly, the maximum value of ΔN_{max} are very close to that of ΔN_{Normal} observed at the right tunnel spring line even though ΔN_{max} are investigated in term of the maximum change. When the pile tip is located below the tunnel (-1.0 D_T), ΔN_{max} significantly increase again with a constant degree of ΔN_{max}.

Together with the ω_N degree in Figure 6.11b, the similar patterns to a distortional degree presented in Section 5.4.4 of Chapter 5 can be seen that the larger ω_N belongs to the larger clearance (for the same pile tip level). With a longer pile, until the pile tip is located at +1.0 D_T, ω_N continues to increase (at the same level of the pile tip, ω_N at a clearance of 4.5m remains the largest), before ω_N becomes

constant when the pile tip is located at above the tunnel lining (+0.5 D_T). Below this level, ω_N increase again before ω_N become constant at 96 ° with extending pile to deepest level in study for the clearance of 0.5 m. The maximum magnitude of ΔN_{Max} occurs at ω_N of 96°. For the other clearances, the constant of ω_N occurs at 112 °. ω_N indicating the positions of ΔN_{Max} can consider the pile tip conditions as "short pile" or long pile". These conditions are consistent with the summary of Chapter 5. These pile tip conditions can provide the range of pile tip affecting on the existing tunnel. The range of pile tip above the tunnel, +3.0 D_T to +0.5 D_T, are defined as the short pile condition where ω_N is positioned between 20° to 60°. For the long pile condition, ω_N are constantly positioned at 96 ° (considering with the clearance of 0.5 m) for the pile tips located the range from +0.5 D_T to -6.0 D_T.

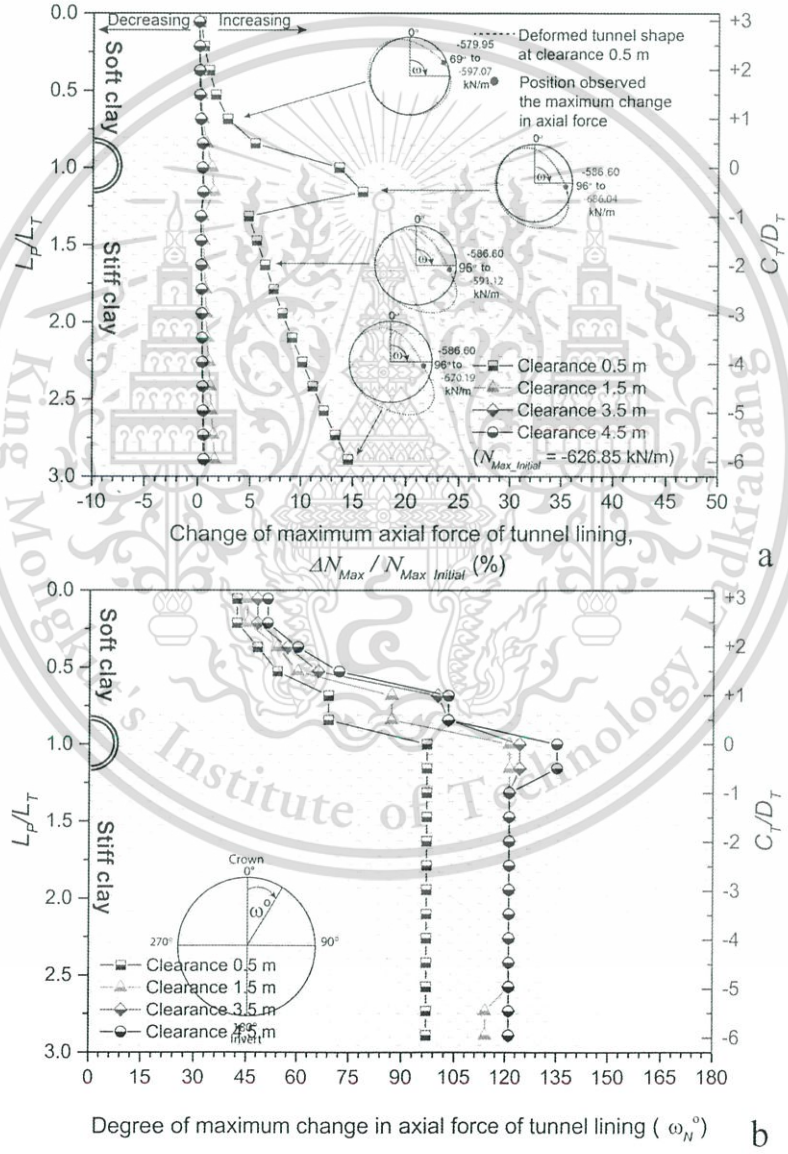

Figure 6.12 Changes of axial forces for tunnel located in stiff clay. (a) the maximum change in axial force. (b) degrees of the maximum change in axial force, ω_N.

For the case of a tunnel in stiff clay as shown in Figure 6.12a and b, the distribution pattern of ΔN_{Max} remain similar to those of ΔN_{Normal} observed at right tunnel spring line as shown in Figure 6.7b for the same case.

The maximum value of 15% by comparing with $N_{Max\_Initial}$ (-626.85 kNm/m), which is very close to those of ΔN_{Normal} at right spring line, still occurs when the pile tip is located at tunnel invert. When the pile tip is extended below this level, the significant increment of ΔN_{Max} can be seen. Likewise, the distribution of ω is similar to that of tunnel located in sift clay. There are two conditions for pile tip defined from the positions of ΔN_{Max}. When considering ω_N for the clearance of 0.5 m, ω_N is different with comparing the case of tunnel in soft clay for short pile condition. Whereas, ω_N is positioned at 96° when the pile tip is located at the range from +0.5 D_T to -6.0 D_T defined as long pile condition. When considering other clearances with long pile condition, ω_N is constant at 120°.

As described above, the maximum values obtained from the ΔN_{Max} and ΔN_{Normal} observed right spring line is very close as 5% and 15% by comparing with each initial maximum axial forces for tunnel located in soft and stiff clay respectively. It can indicate that whatever the assessment methods of changes in axial forces, ΔN_{Normal} or ΔN_{Max}, their maximum values are insignificant. The maximum values of the ΔN_{Max} and ΔN_{Normal} with ω_N at 96° occur when the pile tip is located at tunnel invert for both cases. With comparing between the case of tunnel in soft and stiff clay, when the pile tip is located below the tunnel (- 1.0 D_T to -6.0 D_T), ω_N is constant at 96° even though ΔN_{Max} increases. Additionally, it can be seen that the tunnel deformed shapes depicted as Figure 6.11a and Figure 6.12a are extended but the ω_N is still constant.

2) The maximum changes in bending moment of the tunnel lining

The changes in bending moment of tunnel lining in the circumferential direction, ΔM_{Max}, with its degrees, ω_M, for tunnel located in soft and stiff clay are illustrated in Figure 6.13 and Figure 6.14. ΔM_{Max} is presented with similar presentation of ΔN_{Max} as shown in Figure 6.13a, the initial bending moment indicating the initial behaviour of bending moment after excavated tunnel are shown near left axis (L_P/L_T). The distribution patterns of ΔM_{Max} are obviously different from those of ΔM_{Normal}, but are similar to those of the maximum changes in tunnel diameter as described in Section 5.4.4 of Chapter 5.

The only increasing of ΔM_{Max} for all clearances can be seen. ΔM_{Max} for the clearances of 3.5 m and 4.5 m is close with all levels of extended pile tip. For the clearances of 0.5 m, ΔM_{Max} gradually increases to reach the value of about 50% when the pile tip is located above the tunnel ($C_T/D_T \leq +0.5$). With negative behaviour of initial bending moment, the increasing of ΔM_{Max} means the increasing of compressive bending moment. The sudden decreasing occurs at the pile tip extended to the tunnel spring line (0.0 D_T) where the initial moment becomes the tensile behaviour (positive sign). When the pile tip is located below the tunnel axis ($C_T/D_T \geq 0.0$), the increasing of ΔM_{Max} with tensile behaviour occurs to reach the maximum

value of about 70% at the deepest level considered in this study (−6.0 D_T). By comparing with the value of ΔM_{Normal}, the value of ΔM_{Max} is much larger than that of the ΔM_{Normal} for the same pile length, for example, about 2.5 times greater at +0.5 D_T and −6.0 D_T. This indicates that observing the change in bending moment at tunnel horizontal and vertical axes results in underestimation. However, the initial bending moments at observed positions of ΔM_{Max}, which are shown in Figure 6.13a, are smaller than those of ΔM_{Normal}. Although, the increasing of ΔM_{Max} reaches about 70% of the maximum initial bending moment, the induced bending moment observed at the maximum increasing degree (124°) does not exceed the maximum initial bending moment.

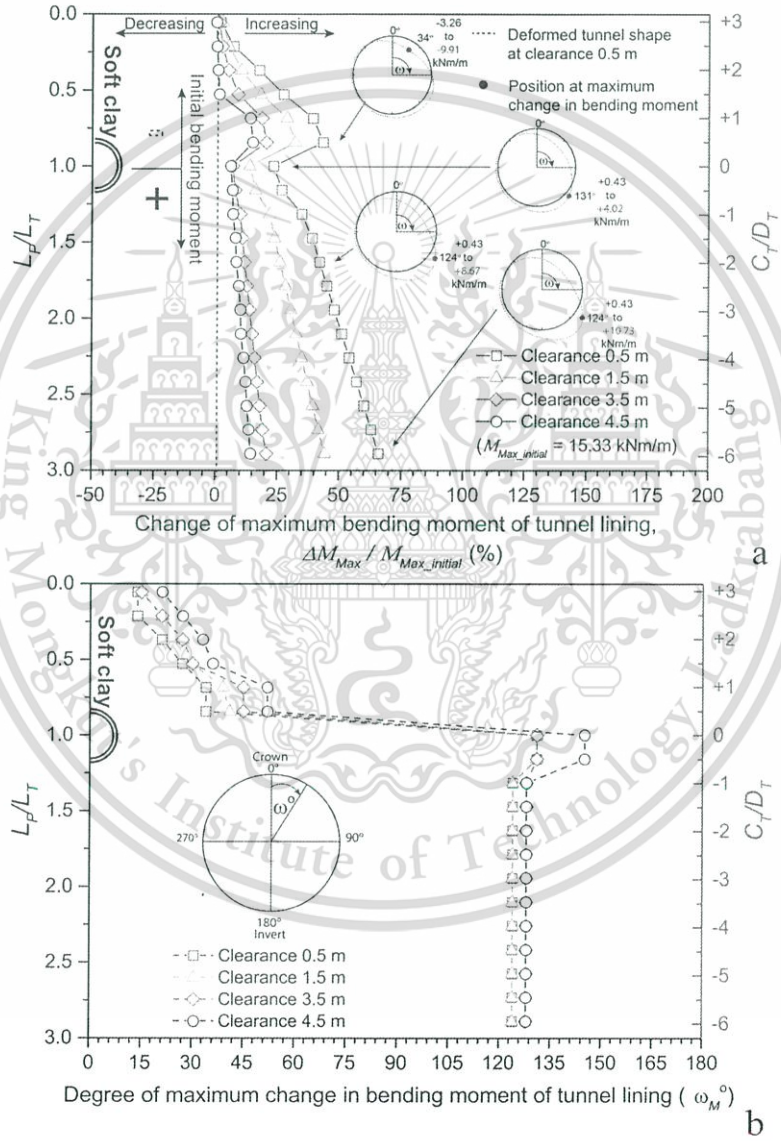

Figure 6.13 Change of bending moment due to a pile under loading with various tips for tunnel located in soft clay. (a) the maximum change in bending moment. (b) degrees of the maximum change in bending moment, ω_M.

Additionally, the tunnel deformed shapes together with observed positions are depicted in Figure 6.13a, it seems to be seen that the positions of the maximum value of ΔM_{Max} are subjected to the pile tip positions obviously. When the pile tip is located

above or below tunnel, the maximum value of ΔM_{Max} is also at the upper tunnel part or below tunnel parts. In order to be clear as mentioned before, the positions of the maximum value of ΔM_{Max} represented by ω_M are further described as below.

By observing ω_M in Figure 6.13b, the distribution patterns of ω_M are divided into two sections and the larger ω_M belongs to the larger clearance case (for the same pile tip level). The first section is the distributions of ω_M positioned between 15° to 50 ° when the pile tip is located above the tunnel axis ($C_T/D_T \geq 0.0$). The second section is the distributions of ω_M positioned between 120 ° to 145 ° when the pile tip is located below the tunnel axis ($C_T/D_T \leq 0.0$). This can also indicate two main behaviour types of pile-tunnel interaction depending on the relative pile length compared to the tunnel position: short pile and long pile conditions according to the summary of previous investigation (in Chapter 5).

For the case of the tunnel located in stiff clay, the initial bending moment of considered positions of ΔM_{Max} are negative bending moment (negative sign). The distribution patterns of ΔM_{Max} as depicted in Figure 6.14a are significantly different with those of the previous case. As seen in this figure, the decreasing of ΔM_{Max} can be obviously observed. The distribution patterns of ΔM_{Max} for the clearance of 3.5 m and 4.5 m are very close. This can imply that the clearance of 4.5 m seems to be safe for influence of adjacent pile under loading on the stability of existing tunnel in this situation. For the other clearances, When the pile tip is located in soft clay (+3.0 D_T to +1.0 D_T), the small increment of ΔM_{Max} occurs with extending pile tip. At the same pile length and clearance, ΔM_{Max} in this case is much smaller than in the previous condition (a tunnel in soft clay). This indicates that, when subjected to the same working load, the ΔM_{Max} in stiff clay is smaller. When the pile tip is extended into stiff clay (+0.5 D_T), the increasing of ΔM_{Max} become larger. The gradually decreasing of ΔM_{Max} occurs when the pile tip is below at the tunnel spring line.

ΔM_{Max} significantly decrease with increasing pile tip to the deepest in study (-0.5 D_T to -6.0 D_T). When the decreasing of ΔM_{Max} reaches to about 20%, the reversed sign of ΔM_{Max}, which means changing the negative bending moment to positive bending moment, occurs. At the deepest of pile tip, the maximum values of 120% of $M_{Max\_Initial}$ (-22.99 kNm/m) occurs. This can firstly indicate that the compressive behaviour of bending moment induced in tunnel lining at initial stage (after excavated tunnel) become the tensile behaviour when the pile tip is located in range from 0.0 D_T to -6.0 D_T for the clearance of 0.5 m. The second finding is that the changing behaviour of bending moment, compressive to tensile behaviours, is induced by tunnel deformation conducted in extension behaviour. Besides, the compressive bending moment is induced by tunnel contraction deformation. This again confirms that the behaviour of ΔM_{Max} is consistent with the behaviour of the maximum changes in tunnel diameter proposed in Section 5.4.4 of Chapter 5. Moreover, as seen in Figure 6.6b. The induced bending moment due to the impact of loaded pile at the degree of 124°, the maximum value of ΔM_{Max} can be observed, exceeds the initial bending moment when the pile tip is located at -6.0 D_T. In this situation, the tunnel stability should be observed by paying special attention. Additionally, by comparing

with the maximum value of ΔM_{Normal}, the value of ΔM_{Max} is much larger than that of the ΔM_{Normal} for the same pile length, for example, about 2.0 and 4.0 times greater at +0.5 D_T and −6.0 D_T respectively.

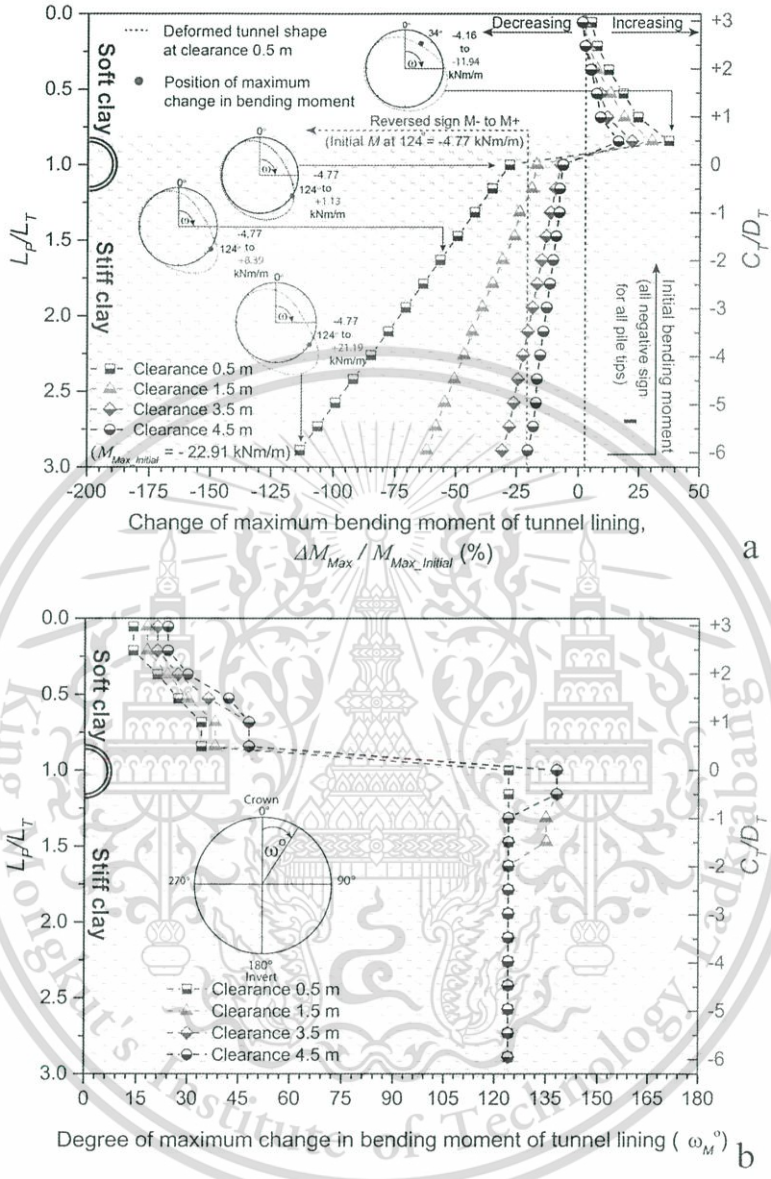

Figure 6.14 Change of bending moment due to a pile under loading with various tips for tunnel located in stiff clay. (a) the maximum change in bending moment. (b) degrees of the maximum change in bending moment, ω_M.

By observing ω_M for tune located in stiff clay as shown in Figure 6.14b, the distribution patterns of ω_M are similar to the previous case (a tunnel in soft clay), but the values are different. The three zones of ω_M distributions can be also observed. However, a small discrepancy can be seen, for example, in the case of a clearance of 1.5 m. With the pile tip extending below the tunnel spring line (0.0 D_T to -6.0 D_T), the positions of ω_M, which occur the maximum values of ΔM_{Max}, are at 124° for the all clearances.

According to the results in Section 5.4.4 of Chapter 5, although the maximum changes in tunnel diameter significantly increase when the pile tip is extended below the tunnel spring line, their distortion degrees are constant. This again confirms that the positions of the maximum change in tunnel diameter are consistent with that of the maximum changes in structural forces. In order to be clear this assumption, the maximum changes in tunnel dimeter proposed in Chapter 5 are further described as below.

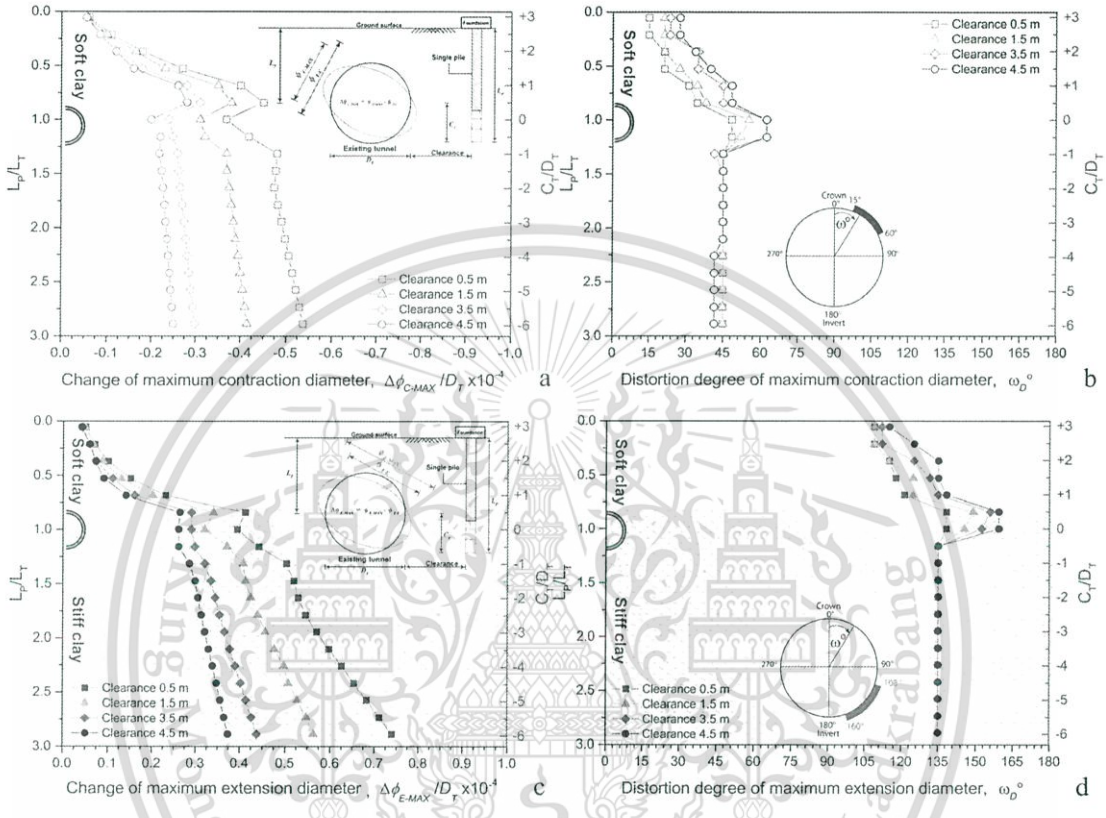

Figure 6.15 Tunnel deformation due to a pile under loading with various tips. (a) Maximum contraction changes in tunnel diameter for tunnel located in soft clay. (b) Distortional degree of contraction changes in tunnel diameter for tunnel located in soft clay, ω_D. (c) Maximum extension changes in tunnel diameter for tunnel located in stiff clay. (d) Distortional degree of extension changes in tunnel diameter for tunnel located in stiff clay, ω_D.

Figure 6.15 shows the maximum contraction change ($\Delta\phi_{C\text{-}MAX}$) and maximum extension change ($\Delta\phi_{E\text{-}MAX}$) in tunnel diameter with distortion degrees started from tunnel crown (ω_D) due to pile loading are presented and discussed in this section. The maximum contraction and extension change ($\Delta\phi_{C\text{-}MAX}$ and $\Delta\phi_{E\text{-}MAX}$) with their distortion degrees (ω_D) are presented for the cases of tunnel located in soft and stiff clay as Figure 6.15a, b and Figure 6.15c, d respectively. The distribution patterns of $\Delta\phi_{C\text{-}MAX}$ and $\Delta\phi_{E\text{-}MAX}$ as depicted in Figure 6.15a and c are similar to that of ΔM_{Max} obviously. Together with the distortional degree (ω_D) in Figure 6.15b and d, the similar distribution patterns of ω_D and ω_M can be seen as described above. ω_D

associated with the $\Delta\phi_{C\text{-}MAX}$ and $\Delta\phi_{C\text{-}MAX}$ are positioned between 15° to 60° and 108° to 160° respectively. However, ω_D remains constant with increasing pile length and reaching the maximum value at 45° and 135° for the assessment method of $\Delta\phi_{C\text{-}MAX}$ and $\Delta\phi_{C\text{-}MAX}$.

6.7 Summary

A series of 3D-FEA were conducted to investigate the tunnel response due to an adjacent pile under loading, in the case of a single pile located on a single side of the tunnel. The results are as follows:

1. The changes in axial force are insignificant, the maximum value is only 15% of maximum initial axial forces. The maximum values of ΔN_{Max} and ΔN_{Normal} at right tunnel spring line are very close. On the other hands, the maximum changes in bending moment, ΔM_{Max} reaches to 120%, should be mainly considered together with the total bending moment induced by loaded pile to pay attention for investigating or planning the impacts due to adjacent loaded pile on existing tunnel in this situation.

2. The induced bending moments due to loaded pile exceed the maximum of initial bending moment (after complete tunnel excavation) when the pile tips are located in the ranges of +1.0 D_T to +0.5 D_T and at -6.0 D_T for both cases considered in this study. The special attention should be paid to trace the exiting tunnel when the pile tips are located these positions.

3. The reversed sign of ΔM_{Max} is established at 124°, compressive bending moment to tensile bending moment, for all clearances in case of tunnel located in stiff clay. This indicates that possible cracking in tunnel lining if the tensile strength of reinforced concrete lining is to be exceeded. Thus, special attention should be paid to this situation.

4. The positions of the maximum changes in lining forces are similar to those of the maximum changes in tunnel diameter, but the values are different. The monitoring instrument for observing the additional lining forces should be especially installed at those positions.

5. The changes in lining forces observed with the maximum value are consistent with the maximum contraction or extension changes in tunnel diameter as proposed in Chapter 5. Obviously, the change in bending moment is subjected to the manner of tunnel deformation. The compressive or tensile bending moment is induced by tunnel contraction or extension deformations respectively.

6. It is postulated that the pile tip at +0.5 D_T above the tunnel spring line, which is considered form the induced bending moment, should be considered for existing tunnel assessment regarding an adjacent pile under loading for a short pile condition in the cases of tunnel located in soft and stiff clay. The greater length of bored pile below +0.5 D_T to the deepest level in engineering practice should be taken into consideration for a long pile condition in both case studies.

7. The clearance of 4.5 m is sufficient distance to be safe for the influences of adjacent loaded pile on the tunnel in this situation.

6.8 References

[1] I.T.A., "Guidelines for the design of shield tunnel lining," *Tunn. Undergr. Sp. Technol.*, vol. 15, no. 3, pp. 303–331, Jul. 2000.

[2] D. Wen, J. Poh, and Y. W. Ng, "Design considerations for bored tunnels at close proximity," *Tunn. Undergr. Sp. Technol.*, vol. 19, no. Ccl, pp. 468–469, 2004.

[3] R. Brinkgreve., E., Engin, W. Swolfs, "*PLAXIS 3D Version 2016 manual*," Chapman, 2016.

[4] H. Mroueh and I. Shahrour, "A simplified 3D model for tunnel construction using tunnel boring machines," *Tunn. Undergr. Sp. Technol.*, vol. 23, no. 1, pp. 38–45, 2008.

[5] F. Tschuchnigg and H. F. Schweiger, "The embedded pile concept - Verification of an efficient tool for modelling complex deep foundations," *Comput. Geotech.*, vol. 63, pp. 244–254, 2015.

[6] S. Likitlersuang, S. Teachavorasinskun, C. Surarak, E. Oh, and A. Balasubramaniam, "Small strain stiffness and stiffness degradation curve of Bangkok Clays," *Soils Found.*, vol. 53, no. 4, pp. 498–509, 2013.

[7] S. Likitlersuang, C. Surarak, D. Wanatowski, E. Oh, and A. Balasubramaniam, "Finite element analysis of a deep excavation : A case study from the Bangkok MRT," *Soils Found.*, vol. 53, no. 5, pp. 756–773, 2013.

[8] T. Schanz, a Vermeer, and P. Bonnier, "The hardening soil model: formulation and verification," *Beyond 2000 Comput. Geotech. 10 years PLAXIS Int. Proc. Int. Symp. beyond 2000 Comput. Geotech. Amsterdam Netherlands 1820 March 1999*, p. 281, 1999.

[9] T. Benz, Small-Strain Stiffness of Soils and its Numerical Consequences. Doctoral Thesis, Institute of Geotechnical Engineering, University of Stuttgart, Stuttgart, 2007.

[10] C. Surarak, S. Likitlersuang, D. Wanatowski, A. Balasubramaniam, E. Oh, and H. Guan, "Stiffness and strength parameters for hardening soil model of soft and stiff Bangkok clays," *Soils Found.*, vol. 52, no. 4, pp. 682–697, 2012.

[11] P. Jongpradist, T. Kaewsri, A. Sawatparnich, S. Suwansawat, S. Youwai, W. Kongkitkul, and J. Sunitsakul, "Development of tunneling influence zones for adjacent pile foundations by numerical analyses," *Tunn. Undergr. Sp. Technol.*, vol. 34, pp. 96–109, 2013.

[12] M. A. Abdel-Motaal, F. M. El-Nahhas, and A. T. Khiry, "Mutual seismic interaction between tunnels and the surrounding granular soil," *Hous. Build. Natl. Res. Cent. J.*, vol. 10, no. 3, pp. 265–278, 2014.

CHAPTER 7

Conclusions and Recommendations

7.1 Conclusion

A series of 3D-FEA were conducted to investigate the tunnel responses due to an adjacent pile under loading, in the case of a single pile located on a single side of the tunnel. Based on the results from this dissertation, the following conclusions are drawn:

1. The tunnel influence zone taking the effect of adjacent loaded pile can be much smaller than the existing zone in which all construction activities are taken into consideration.

2. The tunnel lining deforms as a kidney or rotated ellipse shape when the pile tip is above or below the tunnel spring line, respectively. The tunnel deformation should be thus assessed by the maximum contraction change ($\Delta\phi_{C-MAX}$) and maximum extension change ($\Delta\phi_{E-MAX}$) in a tunnel diameter with distortion degrees (α and β) as proposed in this study.

3. The mechanisms behind the tunnel deformation due to an adjacent pile under loading are principally due to the movement behaviour of soil surrounding the tunnel, which in turn is dependent on the load transfer behaviour from the pile. Thus, the relative position of the tunnel and pile tip, magnitude of the applied load and stiffness of the soil layer in which the tunnel is located play a key role in this complex behaviour.

4. The changes in axial force for all observed points, are relatively small in this situation where the tunnel located in shallow depth. The changes in bending moment should be of concerns.

5. The distribution patterns of the maximum changes in tunnel diameter and bending moment are consistent.

6. It is postulated that the pile tip at +0.5 D_T should be considered for existing tunnel assessment regarding an adjacent pile under loading for a short pile condition in the cases of tunnel located in soft and stiff clay. The greater length of bored pile below +0.5 D_T to the deepest level in engineering practice should be taken into consideration for a long pile condition in both case studies.

7. The influence zone for pile tip proposed in the preliminary investigation is further developed as shown in Figure 7.1. It is reasonable to recommend the range of 1.0 D_T above tunnel spring line and below tunnel spring line to the deepest level in engineering practice should be taken into consideration. For the horizontal clearance, the value of 0.7 D_T or 4.5 m from tunnel surface seems to be sufficient.

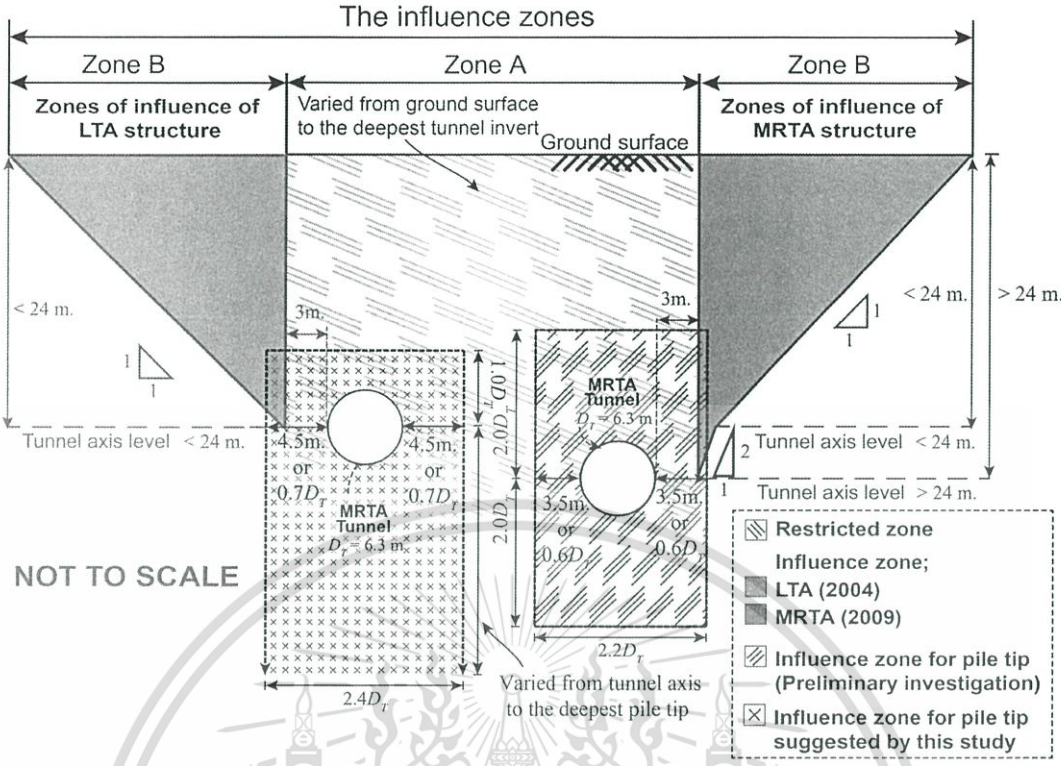

Figure 7.1 The proposed influence zone and the influence zones in previous studies.

7.2 Recommendations for the future works

Further study will be necessary by extending the scope of study to the segmental lining which may be first numerically performed based on the models and parameters derived in the present study. The effect of joints between segmental pieces or rings can then be considered. Additionally, the soil profiles and conditions should be more considered, especially a soil condition where the coefficient of earth pressure at rest, K_0 is more than 1.0. The tunnel responses should be different from this study. Moreover, series of physical model tests will provide the validity of the findings in this study.

BIBLIOGRAPHY

A. Bobet, "Analytical Solutions for Shallow Tunnels in Saturated Ground," *Journal of Engineering Mechanics*, vol. 127, no. 12. pp. 1258–1266, 2001.

A. M. M. Wood, "The circular tunnel in elastic ground," *Géotechnique*, vol. 25, no. 1, pp. 115–127, 1975.

A. S. User, "Abaqus 6.3-1," *Dassault Systèmes Simulia Corp., Provid. RI, USA*, vol. Dassault S, 2008.

A. Verruijt and J. R. Booker, "Surface settlements due to deformation of a tunnel in an elastic half plane," *Géotechnique*, vol. 46, no. 4, pp. 753–756, 1996.

A. W. Skempton,1959. "Cast In-Situ Bored Piles in London Clay," *Géotechnique* 9(4): 153–73, 1959.

A. Wonglert and P. Jongpradist, "Impact of reinforced core on performance and failure behavior of stiffened deep cement mixing piles," *Comput. Geotech.*, vol. 69, pp. 93–104, 2015.

Abu-Krisha "A. Numerical modelling of TBM tunnelling in consolidated clay," Ph.D. Thesis, University of Innsbruck, 1998.

B. Maidl, M. Herrenknecht, and L. Anheuser, L, "*Mechanised Shield Tunneling*," 1996.

B. Stack, "Handbook of Mining and Tunneling Machinery," *John Wiley & Sons*, New York, 1982.

B. B. Broms, "Methods of calculating the ultimate bearing capacity of piles – a summary," *Soils-Soils, No. 18- 19:* 21-32, 1966.

C. J. Lee, "Three-dimensional numerical analyses of the response of a single pile and pile groups to tunnelling in weak weathered rock," *Tunn. Undergr. Sp. Technol.*, vol. 32, pp. 132–142, 2012.

C. Surarak, S. Likitlersuang, D. Wanatowski, A. Balasubramaniam, E. Oh, and H. Guan, "Stiffness and strength parameters for hardening soil model of soft and stiff Bangkok clays," *Soils Found.*, vol. 52, no. 4, pp. 682–697, 2012.

C. Surarak, S. Likitlersuang, D. Wanatowski, A. Balasubramaniam, E. Oh, and H. Guan, "Stiffness and strength parameters for hardening soil model of soft and stiff Bangkok clays," *Soils Found.*, vol. 52, no. 4, pp. 682–697, 2012.

C. T. Tseng, "Three dimension simulation of EPB shield tunneling in Bangkok soft ground", *Master Thesis, Asian Institute of Technology, Thailand*, 2000.

C. W. W. Ng, H. Lu, and S. Y. Peng, "Three-dimensional centrifuge modelling of the effects of twin tunnelling on an existing pile," *Tunn. Undergr. Sp. Technol.*, vol. 35, pp. 189–199, 2013.

C. González and C. Sagaseta, "Patterns of soil deformations around tunnels. Application to the extension of Madrid Metro," *Comput. Geotech.*, vol. 28, no. 6–7, pp. 445–468, 2001.

C. Sagaseta, "Analysis of undrained soil deformation due to ground loss," *Géotechnique*, 37 (3), 301–320, 1987.

C. W. W. Ng, H. S. Sun, G. H. Lei, J. W. Shi, and D. Mašín, "Ability of three different soil constitutive models to predict a tunnel's response to basement excavation," *Can. Geotech. J.*, vol. 52, no. 11, pp. 1685–1698, 2015.

C. W. W. Ng, T. Boonyarak, and D. Masin, "Three-dimensional centrifuge and numerical modeling of the interaction between perpendicularly crossing tunnels," *Can. Geotech. J.*, vol. 50, no. 9, pp. 935–946, 2013.

D. H. Morgan, "A contribution to the analysis of stress in a circular tunnel," *Geotechnique*, 11 (3), 37–46, 1971.

D. Parker, "Pinning hopes," *New Civil Engineer Supplement: Engineering the Millennium Dom*e, 24 February, xiv–xv, 2000.

D. Selemetas, J. R. Standing, and R. J. Mair, "The response of full-scale piles to tunnelling," *Geotech. Asp. Undergr. Constr. Soft Gr. - Proc. 5th Int. Conf. TC28 ISSMGE*, pp. 763–769, 2006.

D. Wen, J. Poh, and Y. W. Ng, "Design considerations for bored tunnels at close proximity," *Tunn. Undergr. Sp. Technol.*, vol. 19, no. Ccl, pp. 468–469, 2004.

E. J. Cording, and W.H. Hansmire, "Displacements around soft ground tunnels," *In: 5th Pan American Congress on Soil Mechanics and Foundation Engineering, General Report-Session IV*, Buenos Aires, pp. 571–632, 1975.

E. M. Comodromos, M. C. Papadopoulou, and G. K. Konstantinidis, "Numerical Assessment of Subsidence and Adjacent Building Movements Induced by TBM-EPB Tunneling," *J. Geotech. Geoenvironmental Eng.*, vol. 140, no. 11, p. 4014061, 2014.

E. O. Measor, and D.H. New, "The design and construction of the Royal Festival Hall." *South Bank. J. Instn Civ. Engrs* 36, 241–318, 1951.

European Committee for Standardization (CEN), Design of steel structures, Part 1–6 general rules: Supplementary rules for shell structures. Eurocode 3. Brussels, Belgium, 1999.

F. C. Schroeder, *"The Influence of Bored Piles on Existing Tunnels,"* A Thesis Submitted to the University of London for the Degree of Doctor of Philosophy and for the Diploma of the Imperial College of Science, Technology and Medicine, 2002.

F. C. Schroeder, D. M. Potts, and T. I. Addenbrooke, "The influence of pile group loading on existing tunnels," *Géotechnique*, vol. 54, no. 6, pp. 351–362, 2004.

F. J. Kaalberg, H.J. Lengkeek, E.A.H. Teunissen, "*Evaluatie van de meetresulaten van het proefpalenprojek ter plaatse van de tweede Heinenoordtunnel.*" Adviedbureau Noord/Zuidlijn Report No. R981382, Amsterdam. (in Dutch), 1999.

F. Tschuchnigg and H. F. Schweiger, "The embedded pile concept - Verification of an efficient tool for modelling complex deep foundations," *Comput. Geotech.*, vol. 63, pp. 244–254, 2015.

F. Ye, C. fei Gou, H. dong Sun, Y. peng Liu, Y. xu Xia, and Z. Zhou, "Model test study on effective ratio of segment transverse bending rigidity of shield tunnel," *Tunn. Undergr. Sp. Technol.*, vol. 41, no. 1, pp. 193–205, 2014.

G. G. Meyerhof, "Bearing Capacity and Settlement of Pile Foundations," *J. Geotech. Eng. Div.*, vol. 102, no. 3, pp. 195–228, 1976.

G. W. Clough, B. P. Sweeney, and R. J. Finno, "Measured Soil Response to EPB Shield Tunneling," *J. Geotech. Eng.*, vol. 109, no. 2, pp. 131–149, 1983.

G. Zheng, T. Zhang, and Y. Diao, "Mechanism and countermeasures of preceding tunnel distortion induced by succeeding EPBS tunnelling in close proximity," *Comput. Geotech.*, vol. 66, pp. 53–65, 2015.

G. Swoboda, "Three-Dimensional Numerical Modelling for TBM Tunnelling in Consolidated Clay," *Tunn. Undergr. Sp. Technol.*, vol. 14, no. 3, pp. 327–333, 1999.

H. Chakeri, Y. Ozcelik, and B. Unver, "Effects of important factors on surface settlement prediction for metro tunnel excavated by EPB," *Tunn. Undergr. Sp. Technol.*, vol. 36, pp. 14–23, 2013.

H. Katebi, A. H. Rezaei, M. Hajialilue-Bonab, and A. Tarifard, "Assessment the influence of ground stratification, tunnel and surface buildings specifications on shield tunnel lining loads (by FEM)," *Tunn. Undergr. Sp. Technol.*, vol. 49, pp. 67–78, 2015.

H. Mroueh and I. Shahrour, "A simplified 3D model for tunnel construction using tunnel boring machines," *Tunn. Undergr. Sp. Technol.*, vol. 23, no. 1, pp. 38–45, 2008.

H. Schmid, "Statische Probleme des Tunnel-und Druckstollenbaues," Berlin, 1926.

H. Y. Liu, J. C. Small, J. P. Carter, and D. J. Williams, "Effects of tunnelling on existing support systems of perpendicularly crossing tunnels," *Comput. Geotech.*, vol. 36, no. 5, pp. 880–894, 2009.

H. H. Einstein, and C.W. Schwartz, "Simplified analysis for tunnel supports," *Journal of the Geotechnical Engineering Division, American Society of Civil Engineers*, 105, 499–518, 1979.

H. Schulze, and H. Duddeck, "Stresses in shield driven tunnels," Beton and Stahlbetonbau 8, 169–175, 1964.

Herrenknecht AG, "Herrenknecht" [Online], Germany, Available: https://www.herrenknecht.com/en/references/references-tunnelling.html [19 August 2016].
hydraulic [19 August 2016].

I. Chudleigh, K.G. Higgins, H.D. St John, D.M. Pott, and F.C. Schroeder, "Pile-tunnel interaction problems," *Proc. of Tunnel Construction and Piling, London*, Great Britain, 172-185, 1999.

I.T.A., "Guidelines for the design of shield tunnel lining," *Tunn. Undergr. Sp. Technol.*, vol. 15, no. 3, pp. 303–331, Jul. 2000.

J. E. Bowles, "*Foundation analysis and design*," *McGRaw-Hill,* New York, 1968.

J. S. Sharma, A. M. Hefny, J. Zhao, and C. W. Chan, "Effect of large excavation on deformation of adjacent MRT tunnels," *Tunn. Undergr. Sp. Technol.*, vol. 16, no. 2, pp. 93–98, 2001.

J. B. Burland and D. Twine, "The shaft friction of bored piles in terms of effective strength." *Proc. 1 st Int. Conf. Deep Foundations on Bored and Augered Piles*. p. 411-420, 1988.

J. B. Burland, "Shaft friction of piles in clay - a simple fundamental approach." Ground Engineering. 6, No. 3, p. 30-42, 1973.

J. D. Morton, and K.H. King, "Effects of tunneling on the bearing capacity and settlement of piled foundations," *In: Tunneling '79. IMM*, London, pp. 57–68, 1979.

J. Yao, R. N. Taylor, and a M. Mcnamara, "The effects of loaded bored piles on existing tunnels," *Geotech. Asp. Undergr. Constr. Soft Gr. - 6th Int. Symp.*, no. 1988, pp. 735–741, 2008.

J. Zou, Y. K. Chow, G. R. Dasari, C. F. Leung, and C. S. Ng, "Pile-soil-tunnel interaction in some layered soil profiles," pp. 1–4, 2002.

K. M. Lee and R. K. Rowe, "An analysis of three-dimensional ground movements: The Thunder Bay tunnel," *Can. Geotech. J.*, vol. 28, no. 1, pp. 25–41, 1991.

K. M. Lee and R. K. Rowe, "Finite element modelling of the three-dimensional ground deformations due to tunnelling in soft cohesive soils: Part I - Method of analysis," *Comput. Geotech.*, vol. 10, no. 2, pp. 87–109, 1990.

K. M. Lee and R. K. Rowe, "Finite element modelling of the three-dimensional ground deformations due to tunnelling in soft cohesive soils: Part II - Results," *Comput. Geotech.*, vol. 10, no. 2, pp. 87–109, 1990.

K. M. Lee, R. K. Rowe, and K. Y. Lo, "Subsidence owing to tunnelling. I. Estimating the gap parameter," *Can. Geotech. J.*, vol. 29, no. 6, pp. 929–940, 1992.

K. Charoenpak, "Finite Element Analysis for Evaluating the Effects of Pile under Loading adjacent to Existing Tunnel," *Master Thesis, King Mongkut's University of Technology Thonburi, Thailand*, 2006.

K.G. Higgins, I. Chudleigh, H.D. St John, and D.M. Potts, "An example of pile tunnel interaction problems." *Proc. Int. Symp. Geotech. Aspects of Underground Construction in Soft Ground, IS-Tokyo '99* (eds O. Kusakabe, K. Fujita and Y. Miyazaki), 99–103. Rotterdam: Balkema, 1999.

Kawasaki Heavy Industries, Ltd., "Kawasaki Heavy Industries" [Online], Japan, Available: https://global.kawasaki.com/en/industrial_equipment/construction/civil/

L. J. Benton, and A. Phillips, "The behaviour of two tunnels beneath a building on piled foundation." *Deformation of Soils and Displacements of Structures; Proc. 10th Eur. Conf. Soil Mech. Fdn Engng*, Florence, 2, 665–668, 1991.

Land Transport Authority, "Code of Practice for Railway Protection", Development and Building Control Department, Singapore, 2004.

M. A. Abdel-Motaal, F. M. El-Nahhas, and A. T. Khiry, "Mutual seismic interaction between tunnels and the surrounding granular soil," *Hous. Build. Natl. Res. Cent. J.*, vol. 10, no. 3, pp. 265–278, 2014.

M. A. Nunes and M. A. Meguid, "A study on the effects of overlying soil strata on the stresses developing in a tunnel lining," *Tunn. Undergr. Sp. Technol.*, vol. 24, no. 6, pp. 716–722, 2009.

M. Abdel-Meguid, R. K. Rowe, and K. Y. Lo, "3D Effects of surface construction over existing subway tunnels," *Int. J. Geomech.*, vol. 2, no. 4, pp. 447–469, 2002

M. Doležalová, "Tunnel complex unloaded by a deep excavation," *Comput. Geotech.*, vol. 28, no. 6–7, pp. 469–493, 2001.

M. J. Tomlinson, "The adhesion of piles driven in clay soils". *Proc. 4th ICSMFE*, England , pp. 66-71, 1957.

M. Kavvadas, D. Litsas, I. Vazaios, and P. Fortsakis, "Development of a 3D finite element model for shield EPB tunnelling," *Tunn. Undergr. Sp. Technol.*, vol. 65, pp. 22–34, 2017.

M. A. Meguid and H. K. Dang, "The effect of erosion voids on existing tunnel linings," *Tunn. Undergr. Sp. Technol.*, vol. 24, no. 3, pp. 278–286, 2009.

Mass Rapid Transit Authority of Thailand, "Restrictive Guideline for Protection Zone in Blue Line Project", Engineering Specifications for MRT Tunnels, Bangkok, 2009 (in Thai).

N. Heama, P. Jongpradist, P. Lueprasert, and S. Suwansawat, "Investigation on tunnel response due to adjacent loaded pile by 3D finite element analysis," *Int. J. GEOMATE*, vol. 12, no. 31, pp. 63–70, 2017.

N. Loganathan and H. G. Poulos, "Analytical Prediction for Tunneling-Induced Ground Movements in Clays," *J. Geotech. Geoenvironmental Eng.*, vol. 124, no. 9, pp. 846–856, 1998.

N. Thasananipan, and M. A. Maung, "Failure Mechanism of Long Bored Piles in Layered Soils of Bangkok," *Civil and Environmental Engineering Conference*, Bangkok, Thailand: V-69 to V-73, 1999.

N. Thasnanipan, A. W. Maung, T. Navaneethan and Z. Z. Aye, "Development and Achievements of Deep-seated Bored Piles and Barrettes Construction in Thailand for the Past Forty Years, A Country Report", *Proc. of the 16th Southeast Asian Geotechnical Conference 8-11 May 2007*, Kuala Lumpur, Malaysia, 2007.

N. Thasnanipan, Zaw Zaw Aye, C. Submaneewong and W Teparaksa, "Performance of Wet- Process Bored Piles Constructed with Polymer-Based Slurry in Bangkok Subsoi," *Proceedings of the International Deep Foundations Congress 2002, Geotechnical Special Publication No. 116, Volume One*, ASCE, February 14-16 2002, Orlando, Florida, USA :143- 157, 2002b.

P. B. Attewell, "Ground movements caused by tunneling in soil," *In: Proceedings International Conference on Large Movements and Structures*, London, pp. 812–948, 1977.

P. B. Attewell, J. Yeates, and A.R. Selby, "Soil Movements Induced by Tunneling and their Effects on Pipelines and Structures." Blackie, Glasgow, pp. 256, 1986.

P. Chiruppapa, *"Cast in-situ bored piles in Bangkok Clay,"* M. Eng. Thesis No. 213, Asian Institute of Technology, Bangkok, Thailand, 1968.

P. Jamsawang, N. Yoobanpot, N. Thanasisathit, P. Voottipruex, and P. Jongpradist, "Three-dimensional numerical analysis of a DCM column-supported highway embankment," *Comput. Geotech.*, vol. 72, pp. 42–56, 2016.

P. Kitiyodom, T. Matsumoto, and K. Kawaguchi, "A simplified analysis method for piled raft foundations subjected to ground movements induced by tunnelling," *Int. J. Numer. Anal. Methods Geomech.*, vol. 29, no. 15, pp. 1485–1507, 2005.

P. Lueprasert, P. Jongpradist, K. Charoenpak, P. Chaipanna, and S. Suwansawat, "Three dimensional finite element analysis for preliminary establishment of tunnel influence zone subject to pile loading," *Maejo Int. J. Sci. Technol.*, vol. 9, no. 2, pp. 209–223, 2015.

P. Suchada, *"Performance of Bored, Driven and Auger Press Piles in Bangkok Subsoils,"* M. Eng. Thesis No. GT 88-12, Asian Institute of Technology, Bangkok, Thailand, 1989 (in Thai).

P. Jongpradist, T. Kaewsri, A. Sawatparnich, S. Suwansawat, S. Youwai, W. Kongkitkul, and J. Sunitsakul, "Development of tunneling influence zones for adjacent pile foundations by numerical analyses," *Tunn. Undergr. Sp. Technol.*, vol. 34, pp. 96–109, 2013.

R. B. Peck, A.J. Hendron, and B. Mohraz, "State of the art of soft-ground tunneling," *In: Proceedings of the North American Rapid Excavation and Tunneling Conference*, Chicago, IL, pp. 259–286, 1972.

R. Brinkgreve., E., Engin, W. Swolfs, "*PLAXIS 3D Version 2013 manual*," Chapman, 2013.

R. Brinkgreve., E., Engin, W. Swolfs, "*PLAXIS 3D Version 2016 manual*," Chapman, 2016.

R. Chen, F. Meng, Z. Li, Y. Ye, and J. Ye, "Investigation of response of metro tunnels due to adjacent large excavation and protective measures in soft soils," *Tunn. Undergr. Sp. Technol.*, vol. 58, pp. 224–235, 2016.

R. J. Chandler, "Discussion on Whitaker and Cooke," *Proc. Symp. Large Bored Piles*. p. 95-97, 1966.

R. J. Chandler, "The shaft friction of piles in cohesive soils in terms of effective stress" *Civ. Eng. and Pub. Works Rev.* Jan 1968. p. 48-51, 1968.

R. J. Finno, G.W. Clough, "Evaluation of soil response to EPB shield tunnelling," *J. of Geotechnical Engineering-ASCE*, 111(2), pp. 155-173, 1985.

R. J. Mair and R. N. Taylor, "Bored tunnelling in the urban environment," *14Th International Conference on Soil Mechanics and Foundation Engineering*, vol. 4. pp. 2353–2385, 1997.

R. J. Mair, R. N. Taylor, and a. Bracegirdle, "Subsurface settlement profiles above tunnels in clays," *Géotechnique*, vol. 45, no. 2, pp. 361–362, 1995.

R. K. Rowe and K. M. Lee, "Subsidence owing to tunnelling. II. Evaluation of a prediction technique: Reply," *Can. Geotech. J.*, vol. 31, no. 3, pp. 467–469, 1994.

R. N. Craig, and A.M.M Wood, "A review of tunnel lining practice in the United Kingdom," *Transport and Road Research Laborat*ory, TRRL Supplementary Report 335, 1978.

R. P. Chen, J. Li, L. G. Kong, and L. jun Tang, "Experimental study on face instability of shield tunnel in sand," *Tunn. Undergr. Sp. Technol.*, vol. 33, pp. 12–21, 2013.K. M. Lee and R. K. Rowe, "Finite element modelling of the three-dimensional ground deformations due to tunnelling in soft cohesive soils: Part I - Method of analysis," *Comput. Geotech.*, vol. 10, no. 2, pp. 87–109, 1990.

R. P. Chen, J. Zhu, W. Liu, and X. W. Tang, "Ground movement induced by parallel EPB tunnels in silty soils," *Tunn. Undergr. Sp. Technol.*, vol. 26, no. 1, pp. 163–171, 2011.S. Bernat and B. Cambou, "Soil-structure interaction in shield tunnelling in soft soil," *Comput. Geotech.*, vol. 22, no. 3–4, pp. 221–242, 1998.

R. P. Chen, L. J. Tang, D. S. Ling, and Y. M. Chen, "Face stability analysis of shallow shield tunnels in dry sandy ground using the discrete element method," *Comput. Geotech.*, vol. 38, no. 2, pp. 187–195, 2011.G. W. Clough, B. P. Sweeney, and R. J. Finno, "Measured Soil Response to EPB Shield Tunneling," *J. Geotech. Eng.*, vol. 109, no. 2, pp. 131–149, 1983.

R. Peck, "Deep excavations and tunnelling in soft ground," *Proc. 7th Int. Conf. SMFE*, pp. 226–290, 1969.

R. Prust, J. Davies, and S. Hu, "Part 6: Tunnels and Underground Structures: Pressuremeter Investigation for Mass Rapid Transit in Bangkok, Thailand," *Transp. Res. Rec. J. Transp. Res. Board*, vol. 1928, no. 1, pp. 205–217, 2005.

S. Babendererde, "Underground Construction in Germany 2000", chapter Verpressen der Schildschwanzfuge hinter einer Tunnelvortriebsmaschine mit T¨ ubbingausbau, STUVA, DAUB, pp. 113–116, 2000.

S. Bernat and B. Cambou, "Soil-structure interaction in shield tunnelling in soft soil," *Comput. Geotech.*, vol. 22, no. 3–4, pp. 221–242, 1998.

S. Bernat, B. Cambou, and P. Dubois, "Assessing a soft soil tunnelling numerical model using field data," *Geotechnique*, vol. 49, no. 4, pp. 427–452, 1999.

S. Likitlersuang, S. Teachavorasinskun, C. Surarak, E. Oh, and A. Balasubramaniam, "Small strain stiffness and stiffness degradation curve of Bangkok Clays," *Soils Found.*, vol. 53, no. 4, pp. 498–509, 2013.

S. Moller, "Tunnel Induced Settlements and Structural Forces in Linings," 2006.

S. Timpong, "Analysis of ground movements in Bangkok MRT Blue Line project", *Master Thesis, Asian Institute of Technology*, Thailand, 2002.

S. W. Jacobsz, J.R. Standing, R.J. Mair, K. Soga, T. Hagiwara, T. Sugiyama, "Tunneling effect on driven piles," *In: Proceedings of the International Conference on Response of buildings to excavation-induced ground movements*. Imperial College, CIRIA, London, pp. 1–15, 2001.

S. Likitlersuang, C. Surarak, D. Wanatowski, E. Oh, and A. Balasubramaniam, "Finite element analysis of a deep excavation : A case study from the Bangkok MRT," *Soils Found.*, vol. 53, no. 5, pp. 756–773, 2013.

S. Suwansawat, "Earth Pressure Balance (EPB) Shield Tunneling in Bangkok: Ground Response and Prediction of Surface Settlements Using Artificial Neural Networks", Ph.D. Thesis, Massachusetts Institute of Technology, USA, 2002.

T. Benz, Small-Strain Stiffness of Soils and its Numerical Consequences. Doctoral Thesis, Institute of Geotechnical Engineering, University of Stuttgart, Stuttgart, 2007.

T. Chapman, D. Nicholson, and D. Luby, "Use of the observational method for the construction of piles next to tunnels," *Proc. Int. Conf. Response of Buildings to Excavation Induced Ground Movements*, (ed F. M. Jardine) London: CIRIA, 2001.

T. Kasper and G. Meschke, "A 3D finite element simulation model for TBM tunnelling in soft ground," *Int. J. Numer. Anal. Methods Geomech.*, vol. 28, no. 14, pp. 1441–1460, 2004.

T. Kasper and G. Meschke, "A numerical study of the effect of soil and grout material properties and cover depth in shield tunnelling," *Comput. Geotech.*, vol. 33, no. 4–5, pp. 234–247, 2006.

T. Rukdeechuai, P. Jongpradist, A. Wonglert, and T. Kaewsri, "Influence of soil models on numerical simulation of geotechnical works in Bangkok subsoil," *EIT Res. Dev. J.* vol. 20 (3), pp. 17–28, 2009

T. Schanz, a Vermeer, and P. Bonnier, "The hardening soil model: formulation and verification," *Beyond 2000 Comput. Geotech. 10 years PLAXIS Int. Proc. Int. Symp. beyond 2000 Comput. Geotech. Amsterdam Netherlands 1820 March 1999*, p. 281, 1999.

W. Broere, R. Brinkgreve, ''Phased simulation of a tunnel boring process in soft soil,'' *in Proc. Conf. on Numerical Methods in Geotechnical Engineering, in Mestat (Ed.), Presses de l'ENPC/ LCPC*, Paris, pp.529-536, 2002.

W. I. Chou and A. Bobet, "Predictions of ground deformations in shallow tunnels in clay," *Tunn. Undergr. Sp. Technol.*, vol. 17, no. 1, pp. 3–19, 2002.

Working Group No. 2, ITA, "Guidelines for the Design of Shield Tunnel Lining," Elsevier Science Ltd: Published, 2000.

Y. J. Lee and R. H. Bassett, "A model test and numerical investigation on the shear deformation patterns of deep wall–soil–tunnel interaction," *Can. Geotech. J.*, vol. 43, no. 12, pp. 1306–1323, 2006.

Y. J. Lee and R. H. Bassett, "Influence zones for 2D pile-soil-tunnelling interaction based on model test and numerical analysis," *Tunn. Undergr. Sp. Technol.*, vol. 22, no. 3, pp. 325–342, 2007.

Y. Xiang and S. Feng, "Theoretical prediction of the potential plastic zone of shallow tunneling in vicinity of pile foundation in soils," *Tunn. Undergr. Sp. Technol.*, vol. 38, pp. 115–121, 2013.

Zheng, T. Zhang, and Y. Diao, "Mechanism and countermeasures of preceding tunnel distortion induced by succeeding EPBS tunnelling in close proximity," *Comput. Geotech.*, vol. 66, pp. 53–65, 2015.

APPENDIX

APPENDIX A

Constitutive Models in This Study

A.1 The Linear Elastic Model

The Linear Elastic model (LE) is based on Hooke's law of isotropic elasticity. It includes two basic elastic parameters, i.e. Young's modulus (E) and Poisson's ratio (υ). Although this model is not suitable for representing soil behaviour, it may be used to model stiff volumes in the soil, like concrete walls, or intact rock formations [1].

A.2 The Mohr-Coulomb Model

The Mohr-Coulomb model (MC) is a simple and well-known linear elastic perfectly plastic model, which can be used as a first approximation of soil behaviour. The linear elastic part of the Mohr-Coulomb model is based on Hooke's law of isotropic elasticity. It includes five input parameters, namely Young's modulus (E) and Poisson's ratio (υ) for soil elasticity, effective shear parameters cohesion (c') and angle of friction (φ') for soil plasticity and (ψ) as an angle of dilatancy. As seen in Figure A.1a for primary loading the stress-strain behaviour is modelled elastic with a constant stiffness up to a certain failure of stress (σ'). Similarly unloading-reloading is modelled, adopting the same material response and stiffness as for primary loading. When the failure stress is reached, perfectly plastic deformation takes place, involving the development of irreversible strains. In order to evaluate whether or not plasticity takes place, yield functions are introduced. The general states of stress soil failure can be represented as a fixed hexagonal yield surface in principal stress space as shown in Figure A.1b. The Mohr-Coulomb yield condition is an extension of Coulomb's friction law to general states of stress. The equations of the hexagonal yield surface are obtained from Eq. A.1- A.3 as below;

$$f_1 = 0 \text{ with } f_1 = \frac{1}{2}(\sigma_2' - \sigma_3') - \frac{1}{2}(\sigma_2' + \sigma_3')\sin\varphi' - c'\cos\varphi' \le 0 \qquad \text{(A.1)}$$

$$f_2 = 0 \text{ with } f_1 = \frac{1}{2}(\sigma_3' - \sigma_1') - \frac{1}{2}(\sigma_3' + \sigma_1')\sin\varphi' - c'\cos\varphi' \le 0 \qquad \text{(A.2)}$$

$$f_3 = 0 \text{ with } f_1 = \frac{1}{2}(\sigma_1' - \sigma_2') - \frac{1}{2}(\sigma_1' + \sigma_2')\sin\varphi' - c'\cos\varphi' \le 0 \qquad \text{(A.3)}$$

Note that compression is considered positive. For stress states that are within this yield surface the MC Model responds linear elastic and all strains are reversible. Adopting Hooke's law in rate formulation the elastic stress-strain relationship is written as Eq. A.4.

$$\dot{\sigma}' = D^e \dot{\varepsilon}^e \qquad \text{(A.4)}$$

Where $\dot{\sigma}'$ is the stress rate, $\dot{\varepsilon}^e$ the corresponding elastic strain rate and D^e is the elastic material stiffness matrix. The latter one is formulated using the two elastic material constants E and υ. The formulation of perfect plasticity decomposes strain rates $\dot{\varepsilon}$ into an elastic and a plastic part as shown in Eq. A.5.

$$\dot{\varepsilon} = \dot{\varepsilon}^e + \dot{\varepsilon}^p \qquad \text{(A.5)}$$

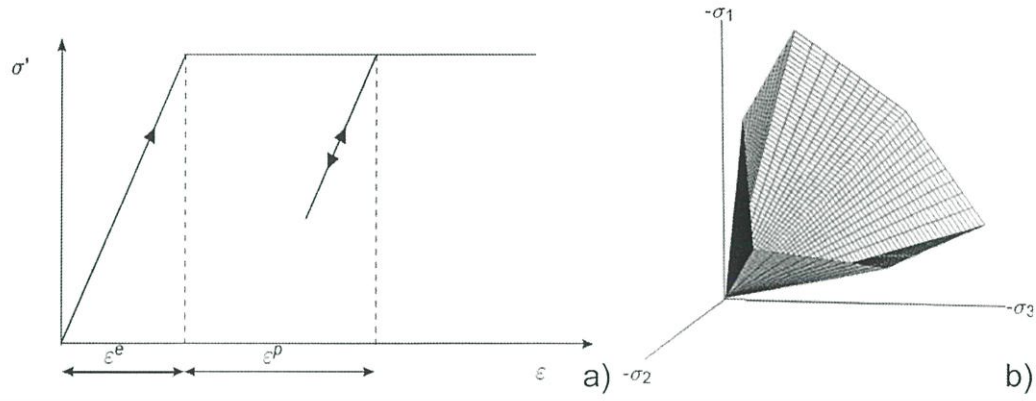

Figure A.1 Basic ideas of MC-Model, a) liner elastic perfectly plastic material behaviour, b) yield surface in principal stress space ($c' = 0$) (modified from [1])

Where $\dot{\varepsilon}^p$ is the plastic strain rate. Combining Eqs. A.4 and A.5 yields is shown as Eq. A6.

$$\dot{\sigma}' = D^e(\dot{\varepsilon} - \dot{\varepsilon}^p) \tag{A.6}$$

If associated plasticity is assumed, the plastic strain rates can then be formulated using the yield function introduced in Eqs. A.1 - A.3., the plastic strain rates then become vectors perpendicular to the surface of the yield function. However, the use of MC type of plastic potential functions would lead to a considerable overprediction of the angle of dilatancy. Therefore, in addition to yield functions, different plastic potential function g is employed. Using the plastic potential functions, non-associated plasticity is adopted and the plastic strain rates are formulated as Eq. A.7.

$$\dot{\varepsilon}^p = \lambda_1 \frac{\partial g_1}{\partial \sigma'} + \lambda_2 \frac{\partial g_2}{\partial \sigma'} + \lambda_3 \frac{\partial g_3}{\partial \sigma'} \tag{A.7}$$

Where λ_1, λ_2 and λ_3 are plastic multipliers. The plastic potential functions are performed as Eqs. A.8-A.10.

$$g_1 = \frac{1}{2}\left|\sigma_2' - \sigma_3'\right| + \frac{1}{2}(\sigma_2' + \sigma_3')\sin\psi \tag{A.8}$$

$$g_2 = \frac{1}{2}\left|\sigma_3' - \sigma_1'\right| + \frac{1}{2}(\sigma_3' + \sigma_1')\sin\psi \tag{A.9}$$

$$g_3 = \frac{1}{2}\left|\sigma_1' - \sigma_2'\right| + \frac{1}{2}(\sigma_1' + \sigma_2')\sin\psi \tag{A.10}$$

The dilatancy angle ψ is used to model positive plastic volumetric strain increments (dilatancy) in case of plastic yielding. Using the consistency condition is shown as Eq. A.11;

$$\dot{f} = \frac{\partial f}{\partial \sigma'}\dot{\sigma}' = 0, \tag{A.11}$$

And employing Eqs. A.6, A.7 and A.11, the plastic multipliers λ_1, λ_2 and , λ_3 are solved from the Eq. A.12.

$$\dot{f}_i = \frac{\partial f_i}{\partial \sigma'} D^e(\dot{\varepsilon} - \lambda_1 \frac{\partial g_1}{\partial \sigma'} - \lambda_2 \frac{\partial g_2}{\partial \sigma'} - \lambda_3 \frac{\partial g_3}{\partial \sigma'}) = 0, \text{ where } i \text{ run from 1to 3} \tag{A.12}$$

For more details on the formulation and implementation of the MC Model that is referred by Smith and Griffith (1982) [2], Van and Vermeer (1990) [3] and Brinkgreve and Vermeer (2001) [4].

A.3 The Hardening-Soil Model

In contrast to an elastic perfectly-plastic model, the yield surface of a hardening plasticity model is not fixed in principal stress space, but it can expand due to plastic straining. Difference can be made between two main types of hardening, namely shear hardening and compression hardening. Shear hardening is used to model irreversible strains due to primary deviatoric loading. Compression hardening is used to model irreversible plastic strains due to primary compression in oedometer loading and isotropic loading. Both types of hardening are contained in the present model.

The Hardening Soil model (HS Model) is an advanced model for simulating the behaviour of different types of soil, both soft soils and stiff soils [4]. When subjected to primary deviatoric loading, soil shows a decreasing stiffness and simultaneously irreversible plastic strains develop. In the special case of a drained triaxial test, the observed relationship between the axial strain and the deviatoric stress can be well approximated by a hyperbola. Some basic characteristics of the HS model are showed as follow:

- Stress dependent stiffness according to a power law Input parameter (m)
- Plastic straining due to primary deviatoric loading Input parameter (E_{50}^{ref})
- Plastic straining due to primary compression (E_{oed}^{ref})
- Elastic unloading / reloading (E_{ur}^{ref}), (υ_{ur})
- Failure according to the Mohr-Coulomb failure criterion Parameters c', φ' and ψ.

In the following basic features of the HS Model will be explained, adopting a standard drained triaxial test. Please note that compression is considered positive.

A.3.1 Hyperbolic stress-strain relationship

When soil is subjected to primary deviatoric loading a decrease in stiffness is observed and irreversible plastic strains develop. Such a relationship was first formulated by Kondner (1963) [5] and later used in the well-known hyperbolic model by Duncan & Chang, 1970 [6]. However, the HS model supersedes the hyperbolic model by far: Firstly, by using the theory of plasticity rather than the theory of elasticity, secondly by including soil dilatancy and thirdly by introducing a yield cap. Although the HS Model by far supersedes the model presented by Duncan & Chang, 1970 [6] one of its basic ideas is the hyperbolic formulation as shown in Eq. A.13.

$$\varepsilon_1 = \frac{q_a}{2E_{50}} \cdot \frac{q}{q_a - q} \tag{A.13}$$

Where q_a is the asymptotic failure stress as shown in Figure A.2.

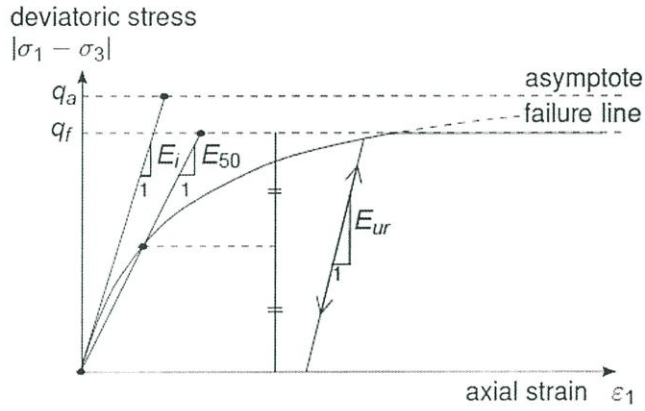

Figure A.2 Hyperbolic stress-strain relation in primary loading for a standard drained triaxial test [1].

This figure also shows the typical curve of a drained triaxial test with constant lateral pressure (σ_3), assuming that under primary loading the behaviour is distinctly nonlinear and hyperbolic up to a Mohr-Coulomb failure stress (q_f). The asymptotic failure stress has the relation as shown in Eq. A.14.

$$q_a = \frac{q_f}{R_f} = (c.\cot\varphi' + \sigma_3') \cdot \frac{2\sin\varphi'}{R_f(1-\sin\varphi')} \tag{A.14}$$

Where $R_f = 0.9$ for many soils. While the maximum stress is determined by the Mohr-Coulomb failure criterion, the hyperbolic part of the curve can be defined using a single secant modulus as additional input parameter. In the HS Model this is the stress dependent modulus E_{50}, as used in Eq. A.13, which is defined as Eq. A.15.

$$E_{50} = E_{50}^{ref} \left(\frac{c'.\cot\varphi' + \sigma_3'}{c'\cot\varphi' + p^{ref}}\right)^m \tag{A.15}$$

Where p^{ref} is the reference confining pressure. Following the ideas by OHDE (1951) [7], the amount of stress dependency is governed by the exponent m, which can be measured both in oedometer tests and in triaxial tests. One tends to find values between 0.4 and 1.0. A value of 0.5 is typical for sands and clays tend to have m = 1.0. In contrast to E_{50}, which determines the magnitude of both the elastic and the plastic strains, E_{ur} is a true elasticity modulus. In conjunction with a Poisson's ratio ν_{ur} it determines the ground behaviour under unloading and reloading; the indices ur stand for unloading/reloading. As the average primary loading modulus E_{50} the unloading modulus E_{ur} is stress-level dependent as shown in Eq. A.16.

$$E_{ur} = E_{ur}^{ref} \left(\frac{c'.\cot\varphi' + \sigma_3'}{c'\cot\varphi' + p^{ref}}\right)^m \tag{A.16}$$

When comparing the hardening model to the previous elastic perfectly-plastic MC Model another significant difference is that plastic strains may already occur before the limit MC-failure stress is reached. This implies that the HS Model incorporates another yield surface, which is not fixed in principal stress space, but it may expand and soil hardening is simulated due to plastic straining. As shown in

Figure A.3a, distinction is made between two types of hardening, namely shear hardening and compression hardening.

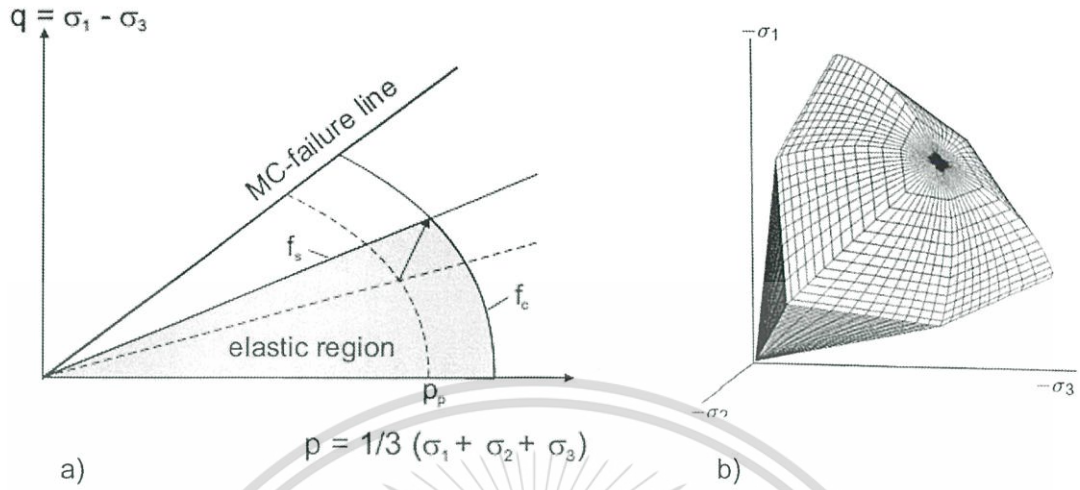

Figure A.3 Yield surface of the HS Model for $c = 0$ a) successive yield loci for shear hardening and compression hardening in p-q-space b) total yield contour in principal stress space (modified from [1]).

For the shear hardening law a yield function (f_s) is introduced, which is a function of the triaxial loading stiffness (E_{50})and for the compression hardening a yield function (f_c) is formulated, being governed by the oedometer loading stiffness (E_{oed}). As also indicated in Figure A.3a for unloading-reloading elastic soil behaviour is assumed, adopting Hook's law with Young's modulus (E_{ur}). Figure A.3b shows the total contour of the HS yield surface in principal stress space.

A.3.2 Yield function

The yield function (f_s) adopted in the HS-Model has the formulation as shown in Eq A.17.

$$f^s = \bar{f} - \gamma^p \tag{A.17}$$

Where $\bar{f}$ is a function of stress and the hardening parameter as shown in Eq. A. 18, and a function of plastic strains (γ^p) is shown in Eq A.19.

$$\bar{f} = \frac{1}{E_{50}^{ref}} \left(\frac{c^{'}.\cot\varphi^{'} + \sigma^{'}_3}{c^{'}\cot\varphi^{'} + p^{ref}}\right)^m \cdot \frac{q}{1 - q/q_a} - \frac{2q}{E_{ur}^{ref}} \left(\frac{c^{'}.\cot\varphi^{'} + \sigma^{'}_3}{c^{'}\cot\varphi^{'} + p^{ref}}\right)^m \tag{A.18}$$

$$\gamma^p = \varepsilon_1^p - \varepsilon_2^p - \varepsilon_3^p = 2\varepsilon_1^p - \varepsilon_v^p \approx 2\varepsilon_1^p \tag{A.19}$$

Similar to the MC Model the HS Model adopts non-associated plasticity to determine the rates of plastic strain with the plastic potential as shown in Eq.20.

$$g^s = (3 - \sin\psi_m) \cdot q - 6\sin\psi_m \cdot p \tag{A.20}$$

with $p = 1/3(\sigma_1 + \sigma_2 + \sigma_3)$. The mobilized angle of dilatancy (ψ_m) is calculated according to the so-called stress-dilatancy equation of ROWE (1962) [8] as shown in Eq. 21.

$$\sin\psi_m = \frac{\sin\varphi_m - \sin\varphi_{cv}}{1 - \sin\varphi_m \sin\varphi_{cv}} \tag{A.21}$$

Where the mobilized friction angle (φ_m) and the constant-volume angle (φ_{cv}) is governed by the Eq. 22 and 23, respectively.

$$\sin\varphi_m = \frac{\sigma_1 - \sigma_3}{\sigma_1 + \sigma_3 + 2c\cot\varphi} \tag{A.22}$$

$$\sin\varphi_{cv} = \frac{\sin\varphi - \sin\psi}{1 - \sin\varphi\sin\psi} \tag{A.23}$$

The dilatancy angle is thus positive as soon as ψ_m exceeds a constant-volume angle φ_{cv}. Considering dense materials contraction is excluded by taking $\psi_m = 0$ for a mobilized friction angle $\varphi_m < \varphi_{cv}$.

Another extension of that early soil model is achieved by introducing compression hardening. The latter is formulated by means of cap-type yield surfaces, which makes the model both suitable for hard soils as well as very soft clays. The cap-type yield function (f_c) has the formulation as shown in Eq A.24.

$$f_c = \frac{q^2}{M^2} + (p + c\cdot\cot\varphi)^2 - (p_p + c\cdot\cot\varphi)^2 \tag{A.24}$$

with

$$M = \frac{6\sin\varphi}{3 - \sin\varphi} \tag{A.25}$$

The position and shape of the cap in stress space is governed by the isotropic preconsolidation pressure (p_p) as also indicated in Figure A.3. The hardening law formulates the relation between the plastic volumetric cap-strain (ε_v^{pc}) and the preconsolidation stress (p_p) as shown in Eq.26.

$$\varepsilon_v^{pc} = \frac{\beta}{1-m}\left(\frac{p_p}{p^{ref}}\right)^{1-m} \tag{A.26}$$

The cap parameter (β) is not used as a direct input parameter. Instead the odometer stiffness (E_{oed})is used as an input parameter which is linked to β. Fig. A.4 shows the typical characteristic curve of an oedometer test. In the HS Model the virgin oedomenter stiffness obeys a stress dependency according to the Eq. A.27.

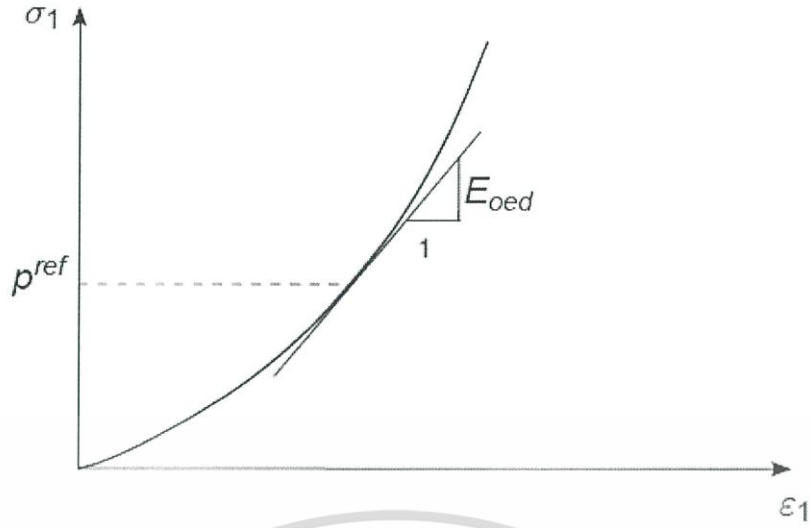

Figure A.4 Definition of E_{oed}^{ref} in oedometer test results [1].

$$E_{oed} = E_{oed}^{ref} \left(\frac{c' \cdot \cot\varphi' + \sigma_1'}{c' \cdot \cot\varphi' + p^{ref}} \right)^m \tag{A.27}$$

where E_{oed}^{ref} is the reference Oedometer Modulus for the axial reference pressure (p^{ref}). In the special case of $m = 1$ one obtains a linear stress-dependency as usual for a clay. In addition, the modulus of E_{50} and E_{ur}, the oedometer modulus (E_{oed}) is also an input modulus for the HS Model. Together with the parameters m, υ_{ur}, c', ϕ' and the dilatancy angle (ψ), there are a total of eight input parameters. To determine the rates of plastic volumetric strains associated plasticity, i.e. $g_c = f_c$ is adopted.

A.3.3 Over Consolidation Ratio (OCR)

Another input parameter which is embedded in the HS Model is the Over Consolidation Ratio. When using the HS Model to consider over consolidated grounds ($OCR > 1$), initial stresses may be modelled according to Eq. A.28.

$$K_0^{OC} = \frac{\sigma_h'}{\sigma_v'} = (1 - \sin\varphi') \cdot OCR - (OCR - 1) \cdot \frac{\upsilon_{ur}}{1 - \upsilon_{ur}} \tag{A.28}$$

The elastic unloading from the maximum vertical overburden stress down to the actual initial stress implies that the actual stress state is not on the yield surface. Contrary to a normally consolidated initial stress state, with the actual stress state located directly on the HS-yield surface, the initial stress state of an overconsolidated ground is in the elastic region, shown in Fig. A.3. Due to the higher unloading-reloading stiffness (E_{ur}), which is used to model the elastic region, overconsolidated grounds in the HS Model have an initially much stiffer response than normally consolidated grounds.

For more information on the formulation of yield functions and for a more detailed description of the implementation of the HS Model can be referred from the publications of Brinkgreve, W. Broere (2013) [1] and Schanz (1999) [4].

A.4 The Hardening-Soil Model with small strain (HS-Small Model) [9]

The HS-Small Model constitutes an extension of the HS-Model. All model features described for the HS Model also hold true for the HS-Small Model. In addition to the HS Model, the HS-Small Model incorporates a formulation of the small strain stiffness. As displayed in Figure A.5, small unloading-reloading stress-strain paths result in a considerably higher elasticity modulus E_0 .

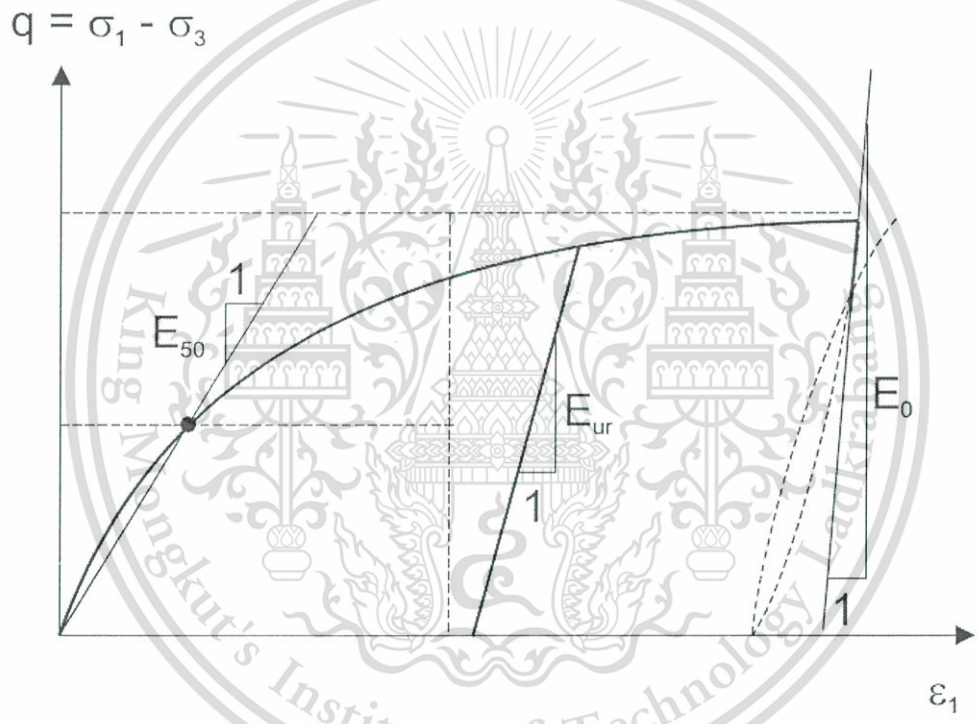

Figure A.5 HS-Small Model: extension of the HS Model incorporating small strain stiffness. [9]

Actually, the maximum soil stiffness is observed at very low strain levels, e.g. strains smaller than 10^{-5} [10]. This is referred to a small strain stiffness. The formulation of small strain stiffness in the HS-Small Model assumes that the decay of small strain stiffness is primarily related to either break up of bonding forces between soil particles or frictional particle forces exceeding their elastic limit. Thus, a drop of stiffness can be observed whenever inter-particle forces are reorganized and concentrated. As shown in Figure A.6, for strains higher than 10^{-5} a rapid drop of small strain ground stiffness is measured, considering shear modulus G . The strain levels obtained here, are far below conventional laboratory testing, requiring special measuring devices such as dynamic methods or local strain gauges.

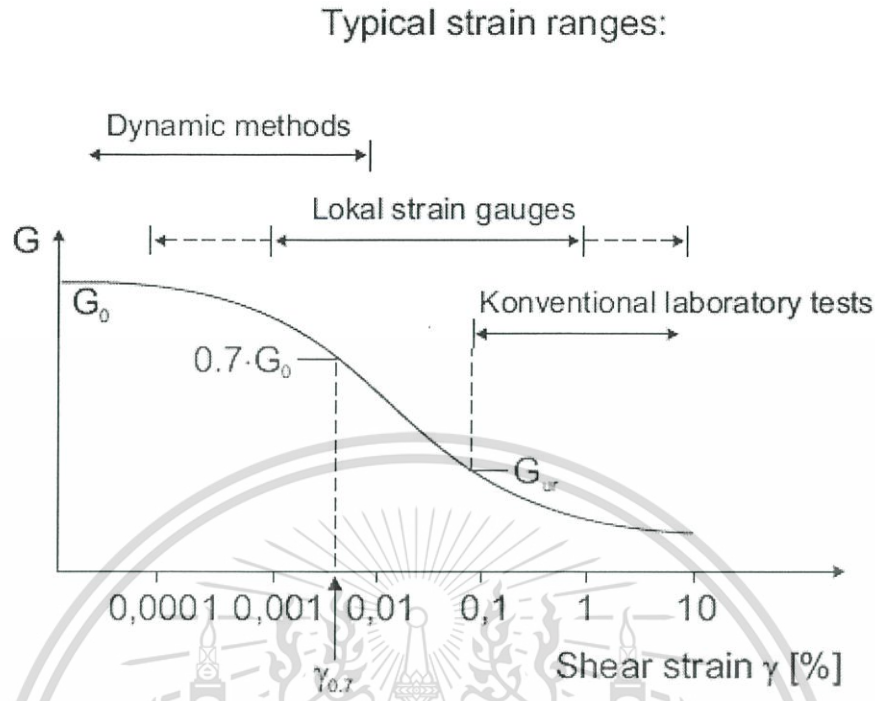

Figure A.6 Small strain stiffness curve for a particular soil adopting shear modulus.

To incorporate small strain stiffness effects into the HS Model a relatively simple expression for the small strain stiffness decay of the shear modulus, similar to the one suggested by Santos and Correia (2001) [11], is adopted

$$G = \frac{G_0}{1 + 0.43 \cdot \gamma / \gamma_{0.7}} \tag{A.29}$$

where G is the actual shear modulus at shear strain γ, G_0 is the initial shear modulus and $\gamma_{0.7}$ is the shear strain at which the initial shear modulus has reduced to $0.7 \cdot G_0$, as shown in Figure A.6. For general states of stress the shear strain is expressed using the strain invariant

$$\gamma = \frac{1}{\sqrt{2}} \cdot \sqrt{(\varepsilon_1 - \varepsilon_2)^2 + (\varepsilon_2 - \varepsilon_3)^2 + (\varepsilon_3 - \varepsilon_1)^2} \tag{A.30}$$

which in the special case of triaxial loading reduces to $\gamma = |\varepsilon_1 - \varepsilon_3|$ While reducing the shear modulus with increasing shear strain, the Poisson's ratio υ_{ur} is kept constant, such that the resulting bulk modulus is not a constant but is also reducing as a function of shear strain.

Conform the ideas by OHDE (1951) [7] and the formulation of stiffnesses in the HS Model, the initial shear modulus G_0 is pressure dependent according to the equation

$$G_0 = G_{ref}^0 \cdot \left(\frac{c' \cdot \cot \varphi' + \sigma_3'}{c' \cdot \cot \varphi' + p_{ref}} \right)^m \tag{A.31}$$

The magnitude of G_{ref}^{0} is strongly correlated to the porosity of the soil. A typical correlation being used is $G_{ref}^{0} = 450 \cdot p_{ref}$ by Biarez and Hicher (1994) [12]. Figure A.6 shows the stiffness degradation curve, reaching far into the plastic material behaviour at larger strains. According to the formulation of the HS Model, stiffness degradation due to plastic straining is modelled by involving material hardening. Therefore, before reaching plastic material behaviour, the formulation of the small strain stiffness curve is cut off at the unloading-reloading shear modulus G_{ur}, defined as

$$G_{ur} = \frac{E_{ur}}{2 \cdot (1 + \upsilon_{ur})} \tag{A.32}$$

The elastic constants E_{ur} and υ_{ur} have already been introduced in the HS Model. Eq. A.32 indicates that G_{ur} is the shear modulus in complete deviatoric unloading as illustrated in Figure A.5. Besides the input parameters as introduced for the HS Model, there are a set of two additional input parameters for the HS-Small Model: the elastic small strain shear modulus G_{ref}^{0} at reference pressure p_{ref} and the threshold value $\gamma_{0.7}$ in primary loading. A more detailed explanation of the HS-Small Model can be found in Be (2006) [13].

A.5 References

[1] R. B. J. Brinkgreve, W. Broere, and D. Waterman, "PLAXIS 3D Manual: Material Models", *Public Work.*, 2013.

[2] I. M. Smith and D. V. Griffith, "Programming the Finite Element Method", *J.Wiley & Sons, Chisester*, UK, 2 edition, 1982.

[3] H. V. Langen and P. A. Vermeer, "Automatic step size correction for non-associated plasticity problems", *International Journal for Numerical Methods in Engineering*, 29:579–598, 1990.

[4] T. Schanz, a Vermeer, and P. Bonnier, "The hardening soil model: formulation and verification," *Beyond 2000 Comput. Geotech. 10 years PLAXIS Int. Proc. Int. Symp. beyond 2000 Comput. Geotech. Amsterdam Netherlands 1820 March 1999*, p. 281, 1999.

[5] R. L. Kondner, "Hyperbolic stress-strain response: cohesive soils," *J. Soil Mech. Found. Div.*, vol. 89, no. 1, pp. 115–144, 1963.

[6] J. M. Duncan and C.-Y. Chang, "Nonlinear analysis of stress and strain in soils," *J. Soil Mech. Found. Div.*, vol. 96, no. 5, pp. 1629–1653, 1970.

[7] J. OHDE. *Grundbaumechanik*. Bd. III. H¨ utte, 1951.

[8] R. K. Rowe, J. R. Booker, and N. P. Balaam, "Application of the initial stress method to soil structure interaction," *Int. J. Numer. Methods Eng.*, vol. 12, no. 5, pp. 873–880, 1978.

[9] S. Moller, "Tunnel Induced Settlements and Structural Forces in Linings," 2006.

[10] J. H. Atkinson and G. Sallfors. Experimental determination of soil properties. In 10th Eur. Conference on Soil Mechanics, number 3, pages 915–956, Florence, 1998.

[11] J. A. Santos and A. Gomes Correia, "Reference threshold shear strain of soil. Its application to obtain an unique strain-dependent shear modulus curve for soil," *Proc. 15th Int. Conf. Soil Mech. Geotech. Eng.*, vol. 1, no. 1993, pp. 267–270, 2001.

[12] J. Biarez and P.-Y. Hicher, "Elementary mechanics of soil behaviour," Technical report, Ecole Centrale de Paris, Cedex, France, 1994.

[13] T. BENZ. Small-Strain Stiffness of Soils and its Numerical Consequences. PhD thesis, Institute of Geotechnical Engineering, University of Stuttgart, Stuttgart, 2006.

CURRICULUM VITAE

NAME	Mr. Prateep Lueprasert
DATE OF BIRTH	August 03, 1985
EDUCATIONAL RECORD	
BACHELOR'S DEGREE	Bachelor of Engineering (Civil Engineering) King Mongkut's Institute of Technology Ladkrabang, 2007
MASTER'S DEGREE	Master of Engineering (Civil Engineering) King Mongkut's Institute of Technology Ladkrabang, 2012
DOCTORAL DEGREE	Doctoral of Engineering (Civil Engineering) King Mongkut's Institute of Technology Ladkrabang, 2017
SCHOLARSHIP	Thailand Research Fund (TRF): Grant Research and Researcher for Industry (RRI), (PHD56I0057), 2013-Present Thailand Research Fund Master Research Grants: TRF-MAG (MRG-WI525E133), 2010-2012
PUBLICATION	**Lueprasert, P.**, Jongpradist, P., Jongpradist, P., & Suwansawat, S. **(2017)**. Numerical investigation of tunnel deformation due to adjacent loaded pile and pile-soil-tunnel interaction. ***Tunnelling and Underground Space Technology***, *70*(March), 166–181. **Lueprasert, P.**, Jonpradist, P., & Suwansawat, S. **(2017)**. Tunneling simulation in soft ground using shell elements and grouting layer. ***International Journal of GEOMATE***, *12*(31), 51–57. Heama, N., Jongpradist, P., **Lueprasert, P.**, & Suwansawat, S. **(2017)**. Investigation on tunnel response due to adjacent loaded pile by 3D finite element analysis. ***International Journal of GEOMATE***, *12*(31), 63–70.

Lueprasert, P., Jongpradist, P., Charoenpak, K., Chaipanna, P., & Suwansawat, S. **(2015)**. Three dimensional finite element analysis for preliminary establishment of tunnel influence zone subject to pile loading. ***Maejo International Journal of Science and Technology***, *9*(2), 209–223.

Lueprasert, P., Jongpradist, P & Suwansawat, S. **(2011)**. Applying 2D for 3D Finite Element Analysis in The Bangkok MRT Blue Line South Extension Project. ***ITA-AITES World Tunnel Congress (WTC) 2011***, *Helsinki, Finland.*

Lueprasert, P., Suwansawat & Jongpradist, P, S. **(2010).** Excavation Scenario Analysis for NATM Tunnel in Bangkok Subsoil. ***ITA-AITES World Tunnel Congress (WTC) 2010***, *Vancouver, Canada.*

Lueprasert, P., Suwansawat & Jongpradist, P, S. **(2010).** 3-D of NATM Excavation for Bangkok MRT Blue Line South Extension. ***ITA-AITES World Tunnel Congress (WTC) 2009***, *Budapest, Hungary.*

Lueprasert, P., Suwansawat & Jongpradist, P, S. **(2008)**. The First Applying of NATM for the Extension MRTA Project in Bangkok. ***Conference of ASEAN Federation of Engineering Organization*** *Bangkok, Thailand (CAFEO'26)*